Terms and Conditions of Use of Digitised Theses from Trinity College Library Dublin

Copyright statement

All material supplied by Trinity College Library is protected by copyright (under the Copyright and Related Rights Act, 2000 as amended) and other relevant Intellectual Property Rights. By accessing and using a Digitised Thesis from Trinity College Library you acknowledge that all Intellectual Property Rights in any Works supplied are the sole and exclusive property of the copyright and/or other IPR holder. Specific copyright holders may not be explicitly identified. Use of materials from other sources within a thesis should not be construed as a claim over them.

A non-exclusive, non-transferable licence is hereby granted to those using or reproducing, in whole or in part, the material for valid purposes, providing the copyright owners are acknowledged using the normal conventions. Where specific permission to use material is required, this is identified and such permission must be sought from the copyright holder or agency cited.

Liability statement

By using a Digitised Thesis, I accept that Trinity College Dublin bears no legal responsibility for the accuracy, legality or comprehensiveness of materials contained within the thesis, and that Trinity College Dublin accepts no liability for indirect, consequential, or incidental, damages or losses arising from use of the thesis for whatever reason. Information located in a thesis may be subject to specific use constraints, details of which may not be explicitly described. It is the responsibility of potential and actual users to be aware of such constraints and to abide by them. By making use of material from a digitised thesis, you accept these copyright and disclaimer provisions. Where it is brought to the attention of Trinity College Library that there may be a breach of copyright or other restraint, it is the policy to withdraw or take down access to a thesis while the issue is being resolved.

Access Agreement

By using a Digitised Thesis from Trinity College Library you are bound by the following Terms & Conditions. Please read them carefully.

I have read and I understand the following statement: All material supplied via a Digitised Thesis from Trinity College Library is protected by copyright and other intellectual property rights, and duplication or sale of all or part of any of a thesis is not permitted, except that material may be duplicated by you for your research use or for educational purposes in electronic or print form providing the copyright owners are acknowledged using the normal conventions. You must obtain permission for any other use. Electronic or print copies may not be offered, whether for sale or otherwise to anyone. This copy has been supplied on the understanding that it is copyright material and that no quotation from the thesis may be published without proper acknowledgement.

Development of Chiral Nanoparticles

By

Mícheál Moloney

A thesis submitted to the University of Dublin for the degree of Doctor of Philosophy

Trinity College

Dublin

October

2008

Declaration

This thesis has not being submitted as an exercise for a degree at any other university. Except where otherwise stated, the work described herein has been carried out by the author alone. The author agrees that the Library may lend or copy this thesis upon request.

Mícheál Moloney

June 2004

Summary

Symmetry and chirality are common occurrences in the natural world. Chiral compounds are extremely important in chemistry, biology and medicine. Chirality has also been envisaged to play an important role in nanotechnology. Most of the research in this field was focused on chiral organic and metallorganic molecules and their supramolecular structures. However, the area of chiral inorganic nanoparticles is currently in the very early stage of its development. There are only a limited number of publications on the preparation of chiral metal nanoparticles. Meanwhile, similar chiral nano-systems based on quantum dots (QDs) have not yet been reported at all. Quantum dots (QDs) are fluorescent semiconductor (e.g. II-VI) nanocrystals, which unlike metal nanoparticles have a strong characteristic spectral emission. This emission is tunable to a desired energy by selecting variable particle size, size distribution and composition of the nanocrystals. QDs have recently attracted enormous interest due to their unique photophysical properties and range of potential applications in photonics and biochemistry as light emitting devices, fluorescent sensors and bioassays.

The main aim of this thesis is develop novel chiral QDs, explore this area in details and establish fundamental principles influencing the structure and properties of chiral QDs. Another objective will be to investigate the specific interactions between chiral QDs and selected enantiomeric biomolecules. Finally we also aim to prepare chiral magnetic nanoparticles and "all in one "fluorescent-magnetic–chiral nanocomposites.

Chapter 1 of the thesis gives a brief introduction to the area of nanotechnology with the particular emphasis of II-VI semiconducting nanoparticles (quantum dots). An overview of quantum dot properties and basic concepts of chirality are considered. A brief review on magnetic materials and magnetic nanoparticles is also given.

Chapter 2 gives a complete listing of all experimental procedures preformed through out the course of this work, as well as detailing the both the equipment and reagents used.

Chapter 3 deals with the synthesis and characterisation of chiral CdS nanoparticles. The chapter explores the presence of optical activity in the bandedge region of these particles and attempt to explain this phenomenon using both

experimental and computational chemistry. It was found that penicillamine stabilised CdS particles have shown both very strong and very broad luminescence spectra. CD spectroscopy studies have revealed that the D- and L- penicillamine stabilised CdS QDs demonstrate circular dichroism and possess almost identical mirror images of CD signals in the range of 200-390 nm. Computer modelling of small chiral CdS-penicillamine clusters using density functional theory demonstrated that penicillamine strongly distorts surface of CdS, transmitting an enantiomeric structure to the surface layers and associated electronic states. However, the quantum dot core was found to remain undistorted and achiral. Therefore the particles posses a chiral shell, but cores of the particles remain achiral. This chiral shell contains chiral defects induced by chiral stabilizer (e.g. penicillamine) on the particle surface. Analyses of PL and CD spectra have shown that there is a clear relationship between defect emission and CD activity.

Chapter 4 is focused on the development of CdSe based chiral quantum dots. These new chiral nanoparticles have been prepared using various enantiomers of penicillamine and cysteine as stabilisers. Again, a clear evidence of the links between defect luminescence and CD activity was observed for CdSe chiral QDs. The potential chiral recognition and sensing properties of the CdSe particles were also examined.

Chapter 5 describes the work on the preparation and characterisation of CdTe based chiral QDs. Unlike the above semiconductors, CdTe nanocrystals possess a cubic structure making it more difficult to synthesis these particles with a chiral shell. A number of synthetic routes were tried before eventually discovering a suitable path. CdTe nanowires were also grown from the chiral quantum dots and initial TEM and spectroscopic studies were carried out on them.

Chapter 6 presents the synthesis of maghemite nanoparticles in which a mixture of Fe^{2+} and Fe^{3+} penicillamine complexes were used to form the particles. FTIR confirmed the presence of the Pen molecules on the surface of the particles and TEM shows them to have a high degree of monodispersity within a 5nm size range. These particles showed superparamagnetic behaviour due to their small size. They also demonstrated different magnetisation values depending on the enantiomer used. Preliminary results on the synthesis and characterisation of magnetic-luminescent-chiral nanocomposites are also presented in this chapter.

Finally, Chapter 7 details the conclusions of this work and also outlines further research on the chiral nanoparticles to be performed in the near future.

Acknowledgements

I would like to thank Professor Yurii K. Gun'ko for all his help and guidance and friendship over the last four years. Still more than that I want to thank him for giving me the opportunity to continue my research and fulfil a life long dream.

My Parents without whose help and encouragement I would never have come so far. I will never be able to pay you back for all you have done for me and allowed me to do.

My sister Jane, without a doubt one of the best friends I've ever had.

My brother John, different sides of the same coin.

All my friends inside, and outside of college you known who you are, there were times I didn't think we going to get out alive.

Everyone in the Chemistry Department and of course the present incarnation of the Gun'ko group Dr Damien Ahern, Dr Amro Satti, Dr Arunas Teišerskis, Michele Byrne, Wei-Yu Chen, Gemma-Louise Davies, Shane Gallagher, Joseph Govan, Joseph McCarthy, Małgorzata Nowostawka, Ian O'Connor, Renata Tekoriūtė.

A special mention for Maciej Stefanko a good man and a good friend whose time was far too short.

The Fibbers collective; Belen, Colin, Kerstin, Lorraine, Saúl and Sophie.

A very special thank you to all the TCD staff both academic and technical who helped me get out of various jams, not to mentioned Fred who could always track down that elusive something or other, no matter how busy he was.

Brendan, Martin, Patsy what can I say that hasn't already being said about these men, legends in their own life times. Thank you for everything, from the day to day banter, to that pinch of something or other, to that piece of equipment that I just couldn't get

to work. I'm still convinced the place would fall apart without you lads holding it together.

This thesis could not have been written without my friends who were, and are, always there for me whenever I needed them. Most of them I have already mentioned with the exception of three very important men. Jonathan, Matthew and Stephen, thank you for everything. I will never be able to pay any of you back but that won't stop me from trying.

Finally and most importantly this thesis is for Ania, whose friendship and love, but most importantly all those bisous for strength have made the last six years the happiest of my life.

.

Table of Contents

Declaration.....II

Summary.....III

Acknowledgements.....IV

Table of Contents.....V

Abbreviations.....IX

Chapter 1 – Conclusion and Future Work.....1

1.1 The Beginning.....1

1.2 Understanding Semiconductors.....2

1.2.1 Exciton.....4

1.2.2 Direct and Indirect Bandgap Semiconductors.....5

1.3 The Neglected Dimension.....6

1.4 Examining size and monodispersity.....7

1.5 Photophysical Properties of Quantum Dots.....11

1.5.1 Absorption.....11

1.5.2 Photoluminescence.....12

1.6 Nanoparticle Surface modification.....17

1.7 Chirality.....19

1.7.1 Circularly Polarised Light and Chirality.....19

1.7.2 Chirality on the nanoscale.....23

1.8 Magnetic Materials.....25
1.8.1 Introduction.....25
1.8.2 Origin of Magnetism.....26
1.8.3 Types of Magnetisation.....26
1.9 Magnetic Materials.....29
1.9.1 The Nano-size Effect.....29
1.10 Aims of this work.....30

Chapter 2 – Experimental.....35

2.1 Starting Materials.....35
2.2 Spectroscopic and Miscellaneous Equipment.....35
2.2.1 UV-Vis Absorption spectra.....35
2.2.2 PL spectroscopy.....36
2.2.3 Circular Dichroism measurement.....36
2.2.4 Infra-Red spectroscopy.....36
2.2.6 Dynamic Light Scattering.....36
2.2.7 Emission Lifetime Decay Measurements.....37
2.2.8 Microwave.....37
2.2.9 Transmission electron microscopy.....37
2.2.10 Magnetisation measurements.....37
2.3 Experimental details for Chapter 3.....38
2. 4 Experimental details for Chapter 4.....38
2.4.1 Preparation of Na_2SeSO_3.....38
2.4.1 Preparation of CdSe nanoparticles.....39
2.5. Experimental details for Chapter 5.....39
2.5.1 Preparation of CdTe nanoparticles.....39
2.5.2. Preparation of CdS/CdTe core-shell structures.....39
2.5.3 Photoannealing experiments.....40
2.5.2 Preparation of CdTe nanowires.....40
2.6. Experimental details for Chapter 6.....41
2.6.1 Preparation of maghemite nanoparticles.....41

2.6.2. Preparation of CdS - maghemite nanocomposites...41

2.7. Experimental details for Chapter 7.....42

Chapter 3 – Cadmium Sulphide.....43

3.1 Introduction.....43

3.2 General synthetic approach 44

3.3 2^2 Statistical Analysis 46

3.4 Circular Dichroism Studies.....55

3.5 TEM studies of Penicillamine stabilized CdS.....60

3.6 Computer modelling of CdS-Pen chiral clusters.....64

3.7 Cystein Stabilized CdS.....71

3.8 Conclusions.....73

References.....75

Chapter 4 – Cadmium Selenide.....77

4.1 Introduction.....77

4.1.1 Aims of this part of the work.....78

4.2 Synthetic of chiral CdSe... 79

4.3 Penicillamine stabilized CdSe.....80

4.3.1 Optimisation of the synthesis.....80

4.3.2 Optical Characterisation.....84

4.3.3 Luminescent Lifetimes of Pen-CdSe.....87

4.3.4 Circular Dichroism measurements.....91

4.3.5 TEM characterisation.....93

4.3.6 Conversion of Defect to Intrinsic emission.....97

4.3.7 Investigation of interactions between chiral QDs and chiral molecular...99

4.4 Cystein Stabilized CdSe QDs.....113

4.4.1 Optimisation of synthesis.....113

4.4.2 Optical Characterisation……116

4.4.3 Fluorescent lifetime measurements……120

4.4.4 CD Studies of Cystein stabilized CdSe……122

4.4.5 TEM of Cysteine stabilised CdSe……124

4.5 Conclusions……125

References……127

Chapter 5 – Cadmium Telluride……129

5.1 Introduction……129

5.2 Synthesis ……130

5.3 Penicillamine stabilized CdTe……131

5.3.1 Optimisation of synthesis……131

5.3.2 Enantiomer and Racemate……133

5.4 Cystein stabilized CdTe dots……135

5.4.1 Optimisation of synthesis……135

5.3.2 Enantiomer and Racemate……137

5.4.3 Fluorescent lifetimes of Cys-stabilised CdTe……139

5.4.4 TEM analysis of Cys-CdTe……140

5.4.5 CD studies of –Cys CdTe……141

5.4.6 Coating of CdTe QDs with CdS shell……143

5.4.7 Cystein- Penicillamine co-stabilized CdTe……148

5.4.8 Synthesis and studies of Chiral CdTe Nanowires..156

5.5 Conclusions……165

References……166

Chapter 6 – Penicillamine stabilized magnetic nanoparticles and their nanocomposites with CdS……168

6.1 Introduction.....168
6.2 Synthesis 169
6.3 Characterisation of magnetic particles.....171
6.3.1 Raman spectroscopy studies.....171
6.3.2 FTIR spectroscopy studies 173
6.3.3 TEM studies 175
6.3.4 Magnetisation measurements.....177
6.3.5 UV-Vis and CD measurements.....179

6.4 Magnetic Luminescent Composites..... 182
6.4.1. Investigation of the interactions between chiral CdS and maghemite nanoparticles...183
6.4.2. In situ grow of CdS shell 187
6.4.3. TEM images of In situ grow of CdS shell 191

6.5 Conclusions.....193
References.....194

Chapter 7 – Conclusions.....196

Publications.....X

Abbreviations

Abs……..…..Absorption

Ems……....Emission

Int……..……Intensity

DLS…….……...……Dynamic Light Scattering

SQUID……...…….. Superconducting Quantum Interference Device

TEM…….……Transmission Electron Microscope

STEM…….……..….Scanning Transmission Electron Microscope

HRTEM……....….High Resolution Transmission Electron Microscope

FT-IR…….……...……Fourier Transform Infra-red

TOPO……... Trioctylphosphine Oxide

TOP…….…....Trioctylphosphine

TBP……Tributylphosphine

Pen……..… Penicillamine

Cys……..……..…….. Cystein

Abbreviations

Abs……..…..Absorption

Ems……....Emission

Int……..……Intensity

DLS……..……...……Dynamic Light Scattering

SQUID……...…….. Superconducting Quantum Interference Device

TEM…….……Transmission Electron Microscope

STEM……..…….…Scanning Transmission Electron Microscope

HRTEM……....….High Resolution Transmission Electron Microscope

FT-IR……..……..……Fourier Transform Infra-red

TOPO……...… Trioctylphosphine Oxide

TOP……..…....Trioctylphosphine

TBP……Tributylphosphine

Pen……..… Penicillamine

Cys……...……...…….. Cystein

Chapter 1. Introduction

1.1 The Beginning

"Neglected Dimensions No Longer"

1915 saw the publication of the now famous book "The World of Neglected Dimensions".[1] In it, the author Wolfgang Ostwald described colloid chemistry, not as a speciality in a much larger subject, but as a science in its own right. Although it would take almost a century for this to be fully realised, his words can certainly be regarded today as prophetic. Throughout the latter half of the 20th century we have seen a return to this "neglected dimension" in which size and shape, two factors that are of little importance in everyday chemistry, play a key role in determining the properties and behaviour of the inhabitants of this "undiscovered country".[2-7]

As this new field grows (along with the interest in it), so too does the terminology associated with it.. The quest for quantum confinement (*a particle is quantum confined when the diameter of the particle is smaller than the Bohr radius of its exciton*) is the quest for a durable, stable material which exhibits properties that are intermediate between the lone molecule and the bulk state.[2] The smallest possible orbit of an electron around a proton, is most likely to be found at a distance from the nucleus called the Bohr radius. Although specific quantum confinement effects are observed in metallic particles (i.e. gold, silver, platinum),[8-14] a great deal of research has centred over the creation of nanosized semiconductor materials such as the sulphides, selenides and tellurides of cadmium, lead, mercury and zinc i.e. the II-VI semiconductors.[15-33] The focus of this thesis is the cadmium based II-VI semiconductor nanocrystals (Quantum Dots). These include CdS QDs, which emit in the near UV-Vis end of the spectrum and, CdSe and CdTe QDs, which emit in the visible regions of the spectrum (**Figure 1.1**). Our main aim is to create semiconductor nanocrystals that are quantum confined, stable in aqueous media, highly luminescent and, in addition, chiral and optically active.

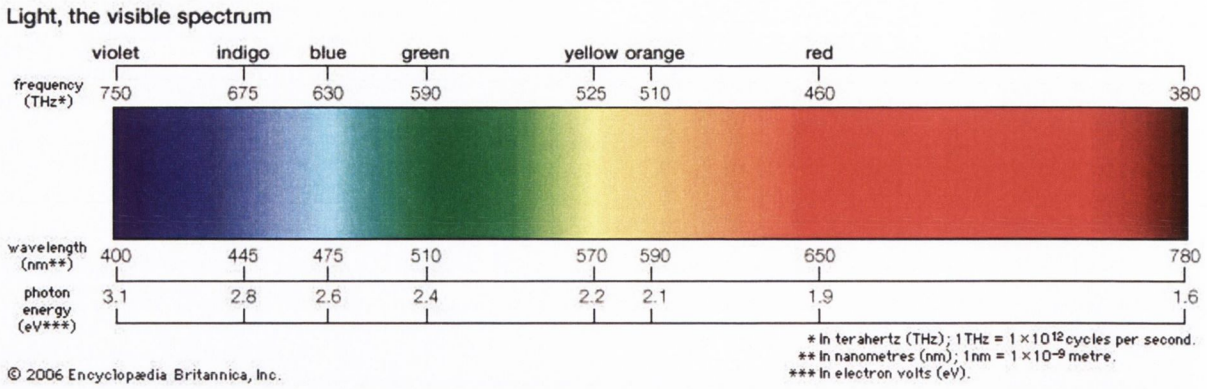

Figure 1.1: Top; The visible spectrum shown in colour, wavelength, frequency and energy. CdS, CdSe and CdTe quantum dots can cover the entire visible as well as the near UV regions of the spectrum. http://updatecenter.britannica.com/eb/image?binaryId=27030&rendTypeId=4.

However before we look into the specifics of creating optically active, or chiral quantum dots, we must first answer some of the basic questions of this field, i.e. what is a semiconductor? What is difference between these materials in the bulk and nano state and what gives them their unique photophysical properties?

1.2 Understanding Semiconductors

Semiconductors are materials which in the bulk state, (as opposed to the nano-state), are solid compounds which are non-conductive when pure or at a low temperature. However, when they are doped with a suitable impurity or raised to a higher temperature exhibit a conductivity which is intermediate between that of any insulator and most metals.[2, 34]

Binary semiconductors are classified according to their metallic element's valence number and their non-metallic element's position in the periodic table, i.e. its group number, ($Cd^{2+}S^{2-}$ for example is a II-VI semiconductor).

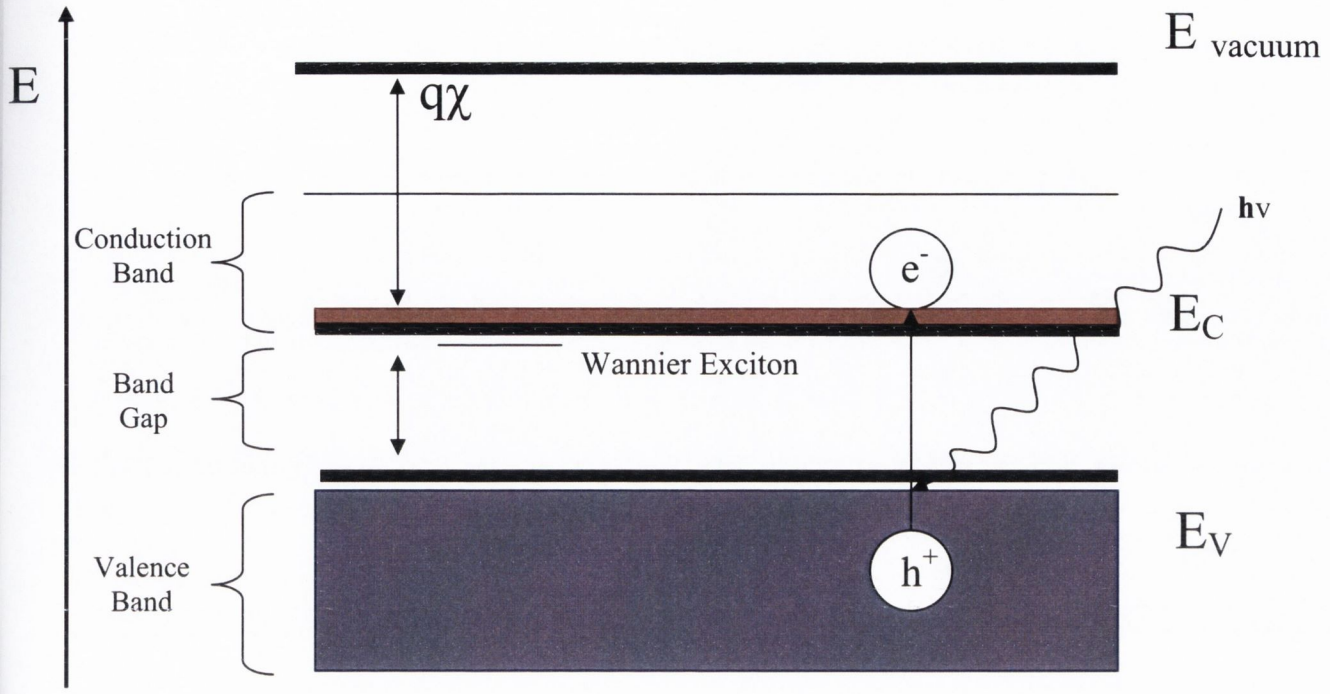

Figure 1.2: Simple energy scheme of a semiconductor. Valence and conduction bands are indicated by their band edges, designated Ev and Ec respectively. The vacuum level, the electron affinity and the electronic charge are indicated by E_{vacuum}, χ and q respectively. Graph was redrawn from reference 3.

The ability of these compounds to exhibit properties intermediate to those of conductors and insulators is a result of the overlapping of their atomic orbitals in an ordered crystalline lattice. The proximity of atomic orbitals creates a continuum of position independent electronic energy levels. A semiconductor possesses not only a valence band but also a conduction band. Energy band diagrams of semiconductors are generally rather complex: however, they can be simplified. Since the electronic properties of semiconductors are subject to the state of the highest partially empty band and the lowest partially filled band, it is sufficient to consider these bands (**Figure 1.2**). At 0 K the valence band in an undoped semiconductor is filled whereas the conduction band is empty. As the temperature is increased, energy is supplied to the system and electrons are promoted to the conduction band. This energy difference which separates the valence and conduction bands from one another is known as the band gap.

It is important to note that the size of the band gap of any semiconductor is dependant on its constituent elements (and temperature) and so a material may be identified by its band energy. As mentioned earlier an impurity, with a smaller band

gap, may be used to "bridge" the larger band gap and allow an electron to be promoted to the conduction band, but the band gap itself cannot be altered. Light may also be used to promote an electron to the conduction band. That is to say that the material may be excited by the energy from a photon of light causing the electron to move from the valence to the conduction band.

1.2.1 Exciton

Once an electron has been promoted from the valence band to the conduction band a "hole" now exists in the valence band. These holes are considered as point positive charges in direct contrast to the point negative charge of the promoted electron. Both the hole and electron can move independently of one another within the lattice allowing the crystal to conduct electricity. Collectively the electron and its corresponding hole are known as an exciton. Although they are not dependent on one another, they are by their very nature drawn to each other. These Coulomb forces create a state similar to that of a hydrogen atom (a negative charge orbiting a positive one), which is known as a Wannier exciton. However if the only force which existed between the electron and hole was a purely electrostatic attraction this would of course lead to the collapse of the exciton. The likelihood of the electron and hole recombining is limited by, firstly, the difficultly of losing the excess energy, so that the exciton may have a relatively long lifetime i.e. several milliseconds. A second stabilizing factor is the spatial overlap of the electron and hole wave-functions. This is essentially a measure of the probability of the hole and electron running to each other.

However, these photo-generated excitons are not stable above 0 K. This instability is a reason for their (the exciton's) small binding energies and large radii. Again using a hydrogen atom as a stable analogous structure and a CdS hole and electron as a typical semiconductor exciton this intrinsic instability is easily seen. A CdS exciton has a binding energy of 0.05 eV and a radius of 25 Å, while a hydrogen atom has a much greater binding energy of 13.51 eV over the much smaller radius of 0.53 Å. So although "structurally" similar a hydrogen atom is stable while a semiconductor exciton is much less so (**Figure 1.2**). The combination of the excitons low binding energy and wide radius results in their rapid dissociation into the free charge carriers as the temperature moves above 0 K.[4] This dependence of the band gap, E_g, on the temperature has been experimentally determined and is expressed by **Equation 1**.[34]

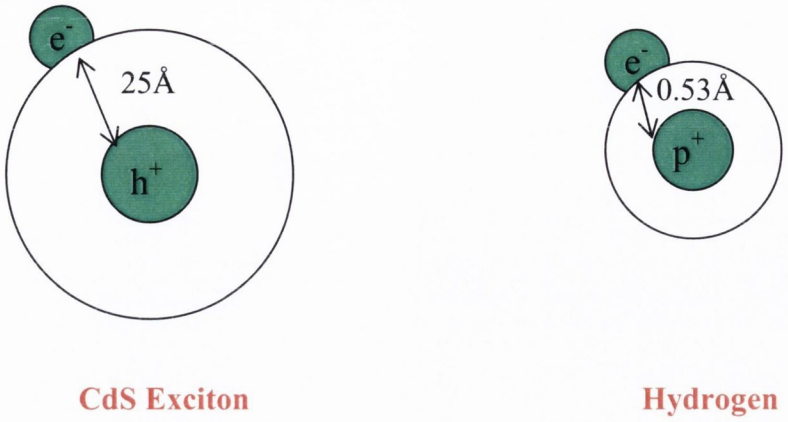

Figure 1.3: Although similar in structure the greater atomic radius and lower binding energy of a semiconductor exciton make it considerably less stable than a typical hydrogen atom.

$$E_g(T) = E_g(0) - \alpha T^2 / T + \beta \qquad 1.$$

Where ,

α and β are the fitting parameters **α = (meV/K)**

$E_g(0)$ = (eV), **β = (K)**

Therefore, it was only at temperatures close to 0 K that excitons, characterised by their sharp absorption and emission lines, were observed.

1.2.2 Direct and Indirect Bandgap Semiconductors

II-VI materials belong to direct semiconductors. A direct bandgap semiconductor is one in which the electron and hole pair which make up the exciton both have the same momentum (**Figure 1.4**). However, in an indirect bandgap material (for example silicon) the electron and hole possess different momentum from one another. This difference in momentum must be corrected before they can recombine with each other. Therefore, for radiative recombination to occur in an indirect-bandgap material, the process must also involve the absorption or emission

of a phonon*, where the phonon momentum equals the difference between the electron and hole momentum. The involvement of the phonon makes this process much less likely to occur in a given span of time, which is why radiative recombination is far slower in indirect bandgap materials than direct-bandgap ones. The fact that radiative recombination is slow in indirect-bandgap materials also means that, under most circumstances, radiative recombinations will be a small proportion of total recombinations, with most recombinations being non-radiative. Therefore indirect bandgap semiconductor materials such as silicon are normally unsuitable for use as an aqueous fluorophores, LEDs and laser diodes.

*A phonon is a quantized mode of vibration occurring in a rigid crystal lattice.

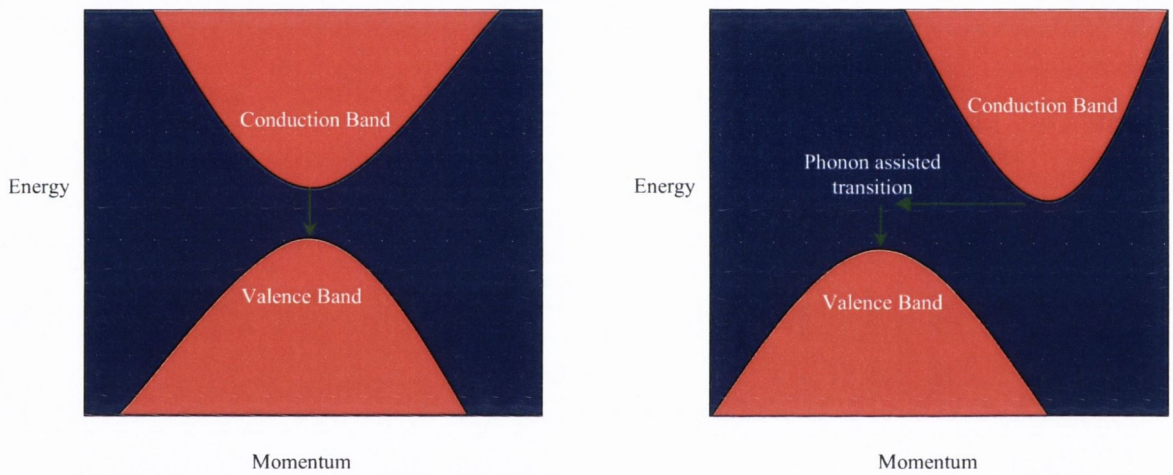

Figure 1.4: Bandgap energy diagrams of direct (left) and indirect (right) bandgaps. Note on the right phonon assisted momentum change must take place before the recombination can occur

1.3 The Neglected Dimension

While all this may be true of the bulk material, when dealing with the same material in the nanosized state the rules are utterly changed. As mentioned earlier a system is quantum confined when its atomic radius is less than the Bohr radius of its exciton. That is to say if CdS (which possesses an exciton radius of 25 Å) was prepared in such a way as to exist in an nanocrystalline form with a particle diameter of 20 Å its exciton would be too "big" for the particle. However by assuming a state of higher

kinetic energy the charge carriers, i.e. the hole and the electron, can fit inside the nanocrystal. This results in the energy bands splitting into discrete quantised levels. The band gap which was believed to be controlled solely by the constituent elements of the semiconductor (or temperature) is now observed to increase as the size of the particle decreases. So the exciton which was once free to move throughout the material is now trapped "in a box", and as this box gets smaller its energy must increase. This results in an increase in the band gap energy, which is accompanied by a decrease in the absorption wavelength. So a blue shift in the absorption wavelength of the substance in question is observed once its size has been reduced by a sufficient degree i.e. to the nano-range.

This change in a substance's optical properties can also be seen by the naked eye. In the case of a semiconductor such as CdS it goes from yellow to colourless as the bandedge moves from the visible at 460nm, (bulk material), to below 400nm, (the ultra-violet), as the material gets smaller. The actual wavelength and therefore size depends on a number of experimental factors which will be seen later on in **Chapter 3**. More dramatic examples can be seen when working with CdTe which spectacularly goes from black in its bulk state to red as quantum confinement takes hold. Depending on techniques used it is possible to move through the visible spectrum creating CdTe particle which absorb from the red through the orange and yellow all the way down to the green. So by controlling the size of the substance it is possible to tune its band gap to whatever is desired. This is essentially physical control of opto-chemical properties.

1.4 Examining size and monodispersity

It is the properties described above as well as other optical (e.g. fluorescent, non-linear) and chemical properties that have attracted the great research interest in semiconductor quantum dots (nanocrystals) of late. These properties, arising from the quantum confinement effect, allow these compounds to exhibit behaviour which is intermediate to that of the lone molecule and the bulk compound, as was mentioned earlier. However many of these properties can only be observed when the size range in which the particles are distributed is quite small, that is, the monodispersity is quite high. Attempts to control

the nucleation and growth of these crystals experimentally and hopefully the monodispersity of the particles are major factors in this work.[2, 35] The possibility of separating the various sized particles after preparation has also been examined. These techniques include the use of classic size separation procedures, such as chromatography (both conventional and HPGC) and gel electrophoresis. These methods have proven reasonably successful as the absorption spectra of a sample of CdS in **Figure 1.5** clearly shows.[2] Once the colloid has been separated into samples with a high degree of monodispersity; so that each sample has a 7-8% derivation from its average particle size, it is then possible to observe fine structure in the samples. The average particle size of the example is believed to be 55Å +/- 4Å with absorption beginning at 500nm accompanied by several weak shoulders at shorter wavelengths. These "bumps" can only be observed once the sample has undergone separation by gel electrophoresis. This fine structure can be observed both at room temperature and at –77K, but can be more clearly seen on the second derivation spectra. The positions of the shoulders in the absorption spectra are mirrored by the minima in the second derivation spectra. These shoulders, which are believed to arise from transitions to discrete higher excitonic levels can only be seen if the standard deviation from the average particles size is less than 20%. However these processes are time consuming and become more difficult as the size range in which we work decreases. So one of the end goal of this work is to create an experimental procedure which will yield a highly monodispersed nanocrystalline sample without the need for complicated separation methods.

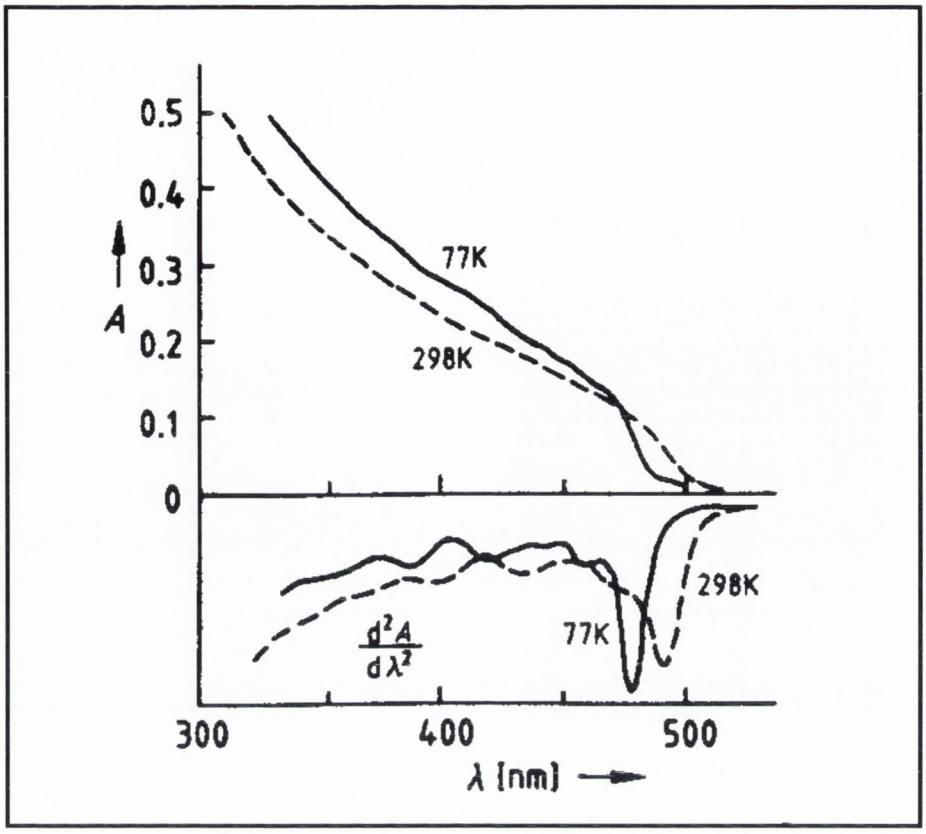

Figure 1.5: Absorption spectra of quantum confined CdS which has been separated by gel electrophoresis, at 298 and 77K, the broken and solid lines respectively. The bottom part is the second derivation spectra. Ref.[2]

The main method for examining the degree of monodispersity of any nanoparticulate sample is of course TEM, (Transmission Electron Microscopy), (**Figure 1.6**), as seeing is believing. Unlike other size measuring techniques such as XRD and Zetasizing averages of numerous sizes are not taken but actual sizes of individual particles can be seen and therefore a clear picture of the monodispersity can be gained.

Any attempt to determine particle size of materials which are below 10 nm is a difficult thing. Their small size, combined with coating in organic stabilizers and of course particle aggregation makes identifying individual particles difficult. While TEM has become the classic technique to determine particle shape and size there is of course a limit to sizes it can observe, however these limits are being extended each day with the invention of more and more sensitive microscopes. TEMs work as conventional microscopes in that optics are used to magnify objects that can not be seen by the naked eye, however instead of using light, these microscopes using

electrons to highlight the samples. Samples are placed on copper grid which can be coated in a number of substances.

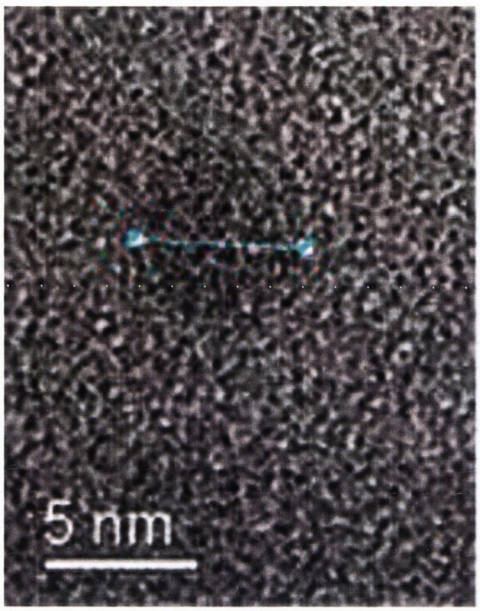

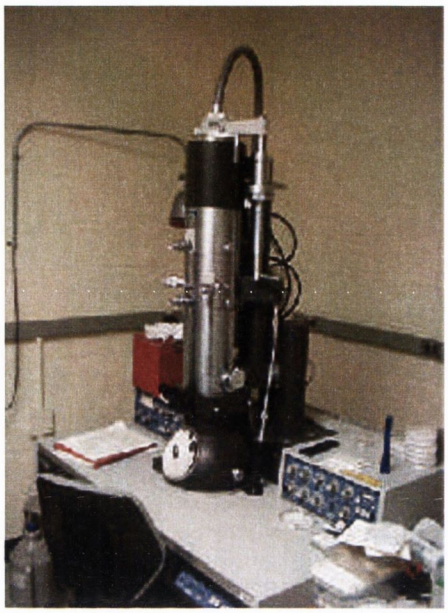

Figure 1.6: LHS: HRTEM image of circular CdS nanocrystals in the 5.5nm size range. Note: It is possible to see the crystal lattices of individual particles using this technique. RHS: Picture of a standard transmission electron microscope (TEM) www.micro.cornell.edu/IMAGES/TEM.sized.jpg.

These include elemental carbon, silicon nitride or an organic polymer such as formvar. While the copper grids are extremely conductive and therefore show up black as they absorb energy from the electrons been fired at them, the substrate does not and therefore appears clear making a perfect background against which to see the nanoparticles. Depending on how conductive a sample is it will appear as a black, (metallic nanoparticles) or grey, (semiconductor nanoparticles), object against the lighter grid background. As nanocrystal sizes move into the <10 nm range they become too small for clear TEM images to be resolved and high resolution TEM (HRTEM) must be employed. Both TEM and HRTEM have been used over the course of this work to elucidate both size and shapes of the particles produced. As mentioned earlier XRD may also be used to determine particle size however any attempt to perform XRD scans of these quantum dots proved unsuccessful. This is more than likely due to small amount of particle produced in each reaction. Also as XRD, (like TEM), must be preformed dry it does not give an accurate picture of the

dots in solution. By using techniques such as zetasizing or dynamic light scattering, DLS, as it is also known, we can get a picture of not only the individual dot sizes but also the size of the aggregates that the dots arrange themselves into. DLS, as the name suggests, combines a light source which passes through the sample being examined and detectors which determine the size of the particles by measuring the angle at which light is back scattered. Again however, this system has it limitations. Firstly the presence of large or sedimenting particles, (such as nanoparticle aggregates), and luminescent material, (i.e. the quantum dots), can affect the PdI or polydispersity index. Any scan which has a PdI greater than 0.4 is considered to be unreliable with 1 been the maximum value. Secondly the Zetasizer's limit is somewhere below 5 nm making size determination of the smaller dots, especially the racemic dots, impossible. Racemic dots are those prepared with an equal mix of D- and L-stabilizer. Despite these drawbacks Zetasizing offers a easy, accessible means to get an idea of particle sizes however it must be used in conjunction with and not as a replacement to TEM, especially when dealing with <10 nm quantum dots. The organic molecules used as stabilizing agents when preparing nanoparticles can obstruct clear TEM images. This problem can be overcome by using gel filtration, for example sephadex columns, to separate nanocrystals from the extra organic impurities which would otherwise cause the aggregation of nanoparticles making individual size determination impossible. Nevertheless, both TEM and the necessary cleaning techniques are expensive and time consuming.

When dealing with fluorescent samples it is possible to examine the monodispersity without using imaging or scattering spectroscopy. By examining the position of the emission at various excitation wavelengths a clear indication of monodispersity can be obtained.[2] As mentioned earlier, the wavelength a nanoparticle of a particular material absorbs at is an indication of its size. This is also true of its emission wavelength. As most quantum dots will only have one emission maxima, and as the emission spectrum is not nearly as complex as the absorption spectra it is a useful tool to identify different sizes within a batch of nanoparticles. A sample with a uniform size distribution will only emit at a single wavelength which corresponds to it size. That is particles with a high degree of monodispersity will emit at the same position despite changes in the excitation wavelength. However, a sample containing varying sizes of particles will not. As the excitation wavelength is changed the particle(s) with the size closest to that wavelength will emit preferentially over the others in the

sample. Therefore the position of the emission maxima will move as the excitation wavelength is changed. Horst et al. reported a way of using this property to their advantage when proving the existence of discrete optical transitions in samples with high size distributions.[2] Observing the emissions with the longest wavelengths (while varying the excitation wavelength) of a given sample at 15 K, the excitation spectra of these emissions was recorded. Since the size of the particle controls the position of the onset of absorption, it therefore controls the position of the emission wavelength whether the emission is intrinsic or to a lesser extent defect. Emissions are either derived from intrinsic properties of the particles (which are observed in the absorption spectra) or are a result of defects in particles structure (these are referred to as defect emissions); again these properties will be dealt with in Section 1.6. Since each excitation spectra corresponded to a single emission which in turn corresponded to particles in a particular size range, it was possible to see the fine structure in the excitation spectra.

1.5 Photophysical properties of Quantum Dots

1.5.1 Absorption

Ultraviolet-visible spectroscopy is used to characterise various organic and inorganic compounds by recording the total light absorbed at wavelengths across the range of ultraviolet and visible region of the electromagnetic spectrum. Using a light source and detector, with the sample placed in the path of the light beam. The difference in the total light emitted by the spectrometer on one side of the sample against the light picked up by the detector on the opposite side at individual wavelengths is used to contrast a typical absorption scan. Wavelength, (measured in nm), is often represented by the symbol λ. For any given substance, the wavelength at which the maximum absorbance in the spectrum occurs is called the λ_{max}. Substances such as ionic crystals

are not "UV active" that is they do not have an absorption spectrum. Organic molecules will only be UV active if they posses a group or bond which can absorb energy, i.e. the presence of carboxyl groups or conjugated systems. As shown above semiconductors contain empty conduction bands which can be occupied by electrons from the valence bands, this of course means they are UV active. As each semiconductor, (in the bulk state), has its own unique bandgap energy, i.e. the energy needed to promote an electron to the conduction band and thereby create an exciton, it is possible to identify various semiconductors from their UV-Vis spectra. Therefore the absorption spectrum of a semiconductor can be described as a visual representation of its band gap energy. So in the bulk each semiconductor has a characteristic bandgap energy and therefore absorption wavelength. However this changes in the nanoscale.

As explained in previous sections the creation of semiconductor nanoparticles results in a quantum confinement effect taking place. This effect causes the bandgap energy of the semiconductor to increase relative to its size. As energy can also be written as $1/\lambda$ this means absorption spectroscopy can not only be used to identify various semiconductors but more importantly it can determine if quantum confinement has indeed taken place. A semiconductive material will usually show a peak of absorbance where the energy of the absorbed light is just higher than the band gap energy. As quantum confinement leads to an increase the energy of the charge carriers, this increases the band gap energy, which is seen as a blue shift in the absorption wavelength of the material. As the particle size decreases the band gap energy increases and the absorption wavelength blue shifts.

The absorption spectra can also give an idea of monodispersity. As the absorption maxima depends on particle size the narrower the absorption peak is the smaller the size distribution, whereas the wider absorption peak or "shoulder" the greater size distribution. Although these shoulders can also be a result of particle aggregation which is also quite common in water based particle synthesis.

1.5.2 Photo-Luminescence

Up to this point we have only dealt with the ability of these quantum confined semiconducting materials to absorb light, while touching briefly on their ability to

"luminesce", that is to emit this light. The photoluminescence of any substance can be studied using PL spectrometer. Like absorbance spectroscopy described above PL spectroscopy involves a light source, usually a tunable laser, and a detector. However unlike absorption spectroscopy the light source emits light at only one wavelength which has been chosen by the operator; this wavelength usually corresponds to the λ_{max} observed in the absorption spectra. If the material is luminescent it will re-emit the light it has just absorbed, the time taken to re-emit this light can be measured as an exponential decay and is referred to as the luminescent lifetime. Another important difference between the set up in a PL as compared to an absorption spectrometer is the light source and detector are at right angles to each other so as to prevent incident light from the laser reaching the detector. As mentioned in Section 1.2 it is possible to excite a semiconductor using light. This causes an electron from its valence band to be promoted to the conduction band, thereby creating an exciton. This electron will not however remain excited indefinitely and eventually it and its corresponding positively charged hole will recombine. As the electron returns to the ground state the energy will be released as light. This is known as a radiative recombination. When dealing with quantum dots however it is not usually that simple. Although, due to their small size factors such as diffusion no longer affect the luminescence there can still be defects within the crystal structure and of course on the surface of the particles which either the electron or the hole can and will recombine with. These "trapped states" as they are known can allow either emissive or non-emissive recombinations to take place and depending on the number of these defects present in and on the particles the quantum dots will express either defect or intrinsic luminescence, but what are these defects? To answer this question we must observe a simple energy scheme of a semiconductor (**Figure 1.7**). Up to this point the band gap was considered a clear boundary between the excitonic levels, however this "no mans land" contains traps for both electrons and holes. These traps in reality can be caused by a number of possibilities. These include interstitial atoms, impurities, dislocations and of course actual defects in the crystal structure. The charge carriers (the electron and hole) can recombine with these traps. However this recombination can be either radiative or non-radiative. In the latter case no emission is observed, but in the former defect emission will be seen. Due to the disturbed bonding forces on the surface of the semiconductor it is here that traps are most commonly found. So in nanocrystals where the surface area to volume ratio is large (there are about as many molecules on the surface as there are in the entire

crystal), the state of the surface i.e. presence or absence of physical defects, is of paramount importance.

This unusual size to surface area ratio combined with the fact that the wave function of the nanocrystals exciton already fills the entire volume of the particle creates an additional problem. In bulk semiconductor material the lifetime of the exciton is governed by diffusion processes which carry the charge carriers from the core where they are formed, to the surface where they are trapped. This is of course untrue of the quantum confined material, since there is a high probability that once an exciton is formed it is already on the surface. Examination of quantum confined ZnS and CdS has shown that the time required for their individual charge carriers to be trapped is ≤ 100 femtoseconds.[2] So in essence the study of the emission properties of various nanocrystalline materials is the study of the state of their surfaces. This feature of nanoparticle chemistry will in turn lead into the motivation for this work. It has been noticed that, as with other nanocrystals, the emission properties of CdS are affected by its surface conditions. The method of preparation, the solvent used, but especially the stabilizer used, all play an important role in determining its emission properties.

Intrinsic luminescence as the name suggest is due to recombinations which are exclusive to the dot itself and is not the result of any defects within the crystal structure. Generally there will always be some loss of energy to the surroundings causing the emission maxima to be slightly red shifted with respect to the absorption maxima, however there are instances where intrinsic emission maxima can have a Stokes shift, (the distance in nm between the absorption and emission maxima), greater than the usual 20-30 nm. Therefore the main characteristic of an intrinsic emission is the width of the peak at half its maximum intensity or its FWHM, this is usually about 30 nm.

Particles which possess intrinsic luminescence therefore only emit over a small wavelength allowing them to be classified by colour with any changes in either the size or surface conditions resulting in a clear and observable colour change. This narrow emission also makes checking the degree of particle monodispersity quite easy as slight changes in the emission maxima will be easily observed, (see **Section 1.4**). If the particle surface posses a large number of surface defects or trapped state then defect emission will be expressed. Unlike the intrinsic form, a defect emission always has a large Stokes shift and FWHM, in the case of Pen-CdS, 160nm and 120nm respectively. This large FWHM means that QDs which express defect

luminescence will not emit single colour but a mixture across the visible spectrum allowing them to emit white light. However they still do have a maximum emission wavelength ensuring the white light has a certain tint depending where the maxima is, e.g. R-Pen CdS emits at 490 nm therefore it emits blue-white light. While particles which possess defect emission may still be used as fluorophores the width of their emission means that any changes in the surface of the particles as a result of interaction with analyte molecules will not be as easily observed as with intrinsic emission.

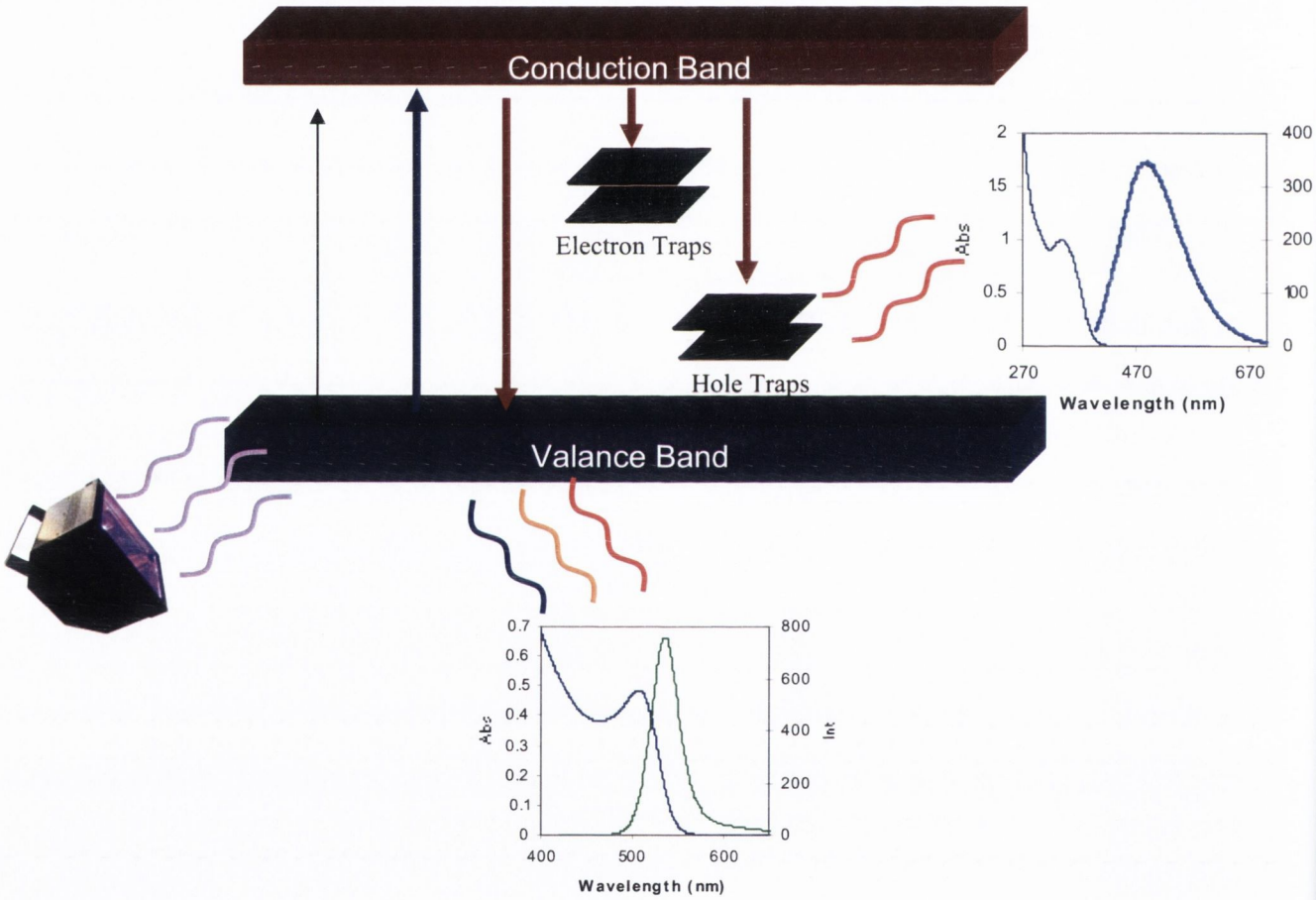

Figure 1.7: Simple energy scheme of a semiconductor showing the creation of the exciton as the material is exposed to UV light. Intrinsic luminescence is generate by particles with no defect present, (Cys-CdTe bottom), but those which posses electron and hole traps exhibit defect luminescence, (Cys-CdS right).

1.6 Nanoparticle Surface Modification

It is relatively easy to produce nanosized crystals immediately upon co-precipitation, however, what is to stop these various nucleation centres from simply amalgamating into the larger bulk material? The simple answer is the introduction of a capping agent or stabilizing molecule. While a large variety of molecules are now being used as "stabilizing agents" in the preparation of nanocrystals, including antigens, antibodies, amino acids, polyphosphates, thiols and silicates, it was simple organic polymers which were the initial molecule of choice.[32, 36-43] Oswalt ripening; the process by which many individual smaller crystals are sacrificed to form one larger single crystal is a process which must be arrested in order to produce stable batches of quantum dots. Initially, it was believed that by lowering the reaction temperature and introducing long chain molecules to increase the viscosity of the solvent and thereby prevent individual nanocrystals from interacting it would be possible to create stable quantum dot colloids. However, it was soon noted that by introducing polymers or long chain molecules which contained functional groups that could co-ordinate to the metal of the nanoparticle that is was possible to create far more stable nanoparticles. Not only this, but depending on the type of stabilizer used, it was possible to control various aspects of the dots. For example, choosing the chain length of the stabilizer used can determine the shape of the particle, i.e. sphere, rod, wires etc.[44] Depending on the hydrophilicity or hydrophobicity of the ligand used, it was possible to create dots which were soluble in either polar or non-polar solvents, and by carrying out ligand exchange reactions dots which were soluble in chloroform could be transferred into something as different as water. It became very obvious very quickly that the stabilizer used was almost as important as the semiconductor itself.[20, 45]

As the importance of the stabilizer became apparent, it also became obvious that if one end of a stabilizer was used to modify the dots surface then the other end could be used as an anchor point for various other analyte molecules. This combined with their ability to not only emit light but also for the colour of this emitted light to be sensitive to surface conditions of the dots made them excellent candidates to be used in biology as sensors and fluorophores.

For use in biological studies quantum dots must fulfil a number of criteria; they must be water soluble and non-toxic, to act as sensors they must be luminescent, to

enter living cells they must be small, and the smaller the better, and of course to permeate the cell membrane they must be biocompatible. Traditionally strongly emitting CdX has only been produced in organic solvents using strongly hydrophobic stabilizers such as TOPO and HDA,[19, 46, 47] these of course are not water soluble making them impractical for biological purposes. While it is possible to exchange these ligands for something more water soluble the results are mixed at best, usually resulting in a large reduction in the quantum yields unless such precautions as the introduction of an epitaxial shell consisting of a second II-VI semiconductor is taken.

It is with this in mind that a considerable amount of effort has been put into finding a simple synthetic route which would allow the use of hydrophilic molecules that are not only biologically active and non-toxic but will also produce strongly luminescent dots to act as the stabilizing molecule. Mercapto group containing molecules such as mercapto-ethanoic or propanoic acids have filled this need nicely.[37, 38, 48, 49] The presence of the sulphur group ensures tight surface binding to any Cd containing quantum dot preventing Oswalt ripening and removing non-radiative traps from the surface, while the carboxyl group at the other end not only increases the dots hydrophilicity but also allows for any number of biologically significant conjugation reactions to be carried out. Sulphur containing amino acids have also proved to be excellent stabilizers with L-Cystein, (a stereospecific analogue of mercapto-ethanoic acid), becoming one of the most popular CdX surface molecules.[20, 50, 51] This use of stereospecific stabilizing molecules opens another avenue in the field of quantum dots as biological sensors, as chirality is of immense importance in biological interaction. This thesis therefore examines the production of the quantum dots CdS, CdSe and CdTe, (as well as the magnetic nanoparticle maghemite and the photosensitive nanoparticle TiO_2) using the dextrorotary, (D-), and levorotary, (L-), enantiomers as well as the racemate, (R-), forms of two separate amino acids. The amino acids used although quite similar are sufficiently different to allow us to show that the chiral effects imbued on the nanoparticles are not simply a property of one molecule alone but of any molecule which contains a chiral group that can co-ordinate to a quantum dot. Over the course of this thesis the two amino acids used, (in both their enantiomeric forms as well as the racemate), will be 2-amino-3-mercaptopropionic acid and 2-Amino-3-mercapto-3-methylbutanoic acid or cystein and penicillamine as they are more commonly known, (**Figure 1.8**). Both compounds are mercapto group containing carboxylic acids which also possess an amino groups attached to their

chiral centre(s). Although the mercapto group is the primary Cd binding group both the amino and carboxyl groups are also believed to be involved.

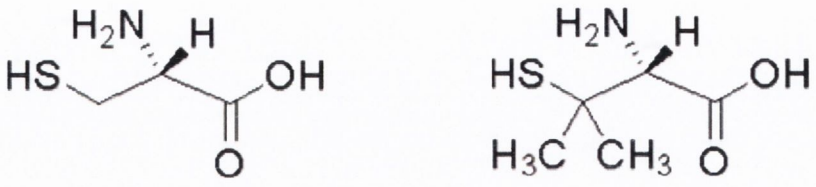

Figure 1.8: Cystein, (left) and Penicillamine, (right).

1.7 Chirality

1.7.1 Circularly Polarised Light and Chirality

Symmetry and chirality are common occurrences in the natural world. [52] A chiral molecule is one that has two mirror-image forms, which are not superimposable in three dimensions. The mirror-image forms of the chiral molecule are classified as enantiomers. Chiral compounds play an extremely important role in chemistry, biology and medicine. Here we are going to discuss some basic concepts and definitions relevant to polarised light (specifically circularly polarised light) and chirality.

While it is possible to consider light to consist of the particles known as photons, it must also be remembered that light is also thought as a self-propagating wave. This transverse electromagnetic wave has a direction of propagation along which it moves; the z axis. The polarisation of the wave describes the behaviour of the troughs and crests of the wave, the vector **E**, along the x and y planes, which are of course perpendicular to the direct of propagation, the z axis. If we consider the light to be unhindered and continuous moving in a single direction then the z axis, the direction

of propagation, is fixed. While it is possible for the vector, **E**, to also be fixed in relation to the z-axis this is not always the case. The vector(s) in unmodified or isotropic light have no set direction or type of movement but consists of all of the possible types of polarisation. The plane of polarisation is the plane created by the z axis and the direction/movement of the vector of a specific wave. If the vector stays in a fixed direction then the wave is said to be linearly polarised. If the vector changes direction randomly with time then the wave is said to be randomly or un-polarised. However the vector can also change direction uniformly over time. Moving circularly in either direction this is known as circular polarisation light and is specified to be left or right handed depending on the direction of rotation, (**Figure 1.9**).

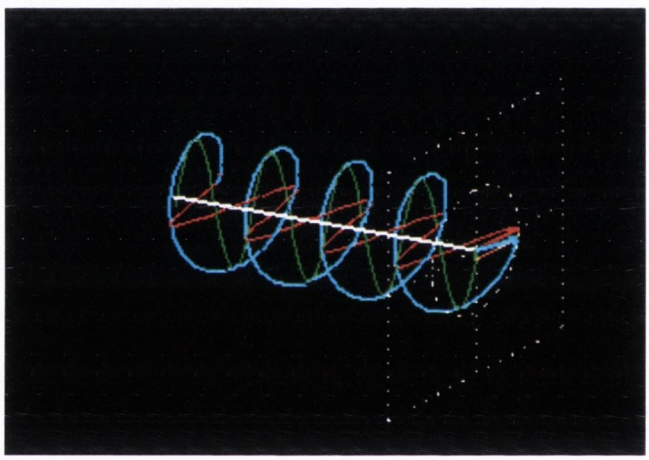

Figure 1.9: Right handed circular polarised light. The white line indicates the direction of propagation. The red and green lines represent the vector E in the x and y axis's respectively. As the wave moves in the z direction the vector E rotates clockwise much like a corkscrew. Diagram referenced from www.ua.es/.../TETS/opfisica/polar/cdedemo/p4.gif

It is this type of light that we are concerned with as it can be preferentially absorbed by secondary structures in certain types of molecules and crystal structures. Therefore circularly polarised light can be used as a tool to confirm the presence of these chiral groups.

The most basic and obvious example of chirality is that of human hands; two objects which are identical mirror images of each other yet cannot be superimposed on top of one another. However chirality is not simply confined to the macroscopic world and can be found everywhere in nature; at the macro scale, the micro scale and

at the molecular scale. Like human hands certain molecules are chemically identical but yet cannot be superimposed onto of one another. These are stereoisomers; molecules which have identical molecular formulas but different structure formulas.

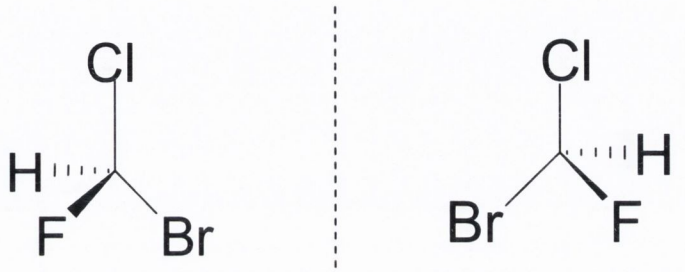

Figure 1.10: One of the simplest examples of molecular chirality bromochlorofluoromethane.

Figure 1.10 shows both enantiomers of bromochlorofluoromethane, one of the simplest examples of chirality on the molecular level. Although both molecules appear identical at first glance, any attempt to superimpose one over the other will prove unsuccessful. If one of the enantiomers is rotated by 180^0C along the C-Cl axis then all atoms in both molecules will be facing in the same direct as we look down. However these molecules are not one dimensional and as the molecules are flipped the atoms which once pointed into the plane of the page now point up, and vice versa. As stated above chiral molecules are also said to be optically active. The reason for this is quite simple chiral molecules depending on the direction of their chirality will preferentially absorb left or right handed circularly polarised light. If a molecule is in the D- or dextrorotary form then it will absorb right handed polarised light, while if it absorbs left hand circularly polarised light then the molecule is said to be in the levorotary or L- conformation. Although the R-(rectus-right), S-(sinister-left), system is more commonly used to name optical active molecules in chemistry, for reasons of simplicity the D-, L- system remains in use for amino acids and so will be used through out this thesis.

It is on this principle of preferential absorbance of circularly polarised light that circular dichroism, CD, spectroscopy works. Unlike absorption spectroscopy where the light is isotropic CD uses mixtures of left and right handed polarised light and

measures which component is removed, according to ΔL-ΔR, therefore if the molecule is left handed a positive scan is attained and consequently if the D-conformation is present in excess then a negative scan is attained. If enantiomers are present in equal amounts then the sample is said to be racemic and no signal is obtained. The chiral centre in an amino acid is usually the carbon to which the amino group is bonded, as with the substituted methane above, (**Figure 1.10**), it is a carbon atom with four different substituents that provides the optical activity. **Figure 1.11** shows the penicillamine in its D- and L- configurations and their corresponding CD scans. Both molecules absorb at 232 nm and would therefore be indistinguishable by UV-Vis spectroscopy but as they preferentially absorb right or left circularly polarised depending on their handedness they are easily separated by CD. A simple rule when determining the handedness with amino acids is to use the acronym **CO.R.N.** Starting with the hydrogen on the chiral centre follow the other substituents in the following order: first the carboxyl group, –COOH, then the -R group and finally the amino group $–NH_2$. If they are arranged clockwise then the molecule is in the L-configuration, if anticlockwise then the D-.

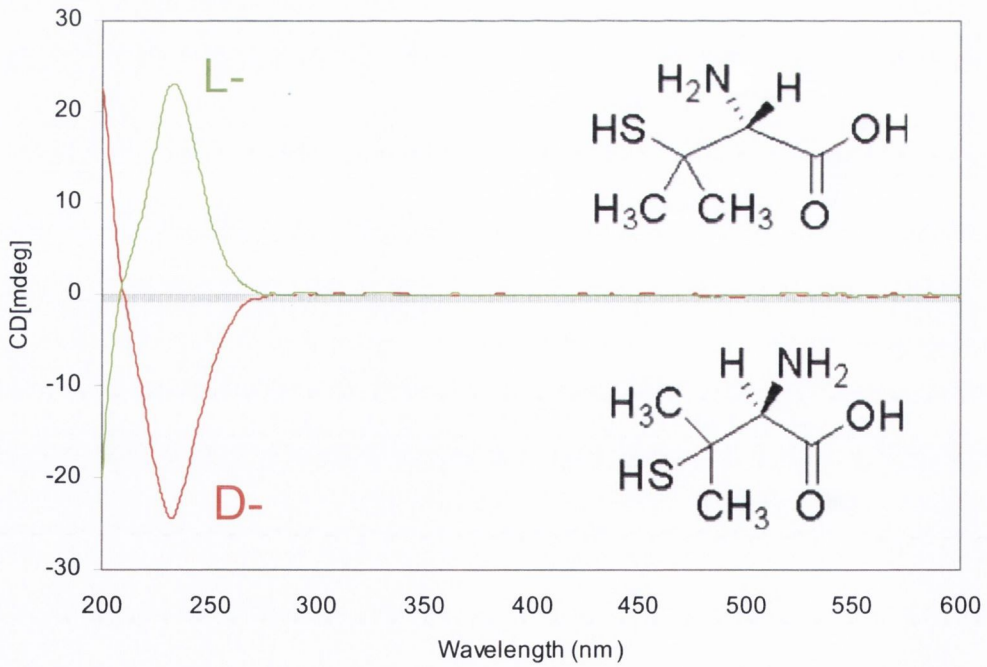

Figure 1.11: CD spectrum showing the scans of free D- and L- Penicillamine. Absorption maxima is at ~234nm for both enantiomers but negative for the dextrorotary and positive for the levorotary enantiomers.

By using chiral molecules as nanoparticle stabilizers it was hoped that they would retain their chirality. This would perhaps allow the particles to be used in chiral interactions and sensing. However, what has become apparent in recent years is that not only do these stabilizers retain their chirality but they also impart it unto the crystal that they are stabilizing.

1.7.2 Chirality on the nanoscale

Although well documented on the molecular scale, chirality in the nanoscale is a relatively new field. Using chiral organic molecules as templates it has become apparent that it is possible to transfer the stabilizers optical activity onto the nanomaterial. Initially, this involved molecules which bridged the gap between the molecular and nanoworlds such as chiral supramolecules like La nanoballs or gold thiol nanoclusters.[53] However as the field has progressed, it has been shown that it is possible to create chiral metallic nanoparticles using chiral molecules as varied as thiol containing chiral ligands, (amino acids) to chiral polymers, (DNA).[9, 10, 54-56]

Initially chiral gold and silver nanoparticles were produced using thiol containing chiral stabilizers. As amino acids represented a ready supply of compounds which fulfilled these two prerequisites the main bulk of the work involving chiral metallic nanoparticles was built around these stabilizers. Much work has been done in this field in recent years with chiral gold and silver nanoparticles being produced from penicillamine, cysteine, N-acetyl cystein, etc, indicating that any chiral thiol can be used as a chiral template. Although it is generally accepted that the source of the chirality, (in this case the amino group), must also be able to co-ordinate to the nanoparticles, although this may not be the case.[57] An interesting phenomenon is that the smaller the particle the greater the degree of optical activity with this effect being more pronounced in silver rather than gold particles.[57]

One of the more interesting chiral stabilizers is without a doubt DNA. Shemer et al. demonstrated that it is possible to grow chiral silver nanoparticles on a DNA template by first functionalising the DNA with silver ions before then reducing the metal ions to form nanoparticles.[55]

DNA is not only an excellent chiral template when growing optically active metallic nanoparticles, it can also be used to produce a chiral response in racemic mixtures of single walled carbon nanotubes.[58] This work was later expanded by Peng et al. who

using chiral diporphyrin as a type of nanotweezers separated carbon nanotubes according to their chirality.[59] Here we see a working example of chiral nanoseperation, and since the porphyrin can be separated and reused the process is also renewable.

While a number of different theories have been put forward trying to explain the origin of chirality in nanoparticles most of them drawn the conclusion that the chirality comes in some shape or form from the chiral stabilizer. Briefly, i). the ligand acts as a template around which the entire particle must grow, meaning the crystal itself is chiral, ii). the ligand only affects the surface atoms of the particles leaving the core achiral or iii). that only the ligand is chiral and this property is somehow transferred onto the plasmon or exciton band of the metal or semiconductor nanoparticle respectively. However, it must also be mentioned that using a combination of trapped-ion electron diffraction, photoelectron spectroscopy and TDDFT calculations a Au_{34}^- cluster was shown to be chiral without the presence of a chiral stabilizer. However, recent publications have dealt with the theory of the chiral footprint. By adding amounts of an enantiopure ligand to nanoparticles which are racemic it is possible to optically activate the particles via ligand exchange, giving credence to the stabilizer theory.[56, 60] It therefore becomes obvious that there is still a long way to go to fully comprehending this phenomenon.

While there is now a great deal of interest in the field of nanoscale chirality, there has been little or no work done outside of metallic nanoparticles and carbon nanotubes. In this thesis we shall concentrate on chirality in quantum dots and magnetic nanoparticles. We hope that these materials will contribute to this already fascinating area and that they may be applied as luminescent enantioselective sensors and enantioselective magnetic separation respectively.

1.8 Magnetic Materials

1.8.1 Introduction

Although known, in its various forms, since the Hellenic age (magnetic ores, compasses etc) it is only in the last two centuries that the naturally occurring phenomenon known as magnetism has begun to be more fully understood.

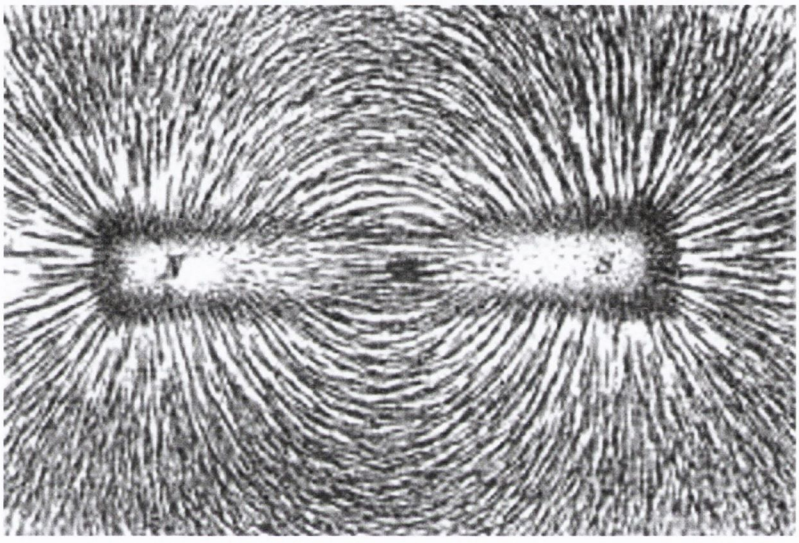

Figure 1.12: The classic pattern of magnetic "lines of force" described by iron filings.[61]

Although classically associated with iron containing compounds, the legend of Magnes tells us of a Shepherd who while tending his flock accidentally strikes the iron tip of his staff against a lodestone and is magically held to the ground by some unseen force), the presence of a magnetic field is not however dependant on the presence of iron ore. Magnetic fields have been found to exist in environments where iron oxide just can't exist, from the earth's core, (where incredibly high temperatures and pressures which would vaporise the oxide), to space born gaseous anomalies, where due to the absence of oxygen iron oxide simply does not exist. Therefore a definition is needed which doesn't include the presence of iron ore as a necessary factor.

1.8.2 Origin of Magnetism

Magnetic fields are generated by the movement of an electric current and vice versa. On a quantum level the movement of electrons orbiting their respective nuclei could explain why some materials were magnetic and others are not. Magnetic fields, or magnetic moments, are a result of two kinds of electron movement. The first is the orbital motion of the electron around the nucleus of the atom and the second is the electron spin dipole magnetic moment. The former can be considered as a current loop, resulting in an orbital dipole magnetic moment along the axis of the nucleus. The latter is a much stronger source of electronic magnetic moment.

The overall magnetic moment of the atom is the net sum of all of the magnetic moments of the individual electrons. However, magnetic dipoles will oppose each other in order to reduce the overall net energy. Therefore in an atom the opposing magnetic moments of some pairs of electrons will cancel each other out both in orbital motion and in spin magnetic moments. Compounds with completely filled electron shell or subshell, will normally completely cancel each other out, diamagnetism, while compounds with partially-filled electron shells have a magnetic moment, whose strength depends on the number of unpaired electrons, paramagnetism. These are the two simplest types of magnetism, however there are others such as antiferro-, ferro-magnetism and superparamagnetism, which will be dealt with in the next section, as well at taking a closer look at dia and paramagnetism.

1.8.3 Types of Magnetisation

Diamagnetism

In diamagnetism, **n**, (the number of unpaired electrons), equals zero. As there is an even number of electrons and an even number of opposite spins they cancel each other out and cause the element to have no magnetic field. Any fixed diamagnetic substance will repel a magnetic field.

Paramagnetism

Paramagnetic materials possess unpaired electrons which may be randomly orientated. When a magnetic field is applied to any such substance the field of the atom aligns with the field of the magnetic field and causes the atom to be slightly

attracted to that magnetic field. This intensity increases depending on the size of **n**, i.e. the number of unpaired electrons. Each electron in an atom possesses a spin magnetic moment which, in turn, possesses an orbital magnetic moment. The combined spin and orbital magnetic moments give rise to the overall magnetic moment of the atom. However, the atom will only show an overall resultant magnetic moment (i.e. display paramagnetic behaviour) if there are unpaired electrons present in its valence shell.

Ferromagnetism

A substance is ferromagnetic when its magnetic dipole moments have a tendency to adopt a parallel arrangement.[62] Ferromagnetism is caused by the parallel spinning of electrons in the atoms of the material, forming domains, or areas of stronger magnetism. In an unmagnetized ferromagnetic material, the domains are aligned at random so there is no overall magnetic effect. If a magnetic field is applied to that material, the domains align to point in the same direction, producing a strong overall magnetic effect. Their ability to retain their magnetism even after the field is removed is probably the most recognizable feature of ferromagnetic materials like magnetite. Permanent magnetism arises if the domains remain aligned after the external field is removed. Ferromagnetic materials, (such as magnetite), exhibit hysteresis*, (**Figure 1.13**).

***Hysteresis:** The most common way to represent the bulk magnetic properties of a ferromagnetic substance is to the magnetic induction **B** at various field strengths **H**. However plots of **M** vs **H** may also be used, (**Figure 1.7**), as $\mathbf{B} = \mu_0(\mathbf{H} + \mathbf{M})$. The loop is used to determine the suitability of ferromagnetic materials for various application. For example, electromagnets need to have low coercivity and remanence in order to reduce the magnetic field to zero as and when needed, whereas permanent magnets need these values to be high in order to retain as much magnetisation as possible.[63]

Anti-ferromagnetism

An antiferromagnetic material is defined as one in which the strongly coupled atomic dipoles favour an antiparallel arrangement.[62] Anti-ferromagnetism is associated with compounds such as manganese oxide (MnO). Adjacent ions behave as tiny magnets

(in this case manganese ions, Mn^{2+}) spontaneously aligning themselves at relatively low temperatures into opposite, or antiparallel, arrangements throughout the material. This causes the material to exhibit almost no gross external magnetism. In antiferromagnetic materials, which include certain metals and alloys as well as some ionic solids, the magnetic moment is cancelled out as the magnetically active atoms or ions align themselves in opposite, antiparallel, directions. These compounds are temperature dependent and at low temperatures exhibit no response to an external field. This is due to the antiparallel ordering of atomic magnets been rigidly maintained at this low energy. As the temperature is increased some atoms break free of this restricted arrangement and align themselves with the external field.

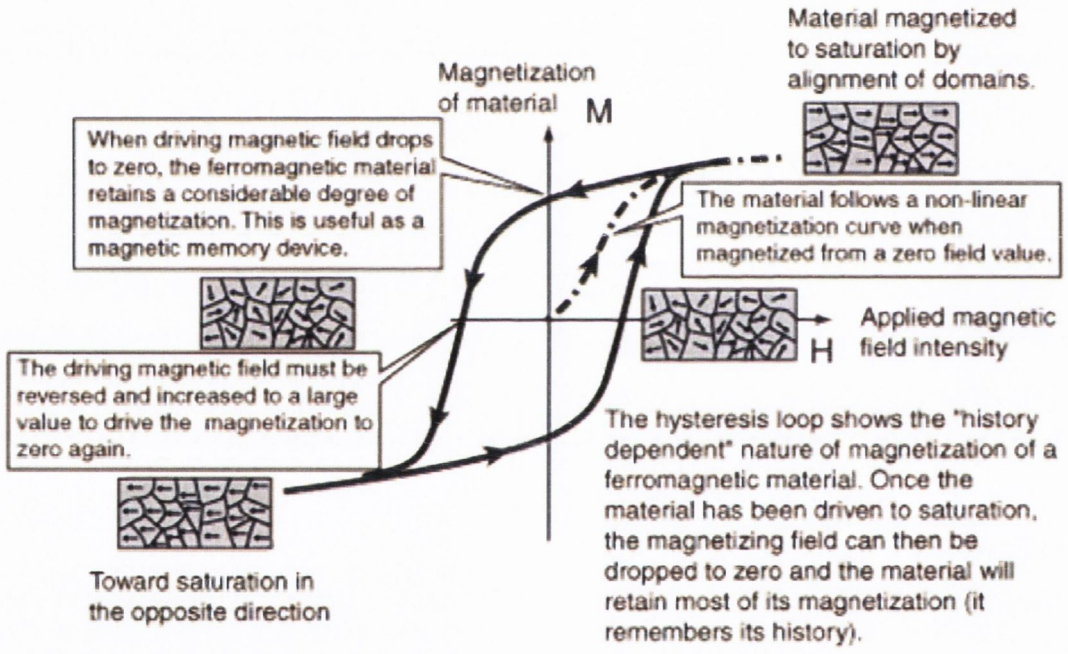

Figure 1.13: Hysteresis curve illustrating the relaxifity, (or lack there of), of a ferromagnetic substance. It is customary to plot the magnetization M of the sample as a function of the magnetic field strength H, since H is a measure of the externally applied field which drives the magnetization.[64]

Ferrimagnetism

A ferrimagnetic material is one in which the magnetic moment of the atoms on different sublattices are opposed, as in antiferromagnetism. However, in ferrimagnetic

materials the opposing moments are unequal and a spontaneous magnetisation occurs. This happens when the sublattices consist of different ions, such as Fe^{2+} and Fe^{3+}, as in magnetite. Ferrimagnetic materials are like ferromagnets in that they hold a spontaneous magnetisation below the Curie temperature, and show no magnetic order, i.e. are paramagnetic, above this temperature. Ferrimagnetism is exhibited by ferrites and magnetic garnets. Magnetite was originally classified as a ferromagnet before Néel's discovery of ferrimagnetism and antiferromagnetism.

1.9 Magnetic Nanoparticles

1.9.1 The Nano-size Effect

One of the most remarkable properties of nanosized magnetic particles is their ability to exhibit superparamagnetism. For example below a certain 'critical size', ~10 nm, magnetic iron oxide nanoparticles exist as a single magnetic domain as opposed to a multidomain in the bulk state.[65] Particles of this size are called superparamagnetic. In this case even though the temperature is below the Curie or Néel temperature and the thermal energy is not sufficient to overcome the coupling forces between neighbouring particles, the thermal energy is sufficient to change the direction of magnetization of the entire nanocrystallite. Superparamagnetic nanoparticles do not retain any residual magnetisation after removal of a magnetic field and for this reason do not agglomerate as much as paramagnetic particles. Ferrofluid, also know as a magnetic fluids, consist of colloidal magnetic nanoparticles (~10 nm) dispersed with the aid of a surfactant, stabilizer, in a continuous carrier phase i.e. water.[66] True ferrofluids are stable, meaning that the solid particles do not agglomerate and phase separate even in extremely strong magnetic fields. If a magnetic colloid does not fit these conditions, i.e. is 1-3 orders of magnitude bigger than 10 nm, agglomerates in the presence of a magnetic field, then it is no longer considered a ferrofuild and is now a magnetorheological fluid.[67] Magnetic fluids are widely used as contrast agents in magnetic resonance imaging (MRI) for medical diagnostics and in magnetic field assisted cancer therapy.[3, 68-70] Magnetic nanoparticles have been extensively studied

because of the increasing interest in applications as different as spintronics and drug delivery systems.[71-75] By producing these ferrofluids using chiral stabilizing ligands we hope to add another dimension to them by allowing them to target chiral centres within the body. However, as these particles are not UV, and therefore CD, active it is quite difficult to prove if particles stabilized with one enantiomer are different from the other. While early magnetic studies do seem to indicate some difference between D- and L- stabilized particles, there is no clear understanding and explanation for these phenomena. Thus this area will require more intensive and detailed studies to be performed in the near future.

1.10 Aims of this work

Chiral compounds are extremely important in chemistry, biology and medicine from molecular recognition to heterogenous catalysis. Chirality has also been envisaged to play an important role in nanotechnology. To date most of the research in this field was focused on chiral organic and metallorganic molecules and their supramolecular structures. However, the area of chiral inorganic nanoparticles is currently in the very early stage of its development. There are only a very limited number of publications on the preparation of chiral metal nanoparticles. These include mainly gold and silver nanoparticles prepared using chiral thiol containing stabilisers. However, surprisingly, similar chiral nano-systems based on quantum dots (QDs) have not yet been reported at all. Thus the main scope of this work is to combine chiral molecules and QDs in one species and produce chiral QDs. The aim of this project is develop novel chiral QDs, explore this area in details and establish fundamental principles influencing the structure and properties of chiral QDs. In this project we are going to produce and investigate new chiral CdS, CdSe and CdTe nanosystems.

Our initial task in this project is to develop and optimise synthesis of chiral QDs using various chiral thiol stabilizers and investigate their structure and optical properties. We plan to prepare a series of new CdS, CdSe and CdTe QDs using commercially

available enantiomeric thiols (penicillamine, cysteine) as capping agents. We also aim to establish a correlation between the ratios of chiral stabilizers and the photophysical properties of chiral QDs. This work will be particularly important for understanding of the fundamental properties of chiral QDs and development of their potential applications. The absorption, luminescence and CD properties of all QD materials prepared will be examined in details. In selected cases we will conduct a very thorough study using time-resolved methods.

Another objective will be to investigate the specific interactions between chiral QDs and selected enantiomeric biomolecules. We believe that chiral QDs have a lot of potential as fluorescent assays for biological and chemical analysis. Certainly, it would be too ambitious to try to investigate interactions of QDs with a large variety of chiral biomolecules. This sort of work would require enormous resources and would be very time consuming. Therefore, in this part of the project we would like to focus our work only on the interaction of chiral QDs with selected chiral amino acids, drugs and DNA samples. We anticipate that chiral QDs should give a characteristic luminescent response (e.g. quenching of the luminescence) while binding to chiral species due to the energy (or charge) transfer processes.

Finally we also aim to prepare chiral magnetic nanoparicles and "all in one "fluorescent-magnetic–chiral nanocomposites.

Chiral QDs and fluorescent-magnetic–chiral nanocomposites are expected to possess very exciting properties, which could lead to a multitude of applications in photonics and biotechnology.

References

[1] W. Ostwald, *Steinkopf, Dresden* **1915**.

[2] W. Horst, *Angewandte Chemie International Edition in English* **1993**, *32*, 41.

[3] J. Chen, A. Zheng, Y. Gao, C. He, G. Wu, Y. Chen, X. Kai, C. Zhu, *Spectrochimica Acta Part A: Molecular and Biomolecular Spectroscopy* **2008**, *69*, 1044.

[4] T. N. Sandeep Kumar, *Small* **2006**, *2*, 316.

[5] W. T. Sun, Y. Yu, H. Y. Pan, X. F. Gao, Q. Chen, L. M. Peng, *J. Am. Chem. Soc.* **2008**, *130*, 1124.

[6] Y. Liu, T. Tan, B. Wang, R. Zhai, X. Song, E. Li, H. Wang, H. Yan, *Journal of Colloid and Interface Science* **2008**, *320*, 540.

[7] P. Dagtepe, V. Chikan, *J. Phys. Chem. A* **2008**, *112*, 9304.

[8] H. Yao, T. Fukui, K. Kimura, *J. Phys. Chem. C* **2007**, *111*, 14968.

[9] C. Gautier, T. Burgi, *J. Am. Chem. Soc.* **2006**, *128*, 11079.

[10] N. Nishida, H. Yao, T. Ueda, A. Sasaki, K. Kimura, *Chem. Mater.* **2007**, *19*, 2831.

[11] T. Shimada, K. Ookubo, N. Komuro, T. Shimizu, N. Uehara, *Langmuir* **2007**, *23*, 11225.

[12] S. Chen, P. J. Ferreira, W. Sheng, N. Yabuuchi, L. F. Allard, Y. Shao-Horn, *J. Am. Chem. Soc.* **2008**, *130*, 13818.

[13] L. Qiu, F. Liu, L. Zhao, W. Yang, J. Yao, *Langmuir* **2006**, *22*, 4480.

[14] S. Y. Zhao, S. H. Chen, S. Y. Wang, D. G. Li, H. Y. Ma, *Langmuir* **2002**, *18*, 3315.

[15] S. D. Elliott, M. Moloney, x, chea, x, P. l, Gun, x, Y. K. ko, *Nano Lett.* **2008**, *8*, 2452.

[16] E. Hao, H. Sun, Z. Zhou, J. Liu, B. Yang, J. Shen, *Chem. Mater.* **1999**, *11*, 3096.

[17] N. Ma, J. Yang, K. M. Stewart, S. O. Kelley, *Langmuir* **2007**, *23*, 12783.

[18] H. Qian, C. Dong, J. Peng, X. Qiu, Y. Xu, J. Ren, *J. Phys. Chem. C* **2007**, *111*, 16852.

[19] P. Reiss, J. Bleuse, A. Pron, *Nano Lett.* **2002**, *2*, 781.

[20] P. Xue, R. Lu, Y. Huang, M. Jin, C. Tan, C. Bao, Z. Wang, Y. Zhao, *Langmuir* **2004**, *20*, 6470.

[21] B. I. Lemon, R. M. Crooks, *J. Am. Chem. Soc.* **2000**, *122*, 12886.

[22] H. Seo, S. W. Kim, *Chem. Mater.* **2007**, *19*, 2715.

[23] H. Kim, M. Achermann, L. P. Balet, J. A. Hollingsworth, V. I. Klimov, *J. Am. Chem. Soc.* **2005**, *127*, 544.

[24] J. M. Tsay, M. Pflughoefft, L. A. Bentolila, S. Weiss, *J. Am. Chem. Soc.* **2004**, *126*, 1926.

[25] M. V. Kovalenko, E. Kaufmann, D. Pachinger, J. Roither, M. Huber, J. Stangl, G. Hesser, F. Schaffler, W. Heiss, *J. Am. Chem. Soc.* **2006**, *128*, 3516.

[26] M. O. M. Piepenbrock, T. Stirner, S. M. Kelly, M. O'Neill, *J. Am. Chem. Soc.* **2006**, *128*, 7087.

[27] B. Tang, F. Yang, Y. Lin, L. Zhuo, J. Ge, L. Cao, *Chem. Mater.* **2007**, *19*, 1212.

[28] M. Kuno, K. A. Higginson, S. B. Qadri, M. Yousuf, S. H. Lee, B. L. Davis, H. Mattoussi, *J. Phys. Chem. B* **2003**, *107*, 5758.

[29] W. W. Yu, J. C. Falkner, B. S. Shih, V. L. Colvin, *Chem. Mater.* **2004**, *16*, 3318.

[30] J. M. Pietryga, R. D. Schaller, D. Werder, M. H. Stewart, V. I. Klimov, J. A. Hollingsworth, *J. Am. Chem. Soc.* **2004**, *126*, 11752.
[31] C. M. Evans, L. Guo, J. J. Peterson, S. Maccagnano-Zacher, T. D. Krauss, *Nano Lett.* **2008**, *8*, 2896.
[32] K. A. Abel, J. Shan, J.-C. Boyer, F. Harris, F. C. J. M. van Veggel, *Chem. Mater.* **2008**, *20*, 3794.
[33] J. E. Murphy, M. C. Beard, A. G. Norman, S. P. Ahrenkiel, J. C. Johnson, P. Yu, O. I. Micic, R. J. Ellingson, A. J. Nozik, *J. Am. Chem. Soc.* **2006**, *128*, 3241.
[34] Semiconductor Fundamentals, B. V. Zeghbroeck, **2007**. http://ece-www.colorado.edu/~art/book/
[35] T. Ni, D. K. Nagesha, J. Robles, N. F. Materer, S. Mussig, N. A. Kotov, *J. Am. Chem. Soc.* **2002**, *124*, 3980.
[36] X. Chen, J. L. Hutchison, P. J. Dobson, G. Wakefield, *Journal of Colloid and Interface Science* **2008**, *319*, 140.
[37] C. A. Constantine, K. M. Gattas-Asfura, S. V. Mello, G. Crespo, V. Rastogi, T. C. Cheng, J. J. DeFrank, R. M. Leblanc, *J. Phys. Chem. B* **2003**, *107*, 13762.
[38] N. Gaponik, D. V. Talapin, A. L. Rogach, K. Hoppe, E. V. Shevchenko, A. Kornowski, A. Eychmuller, H. Weller, *J. Phys. Chem. B* **2002**, *106*, 7177.
[39] B. Huang, D. A. Tomalia, *Inorganica Chimica Acta* **2006**, *359*, 1961.
[40] Y. C. Kuo, Q. Wang, C. Ruengruglikit, H. Yu, Q. Huang, *J. Phys. Chem. C* **2008**, *112*, 4818.
[41] J. Mao, J.-N. Yao, L.-N. Wang, W.-S. Liu, *Journal of Colloid and Interface Science* **2008**, *319*, 353.
[42] R. Sarkar, S. S. Narayanan, L. O. Palsson, F. Dias, A. Monkman, S. K. Pal, *J. Phys. Chem. B* **2007**, *111*, 12294.
[43] S. F. Wuister, A. Meijerink, *Journal of Luminescence* **2003**, *102-103*, 338.
[44] W. Wang, S. Banerjee, S. Jia, M. L. Steigerwald, I. P. Herman, *Chem. Mater.* **2007**, *19*, 2573.
[45] W. Lin, K. Fritz, G. Guerin, G. R. Bardajee, S. Hinds, V. Sukhovatkin, E. H. Sargent, G. D. Scholes, M. A. Winnik, *Langmuir* **2008**, *24*, 8215.
[46] C. T. Yuan, W. C. Chou, Y. N. Chen, J. W. Chou, D. S. Chuu, C. A. J. Lin, J. K. Li, W. H. Chang, J. L. Shen, *J. Phys. Chem. C* **2007**, *111*, 15166.
[47] D. V. Talapin, A. L. Rogach, E. V. Shevchenko, A. Kornowski, M. Haase, H. Weller, *J. Am. Chem. Soc.* **2002**, *124*, 5782.
[48] S. J. Byrne, S. A. Corr, T. Y. Rakovich, Y. K. Gun'ko, Y. P. Rakovich, J. F. Donegan, S. Mitchell, Y. Volkov, *Journal of Materials Chemistry* **2006**, *16*, 2896.
[49] Z. Tang, N. A. Kotov, M. Giersig, *Science* **2002**, *297*, 237.
[50] Z.-X. Cai, H. Yang, Y. Zhang, X.-P. Yan, *Analytica Chimica Acta* **2006**, *559*, 234.
[51] Y. Wu, L. Wang, M. Xiao, X. Huang, *Journal of Non-Crystalline Solids* **2008**, *354*, 2993.
[52] Optics and Photonics: An Introduction, Wiley, F. G. Smith, T. A. King, D. Wilkins, **2007**.
[53] V. Kitaev, *J. Mater. Chem.* **2008**, *18*, 4745
[54] J. T. Petty, J. Zheng, N. V. Hud, R. M. Dickson, *J. Am. Chem. Soc.* **2004**, *126*, 5207.
[55] G. Shemer, O. Krichevski, G. Markovich, T. Molotsky, I. Lubitz, A. B. Kotlyar, *J. Am. Chem. Soc.* **2006**, *128*, 11006.

[56] N. Nishida, H. Yao, K. Kimura, *Langmuir* **2008**, *24*, 2759.
[57] H. Qi, T. Hegmann, *J. Am. Chem. Soc.* **2008**, *130*, 14201.
[58] G. Dukovic, M. Balaz, P. Doak, N. D. Berova, M. Zheng, R. S. McLean, L. E. Brus, *J. Am. Chem. Soc.* **2006**, *128*, 9004.
[59] X. Peng, N. Komatsu, S. Bhattacharya, T. Shimawaki, S. Aonuma, T. Kimura, A. Osuka, *Nat Nano* **2007**, *2*, 361.
[60] C. Gautier, Bu, x, T. rgi, *J. Am. Chem. Soc.* **2008**, *130*, 7077.
[61] V. H. C. M. www.phys.psu.edu/images/research/descriptions/428.gif.
[62] The Physical Principles of Magnetism, Oxford University Press, A. H. Morrish, **1965**.
[63] Introduction to Magnetism and Magnetic Materials, Springer; 1st Edition, D. Jiles, **1991**.
[64] http://hyperphysics.phy-astr.gsu.edu/Hbase/solids/hyst.html.
[65] J. Roger, J.N. Pons, R. Massart, A. Halbreich, J. C. Bacri, *Eur. Phys. J. Appl. Phys* **1999**, *5*, 321.
[66] H. E. Horng, C.-Y. Hong, S. Y. Yang, H. C. Yang, *Journal of Physics and Chemistry of Solids* **2001**, *62*, 1749.
[67] Ferrohydrodynamics, Dover Publications, R. Rosensweig, **1985**
[68] M. Krack, H. Hohenberg, A. Kornowski, P. Lindner, H. Weller, Fo, x, S. rster, *J. Am. Chem. Soc.* **2008**, *130*, 7315.
[69] T. Neuberger, B. Schöpf, H. Hofmann, M. Hofmann, B. von Rechenberg, *Journal of Magnetism and Magnetic Materials* **2005**, *293*, 483.
[70] S. Pathak, M. C. Davidson, G. A. Silva, *Nano Lett.* **2007**, *7*, 1839.
[71] C. Bergemann, D. Müller-Schulte, J. Oster, L. à Brassard, A. S. Lübbe, *Journal of Magnetism and Magnetic Materials* **1999**, *194*, 45.
[72] B. Gleich, J. Weizenecker, *Nature* **2005**, *435*, 1214.
[73] S. Wageh, L. Shu-Man, F. T. You, X. Xu-Rong, *Journal of Luminescence* **2003**, *102-103*, 768.
[74] P. P. C. Sartoratto, A. V. S. Neto, E. C. D. Lima, A. L. C. R. d. Sa, P. C. Morais, *Vol. 97*, Journal of Applied Physics, **2005**, p. 10Q917.
[75] S. A. Wolf, D. D. Awschalom, R. A. Buhrman, J. M. Daughton, S. von Molnar, M. L. Roukes, A. Y. Chtchelkanova, D. M. Treger, *Science* **2001**, *294*, 1488.

Chapter 2. Experimental

2.1 Starting Materials

$Cd(ClO_4)_2.xH_2O$ and thioacetamide, CH_3CSNH_2, 99%+, Na_2TeO_3, 99%, and $NaBH_4$, 99.99%. coumarin 153 and rhodamine B were supplied by Aldrich. The various stabilizers D-Cysteine ≥ 99% and L-cystein ≥ 99.5% were purchased for Fluka while D-Penicillamine, 97-102% [sic] and L- penicillamine, 99% from Aldrich. Na_2SeSO_3 was prepared using Na_2SO_3, 98%, and elemental Se, 99%, which were supplied by Aldrich and Riedel-de Haën respectively. Ferric chloride hexahydrate ($FeCl_3 \cdot 6H_2O$) and ammonium hydroxide (NH_4OH, 0.88M) were obtained from BDH Chemicals, while Ferrous chloride tetrahydrate ($FeCl_2 \cdot 4H_2O$) was obtained from Aldrich. Millipore water was deoxygenated by boiling for 30 minutes and then cooling it to room temperature under argon.

2.2 Spectroscopic and Miscellaneous Equipment

2.2.1 UV-Vis Absorption spectra

UV-Vis absorption spectra were recorded at room temperature using a SHIMADZU UV2101 PC UV-Vis scanning spectrometer. The samples were examined in a 1 cm quartz cell. The solvent used was water. Particle absorption is a function of the Beer Lambert law.

$$A = \varepsilon.c.l$$

Where c is the concentration of the sample, l the path length of the cell and ε the extinction coefficient of the species for a wavelength λ and in a solvent S.

2.2.2 PL spectroscopy

Emission spectra were recorded using a Perkin Elmer LS 50B. Fluorescence was detected at right angles to excitation. All samples were measured in a 1cm quartz fluorescent cell with excitation and emission monochromators, slits, set to 5nm unless otherwise stated. All samples were excited 20 nm below initiation point unless otherwise stated.

2.2.3 Circular Dichroism measurement

CD activity measurements were made on a JASCO J-810 CD/UV spectrometer. As with UV-Vis and PL measurements the samples were examined in a 1 cm quartz cell.

2.2.4 Infra-Red spectroscopy

Infra-red spectra were recorded in the region between 4000 cm^{-1} to 400 cm^{-1} on a Mattson Genesis II FTIR spectrometer. Samples (solid) were dispersed in KBr and recorded as clear pressed discs.

2.2.5 Raman spectroscopy

Raman spectra were measured by Mr Joseph McCarthy, (Chemistry), with a Renishaw 1000 micro-Raman system. The excitation wavelength was 514.5 nm from an Ar^{+} ion laser (Laser Physics Reliant 150 Select Multi-Line) with a typical laser power of 3 mW in order to avoid excessive heating. The 100 × magnifying objective of the Leica microscope was capable of focusing the beam into a spot of approximately 1 μm diameter.

2.2.6 Dynamic Light Scattering

A Malvern Zetasizer was used to elucidate the size of the nanoparticles and aggregates in solution. It employs a light source which emits at 633 nm. The angle of reflection is then used to calculate individual particle sizes.

2.2.7 Emission Lifetime Decay Measurements

Luminescent Exponential decay measurements were performed using a Horiba NanoLED Fluorohub S.P.C.C.

2.2.8 Microwave

The microwave used in these experiments was a conventional domestic microwave, a Samsung TDS Grill. All reactions were heated at 850W for 1min 10sec.

2.2.9 Transmission electron microscopy

All low resolution transmission electron microscopy (TEM) images were taken with the help of Mr Neal Leddy, Centre for Microscopy and Analysis-TCD using a Jeol 2100 TEM. The TEM was operated at a beam voltage of 100 kV. Samples for TEM were prepared by deposition and drying of a drop of the powder dispersed in millipore water onto a formvar coated 400 mesh copper grid. CdTe high resolution images were preformed using STEM and HRTEM and were taken with help of Dr Peter Nelist and Dr. John Hutchisonon, Department of Materials, University of Oxford, using a VG HB 501 STEM and a JEM 4000EX respectively. CdSe AFM and dark field images were taken using a Philips XL30 Scanning Electron Microscope with the help of Dr Kai Sun, University of Michigan.

2.2.10 Magnetisation measurements

Magnetisation measurements were carried out by Dr. Munuswamy Venkatesan (School of Physics, TCD) using a SQUID (Superconducting Quantum Interference Device) magnetometer, which is available in Prof. M. Coey's laboratory in the School of Physics.

2.3 Experimental details for Chapter 3

Preparation of CdS nanoparticles

2ml of a basic aqueous 1 x 10^{-2}M solution of Stabilizer, (2 x 10^{-5} moles of *D*-, *L*- or *Rac*), was added to 45 ml of millipore water in a 100 ml round bottomed flask. The pH was adjusted to 11 by the dropwise addition of 1M NaOH. 4ml of a 1 x 10^{-2} M $Cd(ClO_4)_2.xH_2O$ and 2ml of an 1 x 10^{-2}M of CH_3CSNH_2 were then added and the solution was stirred vigorously. The resulting homogeneous solution was then transferred to a conventional microwave and irradiated for 70 seconds at 850W. The resulting clear, colourless, solution was stored in the dark for at least one day. The volume of the colloid was then reduced to ~5ml using the rotary evaporator and propan-2-ol was added to precipitate out the nanoparticles. The particles were collected by centrifugation. The particles were washed several times with a propan-2-ol, water mixture, (9:1), and finally re-dispersed in millipore water. UV-Vis, CD and fluorescence spectroscopy was carried out on the stable suspensions in water.

Computer modelling of CdS-Pen chiral clusters

Density functional calculations were performed by Dr. Simon D. Elliott (Tyndall National Institute, Cork)

2. 4. Experimental details for Chapter 4

2.4.1 Preparation of Na_2SeSO_3

This water soluble selenium salt was prepared by dissolving 0.0947g of Na_2SO_3 in 50ml of degassed millipore water. Once dissolved 0.0315g of Se was then added. The apparatus was set up for reflux and put under a constant flow of argon. The mixture was stirred vigorously to ensure the insoluble Se did not simply stick to the sides of the round bottom flask. The mixture was heated under refluxed at 110 ^{0}C overnight. The resulting clear colourless solution was used immediately.

2.4.1 Preparation of CdSe nanoparticles

CdSe particles were prepared as above however the thioactemide was replaced with Na_2SeSO_3 and all reactions were carried out in degassed millipore water. The water was degassed by first heating to boiling point and then cooling to room temperature while bubbling with argon from twenty minutes. The resulting clear, yellow, solution was stored in the dark for at least one day. The volume of the colloid was then reduced to ~5 ml using the rotary evaporator and propan-2-ol was added to precipitate out the nanoparticles. The particles were collected by centrifugation. The particles were washed several times with a propan-2-ol- water mixture, (9:1), and finally re-dispersed in millipore water. UV-Vis, CD and fluorescence spectroscopy was carried out on the stable suspensions in water.

2.5. Experimental details for Chapter 5

2.5.1 Preparation of CdTe nanoparticles

CdTe particles were prepared as above however the Na_2SeSO_3 was replaced with Na_2TeO_3. Degassed water was not used however 2ml of 1 10^{-1}M $NaBH_4$ was added before the solution was microwaved. The resulting clear, orange/red, solution was stored in the dark for at least one day. The volume of the colloid was then reduced to ~5ml using the rotary evaporator and propan-2-ol was added to precipitate out the nanoparticles. The particles were collected by centrifugation. The particles were washed several times with a propan-2-ol, water mixture, (9:1), and finally re-dispersed in millipore water. UV-Vis, CD and fluorescence spectroscopy was carried out on the stable suspensions in water.

2.5.2. Preparation of CdS/CdTe core-shell structures

Heating under reflux

40 ml of CdTe core particles were degassed and heated to 40^{O}C under constant stirring. To this colloid was then added, dropwise and concurrently, 4ml of 1 x 10^{-2}M Cd^{2+} solution and 2ml of 1 x 10^{-2}M $Na_2S.9H_2O$ solution. The particles were heated for a further 30 minutes and then examined.

Microwave heating

The above experiment was repeated however the core particles were not heated. The Cd^{2+} and S^{2-} addition were made at room temperature and thioacetamide served as the S^{2-} source. Once the additions were complete the particles were heated in the microwave for 70 seconds at 850 Watts

Ultrasonic treatment

The above experiment was repeated however once the Cd^{2+} and S^{2-} addition were made the particles were then placed in a sonic bath at room temperature and sonicated for an hour. Again the core/shell particles were examined using UV-Vis and PL spectroscopy.

2.5.3 Photoannealing experiments

A 500 Watt Hg lamp was used in the photo-annealing experiment. All annealing took place in a 1cm quartz fluorescent cell and under N_2. A water filled cell was used to filter out any infra-red radiation. 4ml of the Cys-CdTe colloid was placed in a lidded quartz cuvette and bubbled with argon for 10 minutes. The colloid was then exposed to the light for a set period of time and then examined on UV-Vis or PL spectroscopy. The cuvette was then replaced in front of the lamp and the experiment was continued as necessary.

2.5.4 Preparation of CdTe nanowires

As prepared CdTe particles were reduced in volume to around 1ml using a rotary evaporator. 0.5 ml additions of propan-2-ol and methanol were then made until the colloid turned cloudy. The colloid was then centrifuged at 3000 rpms. Once the pellet was isolated it was then redispersed in a 50:50 mixture of a NaOH solution, (p.H = 9), and DMSO. This was then placed in a laboratory oven for up to three hours at $80^{O}C$. µl samples were taken every hour and made up to their original, (prewashing), volume with p.H 9 $NaOH_{(aq)}$ and then examined on UV-Vis, Pl and CD spectroscopy.

2.6. Experimental details for Chapter 6

2.6.1 Preparation of maghemite nanoparticles

100ml of millipore water was first placed in a 250ml round bottomed flask heated to boiling point and then cooled under a constant flow of argon. Simultaneously 5.55 x 10^{-4} moles; 0.153g, of $FeCl_3.6H_2O$ was dissolved in a sample tube containing 5ml of millipore water and 0.056g; 2.77 x 10^{-4} moles of $FeCl_2.4H_2O$ was also dissolved in a separate sample tube containing 5ml of millipore water. To these Fe solutions was then added 0.041g and 0.0136g of penicillamine respectively. These coloured solutions, (Fe^{3+} dark blue; Fe^{2+} lilac), were then combined and added to the 100 ml of degassed millipore water. The resulting solution was continually bubbled with argon for another 1min. 6ml of NH_4OH, (0.88M), solution was then rapidly injected into the iron solution and the flask was capped. The flask was physically agitated over night, turning dark green upon addition of ammonia but turning dark black after 30 seconds or so. The mixture was left shaking overnight. The following day the particles were magnetically separated using 0.5 T magnet and washed several times with millipore water.

2.6.2. Preparation of CdS - maghemite nanocomposites

Core/Shell

2ml of D-Pen maghemite solution, (1.5 x 10^{-3}M), was diluted into 40 ml of millipore water. Under constant stirring was then added, 4 ml of $Cd(ClO_4)_2.xH_2O$, 2ml of Penicillamine and 2 ml of CH_3CSNH_2. All there solution had a molar concentration of 1x 10^{-2} M. The p.h was adjusted to 11 and the resulting solution was microwaved at 850W for 70secs. The flasks containing the resulting solutions were wrapped in tinfoil shaken overnight

Addition of CdS QDs

2ml of maghemite nanoparticle solution was added to 40 ml of as prepared Pen-CdS nanoparticles. The flasks were wrapped in tinfoil and shaken overnight. The product was isolated by magnetic separation and washed several times with water.

2.7. Experimental details for Chapter 7

Preparation of penicillamine functionalised TiO_2 nanoparticles

0.058g of Ti-penicillamine-ethoxide precursor (supplied by Prof. V. Kessler, SLU Uppsala, Sweden) was dissolved in 50 ml of propan-2-ol and heated to reflux under stirring after been bubbled with Ar for thirty minutes. Once at $110^{O}C$ a few drops of ethyldiamine were added follow by 1 ml of freshly prepared 2M NaOH solution. A white precipitate was immediately observed and the solution was refluxed for an hour before being allowed to cool. The solution was centrifuged and the pellet was redispersed in iso-propanol. Both the pellet and supernatant were examined on UV-Vis and CD spectroscopy.

Chapter 3.

Preparation and characterisation of chiral CdS nanoparticles

3.1 Introduction

Due to quantum confinement effects resulting from their nanometer size, fluorescent semiconductor nanocrystals or quantum dots (QDs) have remarkable optical, physical and chemical properties, which differ markedly from the bulk material.[1-5] The ability to tune their optical properties, combined with the ease of surface modification has led to QD's proposed application in *inter alia* light emitting devices, fluorescent sensors and bioassays. [1, 3, 4, 6-9]

As mentioned in the introduction; luminescent semiconducting nanoparticles can be prepared from a variety of materials, which include CdSe, CdTe, ZnS, and PbS and of course CdS.[10-25] Their optical properties are directly related to the particle size, shape and most importantly the condition of the individual particles surface(s). As illustrated in the example of CdTe, Section 1.3, a decrease in particle size is accompanied by a shift in the absorption and emission spectra to shorter wavelengths.[26] Emissions which are near the longest wavelength absorption of the particle are referred to as intrinsic or band edge luminescence. The origin of the intrinsic emission is due to hole/pair radiative recombination from shallow trap states rather than from the band edge.[12] The luminescence which appears at a longer wavelength is due to the recombination of charge carriers via surface traps and is referred to as defect emission. It should be noted that defect emission is one of the very important characteristics of CdS based nanomaterials.[27-33] The coating of these particle's surfaces with a modifier, which usually takes place during particle formation, not only prevents Ostwald ripening from occurring but also decreases the rate of non-radiative decay and normally increases the quantum yield.[26] In addition coating of inorganic CdS nanocrystals with biocompatible ligands not only improves their quantum yields but also increases their hydrophilicity and reduces their toxicity, two important factors

if they are to be used in any biological applications. There are literature reports, which show that CdS as well as other Cd containing quantum dots may be used as probes or sensors.[1, 3, 4, 6-9]

While a lot of work has been carried out using various organic molecules as quantum dot stabilizers, (including the sulphur containing thio-organic acids, alcohols and of course amino acids),[34-39] there has been very little reports on procedural optimisation of QD synthesis.[2, 40] With a few exceptions little has been done in the way of statistical analysis to determine what effects, (if any), the concentrations of the various reactants has on the properties of a family of substances where factors such as size, shape, and surface conditions, are crucial in determining the particles optoelectronic properties.

Chirality is one of the most important factors of molecular recognition and therefore development of chiral luminescent nanosized probes would provide very useful tools for both chemistry and biology. Although there have been some recent publications on the preparation of chiral gold[41, 42] and silver[43, 44] nanoparticles, similar systems based on QDs have not yet been reported.

The main aim of this part of the work is to combine chiral molecules and CdS QDs in one species and produce chiral QDs. We plan to use various chiral stabilisers (for example D- or L- penicillamine) to prepare CdS, CdSe and CdTe based quantum dots and then study their photophysical properties using various instrumental techniques. We also plan to investigate the effects of both D- and L- enantiomers as well as the racemate on the photochemical and photophysical properties and the surface chemistry of these particles.

3.2 General synthetic approach to the preparation of CdS QDs

The dots were prepared using a slightly modified method of that reported by Ni et al.[3] However in this case chiral amino acids stabilizers were substituted for tri-sodium citrate.[3, 36] Also while the stock solution concentrations recommended by Ni et al. were used, a 2^2 statistical study which will be explained in the following section, was then employed for first the penicillamine and then the cystein preparations using quantum yield as the main response.[45]

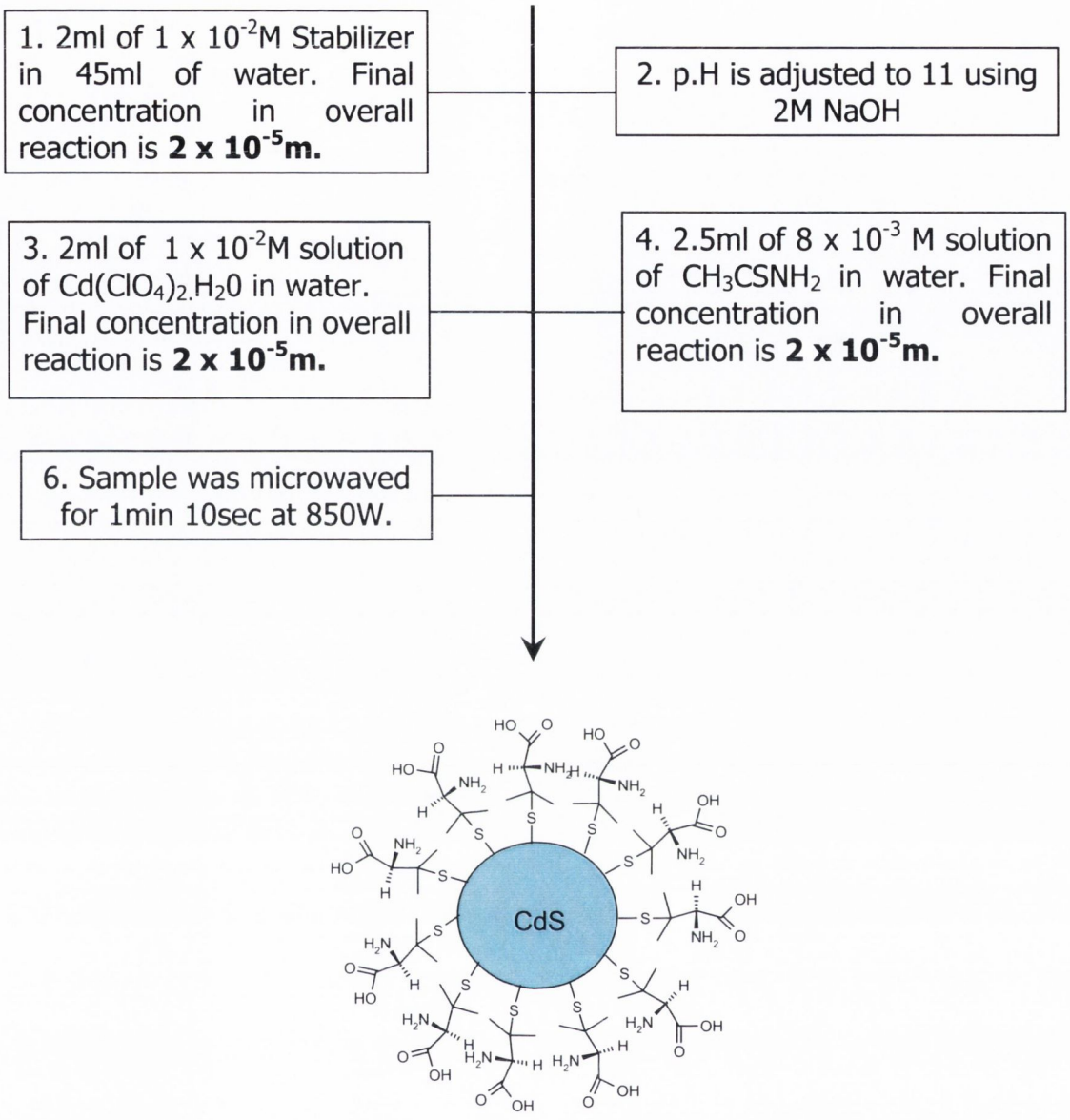

Figure 3.1: Schematic representation of CdS preparation. The example used is the first point in a 2^2 study of CdS. Both Cd and stabilizer concentrations are systematically increased while S concentration stays fixed at 2 x 10^{-5} moles.

The CdS nanocrystals were prepared in water using aqueous solutions of $Cd(ClO_4)_2.6H_2O$ and CH_3CSNH_2. Briefly, as shown in **Figure 3.1**, an aqueous stabilizer solution was first prepared and its pH was adjusted to 11 using NaOH. Both the cadmium perchlorate and thioacetamide solutions were then added. This precursor solution was then place in a microwave and heated for 1min 10 seconds at 850W. The freshly prepared particles were then placed in the dark and allowed to mature for at least 24hrs. This method of reaction initiation ensures that the thioacetamide decomposes in such a way as to release sulphide ions into solution as quickly and

uniformly as possible, therefore allowing for the instantaneous formation of numerous nucleation centres. These numerous nucleation centres should result in nanocrystals of the uniform size.

3.3 2^2 Statistical Analysis for the preparation of Penicillamine capped CdS

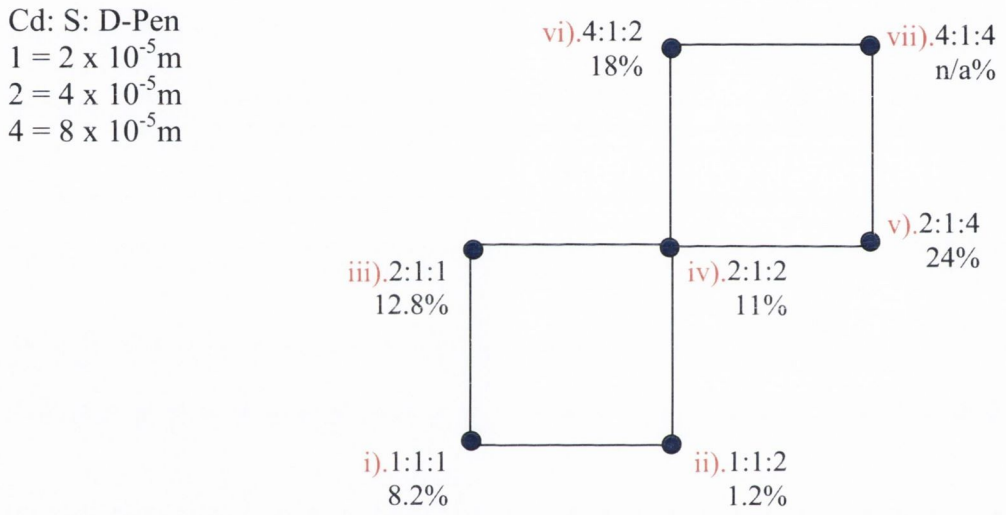

Figure 3.2: 2^2 statistical analysis of D-Pen-CdS. Quantum yields for each point were measured against Coumarin 153 in MeOH.

Keeping the sulfide concentration fixed at point i). of the study, that is at 2ml of a 1 x 10^{-2} M stock solution- (2 x 10^{-5}m). The Pen-CdS system was re-examined using a 2^2 model. The points investigated were at 4 increasing and intersecting levels, **Figure 3.2**. These axis's or levels correspond to the volume of the 1 x 10^{-2}M stock solution used, starting with 2 ml of all three reactants and then doubling the volumes of Cd, along the y axis, and Pen, along the x axis, however the X^{2-} component, in this case S, remained constant at 2ml, (**Figure 3.2**).

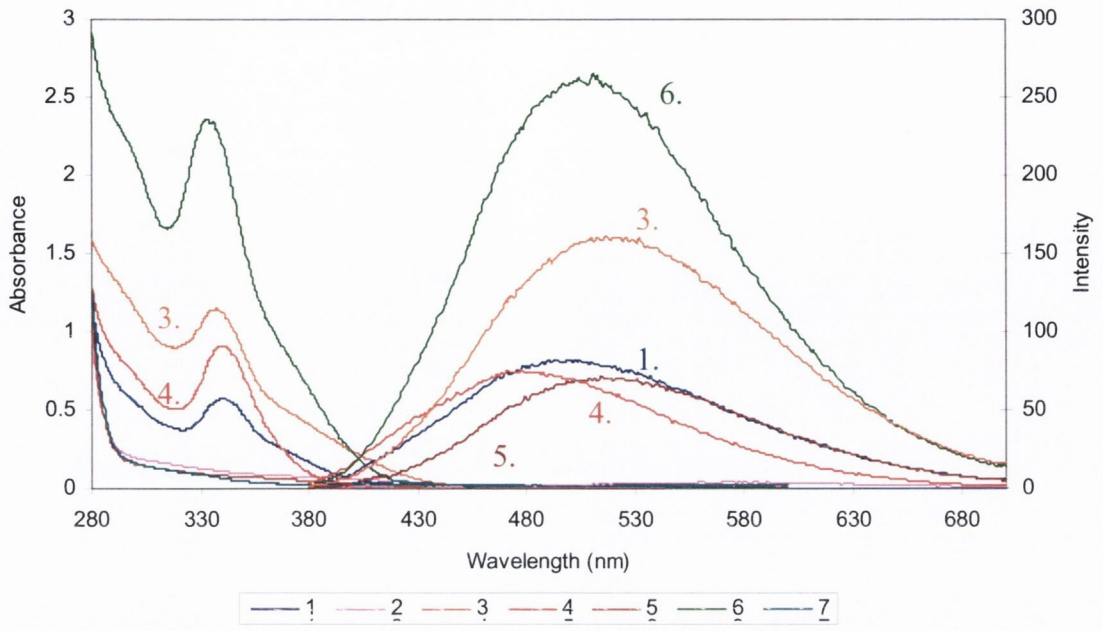

Figure 3.3: Absorption and emission spectra showing points 1-7 of a 2^2 statistical analysis of D-Pen-stabilised CdS QDs. The excitation wavelength in all emission spectra was 360nm.

Although quantum yield was the primary response studied during over the course of this analysis all particles produced were also examined using UV-Vis, PL and CD spectroscopy. Quantum yields were measured against a solution of Coumarin 153 in methanol. **Figure 3.3** shows both absorption and emission spectra for batches 1-7. Batches 2, 5 and 7 demonstrated very poor absorbance and emission properties. Meanwhile batches 1, 3, 4 and 6 demonstrated much better optical properties. In cases where cadmium is in excess (batches 3 and 6), strong distinct band edges are formed, and the luminescence is quite strong and further shifted to the red than others in the batch indicating that these are the larger particles. As the overall concentration of metal and stabilizer are increased relative to the sulfide concentration an increase in both particle concentration and quantum yield occurs. This is more than likely a result of the excess Cd been used to remove hole traps on the surface. Particles which posses an equal ratio of Cd to stabilizer, (1 and 4 but not 7), behaved quite similar to those mentioned above, although their quantum yields were slightly lower. Batch 4 does not posses the initial gradient before reaching the peak and because of this its emission maxima is slightly blue shifted. As the batch 6 demonstrated the highest emission as well as the strongest absorption it was identified as the best in these studies.

Batches where the penicillamine concentration was higher than that of the Cd resulted low concentrations of particles been formed. This is evident from the lack of strong absorbance around the 340nm mark. This low particle concentration is due to the strong chelation effect of penicillamine on the Cd ions present in solution. Once removed there is no longer a driving force to cause the hydrolysis of thioactemide which would otherwise push the particle formation reaction to the right. Using Origin it is possible to present the above quantum yield data as a function of Cd and penicillamine concentrations in the form of 3-D diagram (Figure 3.4).

Table 3.1: Absorption, circular dichroism, emission and excitation, quantum yield for 2^2 statistical analysis of D-Pen CdS.

D-CdS	Abs	CD	Ems	Ext	Q.Y
1	342nm;0.56	386nm;3.2 364nm;-0.9 334nm;10.3	497nm	367nm	8.2%
2	405nm;0.06	n/a	574nm	398nm	1.2%
3	339nm;1.1	377nm;2.7 358nm;2.4 338nm;15	521nm	380nm	12.8%
4	342nm;0.9	376nm;06 358nm;04 340nm;14	477nm	371nm	11%
5	379nm;0.2	384nm;2.2	519nm	348nm	24%
6	335nm;2.3	348nm;3.2 319nm;-5.5 290nm;1.45	509nm	382nm	18%
7	328nm;0.09				

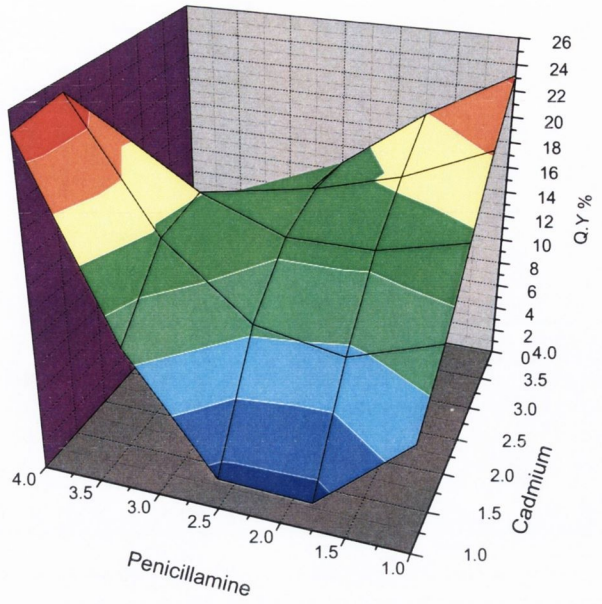

Figure 3.4: 3-D representation of a 2^2 statistical analysis of the formation of D-Pen CdS using quantum yield as the response. Note how the yields peak at points where both metal and stabilizer are opposite to each other. An Origin 7.5 random xyz matrix was used to generate the graph.

Examination of **Figure 3.4,** where the z axis is quantum yield, shows that the particles with the highest luminescence are formed at the two opposite points of the study. That is where the Cd concentration is at its highest and penicillamine is at its lowest and vice versa. However this is a purely mathematical model and does not take into account the chemical constraints. For example, if the penicillamine concentration is too high then the particle formation reaction will not proceed. However, if the Pen concentration is too low then the particles will not be adequately stabilized and will therefore undergo Oswalt ripening. This will eventually either cause the particles to return to the bulk or precipitating from the solution entirely.

By using the statistical study to examine the particles it is possible to see how altering the reactant ratios and concentrations really affect them. For example the Stokes shift between the excitation peak and emission peaks change dramatically depending on the ratio of Cd to Pen, **Table 3.1**. That is to say batches with the same ratio of metal to stabilizer have very similar, though not identical shifts, e.g. 1&3 130 nm and 106 nm, 2&5 176 nm and 171 nm, and 3&6 141 nm and 127 nm. These numbers are quite unusual in that the batch with the highest relative concentration of penicillamine in batches 2&5 are the ones with the largest Stokes shift, this is unusual

as this means that they have the most defective surfaces even though they should be more passivated than the others.

Also close examination of the CD response, **Table 3.1**, shows that there is clearly some link between the quantum yield of the particles and the optical activity. Batch 5, despite having little or no absorbance at the band edge region, still has one of the highest CD response at this region. However, batch number 5 has the highest quantum yield of all particles produced in this study. This premise will be the central theme of this thesis and it is from this point that this work will continue to draw links between both the type and strength of individual particle types luminescence and their optical activity, or lack of it. If the rest of the particles in the study are examined no obvious link is seen between quantum yield and their optical activity. However, if the second and not the first band in the CD spectra are examined a clear relationship is seen between the QY and the second CD peak. As the QY increases so to does the strength of the second CD signal, **Table 3.1**.

The batch number 6 was chosen due to its high QY combined with strong sharp absorbance and high particle concentration. The other samples in the study were then discarded and from here on only penicillamine capped CdS with a ratio of 4:1:2 Cd:S:Pen will be discussed.

As shown in **Figure 3.5** these particles have quite a complex absorbance signal with a shoulder at 379 nm, a peak at 335 nm, and a second shoulder at 301 nm. This type of absorption spectrum has been shown to be quite common for defect emitting CdS nanoparticles. The sharp signal at 335 nm has been previously shown to be pH dependant and generally speaking the higher the p.h the stronger the peak.[46] As the pH of the particle solution is lowered the luminescence is reduced and finally disappears leaving only the CdS absorbance band at ~379 nm. Previous studies of dialysisized CdS particles have concluded that this peak is a result of a charge transfer transition from the carboxylate head group of the complex to an acceptor state at the particle surface.[46]

The signal at 301 nm is believed to be the second exciton peak with the shoulder at 379 nm belonging to the first exciton peak. Another possibility is that the multiple bands are due to the presence of different sizes/types of nanocrystals. However, mixtures of particles can be easily separated using size selective techniques and this will be seen later in this chapter. The production of CdS nanocrystals is confirmed by comparing the energy of the shoulder at 379 nm, (3.27eV), with that of bulk CdS

which absorbs at 478nm, (2.6eV) at room temperature, (**Figure 3.6**). This increase in band gap energy combined with the accompanying decrease in absorbance wavelength can only be accomplished by a decrease in the diameter of the crystal to a point less than that of the Bohr radius of its exciton, i.e. quantum confinement.

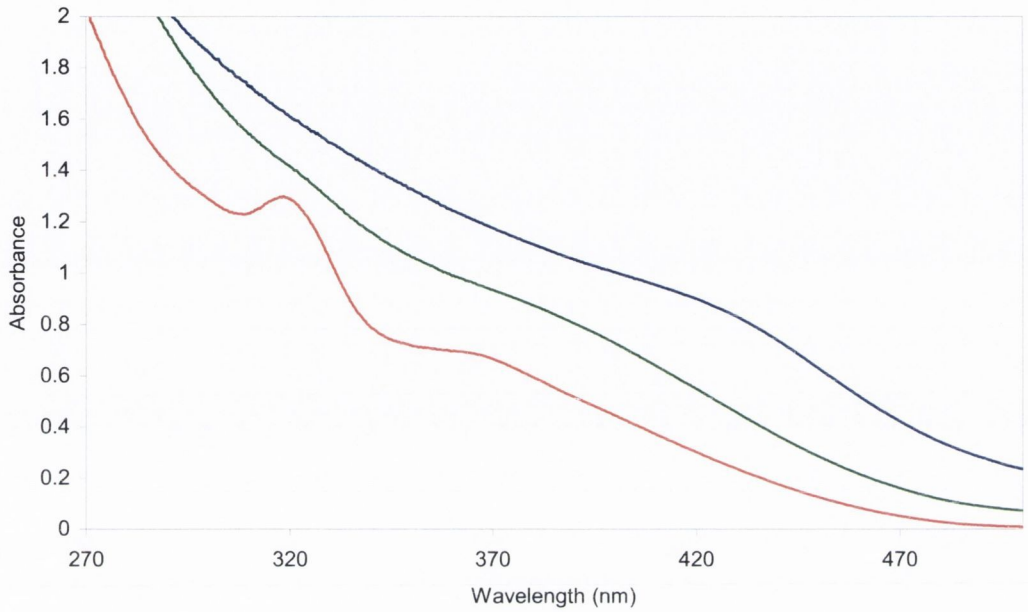

Figure 3.5: Abs spectra of D-Pen capped CdS measured at various pH's 12, 9, and 6. Note the loss of the sharp peak at 320nm as the pH is reduced. This is due to the protonation of the surface carboxyl groups. Note as this protonation also removes the particles negative charge which repels individual particles from one another the bandedge red shifts and scattering increases as individual particles begin to aggregate.

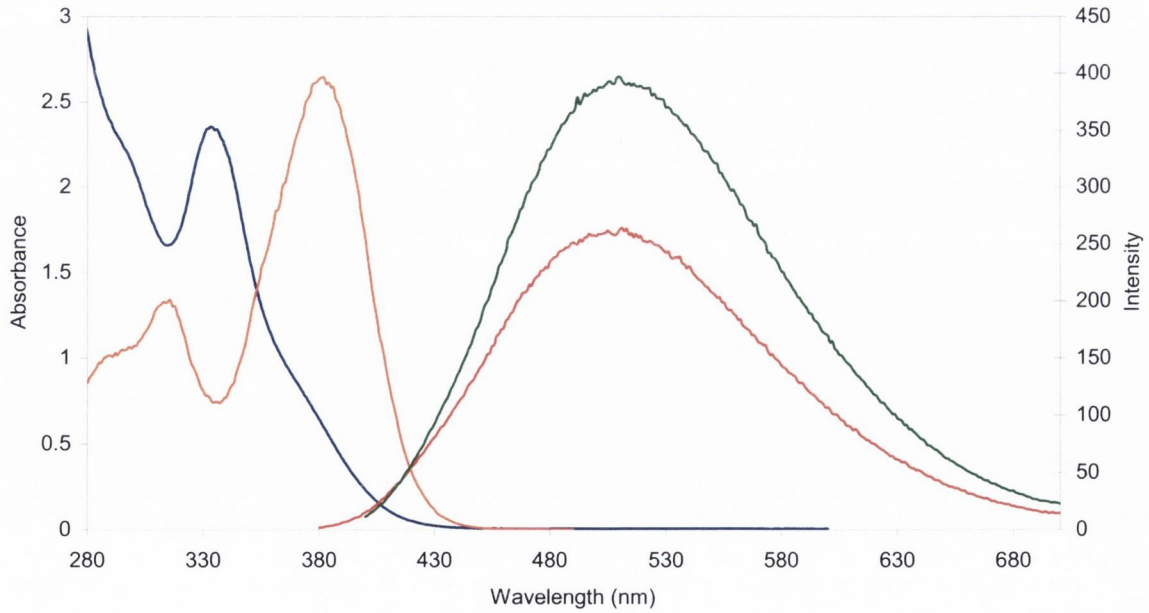

Figure 3.6: Absorption, (blue), emission, (red and green), and excitation spectra of D-Pen CdS. Despite the strong degree of quantum confinement as illustrated by the sharpness of the absorption and excitation shoulder at 337nm and 384nm respectively, the emission scans clearly demonstrate the presence of a large number of surface defects. Emission spectra were excited at 360nm, (red), and 380nm, (green). The excitation spectrum was recorded at 525nm.

Quantum confinement is confirmed by the presence of the shoulder at 379 nm, (3.27eV), when compared with that of bulk CdS which absorbs at 478 nm, (2.6eV) at room temperature, (**Figure 3.6**). This increase in band gap energy combined with the accompanying decrease in absorbance wavelength can only be accomplished by a decrease in the diameter of the crystal to a point less than that of the Bohr radius of its exciton, i.e. quantum confinement. Emission spectroscopy shows the presence of strong defect luminescence present at 510 nm, this is confirmed by the considerable width of the emission, FWHM of 110 nm; particles which emit intrinsically usually have a fwhm of around 30 nm. The dots were excited at two different wavelengths, 360 nm and 380 nm, to check the degree of monodispersity. The emission maximum does red shift by 5 nm when the excitation wavelength was changed indicating a slight variation in particle size, as pointed out earlier on. The excitation spectrum, taken at 500 nm, shows two peaks at 382 nm, 317 nm and a shoulder at 290 nm. Due to their shape both of these should correspond to the absorption signals at 336nm and 299 nm, though red shifted to a large degree, 46nm and 18nm respectively. This loss of energy is expected due to a) the high concentration of the particles and b) the nature of the emission; due to its defective nature energy will be lost to the surroundings as heat and non-radiative recombinations, (**Figure 3.6**). However as mentioned above the strong absorption peak at 336nm is possibly not related to exciton formation but rather another photophysical process involving the stabilizer. With this in mind the two excitation peaks can be assigned to the absorption shoulders at 378 and 300nm meaning the excitation spectra peaks have only red shifted by 6 and 17nm respectively. These more realistic wavelengths combined with the results of the pH experiments in **Figure 3.5** does add credibility to this assignment rather than the former.

Once the D-Pen particles were successfully prepared and characterised CdS dots were then synthesised using a). L-Pen and b). an equal amount of D- and L-penicillamine as the stabilizing molecule(s), which we will refer to as Rac or racemate. The particles were then washed by precipitation in propan-2-ol followed by centrifugation and removal of the supernatant by decanting. After that the particles were redispersed in Millipore water and examined spectroscopically. Both the D- and L- stabilized particles showed identical absorption and photoluminescent spectra.

However, the racemic particles were slightly blue shifted indicating a slightly smaller primary particle size (**Figure 3.7**).

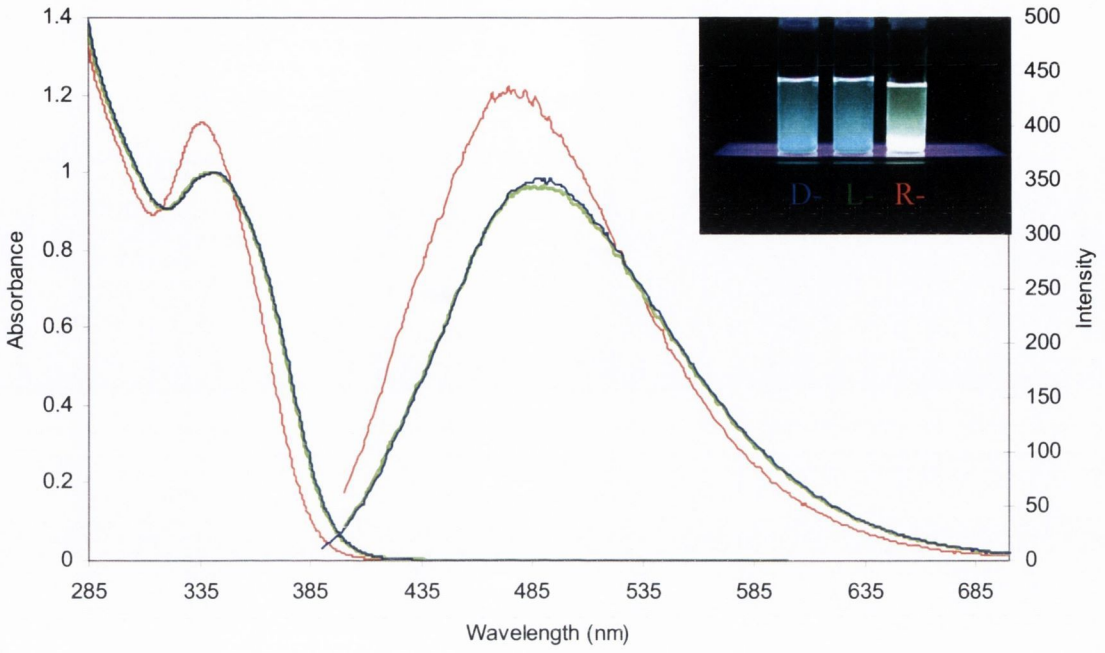

Figure 3.7: UV-Vis and Emission spectra of D-Pen CdS, (Blue), Abs 345nm, Ems 492nm, L-Pen CdS, (Green), Abs 345nm, Ems 492nm, and R-Pen CdS, (Red), Abs 339nm, Ems 478nm. All PL spectra were excited at 360nm. All three types of dots appear clear and colourless in visible light and green/white or blue/white depending on their size. The higher quantum yield of the R- dots is clearly visible in the picture.

Quantum yields, which were calculated using Coumarin 153 in methanol, showed both D- and L- Pen CdS have a Q.Y of 20 ± 2 %, which then increases for the R- sample to 30±4%. These differences in the photophysical properties of the Rac particles when compared with the D- and L- dots is most likely due to the complementary nature of the amino acids allowing for closer packing at the quantum dot surface. This packing of the surface ligands combined with the greater hydrophobic nature of the racemic mixture removes water molecules, and therefore quenching at the particle surface. Water molecules are known to have a quenching effect on quantum dots.[47] As mentioned above absorption spectra of D- and L- enantiomers are almost identical with sharp exciton peaks for both types of dots recorded at 345nm. The racemate absorption spectrum was slightly sharper and shifted to the blue, absorbing at 339nm. The emission spectra show that all three particle types exhibit strong defect luminescence, all excitation spectra are, as seen in the statistical analysis, red shifted by 10nm from the absorbance maxima. The reason for this is believed to be a slight loss of energy due to non-radiative recombinations as

a result of surface defects. It is generally accepted that the photoluminescent decays of quantum dot emission can be approximated using bi-exponential time distribution in the radiative lifetime, where each life time is made up of two components. Typically the shorter lifetime, τ_1, is attributed to the intrinsic recombination of the initially populated core states. The origin of the longer component τ_2 although long disputed is now considered to be a result of the interference of surface states, (i.e. the presence or absence of surface defects), with the recombination of the electron-hole pairs.

Table 3.2: Life time data for D-, L-, and R-Pen CdS nanoparticles, using a tri-exponential fit. Note the higher contribution of τ_1 in the R- particles indicating a greater contribution of core to the overall decay. This is in perfect agreement with the higher defect Q.Y of the R- particles.

	Q.Y%	χ^2	A	τ_1(ns)	B_1	$B_{\%}$	τ_2 (ns)	B_2	$B_{\%}$	τ_3(ns)	B_3	$B_{\%}$
D-	22±2	1.07	21	13.5	3866	37	56.8	4725	45.5	171	1827	17.5
L-	22±2	1.05	30	13	4804	38.3	55.6	5643	44.9	171	2112	16.8
R-	30±2	1.11	22	16	3868	40.7	59	4047	42.6	173	1585	16.7

Although a bi-exponential fit is more common when calculating the lifetimes of quantum dots this proved to be ineffectual here providing poor fits and unacceptable χ^2 values. Also, when dealing with CdS nanoparticles a multi-exponential fit is more common. Therefore a tri-exponential fit will be used to fit the particles. More reasoning for this will be further discussed in the next chapter. Despite the quantum yield of the R-Pen CdS being almost one and a half times that of the D- and L- dots only a slight increase in the life time of the R- dots is seen, **(Table 3.2)**. By examining all three particles, (D-, L- and R-), using a tri-exponential fit in the 1 μs range it is possible to account for these subtle differences. A correlation can be drawn between the lifetime and quantum yield data. This is possible if the overall contribution of the individual lifetimes, the B factors, and not the lifetimes themselves, the τ values are examined. If it is accepted that the smallest lifetime is caused by recombination in the particle core and the medium lifetime is a result of surface recombinations then any increase in intrinsic quantum yields should, (and do), see an increase in the overall contribution of the medium lifetime. However this is not the case here, in fact the overall contribution of the core and not the surface increases for the R-particles. However this is defect and not intrinsic luminescence and any increase in its quantum

yield must be the result of further defect formation on the particle surface which would indeed lead to a decrease in the surface lifetime contribution. Again, the photophysics of these types of particles will be dealt with in further detail in the next chapter.

Finally the third and longest lifetime is believed to be due to the presence of chiral defects on the particles surface. Although it is common for defect emitting CdS to have lifetimes in the 100s nanosecond range these are usually around the 400-550ns mark, the fact that the τ_3 values observed in this work are much lower, and that these values are replicated for other chiral quantum dots, (see later chapters), leads to the believe that they are actually due to the presence of chiral surface defects.

3.4 Circular Dichroism Studies

Circular dichroism (CD) studies of the particles gave particularly striking results. *D*- and *L* - penicillamine stabilized particles produced corresponding mirror image CD spectra (Figure 3) while the particles prepared with a Rac mixture showed only a weak signal.[36]

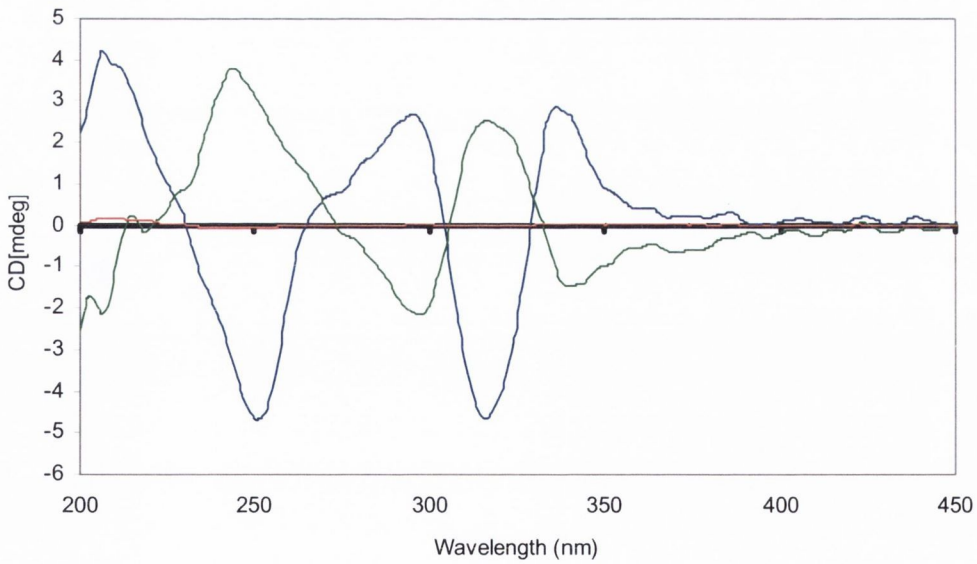

Figure 3.8: CD scan of D-Pen, (Blue), L-Pen, (Green), and Rac-Pen, (Red), modified CdS particles. Note the optically active signals above from 200-400nm. Penicillamine only absorbs at ~234nm, meaning the optical activity has now been transferred onto the quantum dot. (θ deg = δA/32.98).

The CD observed is quite different from that of the free *D*- and *L*- penicillamine which show, as expected, a near symmetrical image with maxima/minima at 234±2 nm. However, the CD spectra of *D*- and *L*- penicillamine stabilized CdS QDs are more complex, with maxima/minima at 208 ± 2, 250 ± 3, 299 ± 1, 318 ± 1 and 340 ± 2 nm, (**Figure 3.8**).

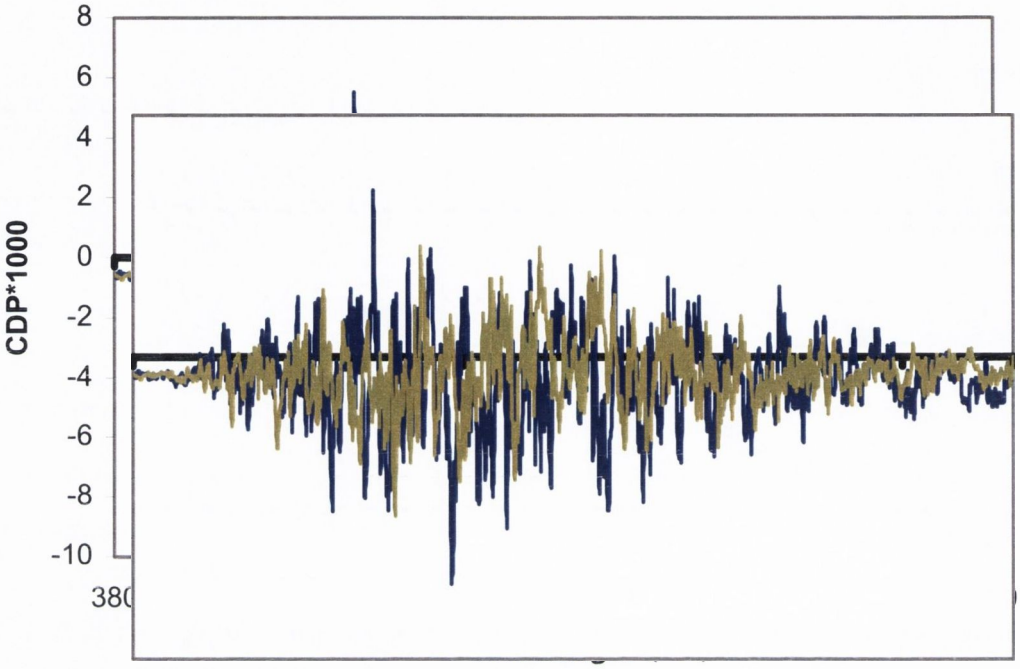

Figure 3.9: CPL of D-CdS, (blue), and L-CdS, (lime). The intensity of the scan has been increased by a factor of 1000 to demonstrate the lack of any real structure, i.e. it is just amplified background noise.

As mentioned earlier, we believe the same surface defects which give the particles their characteristic emission also gives them their optical activity. Therefore, to try and further confirm this hypothesis CDPL studies for D- and L- as well as various, (but not equal), mixtures of D- and L-Pen CdS were also carried out. However, these showed that although these particles preferentially absorb circularly polarised light they do not emit it, **Figure 3.9**.

The opposite preference for left or right polarized light in the region of the CdS exciton bands is particularly intriguing. The presence of optical activity may be due to chirality induced in the quantum dots upon reaction, in a manner similar to that previously proposed for metallic nanoparticles.[13-15] In order to understand the formation mechanism of these chiral QDs, UV and CD measurements were carried out at all stages of the particle preparation, (**Figures 3.10** and **3.11**). Both *L*- and *D*- samples demonstrated similar behaviour but showed bands of opposite chirality.

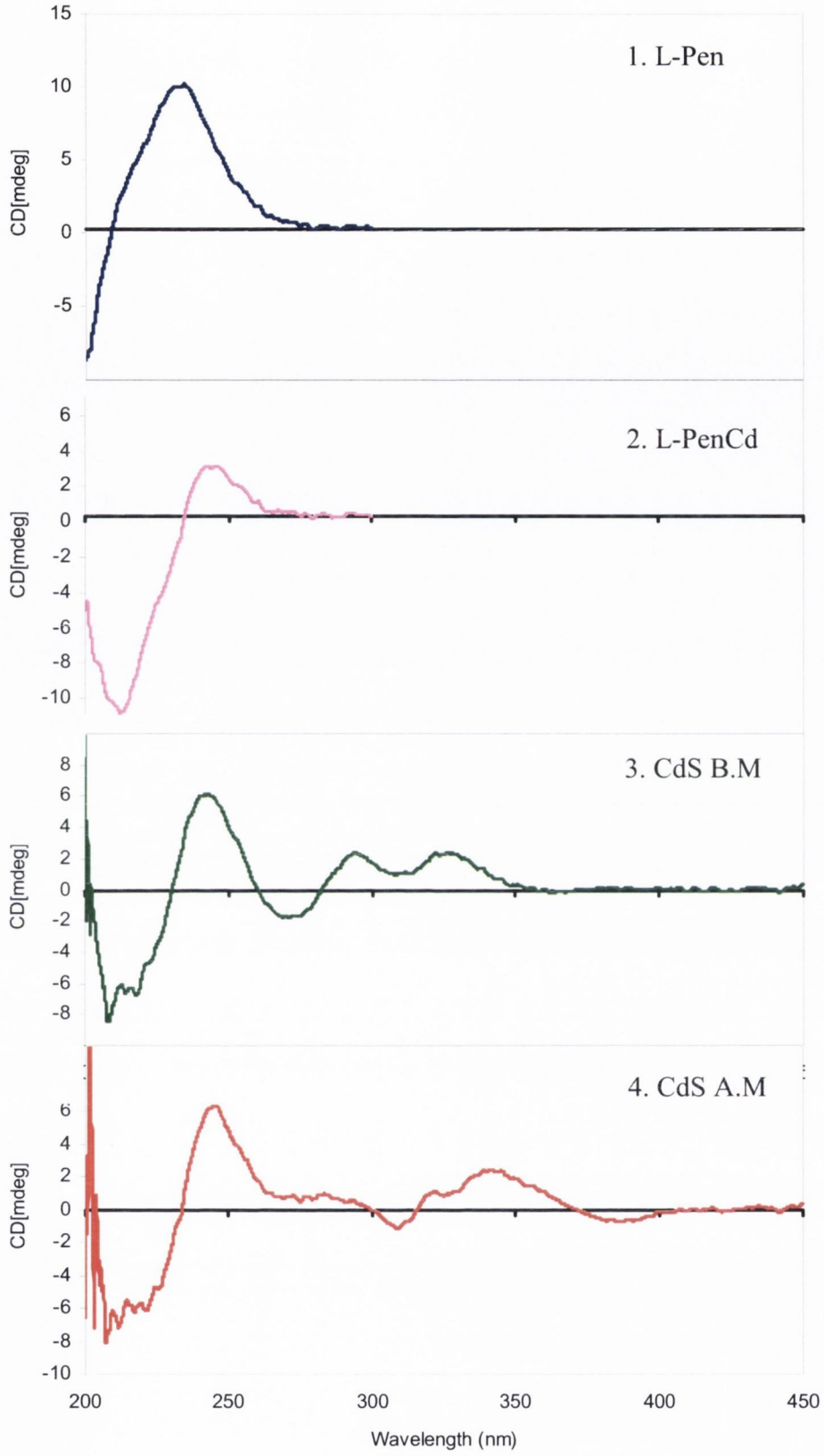

Figure 3.10: CD spectra of L-Pen CdS particles at various stages of preparation. Note the inversion of the signal as the Cd-Pen complex is formed and the subsequent formation and red shift of signals beyond 300nm as the thioacetamide is added and the smaller particles are microwaved. B.M - before microwaving, A.M-after.

According to this data the process initially involves the formation of a Cd penicillamine complex (band around 210 nm), which demonstrates chirality opposite to the starting stabiliser. New species were then formed on addition of thioacetamide. These resulted in the appearance of signals around 290 and 320 nm in the CD spectra. Most likely these are small CdS clusters in which penicillamine is coordinated in a fashion similar to that proposed for other similar CdS systems.[48, 49]

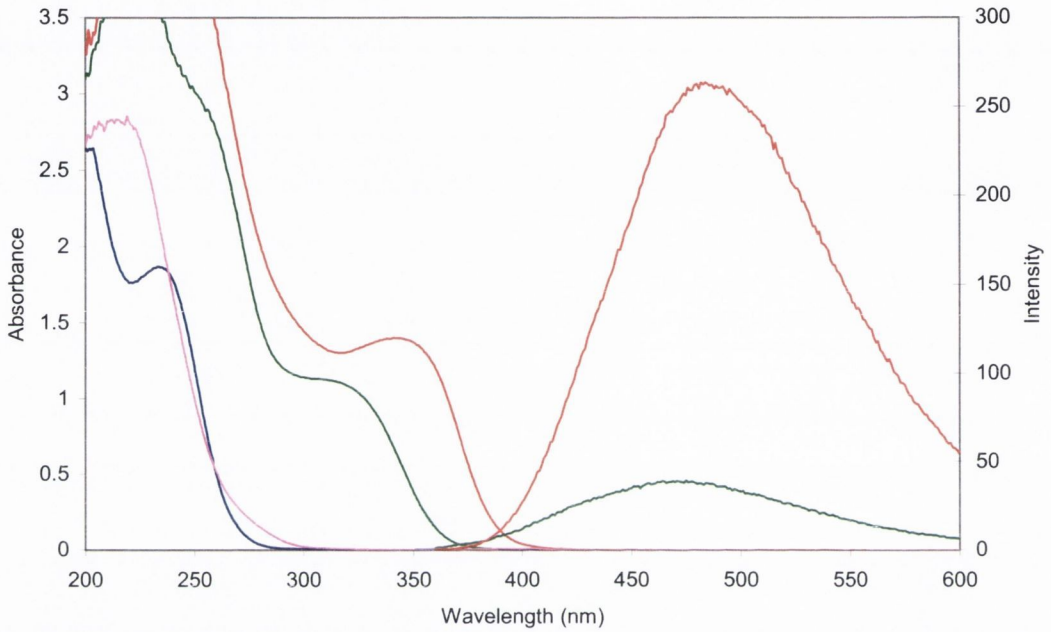

Figure 3.11: UV-Vis and PL spectra of L-Pen CdS monitored through out its formation. Free L-Pen, (blue), absorbs at 232nm. Addition of Cd results in the formation of Cd-Pen complex, (magenta). Addition of thioacetamide forms small luminescing nanoparticles with some remaining tioactemide, (260nm). Once particles are microwaved, (red), their size and luminescence increases as can be seen from the red shift of both abs and ems peaks as well as the greater increase in intensity of the ems peak relative to that of the abs peak.

However examination of these "clusters" using emission spectroscopy showed that they were weakly luminescent; this indicates that they are actually small nanoparticles as clusters do not luminesce. Subsequent microwave irradiation causes these small nucleation centres to grow, forming larger CdS nanocrystals. This results in a red shift in the CdS band edge and corresponding CD signals between 320 and 390 nm respectively. Thus it is obvious that the particle formation and growth takes place involving intermediate chiral species. As a result clusters and corresponding nanoparticles are forced to grow according to a particular chiral pattern introduced by the stabilising ligands.

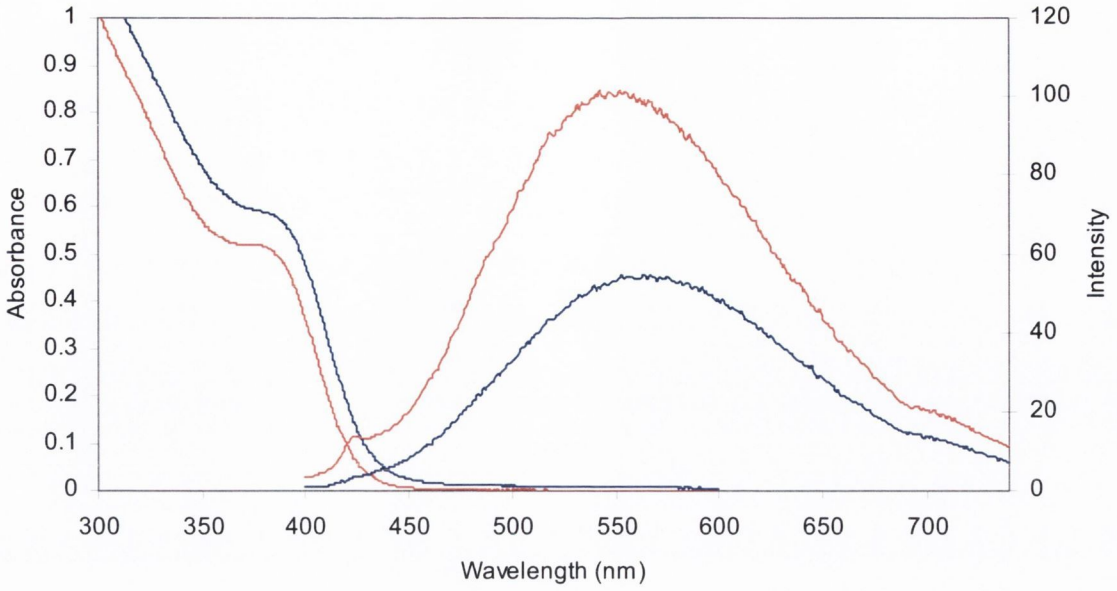

Figure 3.12 UV/Pl of tri-sodium citrate stabilized CdS nanocrystals, (blue), and after addition of D-Penicillamine solution, (red). Pl excited at 380nm. Particles were prepared as described earlier however the penicillamine was substituted with sodium tri-citrate. A ratio of 4:1:4 was used. Once prepared the particles were examined on UV, Pl and CD. 4ml of a D-Pen solution ($1x10^{-2}$M) was then added and the colloid was stirred vigorously. The particles were then re-examined. Ligand substitution can be seen by both the blue shift and removal of scattering in the UV signal, and the increase in the luminescence.

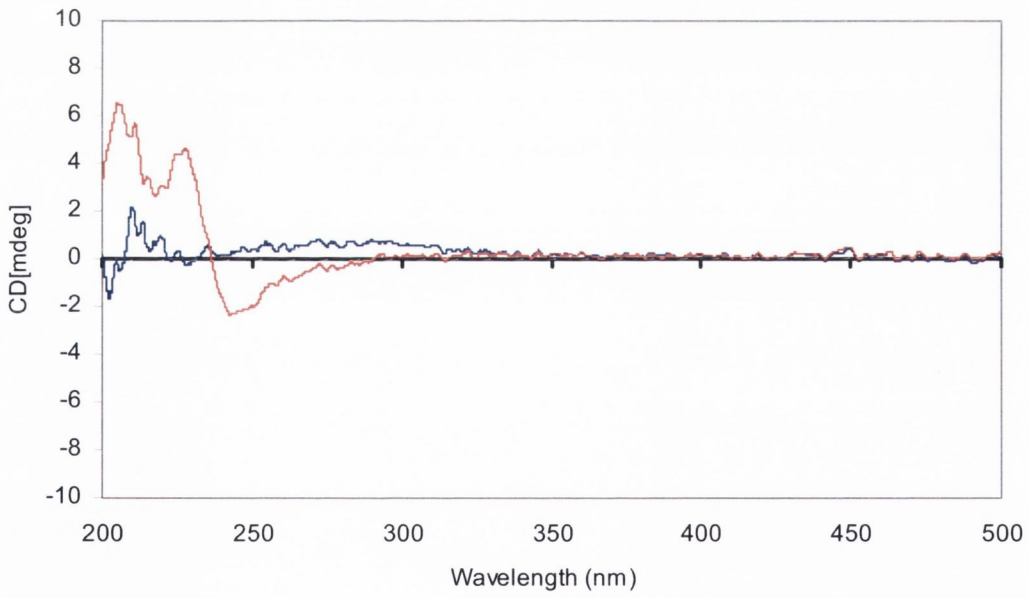

Figure 3.13: CD spectra of tri-sodium citrate stabilized CdS nanocrystals, (blue), and after addition of D-Penicillamine solution, (red). Citrate stabilized CdS particles are not optically active but some scattering is visible between 250 and 350nm. Addition of D-Penicillamine to the particles results in the appearance of signals below 300nm which correspond to the ligand only. The characteristic bands between 290nm and 370nm which are visible when the particles are precipitated in the presence of D-Pen are not present.

To further demonstrate this chiral growth model CdS nanocrystals were prepared using a non-chiral stabilizer, (tri-sodium citrate). Once prepared and characterised D-penicillamine was then added and the ligand exchange was observed on UV-Vis and

Pl however the characteristic CD signal of CdS prepared in the presence of D-Pen was not present, **Figure 3.12** & **3.13**. This further demonstrates the need for a chiral environment *in situ* during co-precipitation to prepare chiral quantum dots. CD spectroscopy was also used to investigate the effects of microwave irradiation on solutions of D-Pen and Cd as well as solutions of Thioacetamide and D-Pen were also carried out as well examining the particle supernatant after precipitation. No unusual chiral signals, i.e. beyond 270nm were seen, **Figure 3.14**.

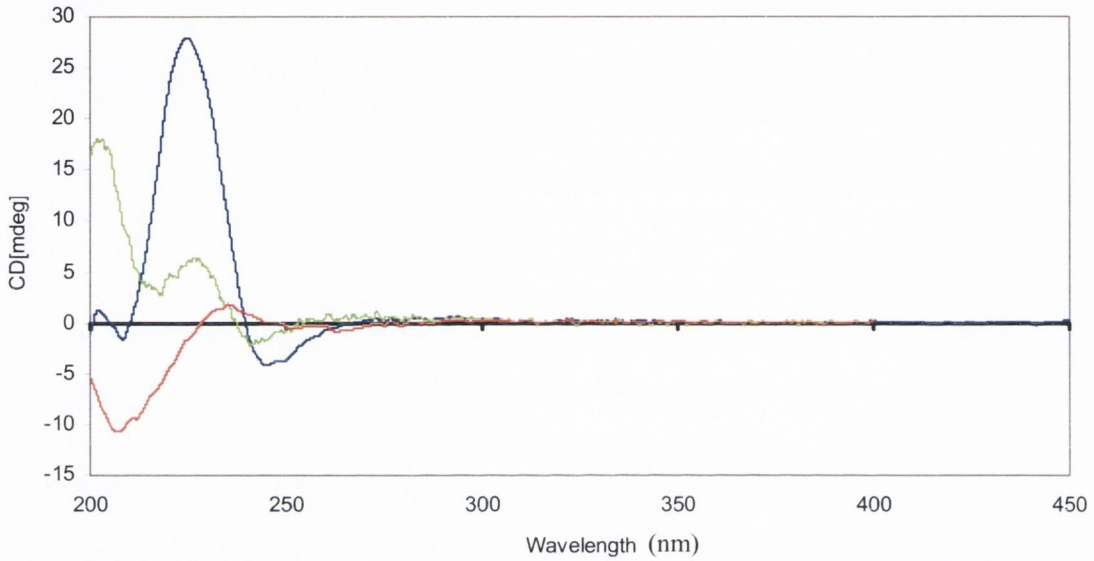

Figure 3.14: CD of D-Pen/Cd, (lime), and D-Pen/Thioacetamide, (red), and CdS co-precipitation supernatant, (blue). All samples were microwaved and left to mature for three days. Note the absence of any signal beyond 270nm. Both the D-Pen/Cd and the D-Pen/Thioacetamide solutions were prepared as a normal D-Pen CdS reaction minus the addition of Thioacetamide or Cadmium Perchlorate solutions respectively. In the case of the supernatant D-Pen CdS was prepared as normal and the supernatant examined.

3.5 TEM studies of Penicillamine stabilized CdS

HR TEM of individual CdS particles showed that the average particle size for D-Pen stabilised CdS nanoparticles to be around 5.5nm, (**Figure 3.15**). This size is conclusive for CdS particles which absorb below 400nm, and is in good agreement with the zeta-sizing results, (**Figure 3.15 left**). Although these spheres were present in D- and L- Pen CdS there were also a large degree of what appeared to be rod like structures in the L-CdS sample, (**Figure 3.16**).

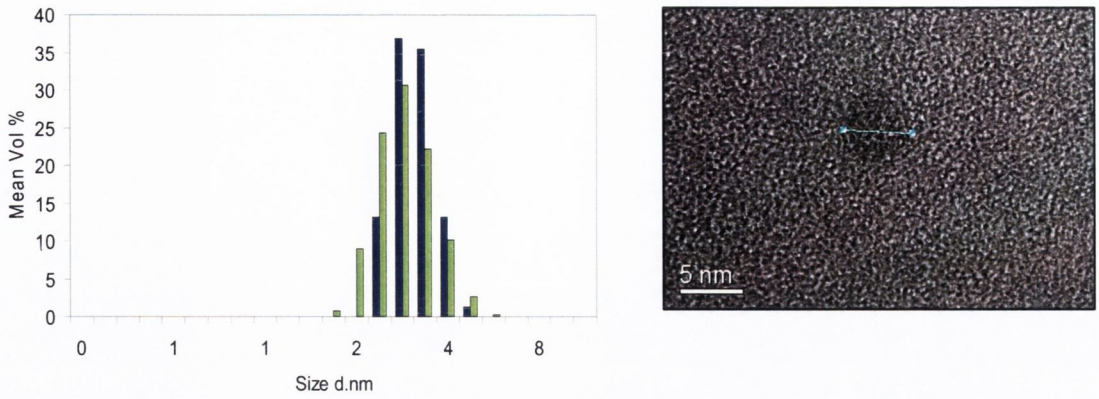

Figure 3.15: Histogram of nanoparticle size distribution from DLS (left) and TEM image, (right), of D-Pen stabilized CdS particles. Histogram shows sizes ranges for D-blue and L-lime stabilized CdS particles, R particles proved too small for instrument to record accurate data. Data was recorded on a Malvern Zetasizer.

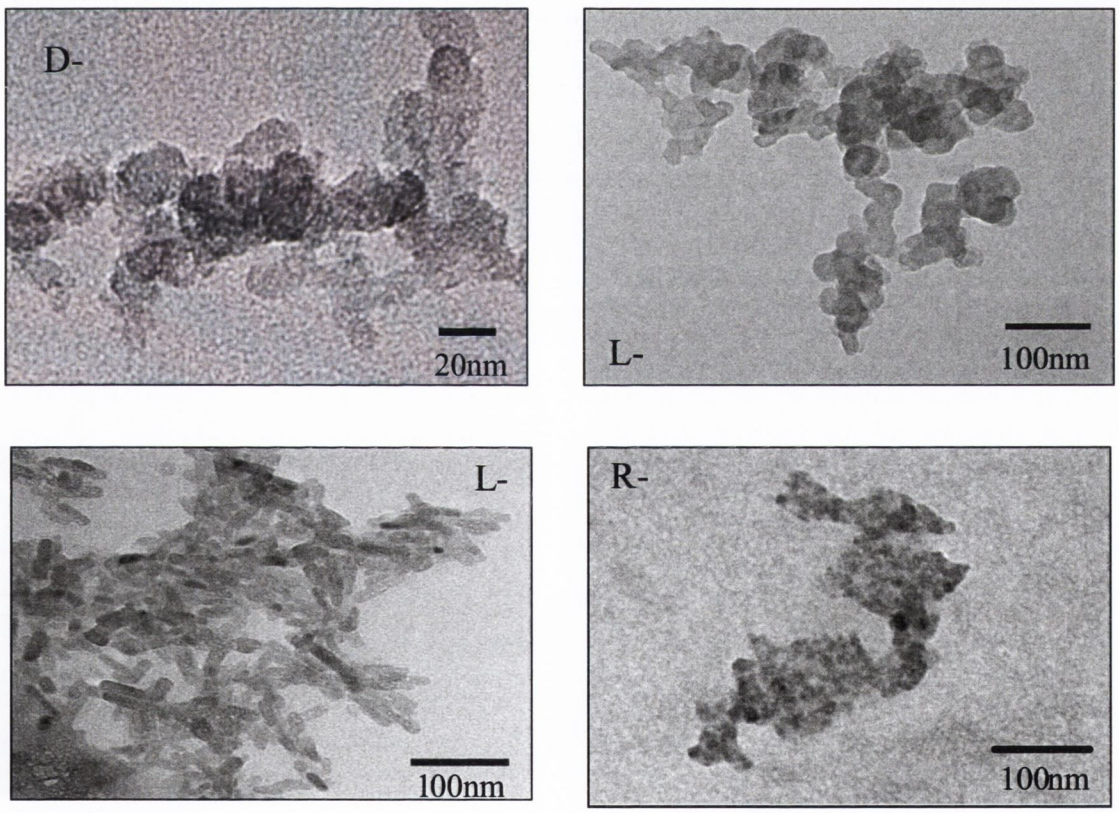

Figure 3.16: TEM image of D-, L- and R-Pen stabilized CdS particles. While 5.5nm particles can be seen among the aggregates the larger 35±6nm particles are more prominent in the non HR images. Both rod and sphere- like structure are also clearly visible in the L-CdS sample.

Size selective co-precipitation was carried out on the L-Pen CdS particles in an attempt to separate the spherical and rod-like aggregates. Once separated each shape's optical properties were then examined. Briefly, L-Pen CdS was prepared and then

taken and reduced in volume to 2ml using rotary evaporation. Once the volume was reduced isopropanol was added dropwise until a cloudy precipitate was observed. Once the particles were precipitated out with the minimum amount of propan-2-ol they were then centrifuged at ever increasing speeds starting at 500rpm's and then doubling the speed each time.

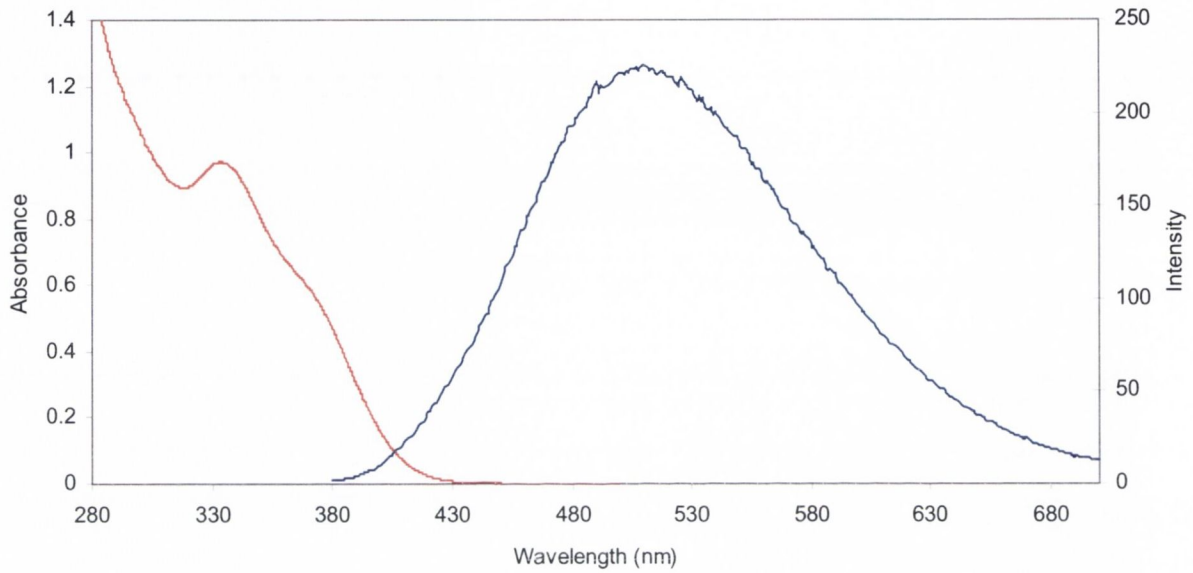

Figure 3.17: UV-Vis and Pl spectra of L-Pen CdS dots before washing with iso-propanol. Note the clear shoulder, (372nm) and peak, (337nm) present in the absorbance spectra. Emission peak is at 510nm and was excited at 360nm.

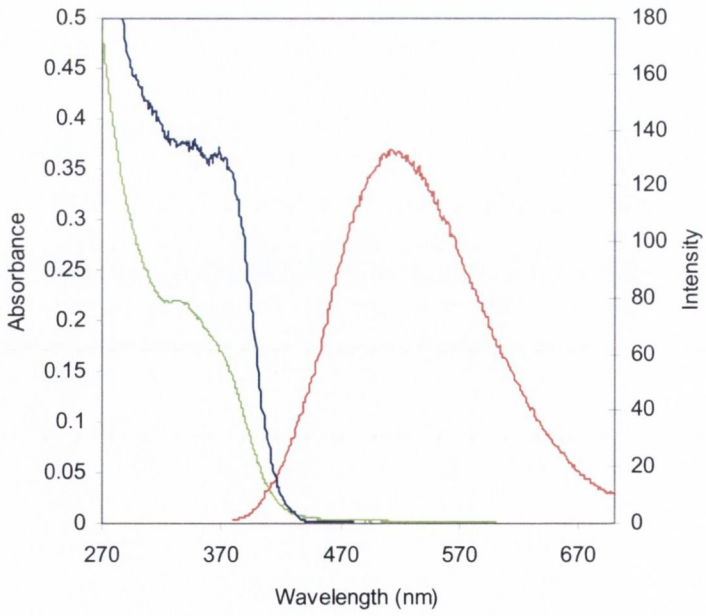

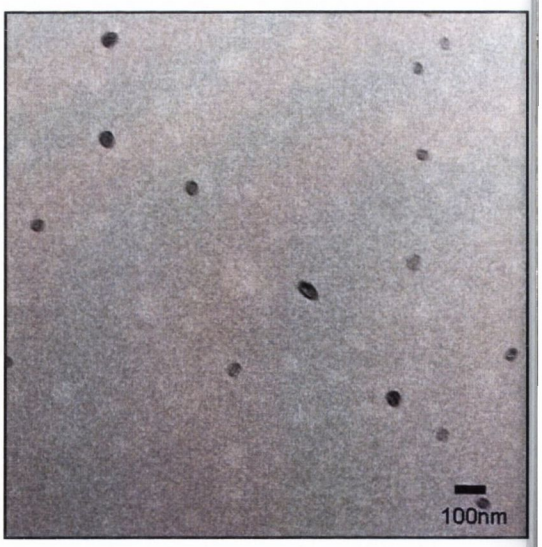

Figure 3.18: L-Pen CdS 500rpm; absorbance, (green), excitation, (blue) and emission, (red). Absorption and emission peaks have red shifted by 6 and 10nm respectively indicating particle growth.

Once a pellet was observed the supernatant was decanted off and the centrifugation continued. Pellets were removed at 500 and 2000rpm and redispersed in millipore water. While the larger rod-like aggregates were expected to come out of solution first it was the smaller spheres which were identified in the 500rpm fraction.

Although still clearly spherical there is what appears to be beginning of an elongation process indicating that the washing process may have destabilized the organic shell slightly. Comparison of the absorption and emission spectra to the unwashed sample show a ~10nm red shift in the both spectra indicating particle growth however the sharp absorption peak at 337nm has been seriously reduced.

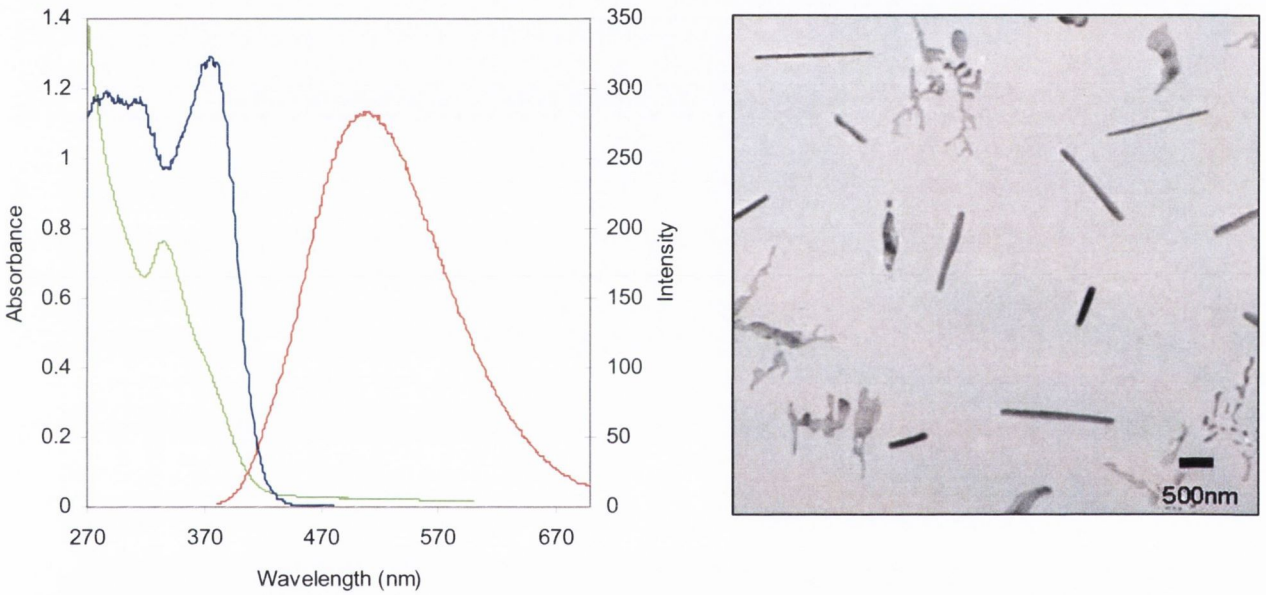

Figure 3.19: L-Pen CdS 2000 rpm; absorbance, (green), excitation, (blue) and emission, (red). Neither the abs or emission peaks have red shifted or changed shape and are identical to the original, (pre-washing), scan. This is strange as the rods have increased in length and width from L=41±8 nm & W=15±2 nm before the washing step to L=1.6± 0.21 μm & W=85±32 nm after.

Examination of the 2000rpm fraction leads to some surprising results. The rods are not only in this fraction, but they have also increased in length and width and are now up to ~1.7 microns long, (**Figure 3.19**). There are also some branched structures present in the grid. A partial explanation for these changes in size and composition may be that the changes are simply due to the destabilization effect of the iso-propanol on the nanorods. Once the nanorods were destabilized then inter particle dipole interactions would cause them to line up end to end, this effect combined with the centrifugal force would cause the nanorods to fuse together end to end and side to

side creating larger nanowire structures. However what is most unusual and cannot be explained is the lack of change in both the absorption and emission spectra despite the increase in the length and apparent solidity of the nanowires. Due to the lack of any spectroscopic changes it must be assumed that these nanowires are despite appearances, not solid, but consist of small individual nanoparticles. The strength of the peak at 337nm, when compared with the smaller circular aggregates, might confirm this if it is indeed due to carboxyl complexation of Cd. However instead of the ligand bending back and co-ordinating to Cd present in the dot it is stabilizing it is acting as bridging ligand between various dots connecting them in the wire-like array.[46] This would account for the lack of any visible red-shifting in the optical spectra.

3.6 Computer modelling of CdS-Pen chiral clusters

In an effort to more fully understand the above phenomenon of optically active semiconductor nanocrystals the system was modeled using Density Functional Theory.[36] The particles before microwaving were modeled as isolated molecules in vacuum. The ground state electronic wavefunction of each cluster was calculated self-consistently within Kohn-Sham Density Functional Theory (DFT) using the TURBOMOLE suite of quantum chemical programs. A good trade-off between accuracy and computational cost was obtained by using the B-P86 functional, the RI-*J* approximation and an atom-centred basis set of valence double-ζ with polarization quality [denoted SV(P)] with a 28-electron effective core potential on Cd. Tests of this method indicated that bond lengths were slightly over-estimated (~5 pm), as is typical of DFT. All species were closed shell. Optimization of the cluster geometry was carried out on the DFT potential energy hypersurface.

The neutral form of penicillamine is shown as $PenH_2$, consequently the dianion is Pen^{2-}, which is the probable charge state of the ligand in these experiments at pH=12. Calculations have indicated that $^{-}SC(CH_3)_2CH(NH_2)COO^{-}$ is the most stable dianionic structure in the gas-phase. Although CdS can adopt either a wurtzite or a zinc-blende structure, it is computed that wurtzite clusters show greater cohesive energy than zinc-blende clusters. With this in mind the former, (wurtzite-based), structure was chosen to study these QDs. HRTEM shows that these particles possess lattice spacings of 3.6 Å, (**Figure 3.15**), where the lattice spacing of bulk wurtzite in

the *a* and *b* planes is 3.81 Å. In the hexagonal wurtzite structure (space group #186, $P6_3mc$), both S and Cd are tetrahedrally coordinated and stacked ABAB along the [0 0 0 1] axis. The experimental Cd-S distance in the bulk is 2.52 Å.

Initial structures for Pen-stabilized CdS QDs were obtained by cutting symmetrical clusters out of the bulk wurtzite structure, so as to expose the (1 0 -1 0) and (0 0 0 1) surfaces. CdS nanoparticles that have been computed in previous DFT studies range in size up to $Cd_{16}S_{16}$, but these are too small for this study. As the point of this study is to elucidate if there is a distortion of the QD core, the smallest useful cluster is one based on Cd_{19} that contains a Cd_4S_4 core capable of distortion/twisting about [0 0 0 1]. {Core atoms, for the purpose of this study, are defined as those that are not bound directly to surface Cd-S units}. A coin-like disc is cut out of the bulk wurtzite structure, consisting of 19 parallel CdS units, each oriented along [0 0 0 1], of which four are bulk-like (Cd_4S_4 core), six form intermediate (0 0 0 1) planes and nine form three equivalent [27] faces around the outside of the QD. The (0 0 0 1) plane was stabilized by H^+ (on S) and SH^- (on Cd), leaving the three {1 0 -1 0} faces of the cluster for adsorption of Pen molecules.

The electronic structure of a semiconductor cluster is notoriously difficult to compute accurately with DFT as with other similar *ab initio* methods. 'Bare' clusters are often unstable and convergent calculations are only possible if the surface is adequately stabilized by ligands in a realistic bonding configuration. Unfortunately, experimental data on the structure of the ligand shell are rarely available, necessitating considerable computational trial and error in the nature and geometry of the ligands. The first criterion is a closed-shell, well-converged electronic structure at the plausible starting geometry. Secondly, it is required that molecular orbitals (MOs) of predominantly Cd:5*s*5*p* character be vacant and low-lying, while ligand valence MOs be occupied. In clusters with poorly-saturated surfaces, the energetic ordering (and thus occupancy) of these MOs is erroneously reversed.

From this model, the bonding of *D*-Pen to {1 0 -1 0} faces of the CdS QD was determined. In the perfect (1 0 -1 0) surface, each topmost S atom caps three Cd, and so it is reasonable to assume that the S atoms of the Pen ligands also assume this position. The amine-N and carboxylate-O of Pen are also basic and each is available for coordination to Cd. Our tests on a variety of small clusters indicate that both N and O can bond to Cd, with a preference for Cd—N, and that neither atom bridges or

caps more than one Cd (although carboxylate may bridge two Cd via two O). This leads us to propose the bonding arrangement shown in **Figure 3.20** for *D*-Pen on a perfect (1 0 -1 0) surface. As the schematic shows, bonding via the carboxylate moiety to a fourth surface Cd atom is asymmetric and lifts the mirror symmetry of the surface. Thus, even without any distortion of the CdS substrate, the adsorption of *D*-Pen is expected to yield an enantiomeric monolayer of ligands. Our calculations aim to see how this affects underlying CdS in the case of a QD.

Our Cd_{19} model cluster has three identical (1 0 -1 0) faces, each consisting of three [0 0 0 1]-oriented CdS units. Using the bonding arrangement outlined above, we substitute *D*-Pen^{2-} for S^{2-} in these faces, so that each face is covered with a band of three Pen ligands, interlocked by H-bonding and co-planar in (0 0 0 1). In order to obtain a reasonable electronic structure, it is necessary to saturate dangling $-COO^-$ at one edge of each face by adding H^+. The cluster formula is thus $[Cd_{19}S_{17}H_{14}(D\text{-}Pen)_6(D\text{-}PenH)_3]^{3+}$. The geometry is fully optimized (first in C_3 symmetry and then without symmetry constraints) and the resulting structure is shown in **Figure 3.21**. This cluster shows a maximum diameter of about 21 Å, measured between outermost H's of the ligand shell, considerably smaller than the final QDs obtained experimentally.

Of the three *D*-Pen ligands bound to each face of the model cluster, the structure of the middle ligand is likely to be most representative of that occurring in the actual QD. The optimized structure shows the middle *D*-Pen coordinating to four Cd in much the same fashion as the starting structure (**Figure 3.20**), with distances Cd—N=2.33±0.06 Å, Cd—O=2.36±0.07 Å, 2.7±0.4 Å and Cd—S=2.58±0.01 Å, 2.78±0.02 Å, 2.9±0.2 Å, all of which suggest strong binding of Pen to the QD surface. The N-Cd-S angle is 82.8±0.4°. The margins of error reflect the slight differences between the three faces, and are perhaps indicative of the geometrical variability that can be expected on imperfect surfaces of actual QDs.

On optimization, the band of three Pen ligands on each face are splayed apart by bulky CH_3 groups, increasing S—S distances within the (1 0 -1 0) face (from 4.0 to 5.3±0.9 Å) and causing rotation of the Cd-S units (tilting clockwise relative to [0 0 0 1] by an average of 41°, standard deviation 14°). This is accommodated by expansion of the cluster perpendicular to the Pen-covered faces, with [0 0 0 1] displacements of 0.5-1.0 Å by intermediate Cd and S atoms (*i.e.* atoms of the $Cd_6(SH)_{12}$ interface

between the $(CdS)_9$ surface and the $Cd_3S_3Cd(SH)_2$ core). As noted above, the asymmetrical orientation of the ligand is dictated by the coordination of carboxylate-O to neighboring Cd, (**Figure 3.21a**). The result is that (*D*-Pen)$_3$ and the underlying Cd and S pack into a segment of left-handed helix on each face, as illustrated in **Figure 3.21b**. Clearly, in an *L*-Pen cluster, the ligands would tilt in the opposite sense (-41°) and form a right-handed helix. This analysis suggests that three factors dictate the cluster geometry: (i) the Pen ligand is slightly bulkier than the space between adjacent Cd on (1 0 -1 0); (ii) surface-Pen bonding is relatively strong and (iii) the Cd-S cluster structure is relatively flexible. As a result, inter-ligand strain is transmitted to the outer layers of the CdS cluster, meaning that the chirality of the ligand shell is transmitted to these layers as well.

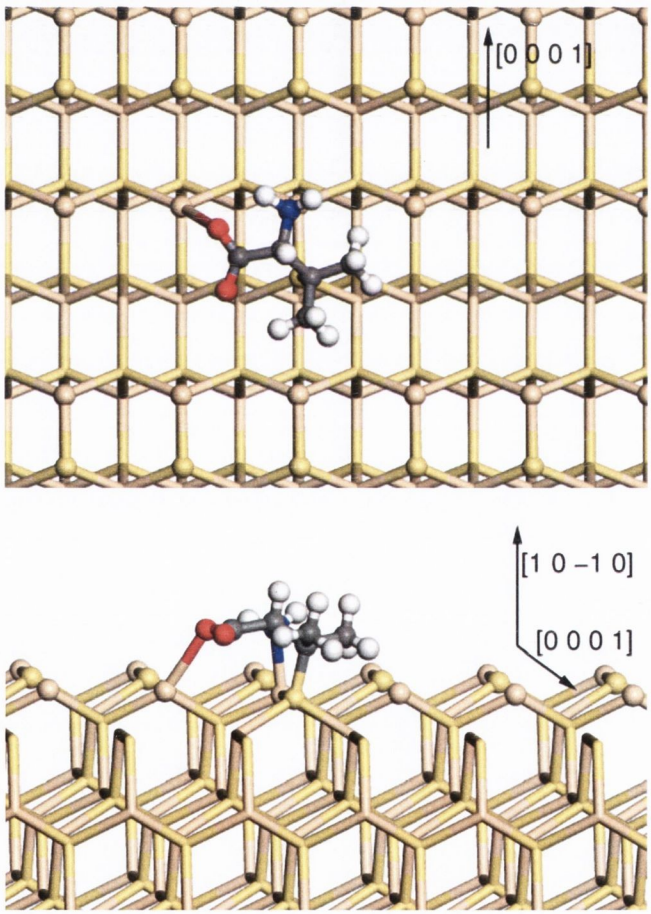

Figure 3.20: Top and side views of the proposed bonding of *D*-Pen to the (1 0 -1 0) surface of wurtzite (Cd=brown, S=yellow, C=grey, O=red, N=blue, H=white, balls=topmost atoms). In the top view, horizontal rows of vertical CdS units are visible at the top and bottom of the figure, while surface S atoms have been removed from the middle row and one has been replaced by the S atom of *D*-Pen, so as to illustrate the bonding pattern found in this study.

It is significant however to observe that the $Cd_3S_3Cd(SH)_2$ core of the QD cluster remains almost undistorted, (**Figure 3.22a**): on optimization, the Cd-S units of the core tilt by only -5° to +2° relative to the perfect crystal, with Cd—S=2.55 Å. The core therefore remains achiral, despite the chiral distortion of the surrounding layers. The defect nature of the particles luminescence combined with further experimental evidence in the later chapters, (Chapter 4-reflux experiments, Chapter 5 degree of intrinsic luminescent vs. level of optical activity), does suggests that this theory is correct.

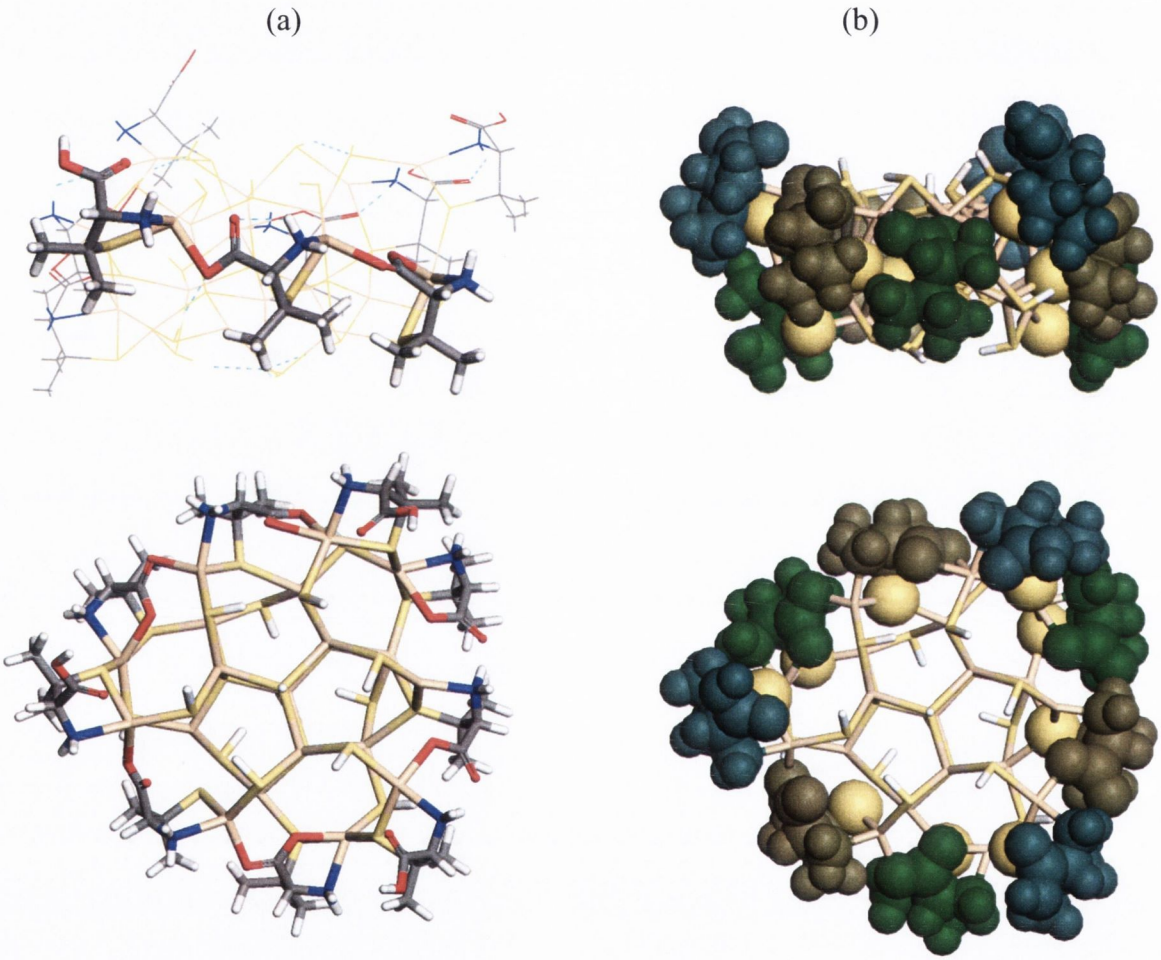

Figure 3.21: Top and side views of a (1 0 -1 0) face of the optimised cluster model of QD: (a) stick representation with PenH-Pen-Pen bonding pattern along one face highlighted in the side view; (b) Pen ligands in space-filling representation, with non-S parts of each ligand coloured differently. Note that *D*-Pen ligands form fragments of a left-handed helix about the QD core.

The Pen-terminated CdS nanoparticles synthesized experimentally are larger and show a wider variety of cluster faces than considered here. Nevertheless, it is

suggested that the relative bond strengths of Pen, Cd and S are universal properties of the system and generally mean that the chirality of Pen is transmitted to the surface and sub-surface layers, but that the QD core remains achiral. Examination of the electronic structure of the computed cluster reveals that the three highest-lying occupied molecular orbitals (MOs) (not shown) are localized on surface S atoms at each corner of the QD (*i.e.* at the junction between {1 0 -1 0} faces). The three lowest-lying unoccupied levels (not shown) are of predominantly Cd character on highly-distorted sub-layer atoms near each corner.

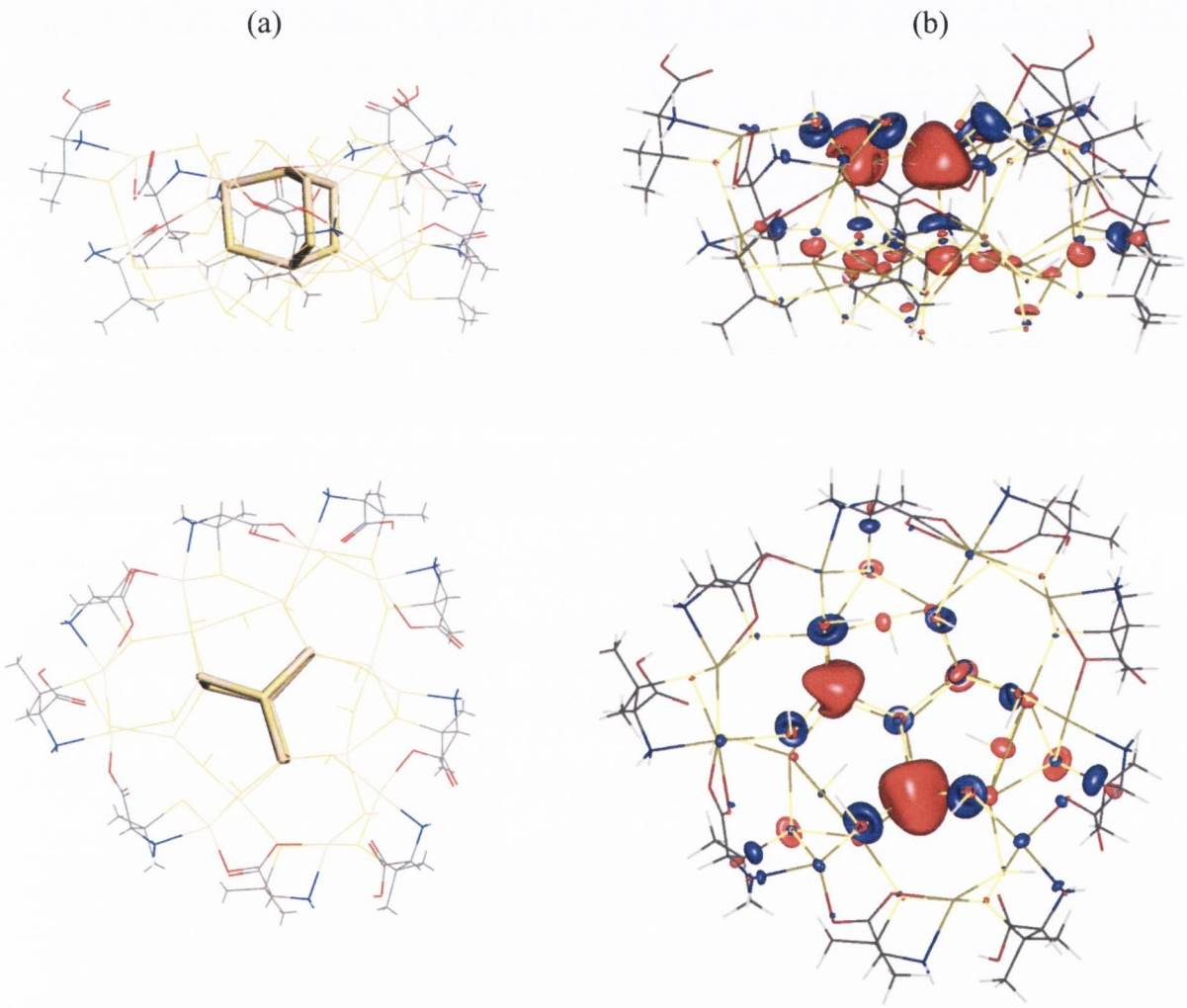

Figure 3.22: Top and side views of optimized cluster model of QD: (a) the Cd_4S_4 core is highlighted; (b) contour plot of empty LUMO+3 molecular orbital, which is mostly of Cd:5*s* character on the QD core.

The corners in our model correspond to defects on a real QD surface. It must be stressed that the unoccupied MOs from a DFT calculation have no direct physical

significance. Nevertheless, it is likely that these or similar chiral states on near-surface Cd are responsible for the long wavelength CD response of small QDs after treatment with thioacetamide (290-390 nm, **Figure 3.10**) and for the defect-related luminescence of the larger QDs. These lies an unoccupied MO of predominantly Cd:5*s* character on the Cd_4S_4 QD core (b). Polarization of this MO is visible, but is minor relative to the strong localization of the other frontier MOs. Optical absorption by the core is therefore predicted to be achiral. This is consistent with our experimental finding, where no new CD states emerge as the size of the QD core increases, (**Figure 3.10-3.14**). It must be concluded that optical absorption by the core is achiral, while absorption at surface defects is strongly influenced by the chirality of the surface layers. To summarise, chiral semiconductor QDs have been synthesized and modeled with density functional theory. This has been achieved by stabilizing CdS nanocrystals with the chiral ligand penicillamine. Weakly luminescent QD nanoclusters were prepared by adding thioacetamide to a solution of cadmium perchlorate and *D*-, *L*- or *Rac*-penicillamine. The QDs stabilized with *D*- and *L*-penicillamine show exactly opposite chiral optical responses. Based on calculated electronic states, we associate the longer-wavelength circular dichroism with near-surface Cd atoms that are enantiomerically distorted by the penicillamine ligands. Subjecting the QDs to microwave irradiation yielded larger, highly luminescent QDs. As mentioned earlier the broadness of the luminescence signal is indicative of a defective surface of the QD. The features in circular dichroism are red-shifted but no new features emerge, which is also consistent with growth of an achiral QD core, as predicted by our calculations.

Models of a typical QD surface show that the penicillamine ligand bonds via N and S to one surface-Cd, and introduces chirality via additional bonding of carboxylate to a neighbouring Cd. The interaction between ligand and cluster is strong, as is the interaction between ligands on the surface, compared to the weaker CdS surface structure. The ligands thus pack into helical bands on the surface and strongly distort the outermost Cd atoms of the QD, transmitting an enantiomeric structure to the surface layers. Significantly however, there is little distortion of CdS geometry in the QD core.

Therefore the three proposed models for circular dichroism in a QD with chiral ligands: (i) the core of the QD is chiral; (ii) the QD surface is chiral; (iii) only the adsorbate is chiral: have all been tested. Both the experimental and theoretical results

seem to the second support model. The control reactions in which tri-sodium citrate is exchanged for penicillamine and the resulting pen stabilized dots do not posses a optically active band edge not only help discount the third model but also reinforce that once the structure of the dots has been finalized there is no going back, (**Figure 3.17** and **3.18**). This is again become apparent in chapter 5 where the rigidness of the cubic structure of intrinsically emitting CdTe allows the quantum dots to exhibit only the weakest optical activity.

3.7 Cystein Stabilized CdS

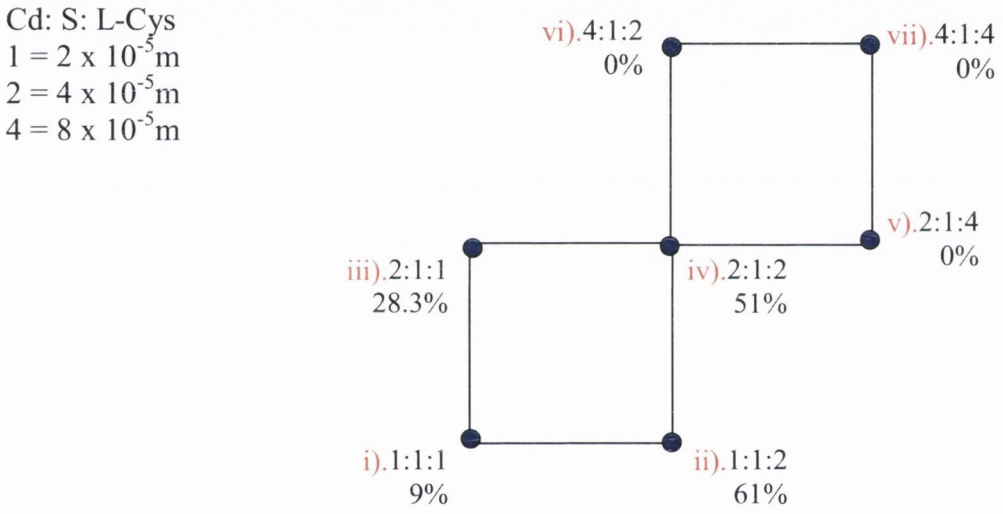

Figure 3.23: 2^2 statistical analysis of L-Cys-CdS. Quantum yields for each point were measured against Coumarin 153 in MeOH.

Cystein unlike penicillamine has been well documented as a quantum dot stabilizer and has been used to produce CdS, as well as CdSe and CdTe quantum dots. However, the CD activity of these nanocrystals has never been checked. To further explore this area for another stabiliser a 2^2 study of cystein stabilized CdS, (**Figure 3.23** & **Table 3.3**), was carried out and the particles were examined using CD spectroscopy. The quantum yields of the particles were also checked to confirm if the above mentioned increased luminescent intensity is actually genuine or just a result of greater particle formation with cystein coated dots.

Although batches 2 and 4 show extraordinary high quantum yields it must be remembered that all samples were excited at 380nm and consequently QYs were measured using this wavelength, (**Figure 3.24**). As both batches 2 and 4 show very little absorbance at this wavelength normalisation of their individual absorbance's with that of the Coumarin 153 lead to dramatic increase in their quantum yields. It is with this in mind that batch 3 was used to determine the presence of optical activity in cystein stabilized CdS.

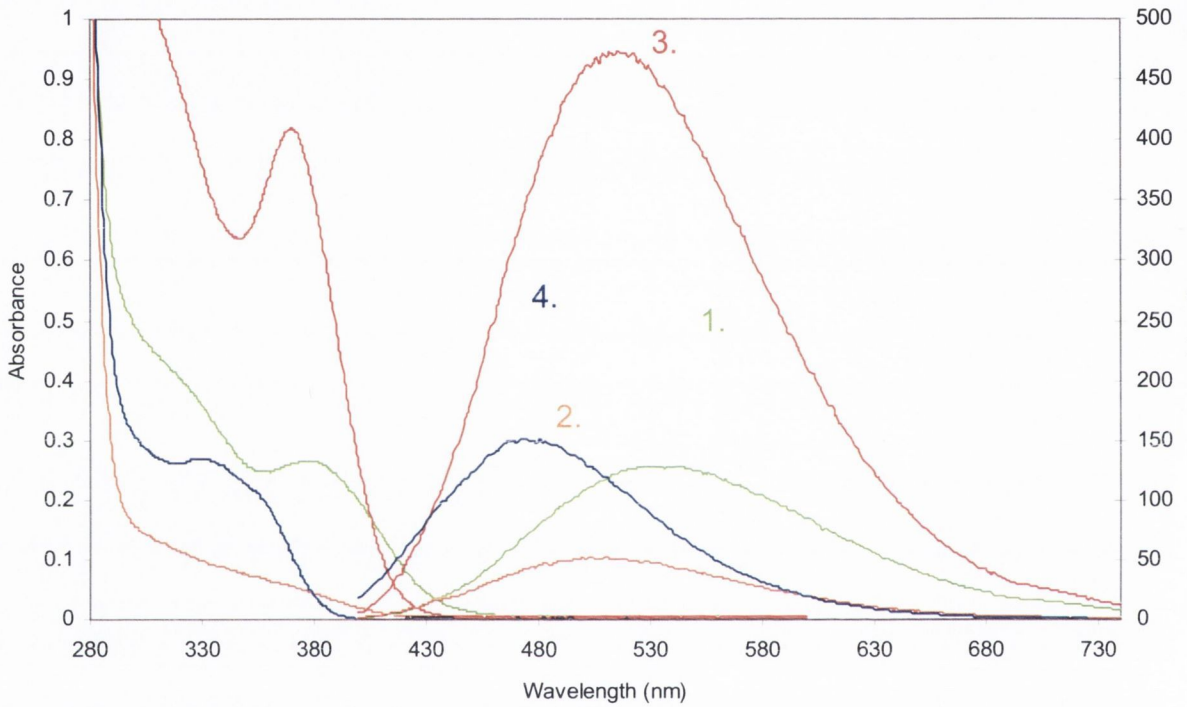

Figure 3.24: UV-Vis and Pl spectra of L-Cys CdS. All emission scans were excited at 380nm. Only samples 1-4 are shown as 5 showed no luminescence or quantum confinement and 6-7 precipitated $Cd(OH)_2$.

Table 3.3: Absorption, circular dichroism, emission and excitation, quantum yield for 2^2 statistical analysis of L-Cys CdS.

L-CdS	Abs	CD	Ems	Ext	Q.Y
1	386nm;0.25	400nm;-4.6 370nm;2.3 340nm;0.5	538nm	380nm	9%
2	377nm;0.06	381nm;-5.6 346nm;4.1 286nm;-3.2	512nm	382nm	61%
3	372nm;0.82	381nm;-5.6 348nm;8 319nm;-2	520nm	370nm	28%
4	360nm;0.18	347nm;-4.5 317nm;2.8	479nm	366nm	51%

Circular dichroism studies confirm that all particles are strongly optically active with very good agreement between the positions of the various CD peaks and positions of the various absorption signals and troughs, (**Figure 3.25**). As can be seen from batch 3, **(Figure 3.24),** the first peak in the CD spectrum is slightly red shifted with respect to the exciton band edge in the absorption spectrum, however as both spectra progress toward the blue region of the spectra they begin to align more closely with one another. This clearly shows that the ability to create optically active quantum dots is not limited to the use of penicillamine as a stabilizing molecule.

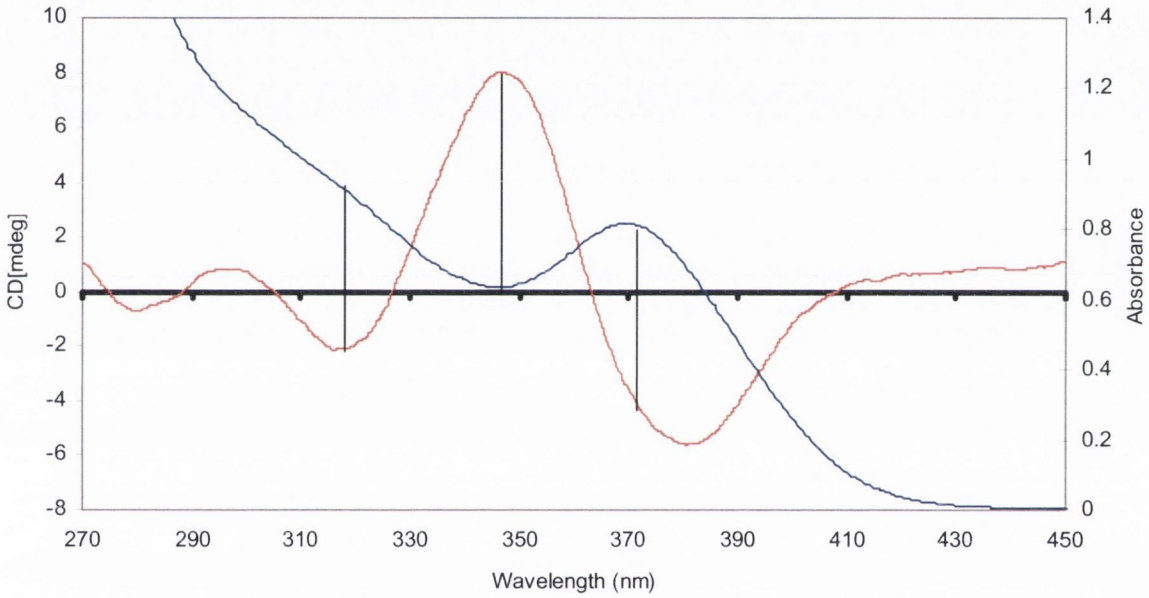

Figure 3.25: UV-Vis and CD spectra of L-Cys CdS. Both the first and second exciton peaks align quite well with the negative peak s in the CD spectrum. Also the trough in the absorbance spectra can be linked to the strong positive peak in the Cd spectrum at ~340nm.

3.8 Conclusions

In conclusion, strongly emitting chiral *D*-Pen and *L*-Pen capped CdS QDs have been prepared by synthesis of CdS particles in the presense of chiral penicilamine and cystein stabilisers. These particles demonstrated very strong and broad luminescence spectra. CD spectroscopy studies have shown that the CdS QDs are optically active and possess almost

identical mirror images of one another in the range of 200-390 nm. Density functional calculations reveal that penicillamine strongly distorts surface Cd, transmitting an enantiomeric structure to the surface layers and associated electronic states. The quantum dot core is found to remain undistorted and achiral. Therefore, although the particles posses a chiral shell and the cores of the particles remain achiral. This chiral shell contains chiral defects induced by chiral stabilizer (e.g. penicillamine) on the particle surface. Analysis of PL and CD spectra have shown that there is a clear relationship between defect emission and CD activity. Therefore we conclude that quantum dots must exhibit defect emission to posses CD activity. Although as the control experiment with non-chiral sodium citrate stabiliser showed, defect emitting dots are not nessecarily chiral. However, only chiral stabilisers can induce the light emmiting chiral defect states. Circularly Polarised Luminescence spectroscopy (CPL) have shown no optical activity in the light emitted by the chiral QDs was observed. This indicates that the luminescence from the defect trapped states on the surface of the particle does not result in circular polarised light.

We think that the ability to create optical active quantum dots is not restricted to penicillamine or cystein and it appears to be possible to create chiral dots using any chiral stabilizer. We also believe that these QDs could find important applications, including their use as fluorescent chemical and biochemical chirality sensors and molecular recognition nanodevices. In the next 2 chapters we are going to expand our investigation to CdSe and CdTe based chiral QDs.

References

[1] P. Alivisatos, *Nat Biotech* **2004**, *22*, 47.

[2] S. J. Byrne, S. A. Corr, T. Y. Rakovich, Y. K. Gun'ko, Y. P. Rakovich, J. F. Donegan, S. Mitchell, Y. Volkov, *Journal of Materials Chemistry* **2006**, *16*, 2896.

[3] N. Gaponik, D. V. Talapin, A. L. Rogach, K. Hoppe, E. V. Shevchenko, A. Kornowski, A. Eychmuller, H. Weller, *J. Phys. Chem. B* **2002**, *106*, 7177.

[4] T. M. Jovin, *Nat Biotech* **2003**, *21*, 32.

[5] A. W. Schill, C. S. Gaddis, W. Qian, M. A. El-Sayed, Y. Cai, V. T. Milam, K. Sandhage, *Nano Lett.* **2006**, *6*, 1940.

[6] W. C. Chan, nbsp, W, S. Nie, *Science* **1998**, *281*, 2016.

[7] M. Kuno, K. A. Higginson, S. B. Qadri, M. Yousuf, S. H. Lee, B. L. Davis, H. Mattoussi, *J. Phys. Chem. B* **2003**, *107*, 5758.

[8] N. N. Mamedova, N. A. Kotov, A. L. Rogach, J. Studer, *Nano Lett.* **2001**, *1*, 281.

[9] S. Y. Zhao, S. H. Chen, S. Y. Wang, D. G. Li, H. Y. Ma, *Langmuir* **2002**, *18*, 3315.

[10] D. Dorfs, A. Eychmuller, *Nano Lett.* **2001**, *1*, 663.

[11] T. Hirai, T. Saito, I. Komasawa, *J. Phys. Chem. B* **2001**, *105*, 9711.

[12] J. R. Lakowicz, I. Gryczynski, Z. Gryczynski, K. Nowaczyk, C. J. Murphy, *Analytical Biochemistry* **2000**, *280*, 128.

[13] B. I. Lemon, R. M. Crooks, *J. Am. Chem. Soc.* **2000**, *122*, 12886.

[14] D. Li, Z.-Y. Yan, W.-Q. Cheng, *Spectrochimica Acta Part A: Molecular and Biomolecular Spectroscopy* **2008**, *71*, 1204.

[15] Y. W. Lin, M. M. Hsieh, C. P. Liu, H. T. Chang, *Langmuir* **2005**, *21*, 728.

[16] Y. Liu, T. Tan, B. Wang, R. Zhai, X. Song, E. Li, H. Wang, H. Yan, *Journal of Colloid and Interface Science* **2008**, *320*, 540.

[17] S. W. Lu, B. I. Lee, Z. L. Wang, W. Tong, B. K. Wagner, W. Park, C. J. Summers, *Journal of Luminescence* **2000**, *92*, 73.

[18] Z. A. Peng, X. Peng, *J. Am. Chem. Soc.* **2001**, *123*, 183.

[19] S. Santra, H. Yang, P. H. Holloway, J. T. Stanley, R. A. Mericle, *J. Am. Chem. Soc.* **2005**, *127*, 1656.

[20] L. Spanhel, E. Arpac, H. Schmidt, *Journal of Non-Crystalline Solids* **1992**, *147-148*, 657.

[21] S. Wageh, Z. S. Ling, X. Xu-Rong, *Journal of Crystal Growth* **2003**, *255*, 332.

[22] S. Wageh, L. Shu-Man, F. T. You, X. Xu-Rong, *Journal of Luminescence* **2003**, *102-103*, 768.

[23] Y. Wu, L. Wang, M. Xiao, X. Huang, *Journal of Non-Crystalline Solids* **2008**, *354*, 2993.

[24] R. Xie, U. Kolb, J. Li, T. Basche, A. Mews, *J. Am. Chem. Soc.* **2005**, *127*, 7480.

[25] W. W. Yu, J. C. Falkner, B. S. Shih, V. L. Colvin, *Chem. Mater.* **2004**, *16*, 3318.

[26] W. Horst, *Angewandte Chemie International Edition in English* **1993**, *32*, 41.

[27] J. Chen, A. Zheng, Y. Gao, C. He, G. Wu, Y. Chen, X. Kai, C. Zhu, *Spectrochimica Acta Part A: Molecular and Biomolecular Spectroscopy* **2008**, *69*, 1044.
[28] Z.-X. Cai, H. Yang, Y. Zhang, X.-P. Yan, *Analytica Chimica Acta* **2006**, *559*, 234.
[29] J.-L. Chen, C.-Q. Zhu, *Analytica Chimica Acta* **2005**, *546*, 147.
[30] Y. Chen, Z. Rosenzweig, *Anal. Chem.* **2002**, *74*, 5132.
[31] H. Li, W. Y. Shih, W. H. Shih, *Ind. Eng. Chem. Res.* **2007**, *46*, 2013.
[32] J. R. Lakowicz, I. Gryczynski, G. Piszczek, C. J. Murphy, *J. Phys. Chem. B* **2002**, *106*, 5365.
[33] J. R. Lakowicz, I. Gryczynski, Z. Gryczynski, C. J. Murphy, *J. Phys. Chem. B* **1999**, *103*, 7613.
[34] M. Kundu, A. A. Khosravi, S. K. Kulkarni, P. Singh, *Journal of Materials Science* **1997**, *32*, 245.
[35] H. Bekele, J. H. Fendler, J. W. Kelly, *J. Am. Chem. Soc.* **1999**, *121*, 7266.
[36] S. D. Elliott, M. Moloney, x, chea, x, P. l, Gun, x, Y. K. ko, *Nano Lett.* **2008**, *8*, 2452.
[37] P. Xue, R. Lu, Y. Huang, M. Jin, C. Tan, C. Bao, Z. Wang, Y. Zhao, *Langmuir* **2004**, *20*, 6470.
[38] W. T. Sun, Y. Yu, H. Y. Pan, X. F. Gao, Q. Chen, L. M. Peng, *J. Am. Chem. Soc.* **2008**, *130*, 1124.
[39] W. Jiang, A. Singhal, J. Zheng, C. Wang, W. C. W. Chan, *Chem. Mater.* **2006**, *18*, 4845.
[40] C. Barglik-Chory, C. Remenyi, H. Strohm, G. Muller, *J. Phys. Chem. B* **2004**, *108*, 7637.
[41] T. G. Schaaff, R. L. Whetten, *J. Phys. Chem. B* **2000**, *104*, 2630.
[42] H. Yao, K. Miki, N. Nishida, A. Sasaki, K. Kimura, *J. Am. Chem. Soc.* **2005**, *127*, 15536.
[43] G. Shemer, O. Krichevski, G. Markovich, T. Molotsky, I. Lubitz, A. B. Kotlyar, *J. Am. Chem. Soc.* **2006**, *128*, 11006.
[44] H. G. P. T. Li, H. S. Lee, S. H. Choi, *Nanotechnology* **2004**, *15*, S660.
[45] E. Mullins, *Statistics for the quality control chemistry laboratory*, **2003**.
[46] D. Lawless, S. Kapoor, D. Meisel, *J. Phys. Chem.* **1995**, *99*, 10329.
[47] J. A. Kloepfer, S. E. Bradforth, J. L. Nadeau, *J. Phys. Chem. B* **2005**, *109*, 9996.
[48] T. Vossmeyer, G. Reck, B. Schulz, L. Katsikas, H. Weller, *J. Am. Chem. Soc.* **1995**, *117*, 12881.
[49] N. Herron, J. C. Calabrese, W. E. Farneth, Y. Wang, *Science* **1993**, *259*, 1426.

Chapter 4.

Cadmium Selenide

Introduction 4.1

CdSe like CdS and CdTe is a II-VI semiconductor which has little applications in the bulk state but over the last ten years there has been an increasing interest in CdSe based nanoparticulate materials.[1-6] A greenish-brown or dark red material with a wurzite structure in the bulk state, it can be quantum confined and depending on the size absorb anywhere between 380-600nm, although CdSe nanoparticles which absorb below 420nm are considered super small and are not commonly reported.[7] As for all quantum dots the photophysical properties of CdSe QDs can be tuned by controlling their size. This level of optical control coupled with their resistance to photobleaching and their high level of solubility in practically any solvent, (depending on the stabilizer used), makes them potentially useful for many applications including light emitting diodes[1] to biological sensors[8] to photovoltalics.[9-11]

Strongly emitting CdSe QDs are normally produced in organic solvents using hydrophobic stabilizers such as TOPO and HDA. These procedures involved the thermal degradation of TOPSe or TBPSe in the presence of a Cd-Alkyl-Phosphine complex; it was also found that control of the alkyl chain length lead to a high degree of morphology control of these particles.[3, 5, 6, 12-19] While these procedures result in strongly emitting monodisperse CdSe nanoparticles, they are not water soluble and this makes them impractical for biological applications. While it is possible to exchange these ligands for something more water soluble the results are mixed at best, usually resulting in a large reduction in the quantum yields unless such precautions as the introduction of epitaxial shell consisting of a second wider bandgap II-VI semiconductor is taken.[20] In this work we focus on the preparation and investigation of water soluble, highly luminescent nanoparticles and therefore only routes to produce the particles directly in water have been explored.[7, 13, 21-26]

4.1.1 Aims of this part of the work

The main aim of this part of our work is to produce and investigate new chiral CdSe based luminescent nanoparticles in aqueous solutions. As we have shown in the previous chapter it is possible to induce the chirality in CdS nanoparticles by using chiral stabilizers. With that in mind this part of our work is focused on developing of novel chiral CdSe QDs using the dextrorotary, (*D*-), and levorotary, (*L*-), enantiomers of appropriate stabilisers. We aim to explore whether the phenomenon of chiral quantum dots is restricted to CdS or if it can be extended to other QD systems. Also as the CdSe particles produced in this chapter both absorb and emit in the visible region it allowed us a chance to appraise their ability to interact with other chiral molecules. This ability to operate in the visible region was important as ultra-violet radiation is harmful to biological systems and if these particles are to eventually be used as fluorophores then they must be excitable at lower energies. One final goal of this chapter is too try and establish the link between type of luminescence and the presence of optical activity. Like CdS, CdSe can also demonstrate defect emission, which can be controlled by heating. We plan to explore the possibilities of controling the chirality and quantum yield of CdSe QDs by varying the synthetic conditions and ratios of chiral stabilisers. Properties of all CdSe QDs are to be investigated by TEM, UV-Vis, PL and CD spectroscopy.

4.2 Synthesis of chiral CdSe QDs

The dots were prepared as described in the previous chapter for CdS QDs by the method reported by Ni et al.[27] However in this case Na_2SeSO_3 was substituted for CH_3CSNH_2 as the X^{2-} source (**Figure 4.1**).[28, 29] The Na_2SeSO_3 was prepared using the method reported by Bhuse et al. and used immediately.[30] Once again 2^2 statistical studies were carried out on both the cystein and penicillamine stabilized dots using quantum yield as the response.[31]

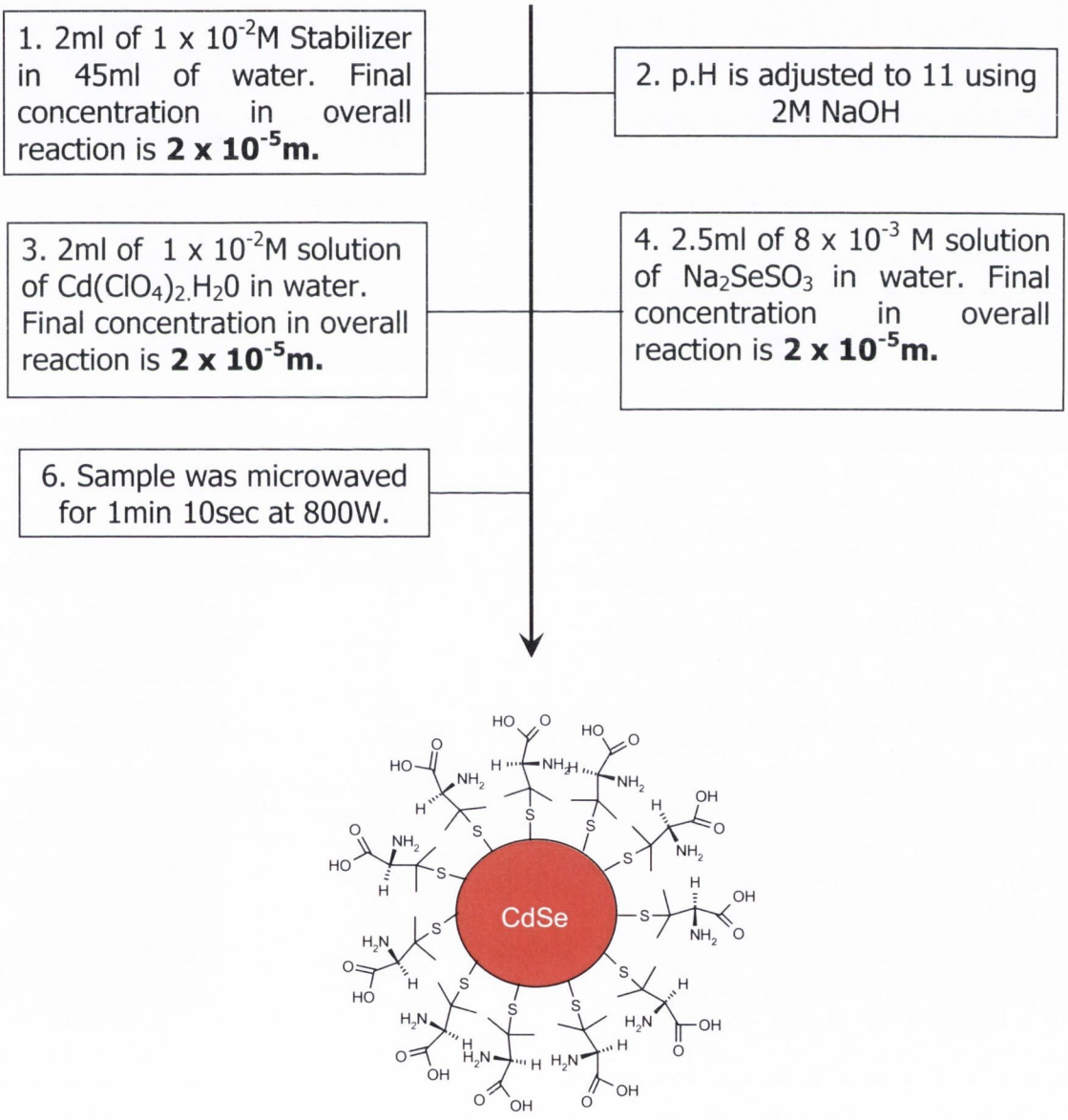

Figure 4.1: Schematic representation of CdSe preparation. The example used is the first point in a 2^2 study of CdSe. Both Cd and stabilizer concentrations are systematically increased while Se concentration stays fixed at 2 x 10^{-5} moles.

Briefly, 2ml of a basic aqueous 1 x 10^{-2}M solution of penicillamine, (2 x 10^{-5} moles of *D*-, *L*- or *Rac*), was added to 45 ml of Millipore water in a 100 ml round bottom flask. The pH was adjusted to 11 by the dropwise addition of 1M NaOH. 2 ml of a 1 x 10^{-2} M $Cd(ClO_4)_2.xH_2O$ and 2.5ml of an 8 x 10^{-3}M of Na_2SeSO_3 were then added and the solution was stirred vigorously. The resulting homogeneous solution was then placed into a conventional microwave and irradiated for 70 seconds at 850 Watts. The resulting clear, yellow solution was then returned to the conical flask and stored in the dark for at least one day. The volume of the colloid was then reduced to ~5ml using the rotary evaporator and propan-2-ol was added to precipitate out the nanoparticles. The particles were collected by centrifugation. The particles were washed several times with a propan-2-ol, water mixture, (9:1), and finally re-dispersed in millipore water. UV-Vis, CD and fluorescence spectroscopy was carried out on the stable suspensions in water.

4.3 Penicillamine Stabilized CdSe

4.3.1 Optimisation of the synthesis (statistical analysis)

As any change in the reaction conditions will affect the properties of the particles it could not be assumed that the cadmium to penicillamine ratio which gave the best results for CdS would do the same for CdSe. So, in order to determine what reaction conditions would give the most luminescent particle a new 2^2 statistical analysis was carried out for CdSe, however this time instead of seven, ten points were examined. The reaction scheme detailed in **Figure 4.1** was used as the starting point for a multi-factor study in which two directions on a Cartesian axis, x = cadmium and y = stabilizer, were investigated at 4 increasing and intersecting levels. These axes or levels correspond to the volume of the 1 x 10^{-2}M stock solution used, starting with 2ml of all three reactants and then doubling the volumes of Cd, along the y axis, and Pen, along the x axis, as in the previous chapter, leaving the X^{2-} component, in this case Se, static at 2ml, **Figure 4.2**.

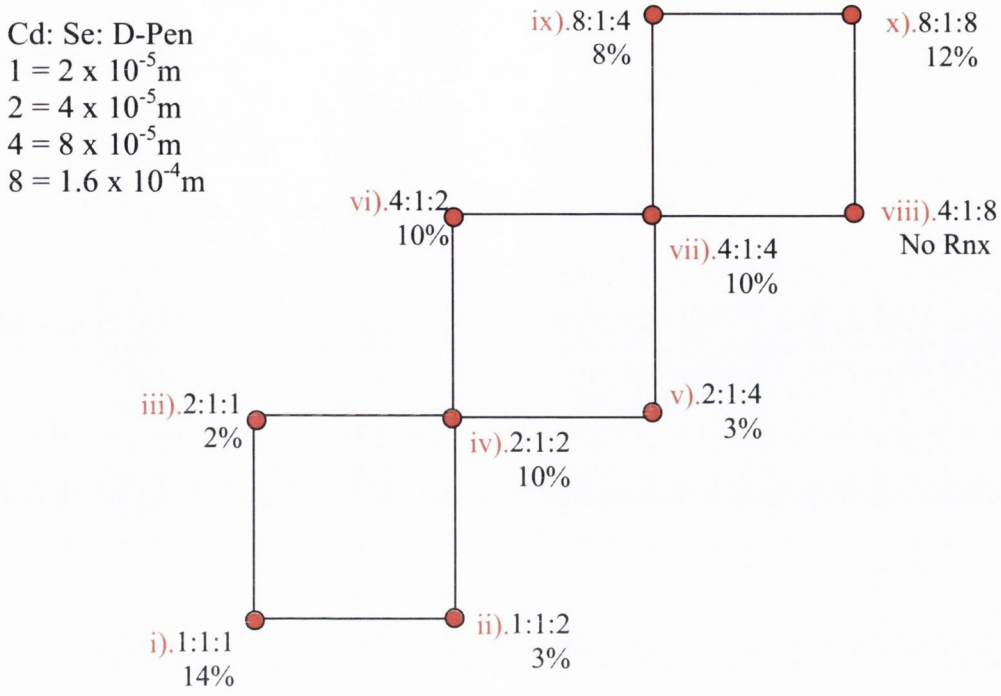

Figure 4.2: 2^2 statistcal analysis of D-Pen-CdSe. Quantum yields for each point were measured against coumarin 153 in MeOH.

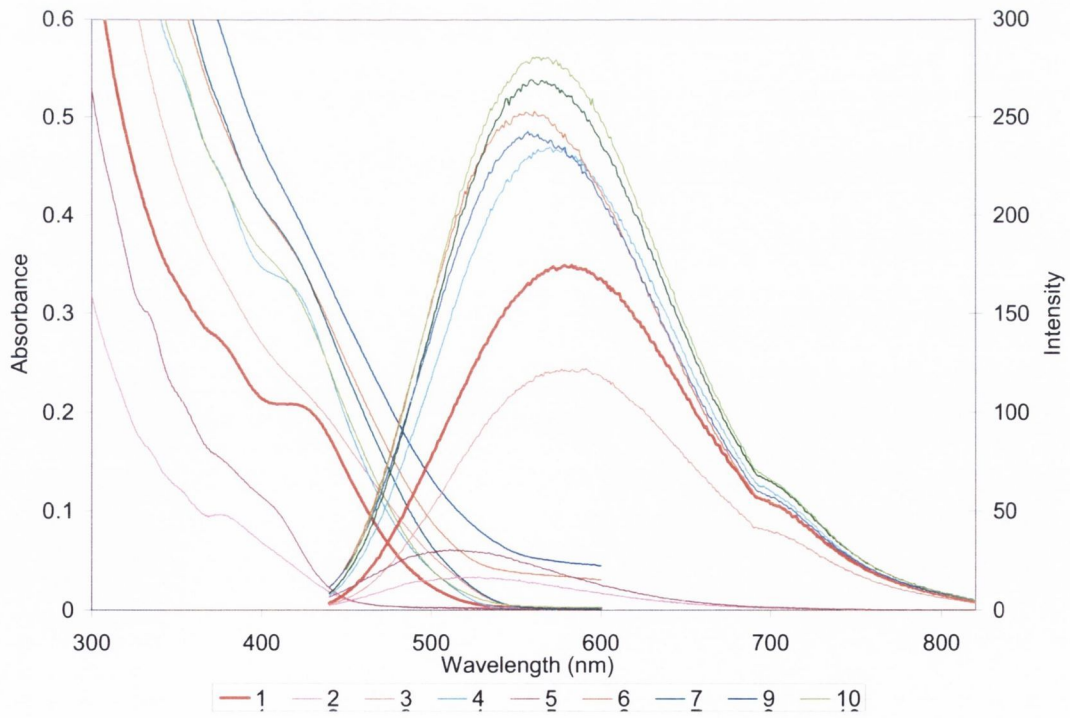

Figure 4.3: Absorption and emission spectra showing batches 1-7 and 9-10 of the above 2^2 statistical analysis of D-Pen-CdSe. All emission scans were excited at 420nm. Reactions where both metal and stabilizer were equal give both the highest QY's and most defined bandedge with point 1 being be far the best of these.

Although quantum yield was the primary response studied over the course of this analysis all particles produced were then examined using UV, PL, CD and PCS spectroscopy. **Figure 4.3** shows both absorption and emission spectra for batches 1-7 and 9-10, no reaction was observed for batch 8. If we split the analysis into three distinct parts by grouping the various batches into a) those with equal Cd to Pen concentrations, points 1, 4, 7 and 10, b) those where Cd is greater than Pen, points 3, 6 and 9, and finally c) those where Cd is less than Pen, points 2, 5 and 8, an unmistakable pattern then emerges.

In cases where cadmium is in excess no distinct band edges (there is no clear band in UV-Vis spectrum) are formed, and the luminescence is quite weak, an increase is only seen when the Cd concentration is doubled with respect to the Se, (points 3 to 6, **Figure 4.2**). The lack of band edge structure in the absorption spectra and the poor luminescence is attributed to poor quantum confinement due to an insufficient amount of stabilizer in the reaction(s). Examination of these particles using Dynamic Light Scattering, also confirmed that they were the largest in the analysis (see **Table 4.1**).

A significant improvement in the structure of the band edge is seen when Pen is in excess of the Cd, (batches 2 and 5 **Figure 4.3**), although the quantum yield remains low. There is an improvement in the structure and a blue shift in the position of the absorption maximum for batch 2, when compared with batches where the Cd concentration is greater than that of the penicillamine. Not only is the exciton peak now quite distinct but the maxima is at 380nm, well into the ultraviolet region of the spectrum indicating that they, (points 2 and 5), are smaller than the remaining particles. This reduction in size was dramatic enough to put them outside the range of the PCS, (Table 4.1). As the Pen concentration is increased the formation of CdSe dots is eventually halted. This is due to the high chelation effect of Pen for Cd and can be seen by the absence of any dots in point 8. Batches where both the Cd and Pen concentrations were equal, (1, 4, 7 & 10), produced dots with the highest quantum yields, (**Figure 4.4**). Interestingly, little or no improvement was seen in the Q.Y's of these particles as the Cd/Pen to Se ratio was increased. Normally increasing the metal concentration leads to an improvement in the luminescence of the particle as the excess Cd binds to the surface traps reducing the number of defects. In fact a negative effect was observed, as we increase the Cd/Pen concentrations. There was also a loss of band edge structure making point 1 not only the batch with the highest quantum yield but also the batch with the highest degree of quantum confinement.

Table 4.1: Absorption, circular dichroism, emission and excitation, quantum yield and size data for 2^2 statistical analysis of D-Pen CdSe.

D-CdSe	Abs	CD	Ems	Ext	Q.Y	Size(nm) from DLS
1	420nm;0.20 379nm;0.27	426nm;-3.3 365nm;-1.1 299nm;-4.8	581nm	434nm	13.6%	4.62±1.39
2	381nm;0.12	423nm;-0.7 392nm;-1.3 364nm;-1.6 267nm;-19	527nm	420nm	3%	n/a
3	428nm;0.2	426.4;-1.3 370nm;-0.4 287nm;-3.7	524nm	436nm	2.3%	10.8±2.04
4	413nm;0.4	425nm;-4.2 370nm;-2.8 300nm;-7.1 269nm;-10	577nm	432nm	9.9%	4.43±1.46
5	379nm;0.2	420nm;-0.5 387nm;-1.7 359nm;-3.1 300nm;-14	517nm	416nm	3.3%	n/a
6	426nm;0.37	421nm;-2 367nm;-0.7 286nm;-6.4	559nm	432nm	9.8%	16±4.38
7	423nm;0.36 381nm;0.53 358nm;0.65	423nm;3.4 368nm;-2.3 346nm;-2 326nm;-2.3 264nm;-23	565nm	436nm	9.5%	5.71±2.55
8	No Rnx	No Rnx	No Rnx		No Rnx	No Rnx
9	441nm;0.31	420nm;-1.9 367nm;-1 347nm;-1.1 325nm;-1.5 263nm;-19	563nm	432nm	8.1%	6.43±1.43
10	421nm;0.33 382nm;0.45 356nm;0.60	422nm;-3.73 367nm;-2.88 326nm;-4.8 283nm;-26.7 267nm;-38.2	566nm	433nm	11.7%	3.41±0.92

The strength of the CD response is of course strongly dependant on not only the presence or absence of optical activity but also on the overall particle concentration. By examining the degree of absorbance at the band edge regions it is easy to see that particle concentration varies from batch to batch, however this alone does not explain the varying degrees of optical activity at the band edge regions of the various particles produced. Close examination of **Table 4.1** shows that batches 1 and 3, although having similar degree's of absorbance at their respective band edge wavelengths of 420 and 428nm, do not have similar millidegree values at these wavelengths. In fact

while batch 1 has a value of -3.3 millidegrees, batch 3 has less than half that at -1.3 mdegs. This disparity in CD values can be seen throughout the stats analysis with particles that possess higher quantum yields having greater optical activity. It is with this in mind that a correlation must be drawn between luminescence and chirality, a premise that will be further investigated later in this chapter.

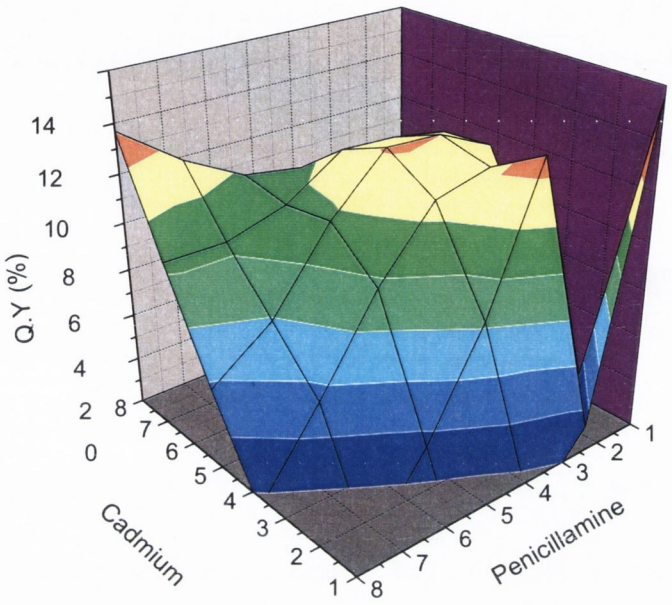

Figure 4.4: 3-D representation of a 2^2 statistical analysis of the formation of D-Pen CdSe using quantum yield as the response. Note how the yields peak at points where both metal and stabilizer are equal to each other. An Origin 7.5 random xyz matrix was used to generate the graph.

4.3.2 Optical Characterisation

Due not only to its high quantum yield but also its sharp absorbance peak and strong optical activity the CdSe particles produced at point i) of the statistical study were chosen as the best. The remainder of the study was then discarded and from now on only penicillamine capped CdSe with a ratio of 1:1:1 Cd:Se:Pen will be discussed. Particles were once again prepared using the D-Pen enantiomer and were re-examined using absorption and photoluminescent spectroscopy.

As shown in **Table 4.1** these particles exhibit an absorbance shoulder at 425nm which we believe corresponds to the exciton formation. A secondary exciton peak is also present at 379nm, this is characteristic for water dispersed quantum confined CdSe. The production of CdSe nanocrystals is confirmed by comparing the energy of

the shoulder at 420 nm, (2.95 eV), with that of bulk CdSe which absorbs at 712 nm, (1.74 eV) at room temperature, (**Figure 4.5**). This dramatic increase in band gap energy and accompanying decrease in absorbance wavelength can only accomplished by a decrease in the diameter of the crystal to a point less than that of the Bohr radius of it's exciton, i.e. quantum confinement.

Emission spectroscopy shows the presence of strong defect luminescence. This is confirmed by a) the large, (160 nm), stokes shift between the absorption and emission maxima's and b) the considerable width of the emission, FWHM of 162 nm, both of which, as mentioned in the previous chapter, are characteristic traits of defect emission. The dots were again excited at two different wavelengths, 420 nm and 450nm, to check the degree of monodispersity.

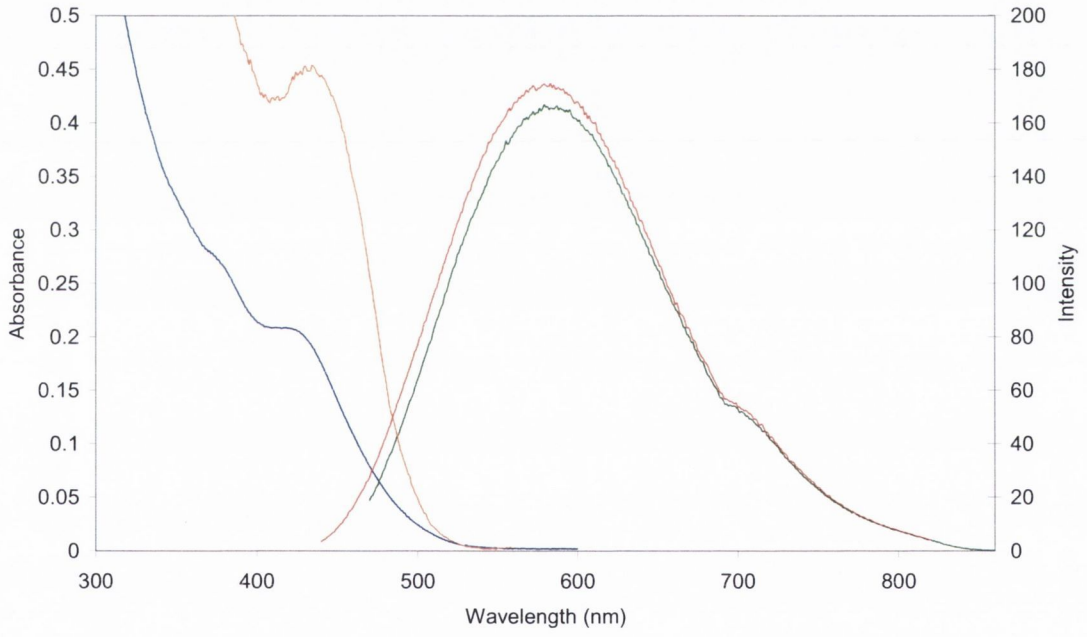

Figure 4.5: Absorption, (blue), emission, (red and green), and excitation spectra of D-Pen CdSe. Despite the strong degree of quantum confinement as illustrated by the sharpness of the absorbance and excitation shoulder at 425nm and 435nm respectively, the emission spectra clearly demonstrate the presence of a large number of surface defects. Emission spectra were excited at 420nm, (red), and 450nm, (green). The excitation scan was recorded at 585nm.

While the emission maximum does red shift by 2nm when the excitation wavelength was changed, indicating a slight variation in particle size, when compared to the width of the emission this shift is negligible. There is also what appears to be a second peak, ~710 nm, partially hidden in the tail of the "main" emission, however since this

second peak does not move when the excitation wavelength is changed, and since it also appears in all of the dots produced during the statistical analysis we assume that it is an integral part of the dot's emission spectrum. The excitation spectrum, taken at 585nm, shows two peaks at 435 nm and 386 nm, both of which correspond to those seen in the absorption spectra. The 10 nm red shift is due to a loss of energy probably via non radiative recombinations caused by the high number of defects on the nanocrystal's surface, **Figure 4.5**. Although not shown an excitation spectrum was also taken at 710nm to try and determine if the "bump" in the tail of the emission was most likely due to the presence of larger particles which were not visible in the absorption spectrum, however the spectrum returned an excitation peak at 435nm.

Once the D-Pen stabilised QDs were successfully prepared and characterised, L-Pen and Rac- stabilised CdSe dots were then synthesised using L-Pen and an equal amount of D- and L-penicillamine as the stabilisers respectively. As with the penicillamine capped CdS, (Chapter 3.), both the D- and L- stabilized particles showed almost identical absorption and photoluminescence spectra, however the racemic particles were once again slightly blue shifted indicating a slightly smaller primary particle size, **Figure 4.6**. Quantum yields, which were once again calculated using Coumarin 153 in methanol as a standard, showed both D- and L- Pen CdSe have a Q.Y of 12 ± 1 %, which then almost doubles for the R- sample to 22%. These differences in the photophysical properties of the Rac-Pen stabilised particles when compared with the D- and L- dots is again attributed to the complementary nature of the amino acids allowing for closer packing of the stabiliser molecules from Racemic mixture at the surface of the quantum dot. Talapin et al. demonstrated that luminescent strength is not simply a factor of particle size nor can it be attributed to shape or relative crystallinity, i.e. similar particles can have different QY.[18] They postulated that particles with the "the smallest net growth rate" would have the highest luminescence, however these were intrinsically emitting particles and so this hypothesis may not be applicable for the CdS and CdSe dots which both demonstrate defect emission. Another possibility is that the greater hydrophobic nature of the Racemic coating excludes water molecules from the surface of the particles which would otherwise quench the luminescence. Perhaps it is a mixture of both these effects. Taking these results into account, (as for all quantum dots reported in this thesis), we suggest that combinations of differing optical isomers affect the way in which that particular ligand controls this net particle growth rate.

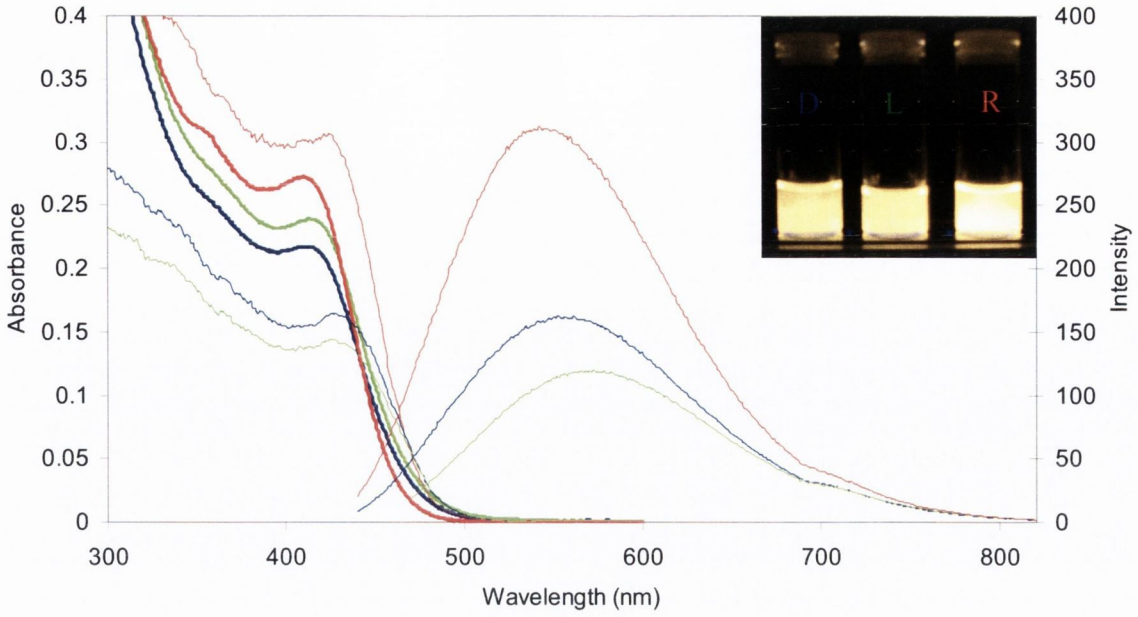

Figure 4.6: UV-Vis and PL spectra of D-Pen CdSe, (Blue), absorption, emission and excitation maximums at 421nm, 562nm, 431nm, respectively. L-Pen CdSe, (Red), Abs 421nm, Ems 577nm, Ext 431nm and R-Pen CdSe, (Lime), Abs 418nm, Ems 550nm, Ext 427nm All Pl emission were excited at 420nm and excitation scan were recorded at 560nm. Inset: Picture of D-, L- and R- emitting yellow-white light while being excited using a 365nm lamp. All three types of dots appear yellow in both visible light. The higher quantum yield of the R- dots is clearly visible in the picture.

Sharp exciton peaks for all three types of dots were recorded around 420nm and as previously reported D- and L- enantiomers are almost identical with the racemate being slightly sharper and shifted to the blue, this is attributed to better packing around the surface of the complimentary amino acids. The emission spectra show that all three particle types exhibit strong defect luminescence, all excitation spectra are, as seen in the statistical analysis, red shifted by 10nm from the absorbance maxima's, again the reason for this is believed to be a slight loss of energy due to non-radiative recombinations as a result of surface defects.

4.3.3 Luminescent Lifetimes of Pen-CdSe

It is generally accepted that the better the intrinsic quantum yield of a quantum dot the closer the decay profile approach a single exponential function.[14, 32] Also when building core/shell, quantum well structures it is not uncommon to move from a single to multi exponential fit as shells are added.[33] Generally, photoluminescent decays of quantum dot emission use bi-exponential distributions in establishing the decay profile; that is each life time is made up of two components.[34, 35] Typically the shorter lifetime, τ_1, is attributed to the intrinsic recombination of the initially

populated core states.[36-39] The origin of the longer component τ_2 although long disputed is now considered to be a result of the interference of surface states, (i.e. the presence or absence of surface defects), with the recombination of the electron-hole pairs.[40, 41]

Table 4.2: Life time data for D-, L-, and R-Pen CdSe nanoparticles, using a bi-exponential fit. τ_1 is believed to be the time taken for the intrinsic recombination of the excitons in the core of the particles, while τ_2 is the recombination of either holes or electrons with surface traps.

	τ_1 (ns)	τ_2 (ns)	χ^2
D-CdSe	3.29	45.4	0.924
L-CdSe	4.83	50.4	0.968
R-CdSe	5.22	53.8	1.04

Initially a bi-exponential fit in the 500ns range was used when calculating the lifetimes of all three types of dots. Despite the quantum yield of the R-Pen CdSe being almost twice that of the D- and L- dots only a slight increase in the life time of the R- dots is seen. L- and D- also have slightly different lifetimes from one another despite have the same quantum yields, **(Table 3.2)**. However examination of the decay curve indicated the presence of a longer component to the overall emission lifetime. Re-examination of the particles over a 1 μs range allowed the decay curve to return to zero giving a much more complete picture of the various emission components. As mentioned above a bi-exponential fit is usually applied when trying to elucidate nanoparticle lifetimes, however any attempt to fit these particles using only two components returned unacceptable χ^2 values, ~2. Another problem with a bi-exponential fit was that the two lifetimes it now gave were a τ_1 in the high 10s of ns and a τ_2 in the 100s of ns, any sign of the core component had been removed. However by using a multi-exponential fit, (in this case three), the shortest, (core), lifetime is retrieved.[2, 38] By examining all three particles, (D-, L- and R-), in the 1 μs range a much clearer picture begins to form, not only do we now see all components of the fluorescent decay but we now also see a correlation beginning to appear between the lifetime and quantum yield data, with D- and L- particles now showing almost the same values for τ_1, τ_2 and τ_3 while the R- particles, which have a Q.Y twice that of D- and L- shows substantial increases in all three components.

Table 4.3: Life time data for D-, L-, and R-Pen CdSe nanoparticles, using a tri-exponential fit. Lifetimes are recorded under air (O2) and under Argon (Ar) . Note the higher contribution of τ_2 in the R- particles indicating a greater contribution of surface states to the overall decay. This is in perfect agreement with the higher Q.Y of the R- particles. Lifetime errors were below 3ns for τ_2 and τ_3, and below 0.5ns for τ_1.

	Q.Y%	χ^2	A	τ_1(ns)	B_1	$B_{\%}$	τ_2 (ns)	B_2	$B_{\%}$	τ_3(ns)	B_3	$B_{\%}$
D-$_{O2}$	10±1	1.062	28.1	9.6	3322	39.5	50.1	3320	39.5	166.5	1751	21
L-$_{O2}$	10±1	1.01	47.7	10.8	3002	38	49.8	3100	39	161.9	1774	23
R-$_{O2}$	23±2	0.99	37.9	14.9	2795	33	67.5	3600	43	186.5	2047	24
D-$_{Ar}$	10±1	1.153	43.2	8.5	4494	46.5	48.3	3445	35.5	168.9	1753	18
L-$_{Ar}$	10±1	1.06	48.7	9.6	2836	36	48.4	3260	41.5	172.2	1771	22.5
R-$_{Ar}$	23±2	0.9	42.3	11.6	2411	28	58.9	3769	44	183	2441	28

Although bi-exponential fits are common for calculation of lifetimes of QDs, multi-exponential fits are used very frequently. For example, Hines et al. working with TOPO capped CdSe and CdSe/ZnS particles demonstrated that the photophysics involved in the calculation of emission decays for mixed emitting, that is defect and intrinsic, particles is far more complex than a simply accounting for a core and a shell component.[2] They also showed that it is not uncommon to have lifetime values in the hundreds of nanoseconds for CdSe, which will be considered at the end of this section.

As more and more work is done on trying to understand the nature of these particles it is becoming more and more widely accepted that it is the overall contribution of the lifetimes, i.e. the **B** factors, rather than the lifetimes themselves which are of importance. Again, Hines et al. showed that by replacing the TOPO shell of CdSe particles with a ZnS shell, which passivated the surface causing an increase in the quantum yield, caused a large increase in the contribution of the 20-30ns component. Also Wang et al. using a process of photo-oxidation to increase the number of defects on the surface of CdSe particles clearly demonstrated that as the quantum yield decreases the contribution of the longer lifetime(s) also decreases.[40]

As stated earlier we believe that the presence of both D- and L- enantiomers on the surface of the R-Pen stabilised particles allows for closer packing of the stabilizer

molecules due to their complimentary nature. This closer packing should results in the greater hydrophobicity of the racemate, removing the quenching water molecules from the surface of the particles, thereby increasing their quantum yields. With the increase in QY, an increase in the lifetimes should also occur, and it does. However according to Wang et al. an increase in the contribution of the longer lifetimes should also occur.[40] If we accept that the shortest component of the lifetime is generated by the initial charge carriers recombining in the core then any longer lifetimes must be due to the interaction of the exciton pair with any surface states. Not only that, but the longer components must be due to radiative recombinations with the charge carriers as the QY increases as the contribution of the longer life times does. By examining the **B** factors of each lifetime of all three types of dots we see that this is indeed the case, (**Table 4.3**). Little or no change is seen in $\mathbf{B_3}$, the longest life time, however while the D- and L- particles have almost identical B values for τ_2 and τ_3, the R-particles show a much higher contribution for τ_2, 68% against D- and L-'s 50%. This indicates a much higher degree of surface related emission in the R- sample, and accounts for it higher quantum yield.

Finally, in the case of CdSe nanoparticles it is unusual, though not uncommon, to see lifetimes in the hundreds of nanosecond range. [2] Although it must be pointed out that it only contributes 20% of the overall lifetime with the bulk of the decay been composed of the small and medium lifetimes. Carrier transfer to non-radiative surface defects usually happen within 10's of picoseconds so these are immediately ruled out. The presence of a CdS shell could also account for the presence of such long lifetimes. However, the presence of such a shell is highly unlikely. The deposition of a CdS shell without the associated extra experimental step is usually accomplished by the decomposition of the core particle's sulphur based stabilizer. This is done through long term heating, or irradiation, or photo-decomposition. However, none of these processes have being applied to these particles. Even though they have been prepared by microwave irradiation, the above described process usually takes hours to accomplish this. [42] These particles however, were only exposed to microwave irradiation for 70 seconds.

Also the long lifetime produced by the presence of a ZnS or CdS shell usually only contributes 10% to the overall lifetime where as the contribution of the 100s of nanosecond lifetimes described here are ~20%.

Normally when CdSe nanoparticles exhibit these kinds of lifetimes it is due to the presence of both intrinsic and defect emission in the particles with the lifetime in the 100 ns range contributing about 50% of the overall lifetime. Although the particles described in this work are already defect emitting they posses two distinct emission peaks, one at 585 nm and one at 700 nm. Size selective co-precipitation as well as numerous photochemical experiments described above has also verified that this peak at 700 nm is an inherent part of the emission profile of these particles and not due to the presence of another, larger, dot. Although no lifetime studies were carried out on them Chen et al.[7] have reported similar emission spectra for mercaptopropanoic acid stabilized CdSe nanoparticles. There is a possibility that the longest lifetime component is caused by the second emission peak at 700nm, as the further into the red the emission the longer its corresponding lifetime.[43]

One last possibility is that both the multiexponential fit and the presence of a lifetime component in the 100s of nanoseconds is a result the chiral shell surrounding the achiral particle core. Although CD and PL spectroscopy studies for CdS proved that the emission for these types of particles is not chiral there are still chiral defects present on the surface of these particles, which give the defect luminescence.

4.3.4 Circular Dichroism measurements

Circular dichroism spectra of the particles showed that, as with the CdS particles discussed in the previous chapter, the particles themselves possessed an optically active bandedge.[44] Spectra of both the D- and L- particles showed them to be optically active from 200nm right out to the onset of absorbance of the particles, i.e. ~485nm, (**Figure 4.7**), with R-CdSe particles showing no optical activity as expected. Although no computational studies were carried out on these particles we believe that model used for penicillamine capped CdS can also be applied to these particles. Therefore the same hypothesis is put forward that the presence of an optically active band edge in these particles is again the result of an achiral semiconductor core surrounded by a chiral semiconductive shell, which is in turn stabilized by chiral ligands. Again the presence of defect emission, which we believe is essential for producing chiral nanocrystals, adds credence to this hypothesis. This connection between defect emission and optical activity will be further discussed later in this

section. Due to the complexity of chiral signal, the CD's spectra showed not only the presence of the ligand but also a chiral exciton bands (**Figure 4.7**), the same monitoring experiments as were carried out on the CdS systems were also carried out here. That is, in order to get a clearer picture of what was happening during the synthesis of these dots, all points of the reaction, {i.e. preparation of penicillamine solution, addition of cadmium, addition of selenium and the eventual microwaving step} were all monitored using absorption and circular dichroism spectroscopy, **Figures 4.8 & 4.9**. Steps 1 and 2 are of course identical to those carried out for penicillamine capped CdS, **Chapter 3**, however, unlike the CdS preparation the addition of the X^{2-} ion, (step 3.), does not result in the formation of luminescent small nanocrystals but non-emitting CdSe nanoclusters with an absorption maxima of 290nm.

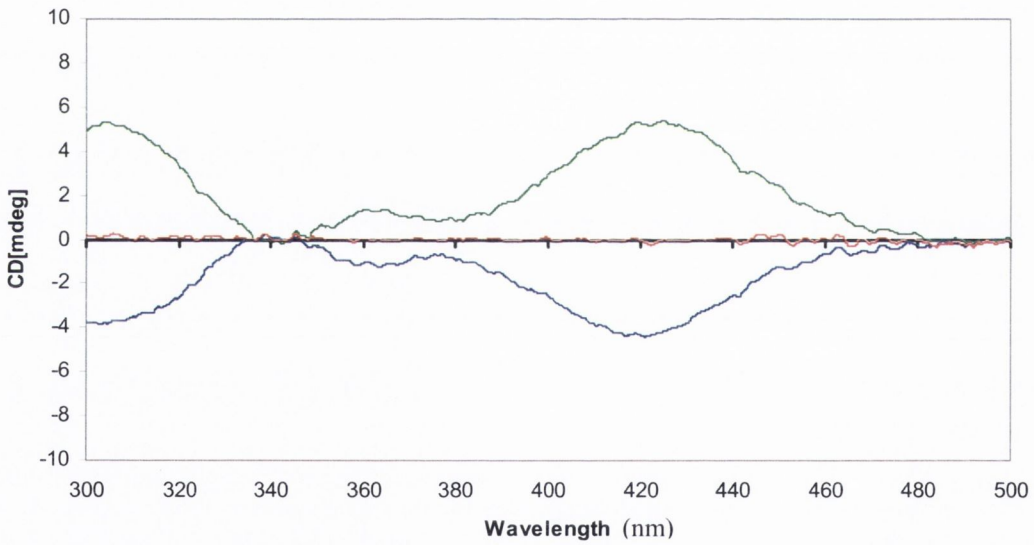

Figure 4.7: CD scan of penicillamine capped CdSe. D-, (Blue) L-, (Green) and Rac-, (Red). (θ deg = δA/32.98).

This difference is probably due to the increase in the penicillamine to cadmium ratio, when compared with the CdS reaction, halting the formation of any larger particles before the heating step. In step 3 we also see a reversal in the chirality of the Cd-Pen complex as the signal at 210nm switches from the negative to the positive region of the spectrum.

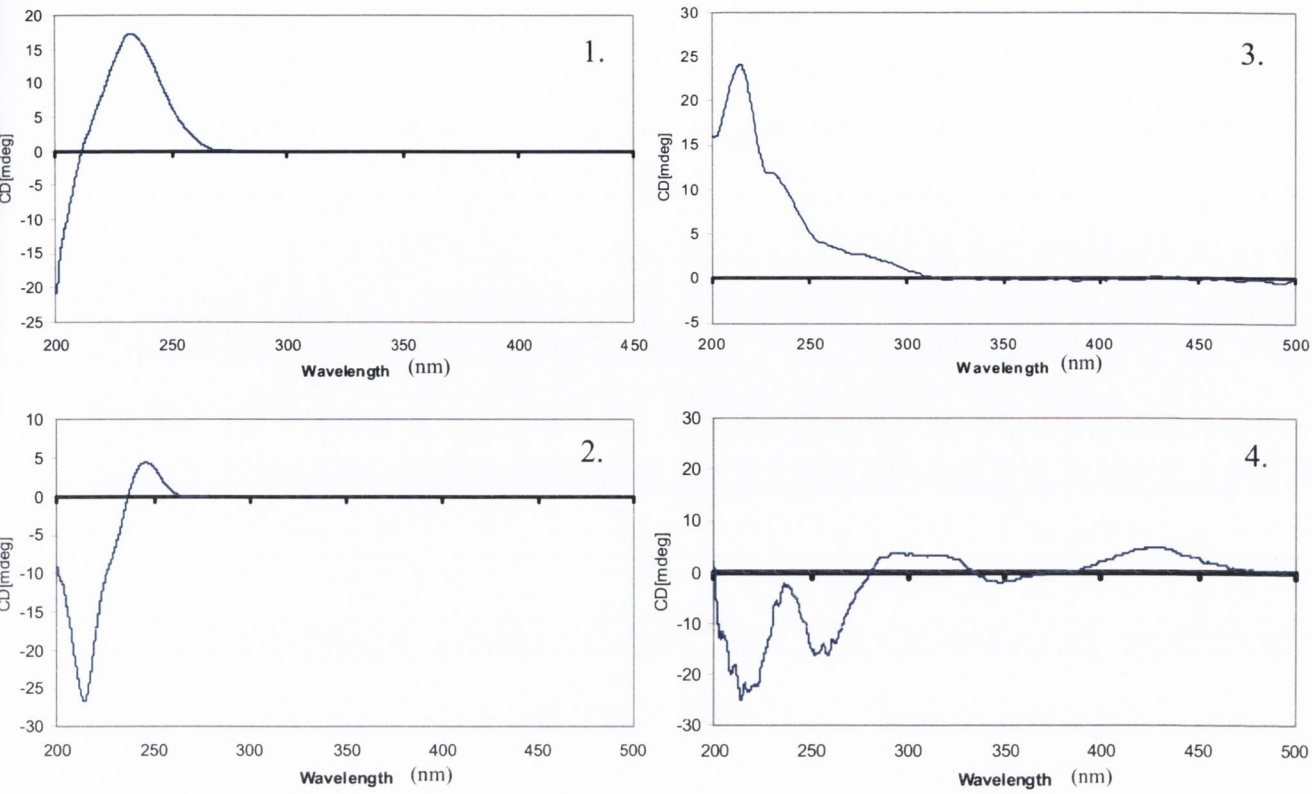

Figure. 4.8: CD monitoring of the formation of L-Pen CdSe. **1.** The free stabiliser is shown at 235nm. **2.** Addition of Cd causes the formation of new bands at 215, (complex), and 250nm, (red shifted Pen band). **3.** Clusters were formed after addition of the Na_2SeSO_3 but before microwave treatment, new bands formed from 250 to 306nm, well in the deep UV, indicating the clusters extremely small size **4.** CdSe nanocrystals formed after microwave treatment, new signals have appeared from 306 to 430nm, including the nanocrystal exciton peak. Note: the final CdSe samples were not purified in these monitoring experiments. Due to the high absorbance between 200-300nm after microwaving the sample was diluted by at least factor of 8 scanned and then normalised hence the high degree of noise in this region.

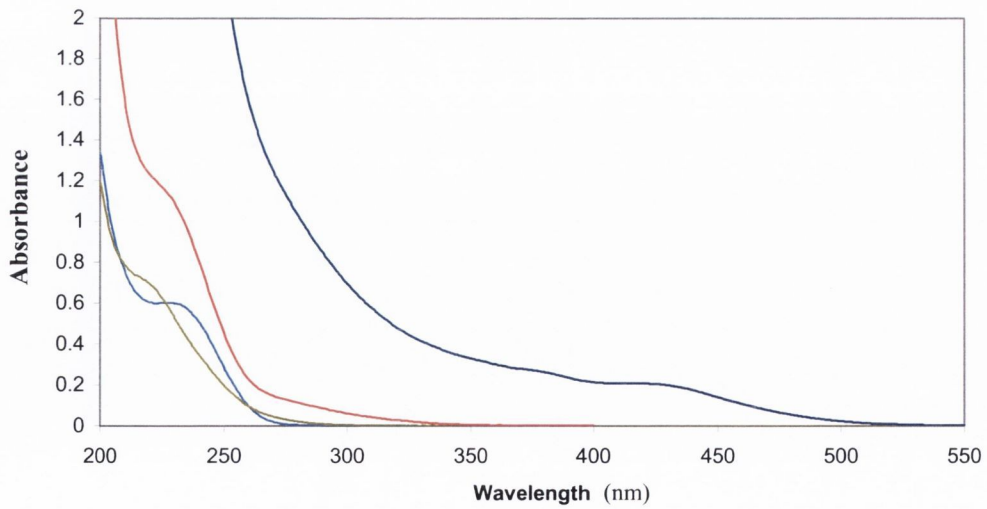

Figure 4.9: UV-Vis monitoring of the formation of *L*-Pen CdSe. **Light Blue:** The free stabiliser is shown at 235nm. **Green;** Addition of Cd causes the formation of new bands at 215, (complex). **Red:** Clusters were formed after addition of the Na_2SeSO_3 but before microwave treatment, Penicillaimne band reappears at 235nm as well as a nanocluster shoulder at 306nm, this is well in the deep UV, indicating the clusters extremely small size **Dark Blue**: CdSe nanocrystals formed after microwave treatment, new signals have appeared at 425 and 381nm which we refer to as the first and second exciton peaks respectively.

After the nanoclusters were heated in the microwave, (Step 4.), we see the formation of the distinct particle exciton band at 424nm as well as another signal at 350nm which we were not able to identify, but appears to correspond to change in the gradient of both the absorption and excitation spectra of the respective particles, **Figure 4.6**. Like the Pen-CdS reported in the previous chapter the CdSe quantum dot appear to grow in a direction opposite to that of the stabilizing ligand however what makes this different from the CdS preparation is that the ligand itself now shows opposite chirality. That is, in the case of L-Pen CdSe for example, the band edge region is now in the positive, (levorotary), region of the spectrum while the L-Pen peak at 232nm has reversed its direction and is now showing a negative millidegree value, i.e. dextrorotary, **Figure 4.8**.

4.3.5 TEM characterisation

TEM imaging of individual Pen-CdSe particles, proved extremely difficult without ADF, **Figure 4.10**. The size of ~5nm is typical for particles which absorb at 420nm and is in good agreement with the zeta-sizing results. However, TEM clearly showed the extent of the aggregation with large spherical "particles" with average sizes of 20nm ± 7nm for D- and 45nm ± 7nm for L- dominating the grids, **Figure 4.10**. {It must be noted that these aggregation effect may be due to the drying of the sample on the TEM grid.}

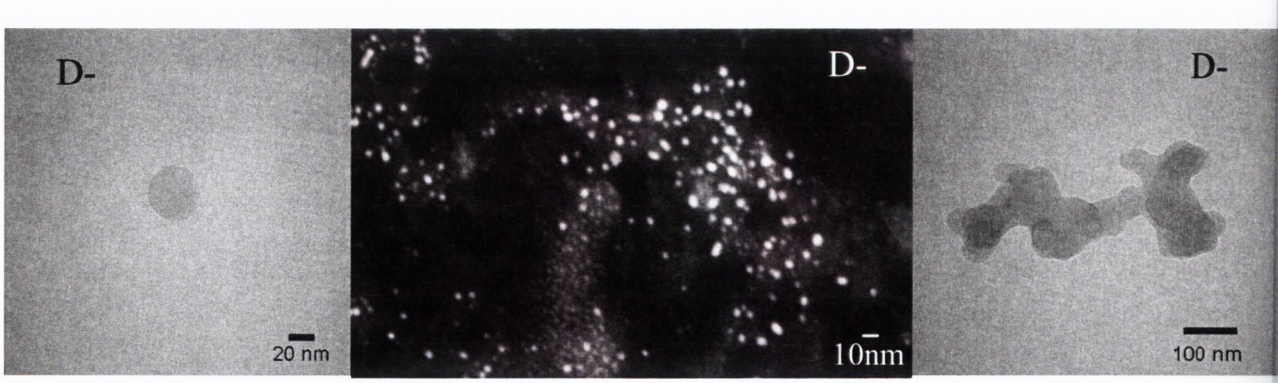

Figure 4.10: TEM (left and right) and ADF (centre) for Penicillamine-CdSe. Both D- and L- particles have identical spectroscopic and image data. Although particles appear to be too large, (~30nm), and aggregate frequently, ADF shows individual particle size to be closer to 5nm the size which is expected for quantum dots with exciton peaks at 420nm.

These sizes are of course much larger than expected for particles which absorb at 420nm and close examination of these large spherical objects showed them to be aggregates of smaller dots. By focusing the beam on these spheres it was possible to break them down into individual particles by burning of the excess stabilizer.

Unlike the D- and L- particles R-Pen stabilized dots have a trend to form high numbers of what appeared to be rod-like structures. Although there were also some spherical particles in the size range of 20±10nm, the sample was mainly made up of 5-10nm thick and 30-70nm long needles, **Figure 4.11**.

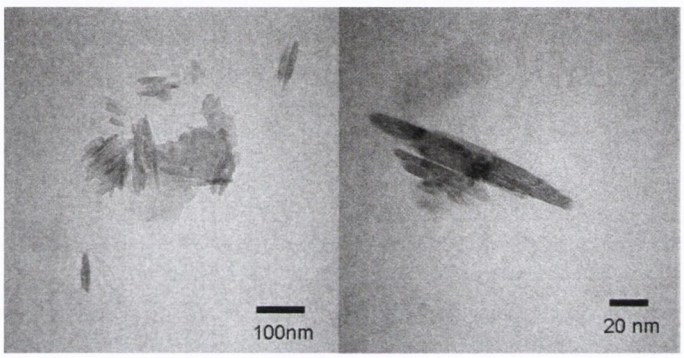

Figure 4.11: TEM for R-Penicillamine-CdSe. Particles aggregate into rod-like formations.

Due to the lack of spectroscopic evidence to suggest the presence of such large structures, whether they are spherical or oblong, we believe that these are in fact not single crystalline objects. Rather they are aggregates which are composed of individual particles. Size selective co-precipitation of the R-CdSe particles allowed us to isolate the rods and using dark field imaging, (ADF), confirmed that they were composed of smaller dots arranged into oblong structure, **Figure 4.12**. Interestingly the rods were found in the supernatant and not the centrifuged fractions. ADF showed that while the nanoparticles contained in the centrifuged fractions were 4.4nm ± 0.7nm the particles which made up the rods were about half that size at 2.4nm ± 0.5nm.

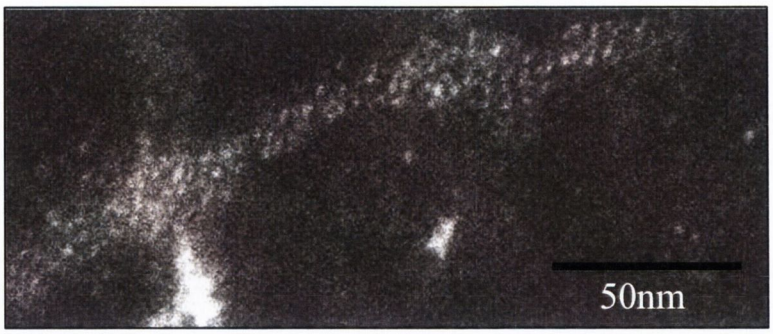

Figure 4.12: ADF image for R-Penicillamine- stabilised CdSe. 5nm particles aggregate into 30-70nm long needle-like assemblies.

This small size not only explains their presence in the supernatant but also the 50nm blue shift in their absorbance spectrum when compared with the recovered fraction, (**Figure 4.13**).

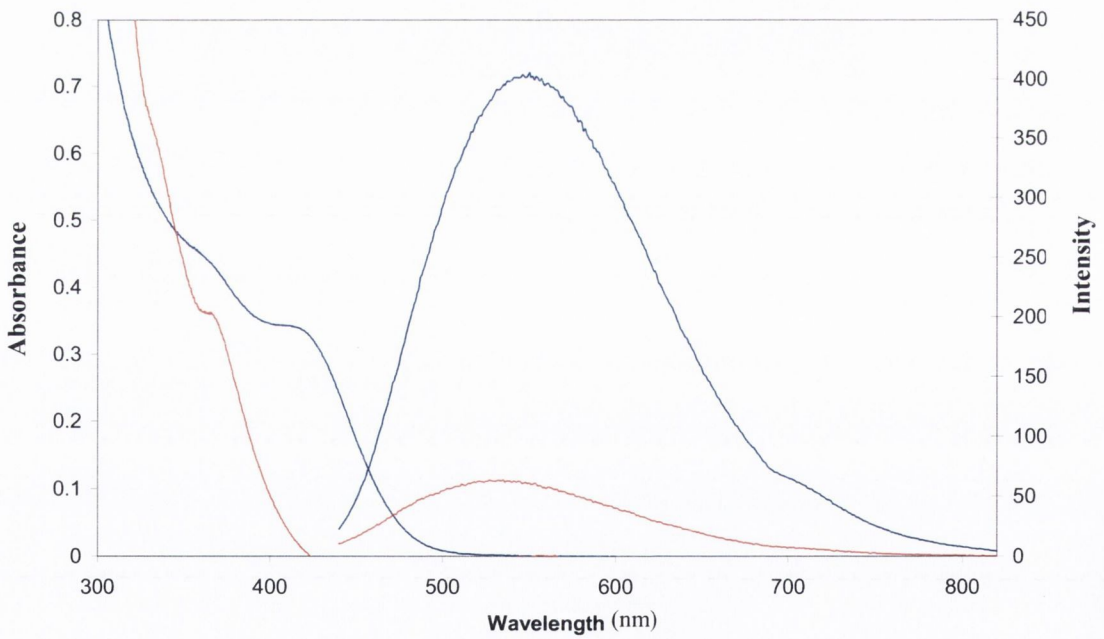

Figure 4.13: Absorption and emission spectra of R-CdSe, blue spectra represents particles which were precipitated out after 1000rpm, (absorbance-419nm, emission-552nm), and the red spectra is the remaining supernatant, (absorbance-367nm emission-535nm).

Nanoparticles, (≤10nm), usually require prolonged heating at high temperatures to form nanorods or other larger morphologies and this growth is always accompanied

by a red shift in both the absorption and emission spectra.[45] However little or no difference is seen in the UV-Vis and Pl spectra for any of the Pen-CdSe particles even though their TEM profiles show particles of radically different size and shapes. As mentioned earlier DLS measurements were inconclusive, however they did suggest the presence, (as does UV-Vis), of nanoparticles in the 5-8 nm range. Another explanation may be that the presence of the complimentary D- and L- amino-acids allows for the formation of a long chain which the particles then grow along. This phenomenon has already being reported with L-Cys stabilized CdTe QDs but it was believed that an excess of Cystein as well as the presence of a co-stabilizer, (Sodium Tri-Citrate), was need to achieve this.[46]

4.3.6 Conversion of Defect to Intrinsic emission

As mentioned in the previous section we believe that for a quantum dot to be optically active it must also express defect emission. These defects are more than likely caused by the presence of the ligand mediated chiral semiconductor shell around our achiral core. To prove this suggestion we attempted to remove these surface, (chiral), defects by annealing the particle surface via heating either by microwaving or heating under reflux.[42] The effect can be seen by the switching, (or not), of the luminescence from defect to intrinsic. An intrinsic emission is different to a defect one in one distinct way; the emission peak appears much narrower than a defect one with a full width half maximum of under 35nm compared to a defect emission FWHM of ~120 nm, there can also be a larger Stokes shift between absorption and emission maxima although this is not always so.

Due to the long refluxing time the concentration of cadmium and penicillamine was increased by a factor of sixteen making the reaction ratio of Cd:Se:Pen; 16:1:16. This high concentration of both metal and stabilizer was chosen to ensure enough of both the metal and stabiliser were present to facilitate a) the eventual particle growth due to the prolonged exposure to high temperatures and b) to replace any stabilizer which may undergo thermal decomposition on the particle surface.

The formation of QDs during heating under reflux was monitored using absorption, emission and CD spectroscopy, (**Figure 4.14**). After an hour the dots, D-Pen CdSe, resembled those produced using the standard microwave technique, that is, they possessed a strong excitonic absorbance band at 424nm and a strong, broad, defect

emission at 580nm. The particles were also optically active at the band edge region. When checked again 16hrs later the absorption band had red shifted and decreased in strength indicating that a certain number of particles had been scarified to produce larger particles.

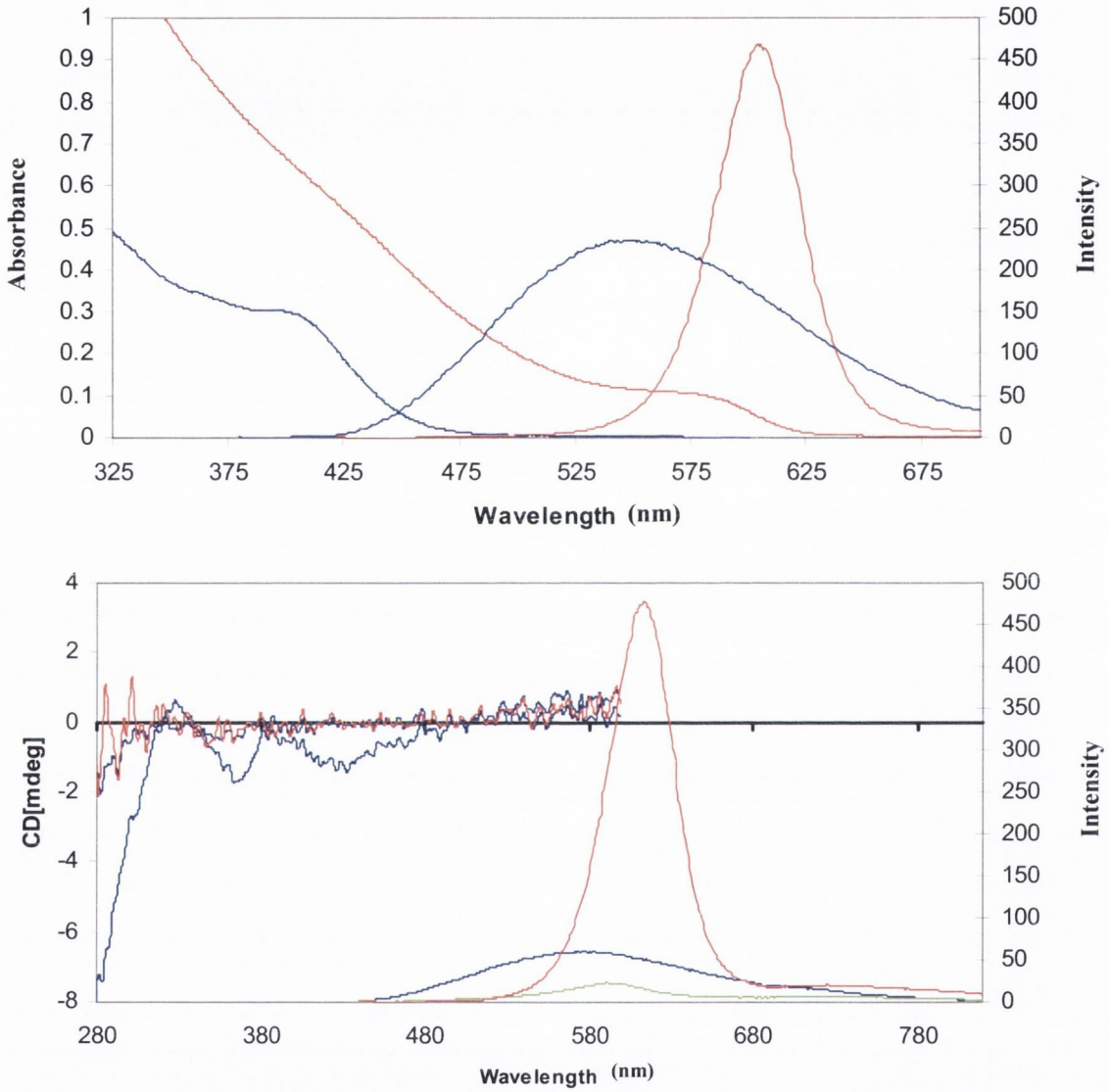

Figure 4.14: Above; absorption and emission and below; CD, spectra of D-Pen CdSe dots examined after 1hr, (blue), and 38hrs, (red) of heating under reflux. The effects of long term reflux can be clearly seen as the dots not only grow in size, (red shifting of absorption), but also in the removal of surface defects, (sharpening of emission and loss of optical activity). Note: Although the absorbance maxima red shifts the emission peak remains stationary causing a decrease in the Stokes shift.

Not only that but the emission had now decreased and narrowed indicating that the process of removing any surface defects had begun. Examination of the CD spectra confirmed this as the particles were no longer optically active in the band edge region.

The particles were examined again 12 hrs later and were found to be now strongly intrinsically emitting without any sign of optical activity at the band edge region. This suggests that is not simply strength but more importantly the type of luminescence (intrinsic or defect) that is important when producing chiral quantum dots.

4.3.7 Investigation of interactions between chiral QDs and chiral molecular species

To explore the possible use of these particles as chiral fluorescent sensors they were tested on a number of well know biologically significant chiral molecules and drugs, as well as on each other. The molecules used included salmon sperm DNA, (both single and doubled stranded), calf thymus DNA, (doubled stranded only), the chiral drug Naproxen, the eight essential amino acids, (listed below) and D- and L-Penicillamine. Complimentary chiral dots were also combined with each other to see if any interaction took place.

The absorption and emission spectra of the dots were then examined for any changes which might indicate an interaction, or more importantly a preferential interaction of one enantiomer over another.

Essential Amino Acids

Out of the twenty six amino acids that humans ingest, eight are considered essential. That is they cannot be synthesis by the body and must therefore be ingested on a regular basis, as the human body cannot store nitrogen containing compounds.[47] The results of emission studies during the interactions between chiral CdSe QDs and selected amino acids are summarised in the **Table 4.4**. All eight acids were made up in Millipore water, (1mg/10ml), and 1ml aliquots of each were added to 3ml of D- or L- CdSe nanocrystals. A control reaction was also carried out in which 1ml of Millipore water was added to both D- and L-CdSe in order to precisely record the dilution effect. A large reduction in particle luminescence was observed when L-Histidine, (**Figure 4.15**) was added to the CdSe colloids, however the effect was almost identical for both D- and L-Pen stabilized particles and so does not show a specific chiral response. None of the amino acids caused an increase the luminescence of the Pen-CdSe particles and not only that but the decreases that were recorded were the same for both D- and L- stabilized particles, with the exception of Leucine and

Trytophane, (**Table 4.4**). Unexpectedly it is the L-Pen and not the D-Pen stabilized CdSe nanoparticles that were more affected by the addition of L-Leucine and L-Trytophane, (**Figure 4.15**).

Table 4.4: Table detailing the emission intensities of CdSe nanoparticles after the addition of essential amino acids. Water was used as a control and therefore all % reductions in emission intensities were calculated from this intensity, thereby removing the need to account for dilution and normalising the results. The addition(s) of L-Leucine and L-Trytophane were the only experiments which gave noticeably different results when looking for chiral recognition. Histidine caused a significant reduction in luminescence of both types of particles.

	D-CdSe Ems Int	% Change	L-CdSe Ems Int	% change
Water	210		255	
Arginine	197	-6	232	-9
Histidine	162	-23	190	-25
Isoleucine	195	-7	240	-6
Leucine	207	-1	239	-6
Lycine	200	-5	239	-6
Threonine	190	-10	223	-12
Trytophane	206	-2	236	-7
Valine	195	-7	245	-4

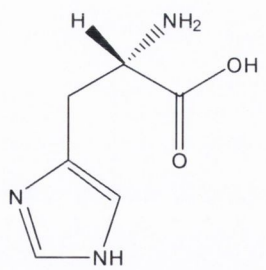

L-Histidine

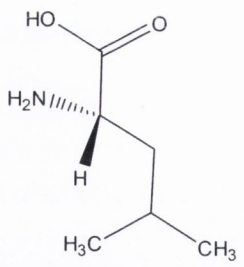

L-Leucine

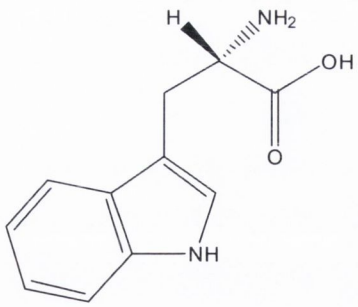

L-Trytophane

Figure 4.15: Diagrams of the three essential amino acids which either have a large effect, (Histidine), or a alternate effect, (Leucine and Trytophane), on the luminescence intensity of D- and L-Pen CdSe nanoparticles.

While the D-CdSe particles show no effect from the addition of these amino acids the luminescence of the L-CdSe nanoparticles decreases by 6 and 7% for Leucine and

trytophane respectively, (**Figure 4.16 and Table 4.4**). This however is a minuscule amount and could not be said to be a noticeable difference making the particles unsuitable as sensors for these amino acids.

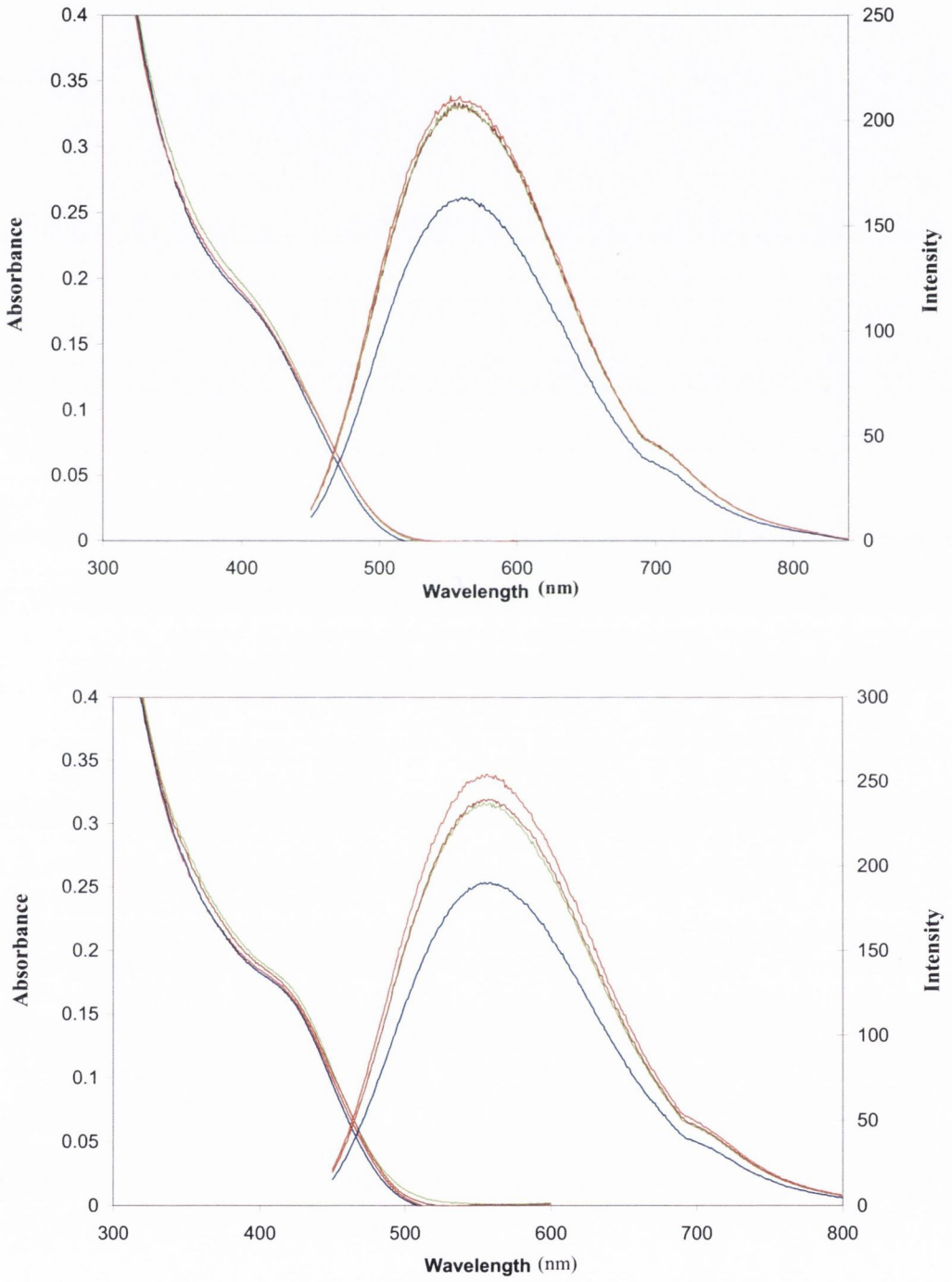

Figure 4.16: Absorption and emission spectra of D-CdSe, (top), and L-CdSe, (bottom), nanoparticles after addition of water, (red), Histidine, (blue), Leucine, (brown) and Trytophane, (green). Partciles were excited at 430nm.

After the preliminary tests above carried out on the essential amino acids it was decided to test the sensitivity of these chiral QDs using the very amino acids which stabilize them. To remove dilution as an experimental factor concentrated solutions of the both D- and L- Penicillamine were prepared, (1 x 10^{-2}M), and µl additions were made over the course of the experiment. Briefly, 3ml of as prepared Pen-CdSe quantum dots were pipetted into a sample tube and 5µl of free penicillamine was pipetted in. The mixture was then incubated in a water bath at 25 ^{0}C for 60 minutes. The particles were then examined, as before, using absorption and emission spectroscopy.

These steps were repeated three more times until 20µl of free Penicillamine in total had being added to the particles.

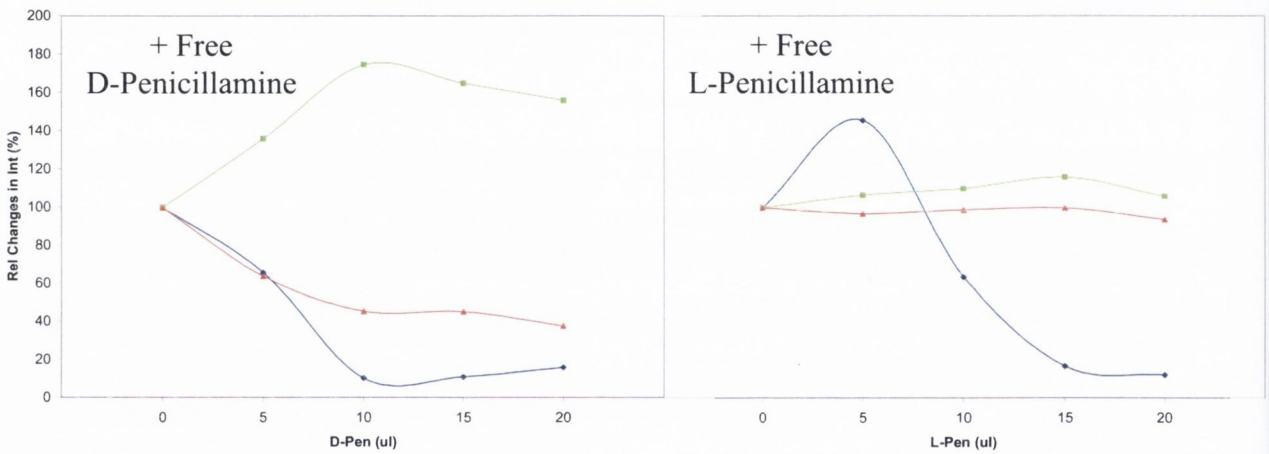

Figure 4.17: Normalised emission data monitoring the addition of D-Pen, (left), and L-Pen, (right), to D-, L- and R-CdSe nanoparticles. Initial addition of the complimentary enantiomer gives an increase in luminescent intensity for both the D- and L- particles, however while further additions of free D-Pen to L-CdSe particles, (left-lime), causes a slight decrease in particle emission, the addition of free L-Pen to D-CdSe results in almost quenching of particle emission, (right-blue). Also while the addition of free D-Pen had a large effect on the emission of the D- and R-CdSe, the addition of free L-Pen had little effect on the L-and R- particles, indicating something more than simple surface interactions are taking place.

While an interaction of particles and amino acid clearly does take place, and the interaction does appear to be dependant on the chirality of either the stabilizer or the dots, **Figure 4.17**, it is far more complex than simply a surface interaction of sensor and analyte, **Figure 4.18**. Initially the experiment appears to be successful, addition of enantiomers to their complimentary particles, i.e. free D-Pen to L-Pen CdSe and *vice versa*, caused an increase in the emission intensities of both types of dots. However as the concentration of free Penicillamine was increased the emission intensity of the L-

CdSe particles plus free D-Pen levels off and begins to decrease slightly while the increased concentration of free L-Pen has a quenching effect on the D-CdSe particles. Also the effects of the free D- or L- Pen on both the racemic particles or their identically stabilized particles is totally different for each enantiomer, (**Figure 4.12**).

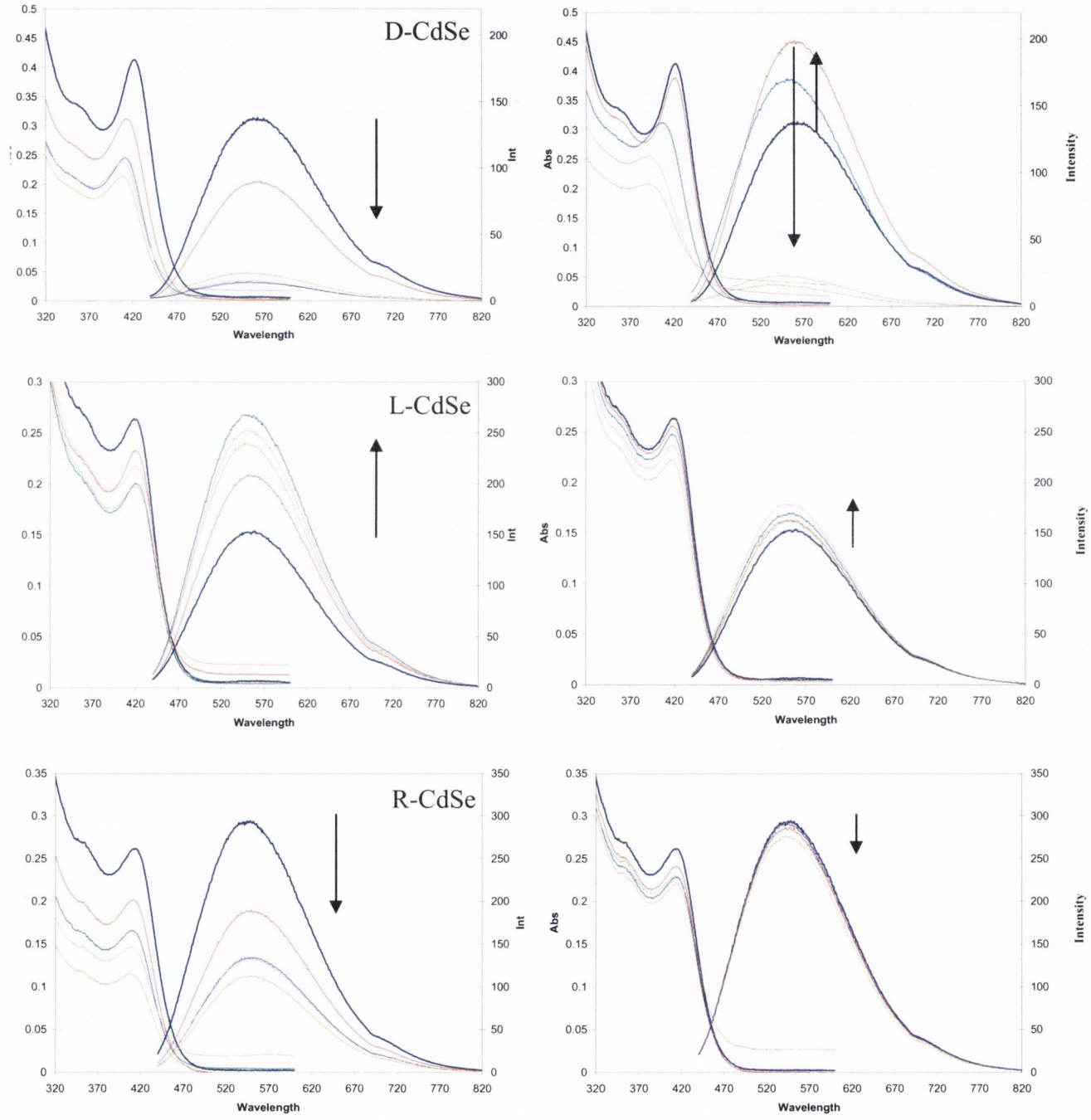

Figure 4.18: Absorption and emission spectra of D-, L- and R-CdSe, top, middle and bottom respectively. Graphs on the left show the addition of D-Penicillamine and graphs on the right show the addition of L-Penicillamine. The graphs are colour coded according to the following plan, 0µl, 5µl, 10µl, 15µl and 20µl. All emission scans were excited at 420nm and the arrows represent the first transition only, i.e. dark blue to red. Wavelength units are nm.

A closer examination of the absorption and emission spectra give a more concise picture of the results and allows an explanation as to what is happening, (**Figure 4.18**). Due to amount of experimental data each nanoparticle type and enantiomer added to it will be considered separately and then the overall results will be examined and a conclusion drawn.

The addition of D-Penicillamine, (5µl), to D-Pen stabilized CdSe causes a 34% reduction in the emission intensity of the dots; however this reduction is accompanied by a 24% reduction in the absorbance of the band edge as well as a noticeable blue shift of the exciton peak from 424 to 415nm indicating not a quenching of the particle luminescence but rather a reduction in both the concentration and size of the particles. As the amount of D-Pen is increased the break down of the particles increases with a reduction in the intensities as well as a continued blue shift of both the absorption, (424 to 410nm), and emission signals, (565 to 554nm). Although the absorption continues to fall the PL recovers on the final addition. UV-Vis spectroscopy also showed a high degree of scattering by the end of the experiment.

The addition of L-Penicillamine, (5µl), to D-Pen stabilized CdSe causes a 45% increase in the emission intensity of the dots which is accompanied by a 7% reduction in the absorbance of the band edge, no blue shift occurs. As the concentration of the L-Pen is increased the same effects which were seen above begin to become evident, a sharp decline in both emission and absorption intensities as well as large blue shift in the wavelengths of both signals; $Abs_{\lambda max}$ 424 to 393nm and $Ems_{\lambda max}$ 565 to 543nm. Also it must be noted that while the exciton peaks of all the samples show a slight loss of shape after the addition of the free Pen, these particles and the R-CdSe with D-Pen sample show an almost total loss of structure by the time the 20µl end point has been reached.

The addition of D-Penicillamine, (5µl), to L-Pen stabilized CdSe causes a 36% increase in the emission intensity of the dots; however this process is accompanied by a 12% reduction in the absorbance of the band edge as well as a slight, 2nm, red shift of the exciton and emission peaks. This red shift can indicate either particle growth or aggregation, either of which can be explained by the addition of extra L-Pen stabiliser onto the surface of the particles. The luminescence increases again after the next addition of D-Pen however from that point on both the absorbance and emission decreases as the D-Pen concentration is increased. A blue shift back to the original

absorption and emission wavelength is also observed as well as a high degree of scattering.

The addition of L-Penicillamine, (5µl), to L-Pen stabilized CdSe causes a 6% increase in the emission intensity of the dots. The reduction is accompanied by a 5% decrease in the absorbance of the band edge. While the exciton peak does not move there is a slight blue shift in the emission intensity, ~3 nm, which increases as the L-Pen concentration is increased. The luminescence increases with the next two additions of L-Pen but begins to decrease when the total volume added equals 20µl.

The addition of D-Penicillamine, (5µl), to R-Pen stabilized CdSe causes a 34% decrease in the emission intensity of the dots which is accompanied by a 23% reduction in the absorbance of the band edge as well as a large, 6 nm, red shift of the emission peak.

Table 4.5: Changes in absorbance and emission of Pen-CdSe after the addition of 5µl, (**left columns**), of analyte, and **right columns**, after 20µl of analyte. The percentage values take T=0 as 100% meaning anything less than 100% is a decrease and vice versa. Note the rapid break down of the D-CdSe particles, which seems to be independent of the analyte added.

+ 5 µl					+ 10 µl			
$Abs_{\lambda max}$	**Abs**	**$PL_{\lambda max}$**	**PL_{Int}**		**$Abs_{\lambda max}$**	**Abs**	**$PL_{\lambda max}$**	**PL_{Int}**
-9nm	76%	n/a	68%	**D-CdSe$_{+D\text{-}Pen}$**	-14nm	51%	-7nm	16%
-1nm	93%	-3nm	144%	**D-CdSe$_{+L\text{-}Pen}$**	-32nm	51%	-19nm	12%
+2nm	88%	+2nm	136%	**L-CdSe$_{+D\text{-}Pen}$**	n/a	73%	-3nm	156%
-2nm	97%	-4nm	107%	**L-CdSe$_{+L\text{-}Pen}$**	-3nm	85%	-7nm	106%
-2nm	77%	+6nm	64%	**R-CdSe$_{+D\text{-}Pen}$**	-4nm	42%	+4nm	38%
-1nm	92%	n/a	97%	**R-CdSe$_{+L\text{-}Pen}$**	-2nm	77%	-2nm	94%

The decreases in both absorption and emission signals are fairly consistent throughout the experiment, expect after the 15µl addition where absorption continues to drop but emission intensity remain constant. Once again a high degree of scattering is clearly seen by the end of the experiment, but the overall particle size seems to be consistent through the experiment.

Finally, the addition of L-Penicillamine, (5µl), to R-Pen stabilized CdSe causes a 3% decrease in the emission intensity of the dots which is accompanied by an 8%

reduction in the particles absorbance. While both the emission and absorbance intensities continue to decline it is nothing when compared to the R-CdSe particles reaction to D-Pen, (**Figure 4.18 bottom left hand corner**). Once again a high degree of scattering is seen at the end, indicating aggregation has taken place. The results of emission studies during the interactions between chiral CdSe QDs and penicillamine are summarised in the **Table 4.5**. A number of conclusions can be drawn from these findings. First and foremost at low concentrations, (5µl, **Figure 4.17**), these dots appear to act as effective fluorescent chiral sensors. Both D- and L- stabilized particles show roughly a 40% increase in luminescent intensity when exposed to their corresponding enantiomer in neutral water. Addition of 5µl of L-Penicillamine to L- or R-CdSe particles has little or no effect on the dots. These results would be excellent if not for the remaining data. Addition of D-Pen to D- or R-CdSe causes a 30-35% reduction in the emission intensity. This drastic reduction in luminescence is accompanied by an equally drastic reduction in absorbance as well as blue shifting of the λ_{max} indicating particle degradation or corrosion which is unusual considering a stabilizing molecule is being added. As the concentration of analyte is increased in all experiments the same phenomenon is observed, that is a drop in absorbance and emission strength. This is particularly true of the D-Pen stabilized CdSe which see the particle concentration half as well as dramatic reductions in particle size as evidenced by the blue shift of the absorption maxima. Another simpler explanation is of course that once added the free amino acid begins to cross link the various isolated dots causing them to aggregate and fall out of solution, however no precipitate was seen during the course of these experiments.

Investigation of the interactions between Calf Thymus DNA and chiral CdSe QDs

Initial experiments investigating the effects of salmon and herring sperm DNA on these dots proved ambiguous as each series of tests gave conflicting results. This was attributed to the poor quality of the DNA being used. To avoid these pitfalls in the previously mentioned experiments we used high quality activated calf thymus DNA. This type of DNA possess a right handed conformation. To prevent the aggregation and clumping of Calf Thymus DNA in solution it must be prepared in an EDTA phosphate buffer. As previously reported EDTA causes Cd based quantum dots to

decompose as the EDTA begins to remove and chelate the Cd ions from the quantum dot crystal structure.[48]

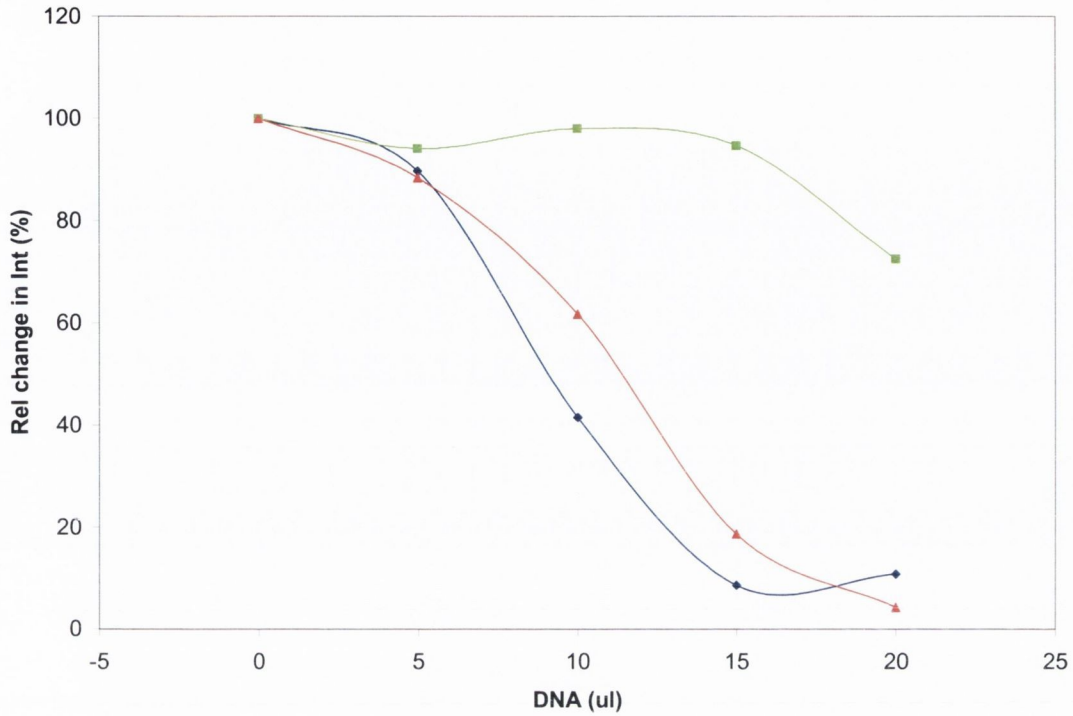

Figure 4.19: Normalised emission data monitoring the addition of calf thymus DNA, to D-, L- and R-CdSe nanoparticles. Initial addition of the DNA has more or less the same effect on all three enantiomers, however as the concentration of DNA is increased the emission intensities of both the D- and R- dots begin to decline rapidly, with the greater effect being on the D- particles. Eventually the L-CdSe begins to loss emission strength. These decreases in emission are accompanied by particle decomposition.

Initially it was believed this would be a problem as the effects of free EDTA buffer on the nanoparticles were also studied. It, EDTA, was found to have a total quenching effect on the particles, even at low concentrations. Instead however it helped to demonstrate the interaction of the right handed DNA with, and subsequent protection of the left handed L-Pen CdSe.

Table 4.6: Changes in absorbance and emission of Pen-CdSe after the addition of 20µl of C.T DNA. The percentage values take T=0 as 100% meaning anything less than 100% is a decrease and vice versa. Note the rapid break down in both the D- and R-CdSe particles.

	$Abs_{\lambda max}$	Abs	$PL_{\lambda max}$	PL_{Int}
D-CdSe	-20nm	56%	-20nm	11%
L-CdSe	+1nm	85%	+10nm	72%
R-CdSe	-15nm	65%	-6nm	7%

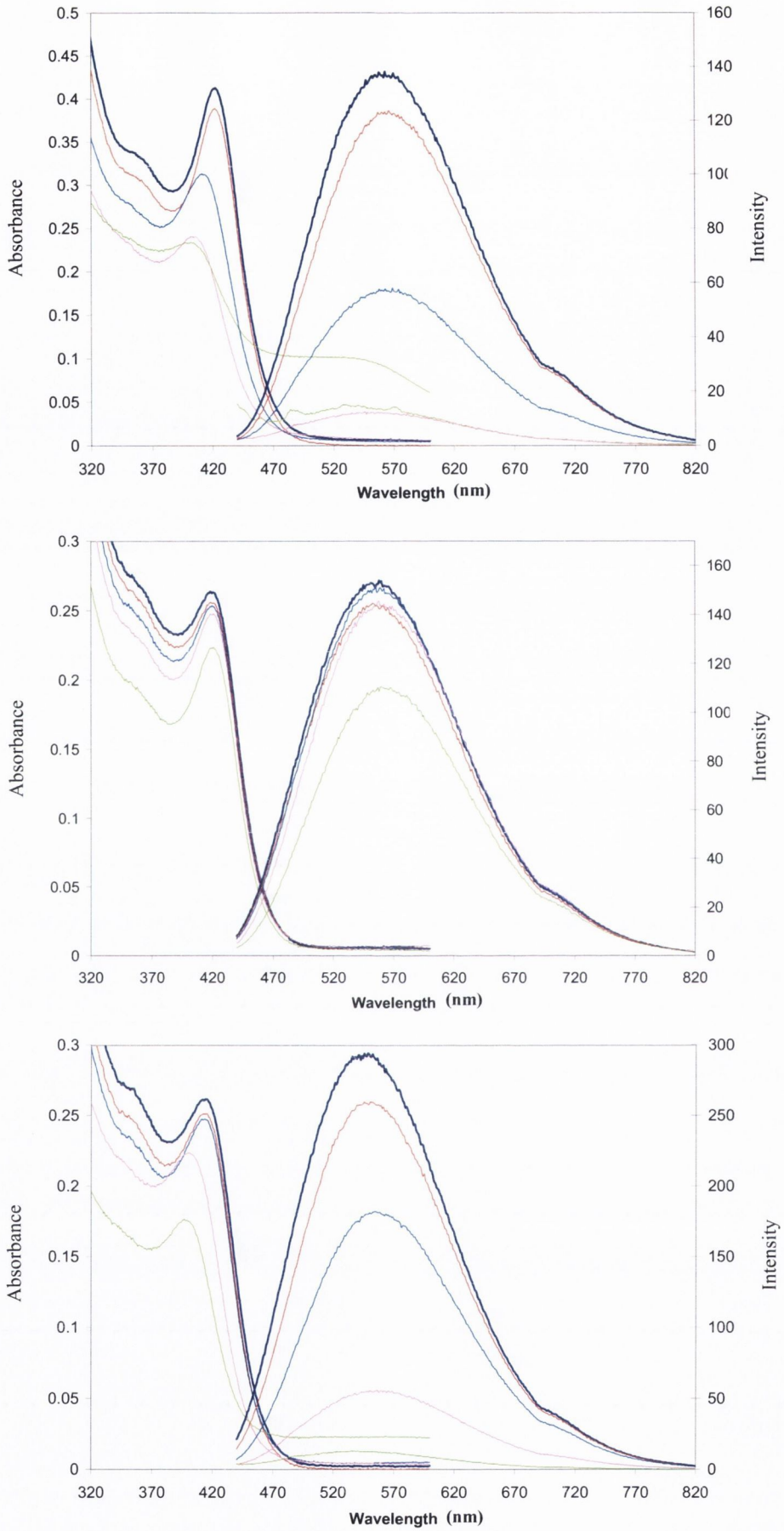

Figure 4.20: Absorption and emission data monitoring the addition of 0μl, 5μl, 10μl, 15μl and 20μl calf thymus DNA, to D-top, L-middle and R-bottom CdSe nanoparticles. Initial addition of the DNA has more or less the same effect on all three enantiomers, however as the concentration of DNA is increased the emission intensities of both the D- and R- dots begin to decline rapidly, with the greater effect being on the D- particles. Eventually the L-CdSe begins to loss emission strength. These decreases in emission are accompanied by particle decomposition.

The changes in emission intensity, (**Figure 4.19** & **4.20** & **Table 4.6**), are more pronounced in the case of the interaction between the D- or R- particles with the DNA (over the L-CdSe). Once again an examination of the absorption spectra show that the D-, (and to a slower, but no lesser, extent the R-), particles are rapidly breaking down as the concentration of DNA, and EDTA, is increased, (**Figure 4.20**, top and bottom). The L-CdSe while presenting a slight decrease in absorbance, (15%), and emission, (28%), intensities does not show a blue but rather a red shift in the λ_{max}. This can be explained by the fact that the right handed DNA is wrapping around the left handed particles which results in their aggregation, as demonstrated by the red shift in both absorption and emission maxima. In addition DNA also protects the L-CdSe QDs from the deteriorating affect of the EDTA.

Investigation of the interactions between Naproxen and chiral CdSe QDs

One of the most common frequently used chiral drugs, Naproxen [(*S*)-(+)-2-(6-methoxy-2-naphthyl) propionic acid] (**Figure 4.21**), was employed to test the response of Pen-CdSe dots. Naproxen was chosen because, a) it is a relatively simple biologically significant molecule and b) it can be made up without the need for buffer or other compounds which may harm the dots.

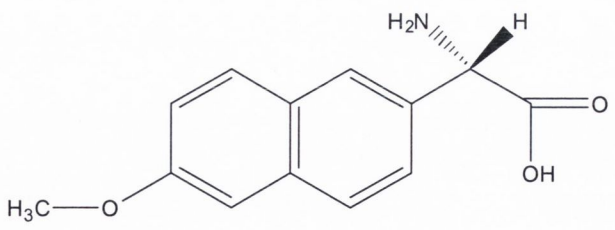

Figure 4.21: The chiral drug Naproxen in the L-, (or S-), conformation. Due to its non-polar character, as a result of its naphthalene ring system it is insoluble in neutral water. However it is readily soluble in methanol.

Table 4.7: Changes in absorbance and emission of Pen-CdSe after the addition of 1ml of Naproxen in methanol, (1mg/10ml). The percentage values take T=0 as 100% meaning anything less than 100% is a decrease and vice versa. Although the naproxen does have an effect on the particles it is not chiral specific

	$Abs_{\lambda max}$	Abs	$PL_{\lambda max}$	PL_{Int}
D-CdSe$_{+MeOH}$	n/a	80%	n/a	69%
D-CdSe$_{+Nap}$	n/a	75%	+2nm	52%
L-CdSe$_{+MeOH}$	n/a	78%	n/a	70%
L-CdSe$_{+Nap}$	n/a	78%	+2nm	51%

The solution of Naproxen was prepared in methanol, because of the low solubility of this drug in water. Although Naproxen is soluble at basic pH in water, this route was avoided as the emission intensity of the quantum dots is extremely pH sensitive. Briefly 1mg of Naproxen was dissolved in 10ml of methanol and 1ml of this solution was added to 3ml of Pen-CdSe dots. The reaction was monitored as before using absorption and emission spectroscopy (**Figure 4.22** & **Table 4.7**). A control reaction was also preformed by adding 1ml of methanol to 3ml of dots to observe the effect, if any on the particles. Addition of methanol caused a 20% reduction in absorbance at 430nm (the excitation wavelength), and a 30% reduction in the emission at λ_{max} in both the D- and L-Pen stabilized CdSe. This reduction in absorbance and the fact it is not accompanied by a shift in the λ_{max} of the exciton peak indicates that the solubility of the quantum dots is significantly reduced in the water/methanol mixture. As Naproxen has low solubility in neutral water and the particles are only slightly soluble in methanol they are expected to stay in their respective phases but to interact at the solution interface. Examination of the absorption and emission spectra show that the particles do interact with the Naproxen as the reduction in the luminescent intensity is far more dramatic than simply with methanol. As there is little change in the position of the exciton peak it is assumed that the dots are stable and not undergoing any form of decomposition. However the Naproxen seems to affect both the D- and L- dots in the same way, reducing the absorption and emission peaks by the same amount and causing the same 2nm red shift in the emission peaks. Although the exciton peak of the L-CdSe dots does appear to sharpen slightly it must be assumed that the chirality of the dots has little or no effect on how they interact with the Naproxen.

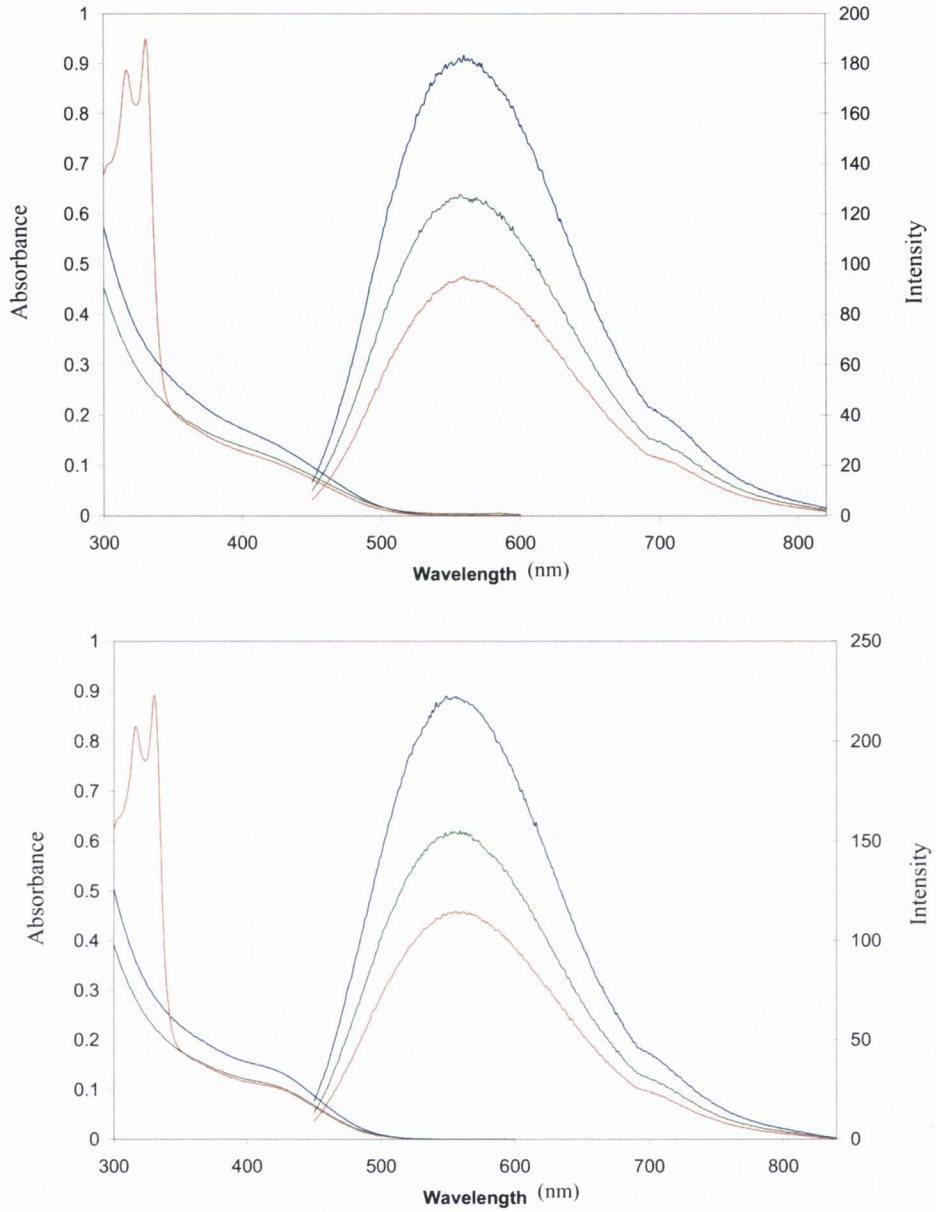

Figure 4.22: Absorption and emission data monitoring the addition of methanolic solution of Naproxen, (red) to D-top, and L-bottom aqueous CdSe nanoparticles, (blue). Samples were excited at 430nm. A control reaction was carried out by adding the same amount of methanol to CdSe particles, (green). As mentioned in abbreviations **Abs** denotes absorption and **Int** denotes emission intensity.

Investigation of interactions between chiral CdSe nanoparticles

In one final experiment to test the chiral interactions between the D- and L- particles, the particles were combined with each other (**Figure 4.23**). Briefly, D- and L-

penicillamine stabilized CdSe particles were diluted to the same optical concentration and then combined in equal volumes. They were monitored using UV-Vis and PL spectroscopy and excited at a point where their absorption spectra crossed, i.e. the isobestic point. If no interaction took place then the emission intensity of the mixed particles would have being half the difference of the individual particle intensities, i.e. D- 202, L- 276, the difference in intensities is 74 so therefore the mixed particles should have an intensity of 202+37=276-37=249. After addition of the D- and L- particles to each other there is no drop in absorbance indicating that the particles are not co-precipitating, which had been an initial worry. Emission spectra show an intensity of 248 which is 4% higher than it should be. The emission intensity continued to rise for the next 20mins eventually levelling off and stabilizing. Particles were continually checked for the next hour but showed no signs of change. The final emission intensity was 257, 7.5% above it should be if no interaction had taken place.

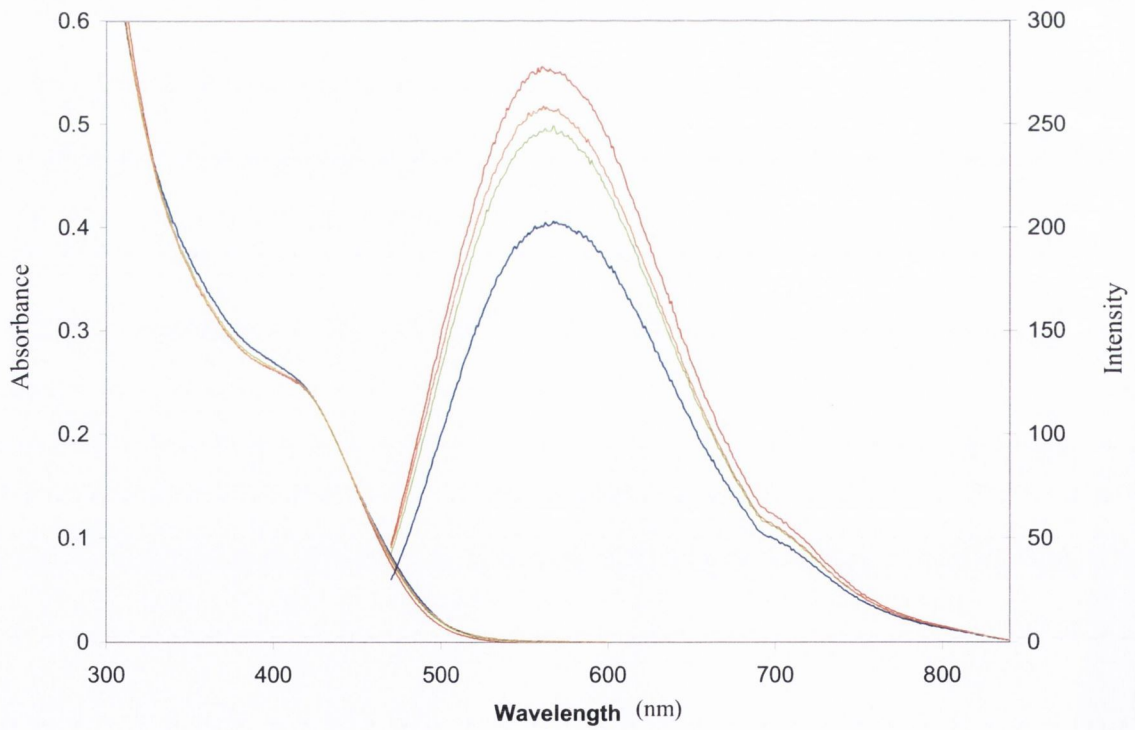

Figure 4.23: Absorption and emission data monitoring the addition D-Pen CdSe, (blue) to L-CdSe, (red). Particles were checked after being combined, (lime) and again after 10mins, (orange). The particles were excited at their isobestic point; 450nm. Abs-Absorption and Int-Intensity.

As no drop in the absorption spectra, or precipitation was observed, it can be assumed that the particles are stable. The slight increase in emission strength does suggest that some interaction has occurred allowing energy transfer to take place. Possibly further investigation will be needed to clarify this.

4.4 Cystein stabilised CdSe QDs

4.4.1 Optimisation of synthesis (Statistical Analysis)

Similarly to the Pen-CdSe, a 2^2 analysis was carried out for the Cystein stabilized CdSe nanoparticles. This time however only, the minimum number of points, seven, were examined. The reaction scheme detailed in **figure 4.1**, (replacing Penicillamine with Cystein), was once again used as the starting point for a multi-factor study. Again the starting point was 2ml of aliquots of 1 x 10^{-2}M stock solutions in 40ml of Millipore water. The volumes were then doubled, the Cd along the y axis, and the Cystein along the x axis. Again the Se^{2-} concentration remained static at 2ml of 1 x 10^{-2}M, (2 x 10^{-5} moles), (**Figure 4.24**).

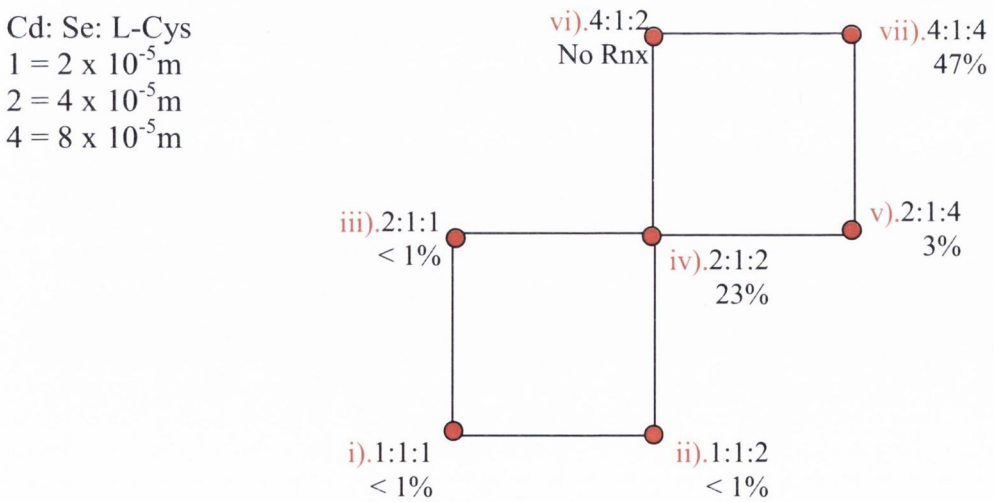

Figure 4.24: 2^2 statistical analysis of L-Cys-CdSe. Quantum yields for each point were measured against Coumarin 153 in MeOH.

Again while the quantum yield was the primary response studied over the course of this analysis all particles produced were then examined using UV, PL, CD and PCS spectroscopy, (**Figures 4.25 & 4.26**). **Figure 4.26** shows both absorption and emission spectra for batches 1-7 no reaction was observed for batch 6. Although, most of the reactions produced quantum confined semiconductor particles, as can seen from a) their absorption peak positions but also b). the sharpness of those exciton peaks, only batches where the Cd and Cys concentrations were double that of the Se gave particles with anything approaching strong luminescence. All particles exhibited defect luminescence.

Close examination of **Table 4.7** shows that the more blue shifted the exciton peak, and therefore the smaller the particle, the higher the quantum yields. This is probably due to the increased concentration of Cd atoms on the outer shell of the dots i) removing any electron traps and ii) allowing for the closer packing of Cystein stabiliser at the dot surface. The added Cd increases the luminescence while the increased cystein concentration and the mostly cadmium shell means closer ligand packing and therefore smaller dots.

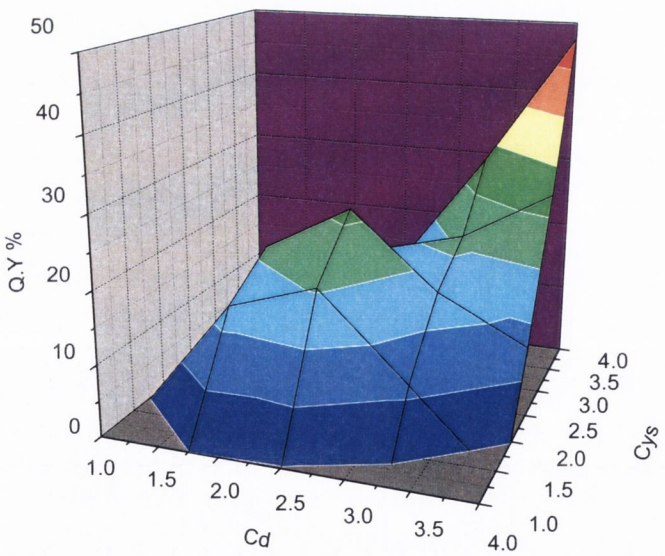

Figure 4.25: 3-D representation of a 2^2 statistical analysis of the formation of L-Pen CdSe using quantum yield as the response. Note how the yields peak at points where both metal and stabilizer are at their highest. An Origin 7.5 random xyz matrix was used to generate the graph.

The increase in the metal/stabilizer to selenium ratio also meant that more nucleation centres would be formed and as a result of the greater Cd to Se ratio particle growth would be slower. This decrease in the overall particle growth rate would also increase the quantum yield.[18] So, while the smaller dots are unquestionably brighter it is not their size but their rate of growth and surface chemistry which gives them their enhanced luminescence. The disparity in particle size was confirmed by DLS zetasizing, **Table 4.7**.

Again a direct correlation can be drawn between the strength at which each particle batch emits and its optical activity. Despite the highly structured, strong exciton peaks of batches 1, 2 and 5 their optical activity at their bandedge regions is quite low, (1-2 millidegrees), while those of batch 4 and 6 are in the 4 and 12 millidegree regions respectively, **Table 4.7**, indicating a link between highly defective particle surfaces and optical activity.

It is also remarkable that by simply varying the concentrations of two reactants it is possible to synthesis semiconductor nanoparticles with largely divergent bandedge energies; 2.93 and 2.38 ev's, (batches 2 and 7 respectively). This demonstrates quite effectively the kind of control which nano-chemistry can allow.

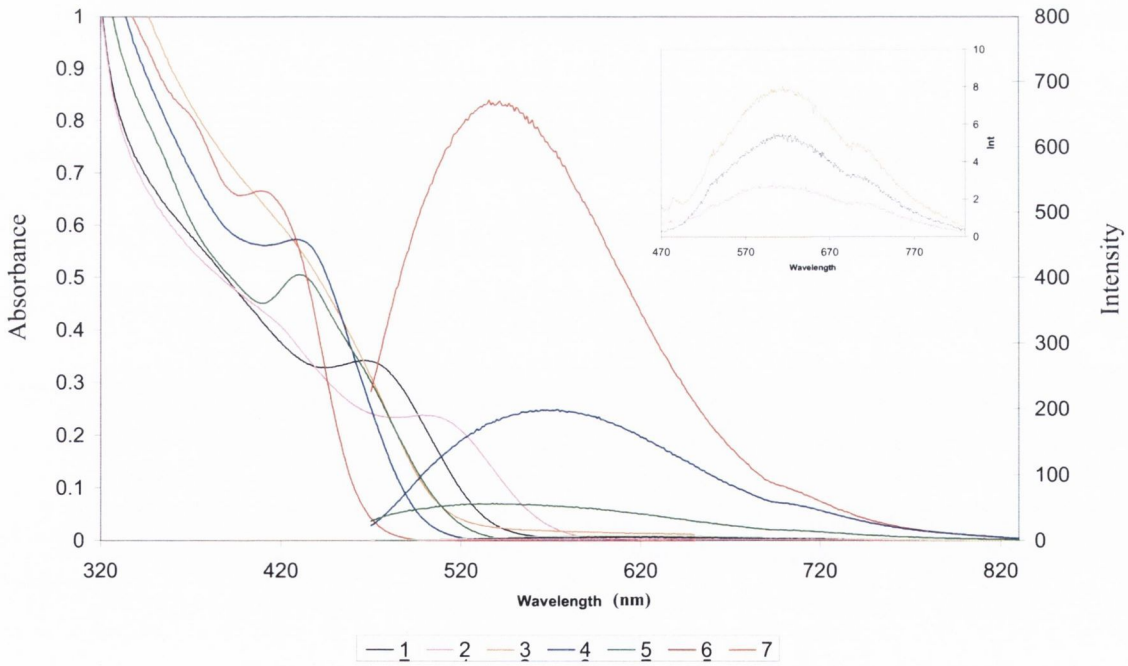

Figure 4.26: Absorption and emission spectra showing points 1-7 of the above 2^2 statistical analysis of L-Cys-CdSe. Inset: emission scans of batches 1, 2 and 3. All emission scans were excited at 450nm.

Batch 7 was chosen as it had the highest quantum yield. Although examination of the xyz scatter plot, **Figure 4.25**, suggested particles with higher quantum yields could be synthesised by increasing the concentration of both the Cd and Cystein this simply lead to the formation of insoluble $Cd(OH)_2$, so with this in mind batch #7 of this analysis was deemed to be the best and therefore used to create the L- and R-particles.

Table 4.8: Absorption, circular dichroism, emission and excitation, quantum yield and size data for 2^2 statistical analysis of L-Cys CdSe. Emission scans were excited at 450nm, excitation scans were recorded using the emission maxima's.

D-CdSe	Abs	CD	Ems	Ext	QY	Size(nm)
1	467nm;0.34	461nm;-2.1 383nm;+1.1 356nm;+2.0 317nm;-1.2	613nm; 5.3	467nm; 6.0 341nm; 7.7	~1%	9.7
2	514nm;0.24	n/a	605nm;2.7	479nm; 3.2 337nm; 4.2	n/a	5.0
3	437nm;0.5	430nm; -1	614nm;8	464nm; 8.4 345nm; 9.5	n/a	11.0
4	430nm;0.57	425nm;-4.2 370nm;-2.8 300nm;-7.1 269nm;-10	567nm;198	449nm; 198 346nm; 247	23.5%	3.6
5	331nm;0.5	479nm;+1 443nm;+1.6 425nm;-5.5 366nm;+5.2 323nm;-7.2 290nm;+8.7	538nm;56	448nm; 57.3 344nm; 73.1	3.2%	3.3
6	No Rnx					
7	413nm;0.6 373nm;0.8	422nm;-12 380nm;+3.2 285nm;-13.2	541nm;665	420nm; 950 345nm; 1020	47%	3.5

4.4.2 Optical Characterisation

Due to its high quantum yield and strong CD response, (which appear to go hand in hand), the particles produced at point **vii)** of the statistical study were chosen as the best. The remainder of the study was then discarded, as before, and from here on only the particles with the ratio of 4:1:4 Cd:Se:Cys will be discussed. Particles were once again prepared using the L- enantiomer and were re-examined using absorption and photoluminescent spectroscopy.

As shown in **Table 4.8** these particles exhibit an absorbance shoulder at 413nm with a secondary exciton peak at 373nm. As with the Pen capped dots the secondary exciton peak is clearly visible and the distance between primary and secondary peaks is the same ~40nm for both Cys and Pen stabilized dots. Once again the formation of CdSe nanocrystals is confirmed by increased bandgap energies, and consequential blue shift in absorbance, of the dots when compared with CdSe in the bulk phase.

Emission spectroscopy confirms that these dots are also strongly defect emitting, with a Stokes shift of 120 nm, (40 nm less than that seen for the Pen dots), and a FWHM of 139 nm, (23 nm smaller than the FWHM of the Pen CdSe particles). The dots were once again excited at two different wavelengths, 420 nm and 450 nm, to check the degree of monodispersity. The emission maximum does red shift by 9 nm when the excitation wavelength was changed indicating a slight variation in particle size.

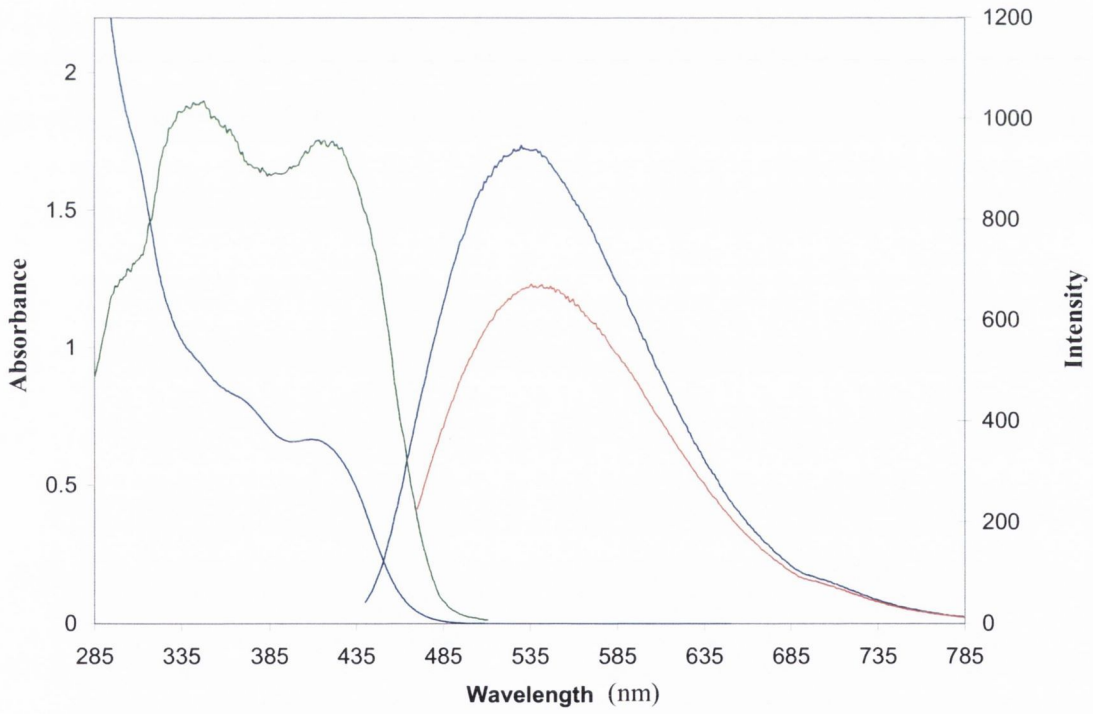

Figure 4.27: Absorption, (blue), emission, (red and dark blue), and excitation spectra, (green), of L-CdSe. Despite the strong degree of quantum confinement as illustrated by the sharpness of the abs and excitation shoulder at 413nm and 373nm respectively, the emission scans clearly demonstrate the presence of a large number of surface defects. Emission scans were excited at 420nm, (blue), and 450nm, (red). The excitation scan was recorded at 530nm.

The tail emission is also present in these Cys stabilized particles, (**Figures 4.26** and **4.27**), excitation spectra taken at this wavelength are different to those taken at 535nm in that the slight shoulder at 435nm which proceeds the main peak at ~430nm in the 535nm excitation scan is now the main peak, this suggests the Once again the second peak does not move when the excitation wavelength is changed. The excitation spectrum, taken at 535nm, shows two peaks at 418nm and 345nm. The peak at 418nm corresponds well to the exciton peak at 413nm with the 5nm red shift caused by a slight loss of energy as nonradioactive recombinations. The excitation peak at 345nm does not match the position of the second exciton peak in the absorption spectrum, however examination of the absorption excitation spectrum for batch 4 of the statistical analysis show that while a second exciton peak cannot be seen in the absorption scan the second excitation peak is clearly visible at 345nm. The fact is that all particles produced in the analysis have this secondary peak at 346nm. All particles prepared in the stats study possess this second excitation peak whether they have a visible second exciton peak or not. While this secondary excitation peak, PL, does not appear to correspond to the secondary exciton peak, (Abs), it is dependant on the position of the primary excitation peak. Examination of the excitation spectra for all six samples shows that there is roughly a 20% different in the intensity and wavelengths of the first and second excitation peaks, (**Table 4.7**).

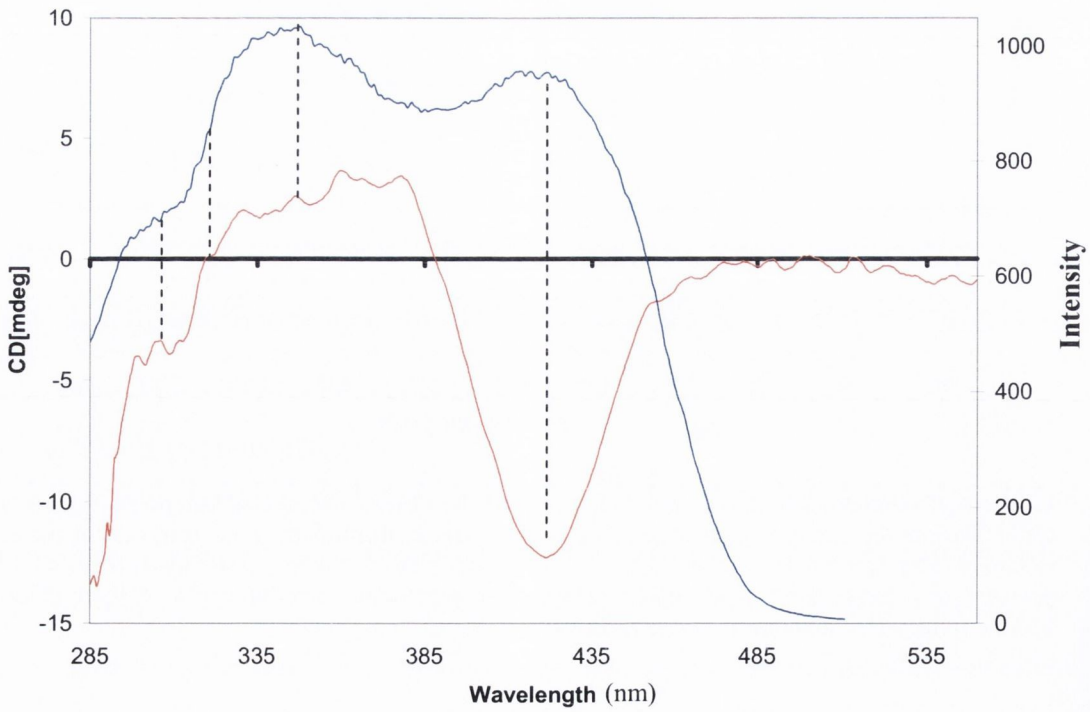

Figure 4.28: CD and excitation scan of L-Cys CdSe particles. All three excitation peaks, 297nm, 345nm and 420nm correspond with either a peak or valley in the CD scan indicating a close link between the photophysical, (emissive), and optically active surface components of the particle.

Although an excitation spectrum is usually only used to confirm the link between the absorption and emission spectra, it is far more useful than simply an analytical tool, especially when examining chiral dots. An excitation scan is essentially an absorption scan taken using a photoluminescent spectrometer, however because it is generated from the emission data it allows us to get a far clearer picture of the particles surface than an absorption scan would. As has been discussed in the previous section there is a clear link between particle luminescence and the presence of optical activity, however the CD spectra are usually more complex than their corresponding absorption spectra. Due to the reduced Stokes shift in the Cys, (as compared to the Pen), stabilized CdSe nanoparticles it was possible to perform excitation spectra as far back as 285 nm while still using the emission maximum. This allows a comparison between CD and excitation spectra from the position of the exciton peak right back to the deep UV region of the spectrum, (**Figure 4.28**). Here we see a clear connection between the peaks and troughs of the CD scan and the various peaks and shoulders of the excitation spectra. This allows us to further identify the various CD signals as corresponding to different particle surface structures that are invisible to absorption spectroscopy and strengthens the link between particle emission and chirality, as the surface conditions that the excitation scan highlights are responsible for both these phenomena.

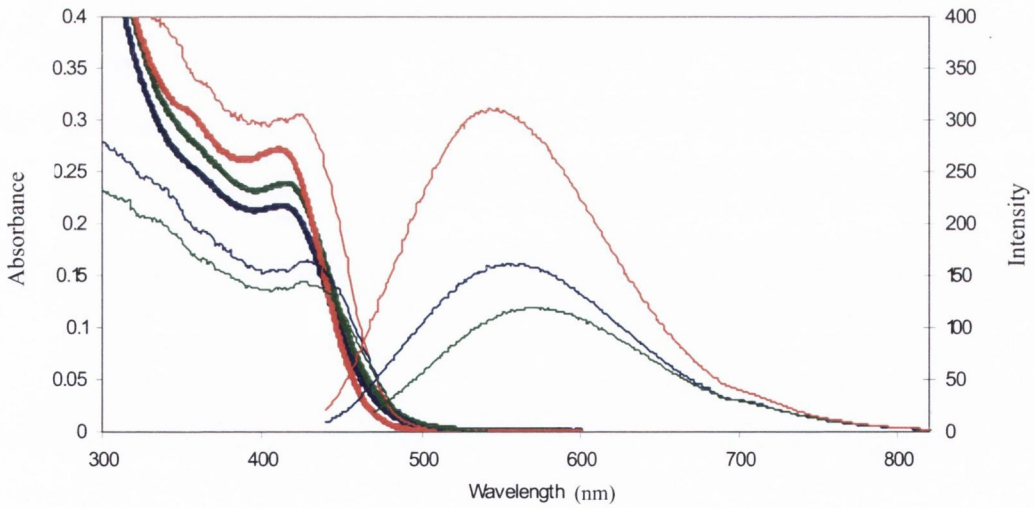

Figure 4.29: Absorption and emission scans of D-, L- and R-Cys CdSe particles. All three excitation spectra were recorded using their corresponding emission maxima. All particle types were excited at 420nm. Absorption scans are in bold. R- stabilized particles are again blue shifted when compared with the D- and L- enantiomers.

Once the L- and R- Cystein stabilized particles were prepared absorption and photoluminescence spectra of each type of dot were recorded and examined. Again D- and L- stabilized particles are quite similar to each other while both the absorption and emission spectra of the R- stabilized particles are shifted to the blue, **Figure 4.29**. Interestingly, the excitation spectrum of R-Cys particles is red shifted by 20nm when compared to its corresponding enantiomers. This increased proximity of the emission and excitation peaks combined with its relatively low defect quantum yield is probably due to the R- particles more ordered surface.

The quantum yield of these particles was again measured using Coumarin 153 as the luminescent standard. D- and L- stabilized dots showed a remarkably high quantum yield for CdSe particles in water at 40±7% for both types of dots. R- on the other hand shows a marked decrease to 13%. The quantum yield of the R-Cys particles are quite close to those already reported in the literature for water soluble CdSe particles however the remaining dots are much higher with such yields only been achieved for CdSe which have either been prepared in organic solvents or have had another semiconductor introduced to form either core/shell or alloy particles. Again, Talapin et al. demonstrated that luminescent strength is not simply a factor of particle size nor can it be attributed to shape or relative crystallinity, i.e. outwardly similar particles can have different QY.[18] They postulated that particles with the smoothest surfaces, (trap and defect free), and therefore the best luminescence were those which would have the "the smallest net growth rate". With this in mind we suggest that combinations of differing optical isomers affect the way in which that particular ligand controls this net particle growth rate, which results in a loss of quantum yield attributed to defect emission.

4.4.3 Fluorescent lifetime measurements

Time-dependent luminescence intensity decay curves for these CdSe nanoparticles were fitted using a tri-exponential analysis over a 1 μs TAC range as their behaviour was quite similar to the Pen-stabilized CdSe. Again lifetimes do not correspond to the individual batches quantum yields with D- and L- having much larger QY than the R-stabilized particles yet the τ values for D- and R- particles are much closer to one another than for D- and L-, (**Table 4.8**). As the D- and L- particles showed a much

larger quantum yield than the R- stabilized particles the contribution of their surface states, (τ_2), to the overall luminescence was higher, (42% when compared to the R-CdSe's 39%, **Table 4.9**).

Table 4.9: Lifetime data for D-, L- and R-Cys CdSe particles using emission maxima to record data. As with the Pen stabilized dots it is the contribution to the overall lifetime, (B factors), and not the lifetimes themselves that agree with the quantum yields.

568nm	Q.Y%	χ^2	A	τ_1 (ns)	B_1	$B_{\%}$	τ_2 (ns)	B_2	$B_{\%}$	τ_3(ns)	B_3	$B_{\%}$
D-	40±7	1.1	113	*13*	10267	36.4	*56*	11919	42.3	*173*	6017	21.3
L-	40±7	1.1	106	*14*	8953	34.1	*61*	11104	42.2	*178*	6240	23.7
R-	13	1.1	193	*11*	12548	46.4	*51*	10531	38.8	*200*	4025	14.8

Lifetimes were also taken at 700nm in an attempt to understand the nature of this secondary peak, **Table 4.10**. While there was little change in the short lifetimes both the medium and long lifetimes changed considerably which is expected as these lifetimes are believed to be linked to the various surface states. This also further strengths the hypothesis that the tail emission which we see in these optically active dots is due to the chiral nature of the quantum dots shell.

Table 4.10: Lifetime data for D-, L- and R-Cys CdSe particles recorded at 700nm. The longest lifetimes of the D- and L- particles was considerably lengthened while the R- was shortened when compared with the lifetimes recorded at particles emission maxima.

700nm	Q.Y%	χ^2	A	τ_1(ns)	B_1	$B_{\%}$	τ_2 (ns)	B_2	$B_{\%}$	τ_3(ns)	B_3	$B_{\%}$
D-	40±7	1.1	1072	14	9062	32.3	63	11189	40	202	7753	27.7
L-	40±7	1.1	2699	12	5753	29	57.5	7220	39.5	202	5753	31.5
R-	13	1.1	5144	12	8183	38	48	9131	43	191	3958	19

4.4.4 CD Studies of Cystein stabilized CdSe

Circular dichroism spectra of the particles confirmed that the particles were chiral right out to their bandedge regions, (**Figure 4.30**), with R-particles showing no optical activity as expected.

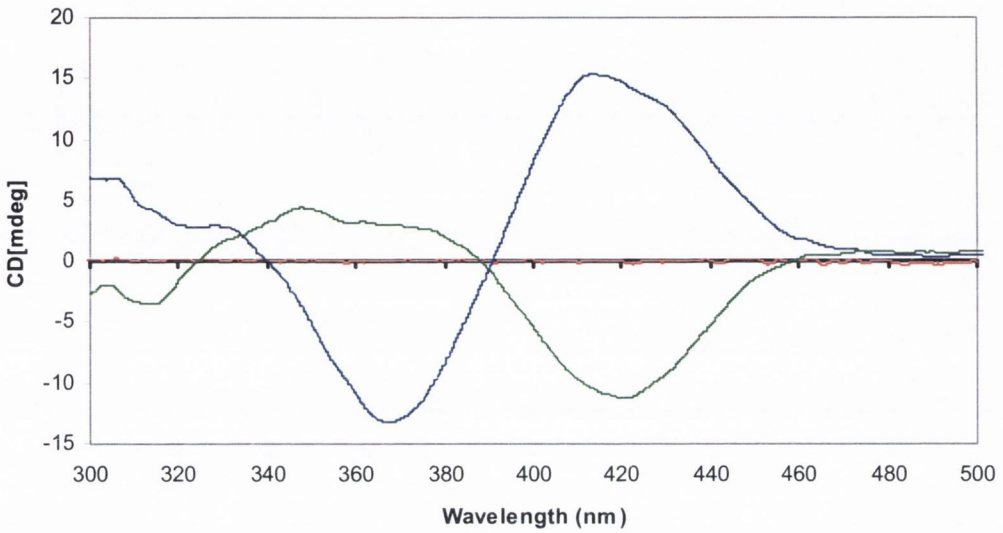

Figure 4.30: CD scan of cystein capped CdSe. D-, (Blue) L-, (Green) and Rac-, (Red). (θ deg = δA/32.98). The lack of symmetry is put down to the higher purity of D- over L-Cystein

Like all previously reported particles these Cys-CdSe quantum dots appear to grow in a direction opposite to that of the stabilizing ligand. However unlike the Pen-CdSe dots where the stabilizer reversed chirality allowing the particles to be formed in the direction of the stabilizer used, i.e. D-stabilized dots which absorbed in the negative region of the spectrum and vice versa, these Cys stabilized CdSe particles repeated the behaviour seen in the CdS particles. That is, the stabilizer retained their original chirality and the particles grew around them producing dots with the opposite chirality, i.e. D- stabilized dots absorbing in the positive region of the spectrum and vice versa.

Once the CD spectra were complete and particle chirality was confirmed the formation of the D-particles were re-examined step by step using CD, UV and PL, (**Figure 4.31**).

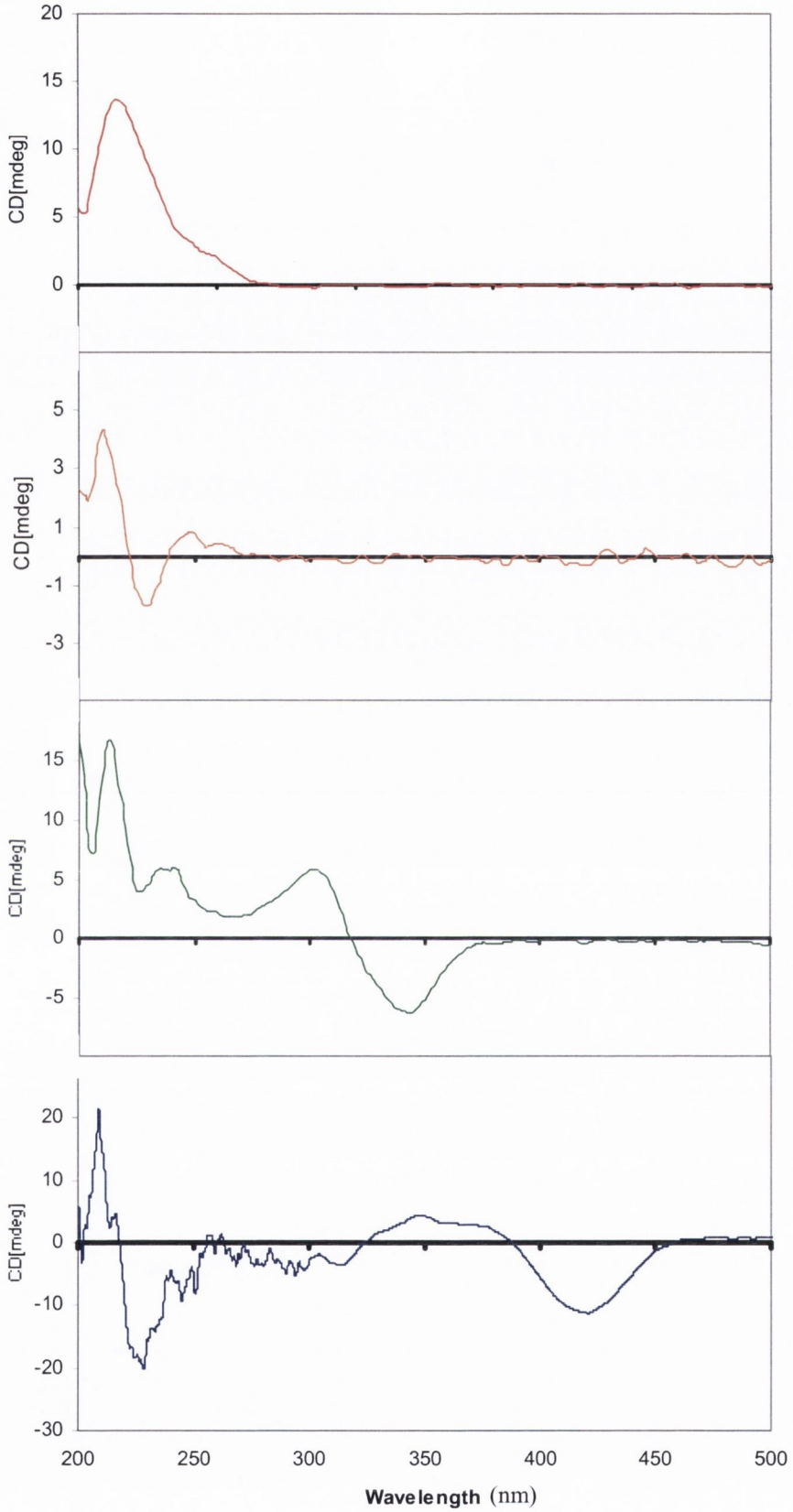

Figure 4.31: CD monitoring of the formation of D-CdSe. **1.** Free Cystein Free with absorption maxima of 216nm **2.** Formation of the Cd-amino acid complex, new bands appear at 230, 251 and 262nm, the band at 216nm blue shifts to 212nm. **3.** The small nanoparticles formed after the addition of the Na_2SeSO_3 but before microwave treatment, new bands fromed from 260 to 346 nm. **4.** The CdSe nanocrystals after the microwave treatment new bands from 350 to 420 nm. The spectra have been recorded using Jasco J-810 Spectropolarimeter. Note: the final CdSe samples were not purified in these monitoring experiments. Due to the high absorbance between 200-300nm after microwaving both samples were diluted by at least factor of 8 scanned and then normalised hence the high degree of noise in this region.

Unlike the penicillamine stabilized particles the cystein particles did exhibit luminescence before microwaving indicating that nanoparticles and not nanoclusters were formed. Steps 1 and 2 are of course identical to those carried out for cystein capped CdS, (**Chapter 3**.) Step 3 sees the formation of luminescent super small CdSe QDs. In step 3. we also see the diminishing and possible reversal of the chirality of the Cd-Cys complex as the signal at 239nm switches from the negative to the positive region of the spectrum, although this may be simply due to the appearance of the quantum dots signal at 350 nm changing the overall shape of the signal. After the nanoclusters were heated in the microwave, step 4, we see the creation of the distinct particle exciton band at 423 nm as well as another signal at 381 and 351 nm which correspond to the fine structure of the excitation scan, (**Figure 4.28**).

4.4.5 TEM of Cystein stabilised CdSe

Unlike the Pen capped CdSe no rod-like nanostructures were found in the TEM images of the cystein capped particles. All batches showed large 20 nm aggregates through each sample. As these are too big to be individual particles with band edges at ~420nm we must assume that they are aggregates of smaller individual particles, (**Figure 4.32**). Unlike the penicillamine stabilized CdSe, it was possible to carry out DLS measurements on these particles with acceptable PdI results.

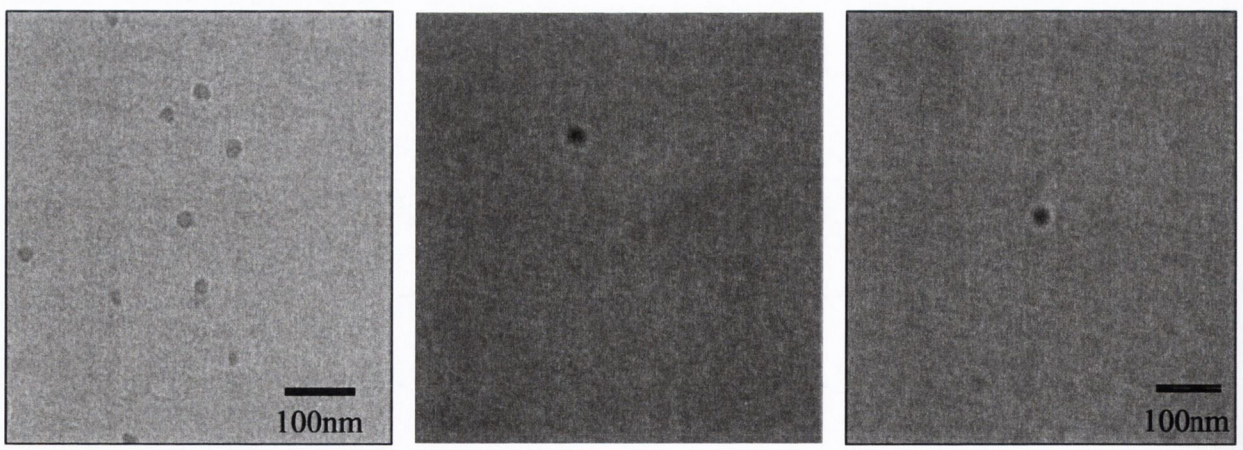

Figure 4.32: TEM images of D-, L- and R- Cys CdSe. All particles appeared spherical with diameters of 19±4nm.

These zetasizing spectra, (**Figure 4.33**), show the dots inhabiting the 3-8nm range, again with the R-CdSe particles being the smallest.

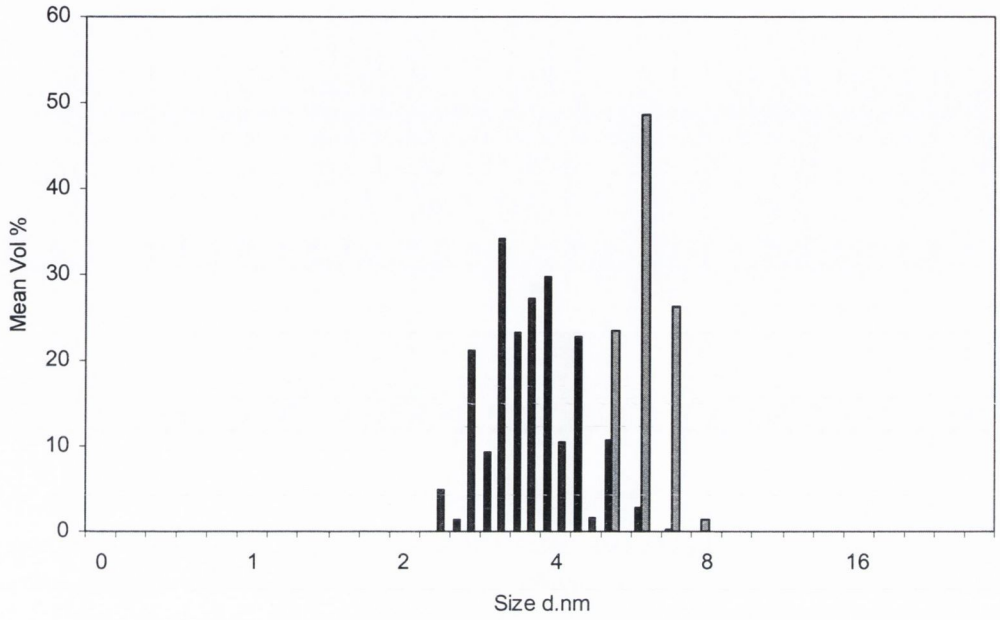

Figure 4.33: Dynamic Light Scattering, DLS, scan of D-, L- and R- Cys CdSe. While D- and R- appear to be around the 3.5nm mark the L-particles are almost double that. This data does not corresponds with UV-Vis data and therefore again shows the limits of this technique.

4.5 Conclusion

Thus we have successfully prepared and characterised penicillamine and cysteine stabilised chiral CdSe QDs. We have found that defect emission of these nanocrystals is strongly related to their CD properties. By comparing the CD and excitation spectra of individual particles it is possible to correlate the various CD peaks with those appearing on the excitation spectra. This would seem to indicate a link between the various surface defects which contribute to the luminescence and those defects where allow the band edge to be optically active. Refluxing was used to remove all surface defects creating a smoother trap free surface which allowed the particles to emit

intrinsically, however by removing these surface defects we also removed the optical activity. This is a strong link between emission type and particle chirality.

In our studies of chiral CdSe QDs, we have found that the defect luminescence plays a vital role in the presence or absence of circular dichroism in nanoparticles. This was confirmed by converting defect emitting dots into particles with intrinsic emission, that resulted in QDs, which do not show any CD activity.

We have also performed preliminary tests on sensing of selected chiral molecules using our new chiral CdSe QDs. While some sensing studies were carried out the results appear to be inconclusive and will need further study although it must be noted that the use of any material which can chelate Cd as an analyte, such as thiol-containing amino acids can partially destroy the particles.

Interaction studies between chiral CdSe dots and DNA also showed some interesting results. It was found that right handed DNA protects preferentially the L-Pen stabilised CdSe particles from the damaging affects of the EDTA buffer solution while both the D- and R- particles experienced a drop in luminescence. We believe this protection comes from the DNA's ability to selectively wrap more tightly around a complementary structure of L- stabilized particles. This demonstrates the potential of chiral CdSe based QDs as fluorescent chiral nano-sensors.

References

[1] M. Achermann, M. A. Petruska, D. D. Koleske, M. H. Crawford, V. I. Klimov, *Nano Lett.* **2006**, *6*, 1396.

[2] M. A. Hines, P. Guyot-Sionnest, *J. Phys. Chem.* **1996**, *100*, 468.

[3] Y. W. Lin, M. M. Hsieh, C. P. Liu, H. T. Chang, *Langmuir* **2005**, *21*, 728.

[4] F. Shieh, A. E. Saunders, B. A. Korgel, *J. Phys. Chem. B* **2005**, *109*, 8538.

[5] D. V. Talapin, I. Mekis, S. Gotzinger, A. Kornowski, O. Benson, H. Weller, *J. Phys. Chem. B* **2004**, *108*, 18826.

[6] S. Wageh, L. Shu-Man, F. T. You, X. Xu-Rong, *Journal of Luminescence* **2003**, *102-103*, 768.

[7] X. Chen, J. L. Hutchison, P. J. Dobson, G. Wakefield, *Journal of Colloid and Interface Science* **2008**, *319*, 140.

[8] Q. Zhang, T. P. Russell, T. Emrick, *Chem. Mater.* **2007**, *19*, 3712.

[9] J. Liu, T. Tanaka, K. Sivula, A. P. Alivisatos, J. M. J. Frechet, *J. Am. Chem. Soc.* **2004**, *126*, 6550.

[10] J. Locklin, D. Patton, S. Deng, A. Baba, M. Millan, R. C. Advincula, *Chem. Mater.* **2004**, *16*, 5187.

[11] C. Querner, A. Benedetto, R. Demadrille, P. Rannou, P. Reiss, *Chem. Mater.* **2006**, *18*, 4817.

[12] Z. Deng, Y. Zhang, J. Yue, F. Tang, Q. Wei, *J. Phys. Chem. B* **2007**, *111*, 12024.

[13] E. Hao, H. Sun, Z. Zhou, J. Liu, B. Yang, J. Shen, *Chem. Mater.* **1999**, *11*, 3096.

[14] J. A. Kloepfer, S. E. Bradforth, J. L. Nadeau, *J. Phys. Chem. B* **2005**, *109*, 9996.

[15] I. Mekis, D. V. Talapin, A. Kornowski, M. Haase, H. Weller, *J. Phys. Chem. B* **2003**, *107*, 7454.

[16] D. V. Talapin, R. Koeppe, S. Gotzinger, A. Kornowski, J. M. Lupton, A. L. Rogach, O. Benson, J. Feldmann, H. Weller, *Nano Lett.* **2003**, *3*, 1677.

[17] D. V. Talapin, J. H. Nelson, E. V. Shevchenko, S. Aloni, B. Sadtler, A. P. Alivisatos, *Nano Lett.* **2007**, *7*, 2951.

[18] D. V. Talapin, A. L. Rogach, E. V. Shevchenko, A. Kornowski, M. Haase, H. Weller, *J. Am. Chem. Soc.* **2002**, *124*, 5782.

[19] D. V. Talapin, E. V. Shevchenko, C. B. Murray, A. Kornowski, S. Forster, H. Weller, *J. Am. Chem. Soc.* **2004**, *126*, 12984.

[20] J. M. Tsay, M. Pflughoefft, L. A. Bentolila, S. Weiss, *J. Am. Chem. Soc.* **2004**, *126*, 1926.

[21] J. Chen, Y. Gao, C. Guo, G. Wu, Y. Chen, B. Lin, *Spectrochimica Acta Part A: Molecular and Biomolecular Spectroscopy* **2008**, *69*, 572.

[22] N. Gaponik, D. V. Talapin, A. L. Rogach, K. Hoppe, E. V. Shevchenko, A. Kornowski, A. Eychmuller, H. Weller, *J. Phys. Chem. B* **2002**, *106*, 7177.

[23] F. Huang, G. Chen, *Spectrochimica Acta Part A: Molecular and Biomolecular Spectroscopy, In Press, Corrected Proof.*

[24] F. C. Liu, T. L. Cheng, C. C. Shen, W. L. Tseng, M. Y. Chiang, *Langmuir* **2008**, *24*, 2162.

[25] S.-M. Liu, H.-Q. Guo, Z.-H. Zhang, R. Li, W. Chen, Z.-G. Wang, *Physica E: Low-dimensional Systems and Nanostructures* **2000**, *8*, 174.
[26] Y.-h. Zhang, H.-s. Zhang, X.-f. Guo, H. Wang, *Microchemical Journal, In Press, Corrected Proof.*
[27] T. Ni, D. K. Nagesha, J. Robles, N. F. Materer, S. Mussig, N. A. Kotov, *J. Am. Chem. Soc.* **2002**, *124*, 3980.
[28] A. E. Raevskaya, A. L. Stroyuk, S. Y. Kuchmiy, Y. M. Azhniuk, V. M. Dzhagan, V. O. Yukhymchuk, M. Y. Valakh, *Colloids and Surfaces A: Physicochemical and Engineering Aspects* **2006**, *290*, 304.
[29] Y. J. Yang, B. J. Xiang, *Journal of Crystal Growth* **2005**, *284*, 453.
[30] V. M. Bhuse, P. P. Hankare, K. M. Garadkar, A. S. Khomane, *Materials Chemistry and Physics* **2003**, *80*, 82.
[31] E. Mullins, *Statistics for the quality control chemistry laboratory*, **2003**.
[32] S. F. Wuister, C. deMelloDonega, A. Meijerink, *J. Phys. Chem. B* **2004**, *108*, 17393.
[33] P. T. K. Chin, C. deMelloDonega, S. S. vanBavel, S. C. J. Meskers, N. A. J. M. Sommerdijk, R. A. J. Janssen, *J. Am. Chem. Soc.* **2007**, *129*, 14880.
[34] R. Gill, I. Willner, I. Shweky, U. Banin, *J. Phys. Chem. B* **2005**, *109*, 23715.
[35] D. Pan, Q. Wang, J. Pang, S. Jiang, X. Ji, L. An, *Chem. Mater.* **2006**, *18*, 4253.
[36] M. G. Bawendi, P. J. Carroll, L. W. William, L. E. Brus, *The Journal of Chemical Physics* **1992**, *96*, 946.
[37] V. I. Klimov, D. W. McBranch, C. A. Leatherdale, M. G. Bawendi, *Physical Review B* **1999**, *60*, 13740.
[38] G. Schlegel, J. Bohnenberger, I. Potapova, A. Mews, *Physical Review Letters* **2002**, *88*, 137401.
[39] W. Xiao-Yong, Z. Jia-Yu, A. Nazzal, M. Darragh, X. Min, *Applied Physics Letters* **2002**, *81*, 4829.
[40] X. Wang, L. Qu, J. Zhang, X. Peng, M. Xiao, *Nano Lett.* **2003**, *3*, 1103.
[41] K. Zhao, J. Li, H. Wang, J. Zhuang, W. Yang, *J. Phys. Chem. C* **2007**, *111*, 5618.
[42] H. Qian, L. Li, J. Ren, *Materials Research Bulletin* **2005**, *40*, 1726.
[43] J. Jack Li, J. M. Tsay, X. Michalet, S. Weiss, *Chemical Physics* **2005**, *318*, 82.
[44] M. P. Moloney, Y. K. Gun'ko, J. M. Kelly, *Chemical Communications* **2007**, 3900.
[45] G. D. Lilly, J. Lee, K. Sun, Z. Tang, K. S. Kim, N. A. Kotov, *J. Phys. Chem. C* **2008**, *112*, 370.
[46] E. W. S. D. Haifeng Bao, *Small* **2006**, *2*, 476.
[47] P. Furst, P. Stehle, *J. Nutr.* **2004**, *134*, 1558S.
[48] Z. Tang, Y. Wang, S. Shanbhag, M. Giersig, N. A. Kotov, *J. Am. Chem. Soc.* **2006**, *128*, 6730.

Chapter 5.

Cadmium Telluride

Introduction 5.1

Unlike previously discussed CdS and CdSe QDs, CdTe is arranged in a cubic, zinc blende, and not wurzite crystal structure. It has a band gap energy of 1.56 eV, ~795 nm, when in the bulk state, and is transparent to infrared radiation out to 20 μm. It was hoped that it could be used to make optical windows and/or lenses. However, due to its high toxicity this was abandoned. Again like CdS and CdSe there has been a large resurgent of interest in this material over the last twenty years or so, but in the nano and not bulk state. By contrast to CdS and CdSe, it is quite easy to prepare intrinsically emitting highly stable CdTe nanocrystals in water using microwave synthesis[1-3]. In addition intrinsically, emitting dots have demonstrated a great potential as fluorescent biological sensors.[4-10] CdTe, like most other semiconductor nanoparticles, are expected to also have applications in optoelectronic and photovoltaic devices.[11-15] However it has also been reported that CdTe nanoparticles may be treated to produce nanorods and nanowire structures.[16-18] This is of interest as nanowires are known to emit polarised light and this may give us the opportunity to produce nanostructures which preferentially absorb and emit polarised light.[19-21] Although the main aim of this part of our work is to develop new CdTe based chiral QDs and investigate their properties. Another important objective is to explore the possibility of enantiomeric control of quantum yield in QDs using various ratios of chiral stabilisers and establish a relationship between chirality and quantum efficiency of CdTe QDs. Finally we also plan to prepare chiral quantum wires based on CdTe, using the above reported techniques.

5.2 Synthesis

1. 2ml of 1 x 10^{-2}M Stabilizer in 45ml of water. Final concentration in overall reaction is **2 x 10^{-5}m.**

2. p.H is adjusted to 11 using 2M NaOH

3. 2ml of 1 x 10^{-2}M solution of $Cd(ClO_4)_2.H_20$ in water. Final concentration in overall reaction is **2 x 10^{-5}m.**

4. 2ml of 8 x 10^{-2} M solution of Na_2TeO_3 in water. Final concentration in overall reaction is **2 x 10^{-5}m.**

5. 2ml of 8 x 10^{-1} M solution of $NaBH_4$ in water. Final concentration in overall reaction is **2 x 10^{-4}m.**

6. Sample was microwaved for 1min 10sec at 800W.

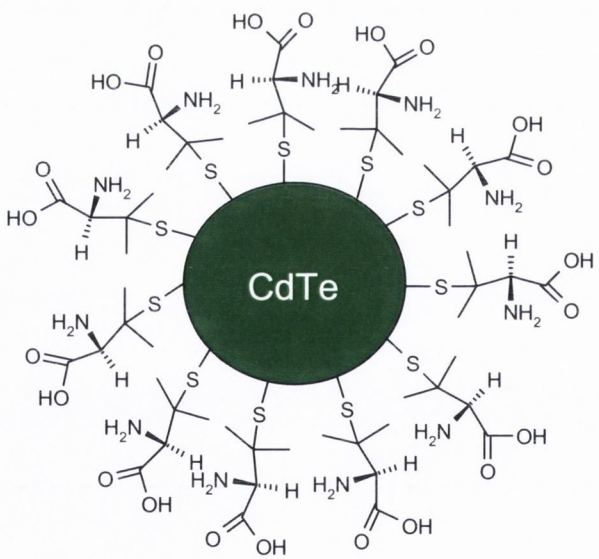

Figure 5.1: Schematic representation of CdTe preparation. The example used is the first point in a 2^2 study of CdTe. Both Cd and stabilizer concentrations are systematically increased while Te concentration stays fixed at 2 x 10^{-5} moles.

The CdTe QDs were prepared using a modified version of the method reported by Bao et al.[22] However the synthesis of QDs was altered to resemble as closely as possible the CdS and CdSe preparation as in the previous chapters. While Na_2TeO_3 took the place of CH_3CSNH_2 or Na_2SeSO_3 the other main change to the reaction scheme was the introduction of $NaBH_4$ to act as a reducing agent releasing Te^{2-} into solution. Briefly, the particles were prepared using microwave induced heating of a solution of $Cd(ClO_4)_2.6H_2O$, stabilizer-(cystein or penicillamine), Na_2TeO_3 and $NaBH_4$. Microwave irradiation was again used to produce highly luminescent CdTe nanocrystals as it has proven to be a very efficient in several previous publications,[2, 3] as well as within this thesis. The Racemic (*Rac*), Dextro (*D*-), and Levorotary (*L*-), enantiomeric forms of cysteine (Cys) were used individually as the stabilizers.

5.3 Penicillamine stabilised CdTe QDs

5.3.1 Optimisation of synthesis (Statistical Analysis)

Initially it was expected that CdTe dots could be produced using penicillamine as the stabilizer. Although penicillamine coated CdTe dots have never being reported in the literature this was not considered a problem as Pen coated CdS or CdSe also had not being reported and as we have discussed in the previous chapter's penicillamine can be used to produce highly luminescent optically active quantum dots. As with the previous 2^2 statistical studies it was the cadmium and stabilizer concentration which were altered; the Te concentration remained fixed throughout the study. Therefore no problems were foreseen when the usual 2^2 statistical analysis was preformed on a Penicillamine CdTe system.[23] The reaction scheme and concentrations were identical to those used in previous chapters and Na_2TeO_3 replaced Na_2SeSO_3 as the X^{2-} source, again luminescence was used as the response.

The results of these experiments were extremely inadequate, because only dots which had barely any luminescence, were produced (**Figure 5.2** and **5.3**).

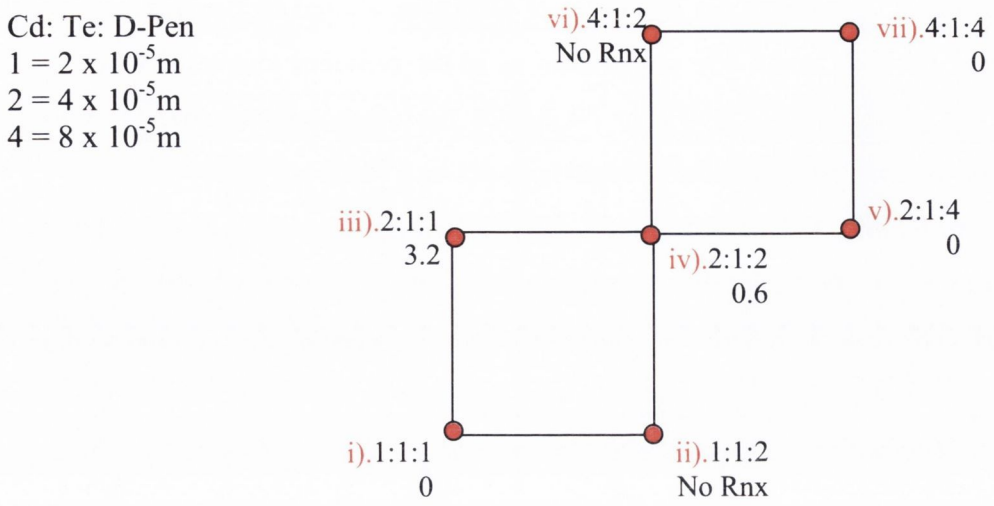

Figure 5.2: 2^2 statistical analysis of D-Pen CdTe. Quantum yields were not measured as luminescence was too low. PL intensities were used as the response instead.

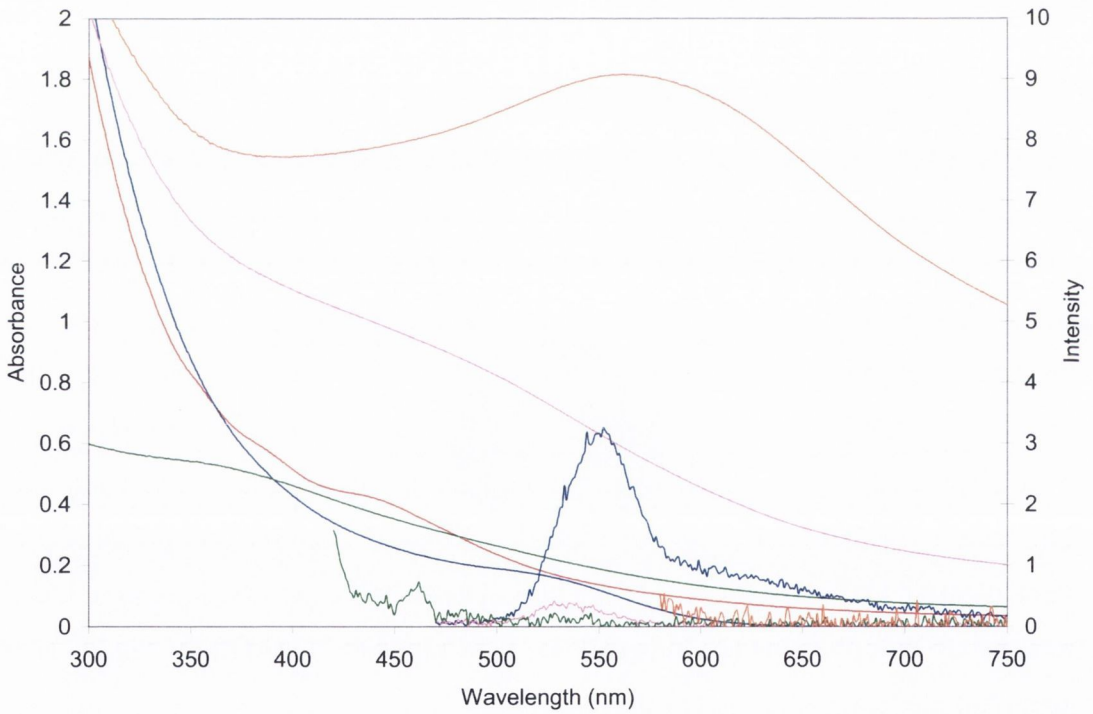

Figure 5.3: Absorption/PL spectra of stats study of penicillamine capped CdTe, 1-orange, 3-blue, 4-pink, 5-green, 7-red. Particles were excited at their various absorption maximas. With the exception of batch 3 none of the samples produced characterisable emission spectra.

5.3.2 Enantiomer and Racemate of Pen stabilized CdTe

Out of the seven batches prepared only number 3 produced dots with what could be called structured emission spectra, **Figures 5.2 and 5.3**. Examination of the CD spectra of these particles showed them to be optically active however the lack of luminescence caused them to be abandoned for the more promising cystein capped nanoparticles. [22, 24, 25]

Examination of the absorption spectra's of the D-, L- and R- Pen-CdTe particles show strong well defined exitonic bands, **Figure 5.4.** In contrast to most other of the particle types reported in this thesis the R-Pen CdTe has an absorption maxima which is red shifted when compared to that of its D- and L- counter parts. This indicates that they, (the R-CdTe), are slightly bigger than the D- and L-CdTe QDs

D-, L- and R- dots absorb at 505nm, 524nm and 537nm respectively. While the D-stabilized particles show mostly intrinsic emission at 555nm both L- and R- particles have a combination of intrinsic and defect peaks, L- 562nm and 617nm, and R- 546nm and 617nm, allowing them to emit white light.

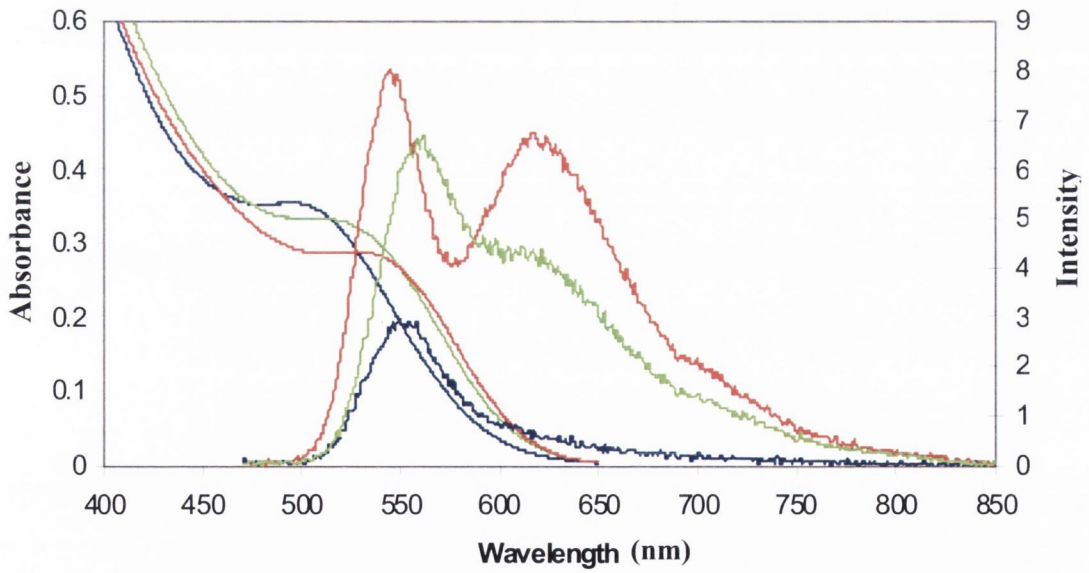

Figure 5.4: Absorption/PL spectra of D-blue, L-lime, and R-red penicillamine capped CdTe. Particles were excited at 450 nm. It is interesting to note the presence of both intrinsic and defect peaks in the L- and R- samples. In the case of L- this defect peak disappeared after a week but remained in the R sample.

The proximity of the absorption and emission maxima in the R-sample show that complimentary enantiomer effect is once again taking place here. This is in stark

contrast with both the greater lamda max of the R-absorption spectrum and the fact it has the largest defect emission of the three particle types.

CD spectroscopy, **Figure 5.5**, shows that both D- and L- Pen-CdTe particles are indeed optically active in the band edge region. R- Pen- stabilised CdTe QDs are of course CD neutral. Despite the optically weak concentration of the particles, (0.35 at the bandedge regions), they are still strongly optically active, (5 millidegrees at the bandedge region).

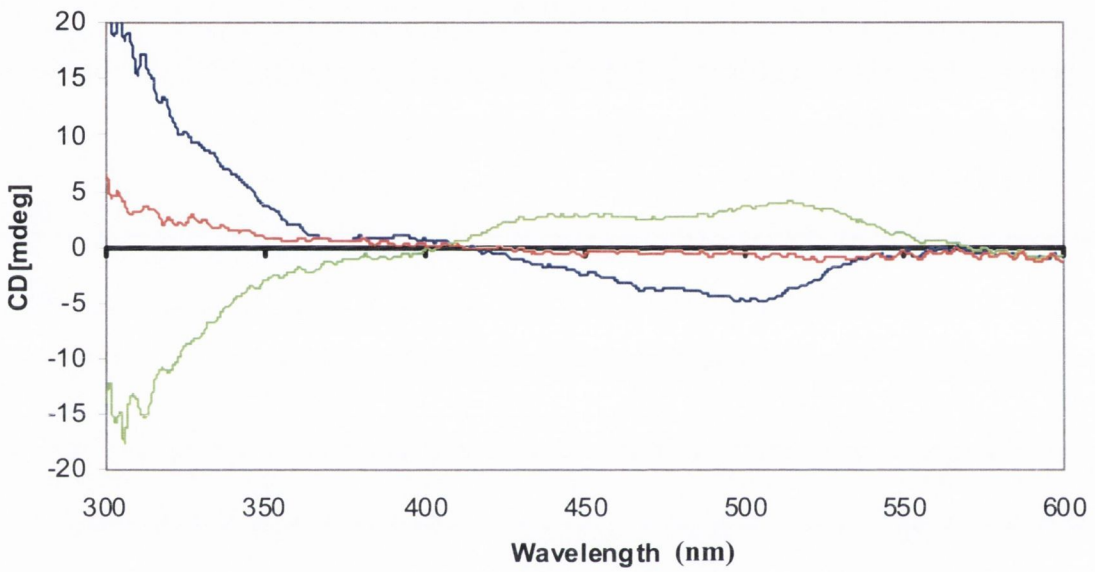

Figure 5.5: CD spectra of D-blue, L-lime, and R-red penicillamine capped CdTe. Particles show a strong CD response from their exciton band down. D- particles are slightly smaller and are therefore blue shifted when compared to the L-.

However, these penicillamine coated CdTe particles demonstrated very weak luminescence. Therefore due to the poor nature of their luminescence the synthesis of penicillamine stabilised CdTe QDs was abandoned and a more conventional, but still chiral, CdTe stabilizer, (Cystein), was used instead.[1, 8, 18, 26]

5.4 Cystein stabilised CdTe QDs

5.4.1 Optimisation of synthesis (Statistical Analysis)

Experiments on the preparation of Cys-CdTe and their optimisation using a 2^2 statistical analysis enabled us to prepare a series of highly luminescent CdTe nanoparticles. Again a seven point study was used and examined with quantum yield as the primary response.[23] The reaction scheme detailed in **Figure 5.1**, (replacing Penicillamine with Cystein), was once again used as the starting point for a multi-factor study. Again the starting point was 2ml of aliquots of 1 x 10^{-2}M stock solutions in 40ml of Millipore water, doubling the volume of one reactant in one direction at a time Again the Te^{2-} concentration remained static at 2ml of 1 x 10^{-2}M, (2 x 10^{-5} moles), (**Figure 5.6**). The quantum yield was the primary response studied over the course of this statistical analysis.

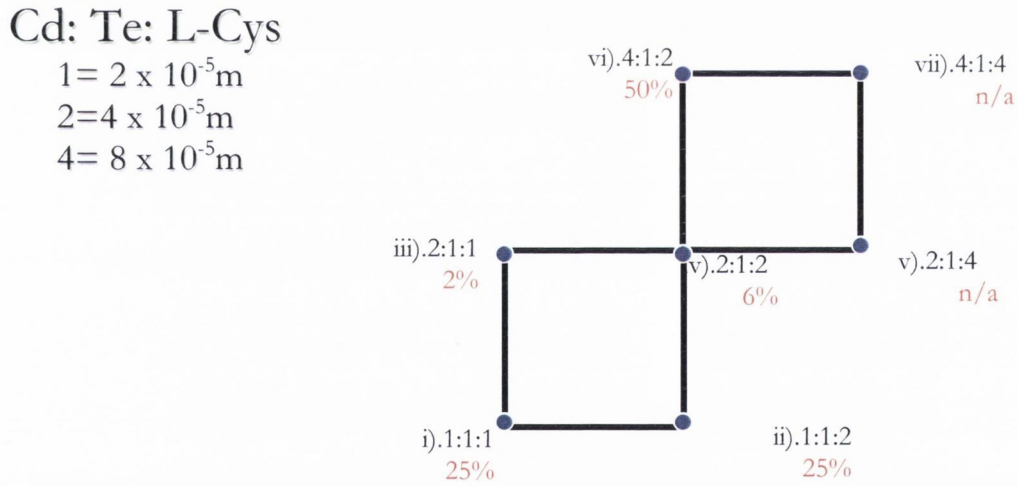

Figure 5.6: 2^2 statistical analysis of L-Cys-CdSe. Quantum yields for each point were measured against Coumarin 153 in MeOH.

All particles produced over the course of the study were of course examined using UV, PL and CD spectroscopy, creating a fuller picture of the effect of the alternate ratios on the dots.

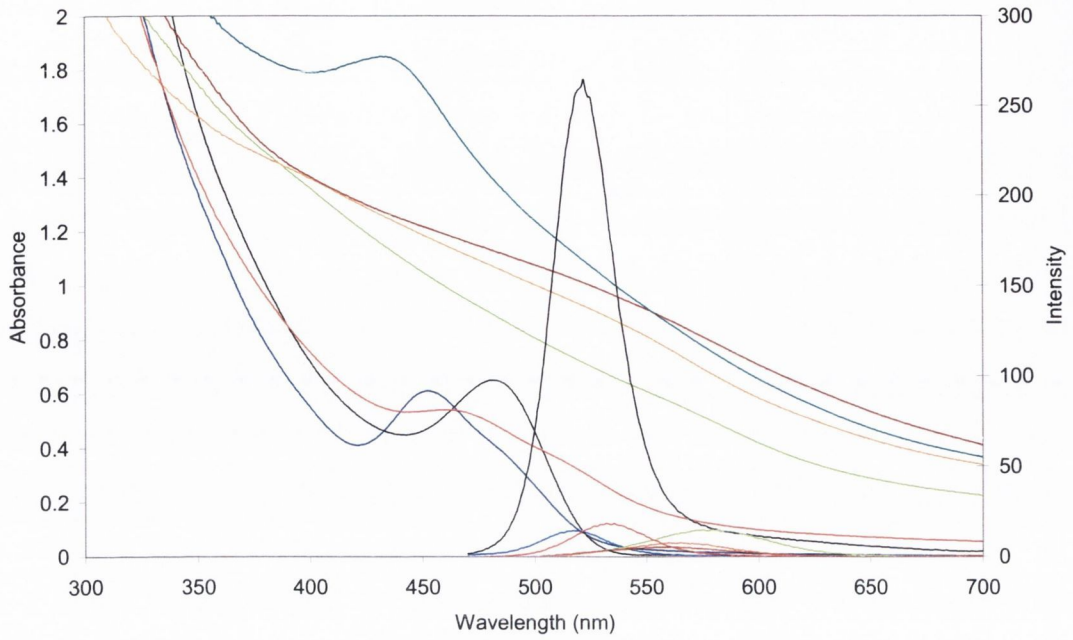

Figure 5.7: Abs/Pl spectra of statistical analysis of Cys-CdTe. PL's were excited at 450nm. 1-lime, 2-orange, 3-blue, 4-red, 5-brown, 6-black, 7-aqua.

Figure 5.7 shows both absorption and emission spectra for batches 1-7. It is obvious that batch #6 gives not only particles with the highest quantum yields but also the most structured exciton band. Again, as seen in the penicillamine CdTe studies, a high degree of scattering and low emission from the other batches within the analysis is clearly visible however the batches that did work produced highly luminescent particles. Due to the high degree of scattering and lack of definite band edge structures for most of the other batches it was difficult to elucidate any discernable pattern as was possible with the previous CdS and CdSe statistical analyses. Optimisation of L-Cys stabilised CdTe nanoparticle synthesis is presented as 3-D diagram of a 2^2 statistical analysis in **Figure 5.8.** The experiments with CdSe considered in the previous chapter showed that as the particles luminescence became more intrinsic its optical activity diminished significantly. We anticipated that the CdTe particles produced in our work could demonstrate CD activity, although possessing intrinsic luminescence.

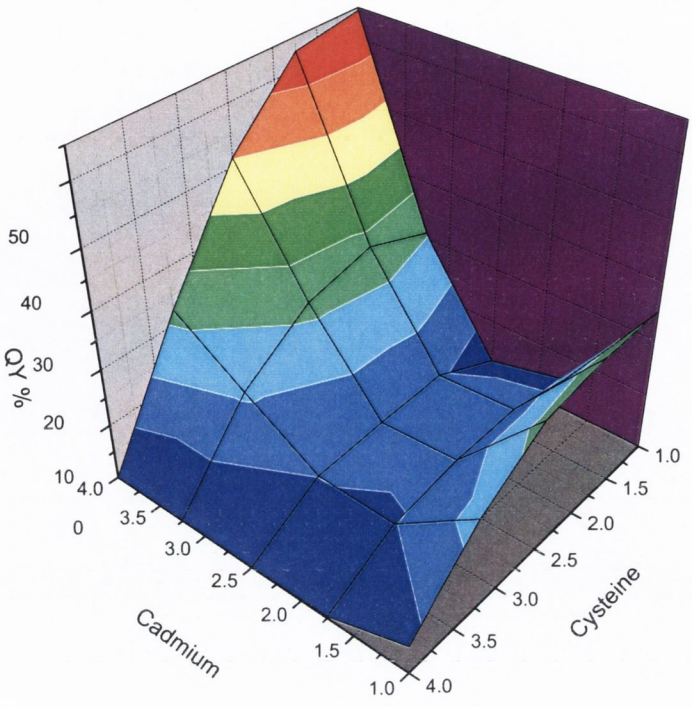

Figure 5.8: 3-D representation of a 2^2 statistical analysis of the formation of L-Cys CdTe using quantum yield as the response. An Origin 7.5 random xyz matrix was used to generate the graph.

5.4.2 Preparation and characterisation of Cys-CdTe Enantiomers and Racemate

D-, L- and R- Cys stabilised CdTe nanoparticles have been prepared by microwave synthesis as described above, (**Figure 5.1).** To determine the level of reproducibility each particle type, (D-, L-, R-), were prepared three times were examined using UV-Vis and photoluminescence spectroscopy. TEM and fluorescent lifetime data were also recorded for all nine samples. The QYs of these QDs were calculated at 470nm using Rhodamine G as a standard, as Coumarine 153 was inappropriate for nanoparticles in this region of the spectrum.

The average absorbance maxima were: 525 nm for D-, 527 nm for L- and 520 nm for R- QDs, (**Figure 5.9**). All CdTe nanoparticle samples emitted strongly in the green-yellow region of the spectrum when excited at 470nm, with average maximas of D- 550 nm, L- 550 nm and R- 546 nm, S.D's were 6.5, 2 and 7.7nm for D-, L- and R- respectively with FWHM of 35 ± 3 nm, (**Figure 5.9**). Excitation spectra taken at 580 nm agreed with their corresponding absorption spectra within 1 - 2 nanometre deviation. These spectral characteristics are typical for CdTe nanocrystals with

excitonic emission, which possess a high degree of monodispersity and have very little surface defects. Due to the particle absorbance from 570nm on, the particles appeared red in visible light, however their high QY gave them a strong green glow clearly visible to the naked eye.

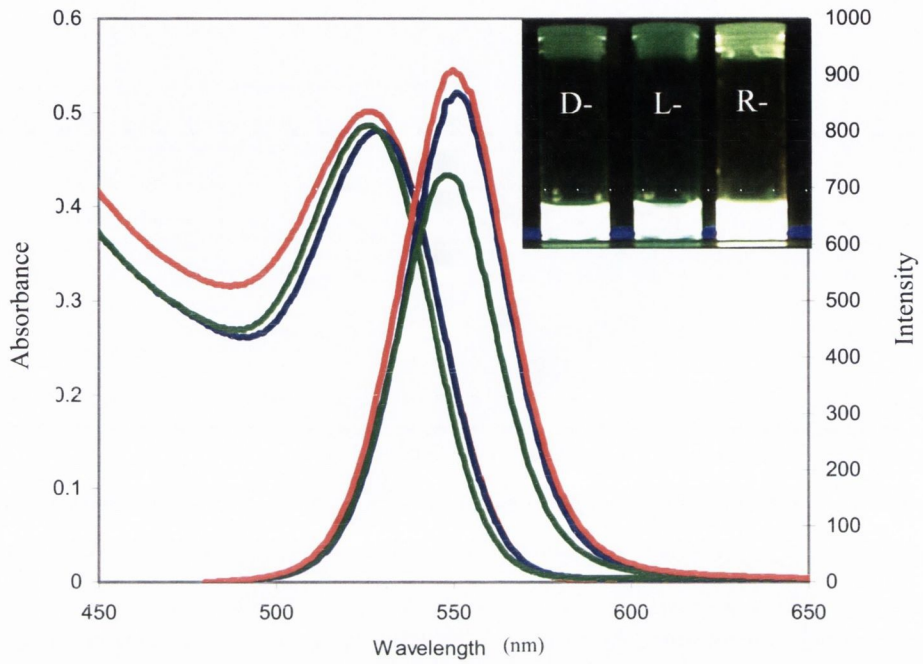

Figure 5.9: Optical spectra (UV-Vis absorption – left and emission – right) of CdTe nanocrystals stabilized with D-Cys (blue), L-Cys (green) and Rac-Cys (Red). Excitation wavelength for all emission spectra is 470nm.

Our measurements of quantum yields gave values of 24±9, 26±1 and 32±1% for D-, L- and R- respectively. The increase in the QY when using a racemic stabiliser is again attributed to the complementary nature of the racemate, as explained in previous chapters, allowing for closer packing of the stabiliser on the nanoparticle surface. This increase in the hydrophobic nature of the QD's surface results in a more efficient elimination of surface bound oxygen and water molecules. As these molecules acts as potential hole traps for surface recombining excitons, their removal contributes to the observed luminescence and QY increases. In order to further examine the dependence of the quantum efficiency on the enantiomeric ratio, 1:3 and 3:1 mixes of D- and L-Cys CdTe were also prepared and their QY recorded. These mixtures resulted in the formation of QDs with lower QYs, which were close to ones for the individual D- or L- enantiomer stabilised particles. In this case the reduction in the QY can be

explained by the non-uniform distribution of D- and L- stabiliser molecules on the QD surface leading to extra defects and kinks (**Figure 5.10**).

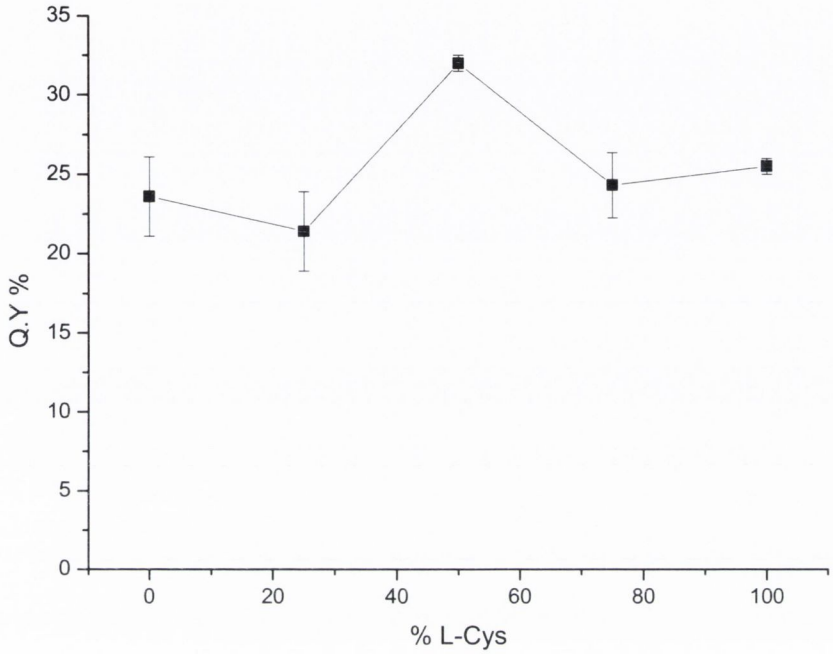

Figure 5.10: Graph detailing the changes in QY as the chirality of the surface stabilizer is altered, starting with pure D, (0% L-Cys), and ending with pure L-, (100% L-Cys). Note the large increase in the QY at 50% where D- and L- are equal, i.e. the racemate.

5.4.3 Fluorescent lifetimes of Cys-stabilised CdTe QDs

Examination of the emission lifetime decays of D- L- and R- Cys- CdTe particles using a bi-exponential fit showed that all three types of particles despite having different quantum yields had remarkably similar lifetime components, (**Table 5.1**). However this can be explained by comparing the contributions of the short life time, (core), and the long life time, $\mathbf{B_2}$, (shell) with the quantum yields of the individual particles. According to table 5.1 as the quantum yield increases in the R-CdTe particles so to does the contribution of the longer life time , which can be attributed to the removal of non-radiative defects on the surface of these particles.

Table 5.1: Lifetime data for Cys stabilized CdTe nanoparticles. Although the trend is not exactly linear there is a noticeable increase in the contribution of the longer lifetime when the quantum yield increases in the R- sample.

	Q.Y	A	χ^2	τ_1	B_1	$\%_{B1}$	τ_2	B_2	$\%_{B2}$
D-	28%	5.4	1.1	12ns	542	61%	32ns	361	39%
L-	27%	7.43	1.1	12ns	493	56%	34ns	406	44%
R-	33%	7.5	1.0	10ns	450	48%	30ns	492	52%

5.4.4 TEM analysis of Cys-CdTe

HR TEM (**Figure 5.11**) showed the dots to have an average diameter of 4-5nm which is consistent with CdTe which absorbs at 520nm.

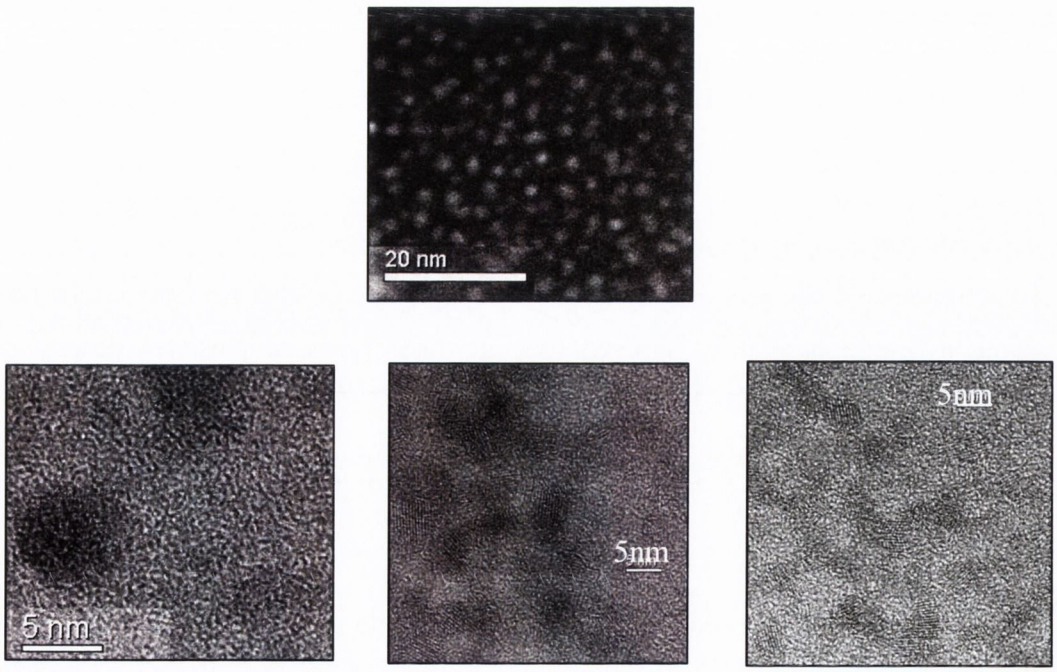

Figure 5.11: Above; Dark field STEM, (D-), and bottom; HRTEM of D-, L- and R- of Cys CdTe nanocrystals.

5.4.5 CD studies of –Cys CdTe

Examination of these particles using CD spectroscopy showed that while a structured CD signal was present it was very weak, (**Figure 5.12**). As mentioned earlier the presence of surface defects in the previously reported CdS was due to the formation of a chiral shell on an achiral core.[27] These defects were also expressed by the broad red shifted defect emission. However these particles, unlike the CdS and CdSe particles do not exhibit defect but intrinsic luminescence and consequently express only a very weak chirality. As discussed above for CdS and CdSe dots, defect emission must be present in dots which give a strong CD signal.

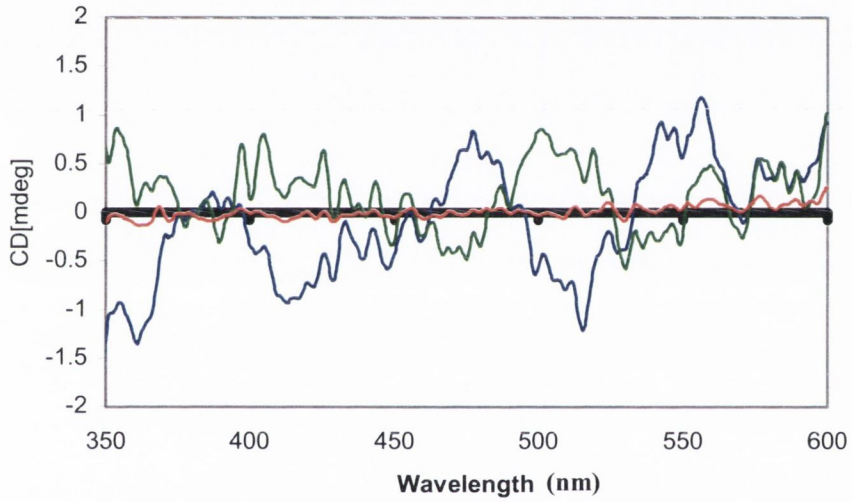

Figure 5.12: CD spectrum of D-, L- and R-Cystein stabilized CdTe. Although very weak the spectra posses a clear structure with sharp signals at 500nm for both the D- and L- particles.

As close examination of previously prepared particles, i.e. CdS and CdSe, revealed the formation of chiral Cd-stabilizer complexes and chiral nanoclusters before eventual nanoparticles formation it was considered unusual that no strong CD signal were visible in these dots. To explore this system CD response monitoring experiments were carried out during the preparation of these particles similarly to CdS and CdSe systems described in previous chapters. As expected, initial spectra of the stabilizer, cystein, before and after addition of the Cd showed the presence of chirality. Initially we see a signal at 210nm from the pure cystein, and then an additional signal at 215nm from the chiral Cd-Cys complex, (**Figure 5.13**).

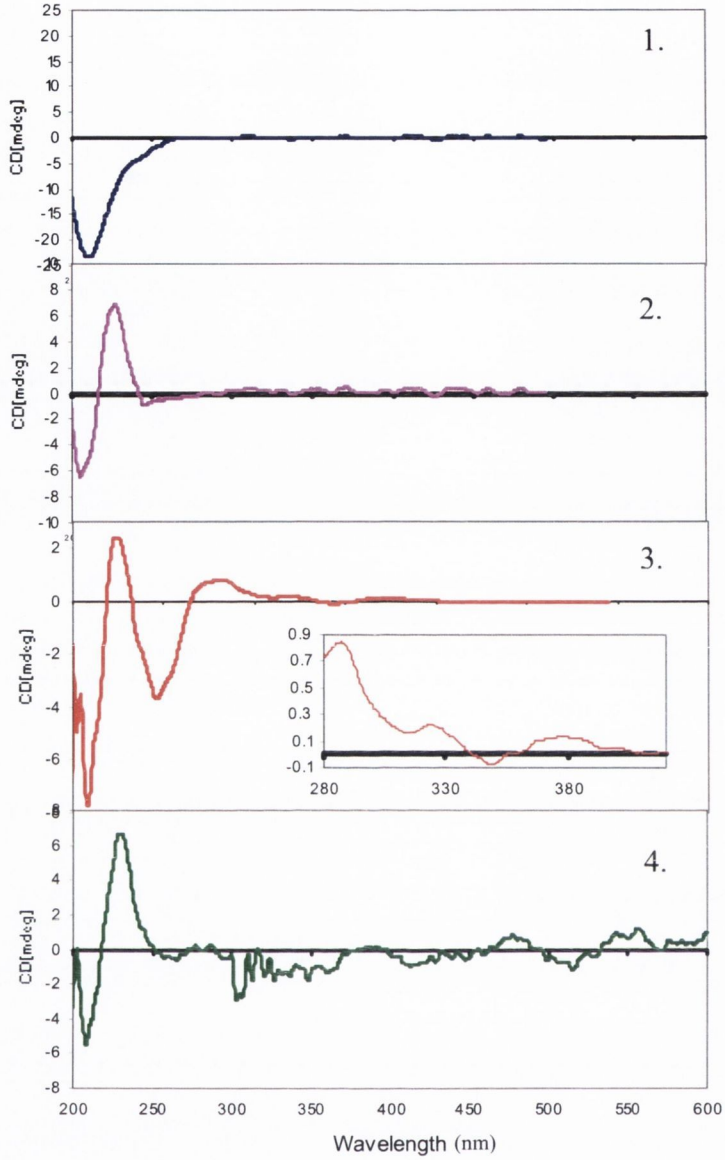

Figure 5.13 CD spectra monitoring the formation of *D*-Cys CdTe QD's. **1.** Cys absorbs negatively at ~210 nm. **2.** The addition of Cd ions forms a Cd-Cys complex and causes the appearance of a new band at ~233nm. **3.** The clusters after addition of the sodium tellerite before the microwave treatment – new bands from 250 to 405 nm (blue). **4.** CdTe QD's after the microwave treatment –all signals beyond 255nm have practically disappeared with only the Cd-Cys complex signal remaining strong. Region from 255-600nm was multiplied by a factor of 5 to make viewing easier, hence the high degree of signal noise.

Upon the addition of Te^{2-} ions small chiral weakly luminescent nanoparticles are formed as can seen by the appearance of signals out to 400 nm. This shows that chiral nanoparticles were indeed formed. Again the presence of luminescence shows that these are nanoparticles and not nanoclusters. However, after microwave irradiation these particles rearrange as highly intrinsic luminescent nanocrystals. The CD signal red shifts as reported before[27] in accordance with particle growth. However, the

heating and consequent growth processes result in the partial removal of surface defects and consequently in the reduction and near complete loss of any CD signal.

5.4.6 Coating of CdTe QDs with CdS shell

In an attempt to introduce chirality into CdTe particles two different routes were explored. The first involved the building of a chiral CdS shell around the achiral CdTe core, this can be done by one of two well known methods i). chemical growth of CdS onto the particles or ii). the use of a high powered light source to photochemically decompose the cystein stabilizer around the dots again forming a chiral CdS around the CdTe core, excess cystein in solution would then be available to stabilize the new CdTe/CdS particles. The second route would involve going back to the start and attempting to synthesis CdTe particles using a mixture of both cystein, (for luminescence), and penicillamine, (for optical activity), this route will be discussed in the next section. The methods of growing one type of semiconductor shell around another are well established and has been reported many times.[28-32] Once the core particles are prepared a second semiconductor, usually with a larger bandgap energy is chemically grown onto the core usually by the slow addition of either the metal followed by the non first metal, or vice versa, or by addition of small volumes of the metal and non-metal one after the other until the desired concentration is reached.

Chemical Deposition of CdS shell

While these additions are normally carried out at slightly above room temperature they can also be done, (depending on the solvent), at extremely low, (-70°C in methanol) or extremely high, (200°C lauric acid) temperatures. In essence there is no hard and fast rule to grow heterogeneous shells on quantum dots. So with this in mind three different routes were attempted in our work. These included heating at room temperature, microwaving and sonication.

The first method involved the heating of degassed core particles at 40°C while 1 x 10^{-2}M aqueous solutions of $Cd(ClO_4)_2.6H_2O$ and $Na_2S.9H_2O$ were added alternately drop by drop. While this lead to an increase in particle size as can be clearly seen by the red shift in the absorbance and emission peaks it also caused a drastic decrease in

the quantum yield of the particles as well as having no effect on the CD activity, (**Figure 5.14**). The experimental setups for the microwaving and sonication routes were similar to that described above with two notable exceptions. Firstly, thioactemide and not sodium sulphide was used as the sulphur source, and secondly, all the shell precursors were added before irradiation commenced. The results, however, were very similar to those observed for the heating method used above. That is, the particles showed an increase in size and decrease in luminescence, but no change in the degree of optical activity, (**Figures 5.15 and 5.16**).

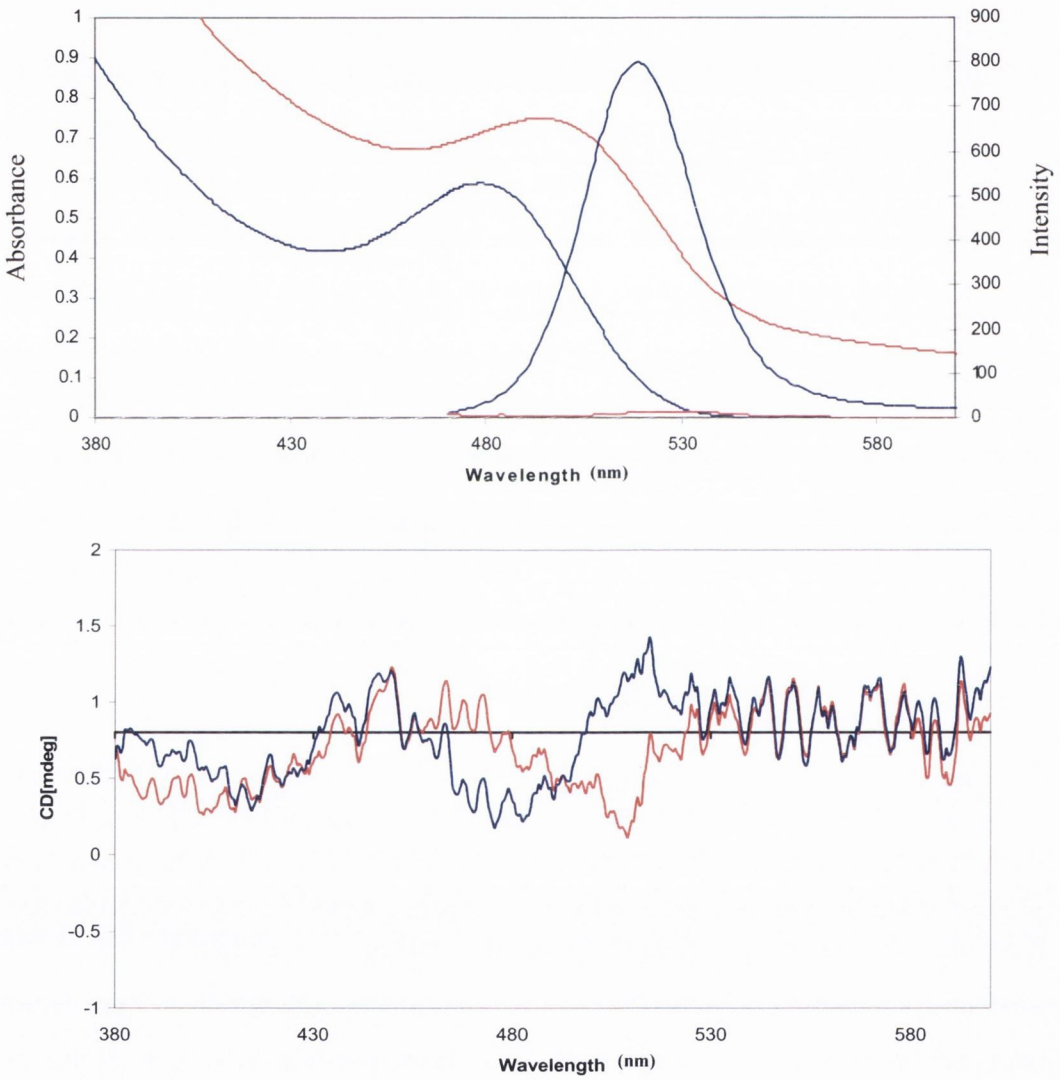

Figure 5.14 Above; Absorption and emission spectra of Cys-CdTe particles before, (abs-481nm and ems-520nm), and after, (abs-497nm and ems-529nm), heating at 40°C for an hour. The red shift in both the absorbance and emission peaks indicates a growth in particle size which is indicative of shell formation. The increased scattering confirms this size growth. Below; CD spectrum of particles before and after shell formation although the shape of the signal has changed there is no increase the strength of the signal.

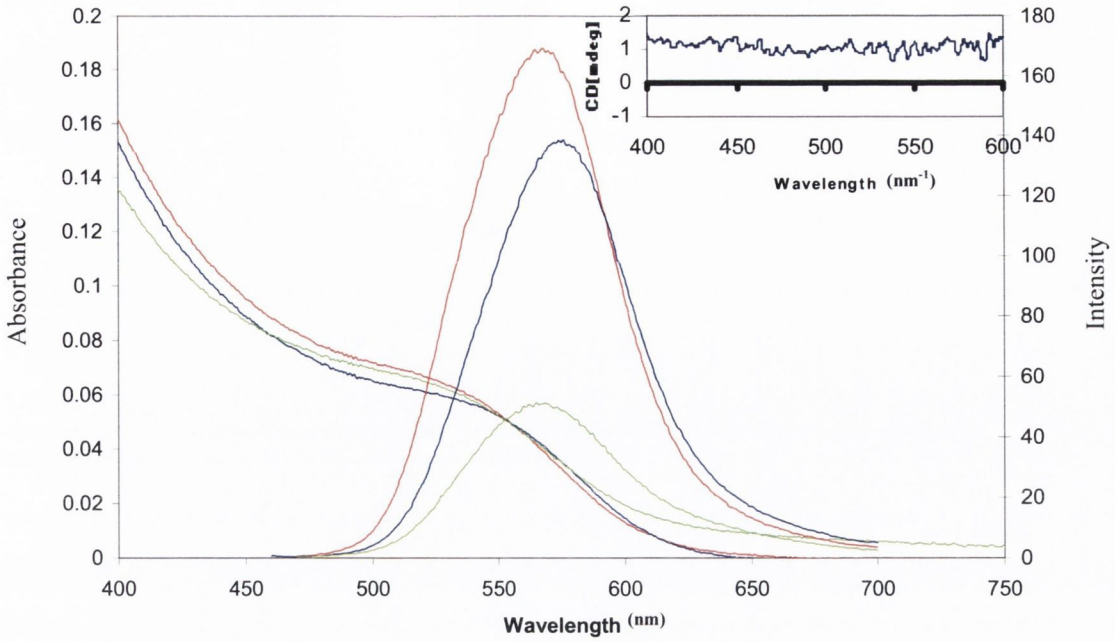

Figure 5.15 Absorption and emission spectra of Cys-CdTe particles before, (abs-526nm and ems-569nm), and after addition of thioactemide, (abs-539nm and ems-576nm), and after 2hrs, (abs-528nm and ems-569nm), of sonication. The red shift in both the absorbance and emission peaks indicates a growth in particle size which is indicative of shell formation. The increased scattering confirms this size growth. Inset; CD spectrum of particles after sonication no CD signal has appeared

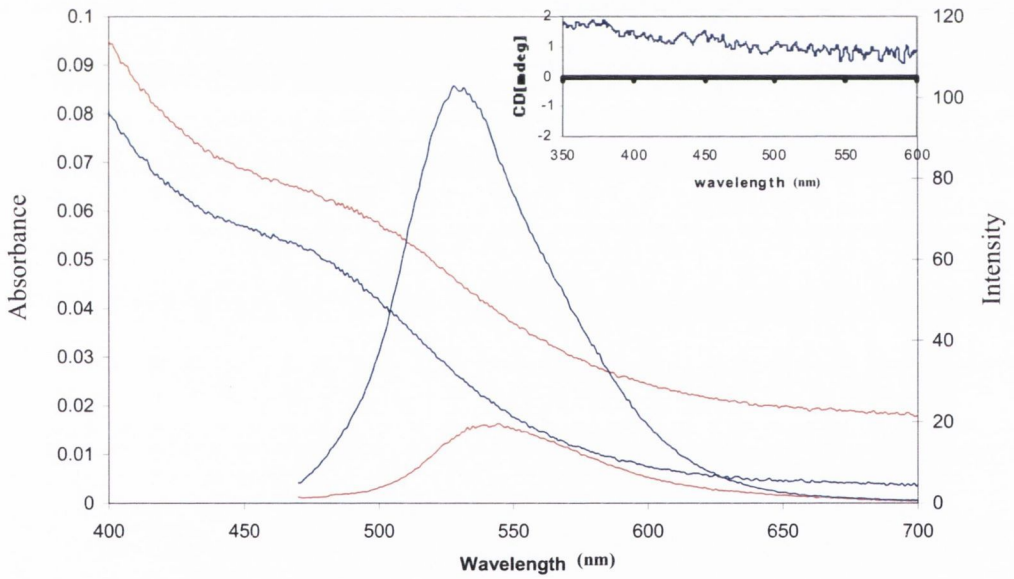

Figure 5.16 Absorption and emission spectra of Cys-CdTe particles before (blue curve), (abs-476nm and ems-531nm), and after (red curve) microwaving, (abs-501nm and ems-545nm). The red shift in both the absorbance and emission peaks indicates a growth in particle size which is indicative of shell formation. The increased scattering confirms this size growth. Inset; CD spectrum of particles after sonication no CD signal has appeared.

In the third approach after 2hrs of sonication in ultrasonic bath at room temperature the particles absorption and emission peaks had shifted back to where they were, (569nm), this is more than likely due to rearrangement of the nanocrystals lattice to

form an alloy of CdSTe, with a bandgap energy intermediate to the two types of semiconductors and therefore more to the blue region of the spectrum than simple core/shell particles.[33]

Photoannealing of Cys-stabilised CdTe particles

Another approach was to expose the degassed unwashed particles to a high powered Hg lamp for short periods, (10mins), of time. It was anticipated that this would form a chiral CdS shell around the CdTe particles through anaerobic photodecomposition of the stabilizer.[1, 34] The Cd-S bond, being too strong to break, remains intact leaving dangling sulphur atoms on the surface of the particles. The excess Cd in solution would immediately bond to these sulphur atoms and the excess cystein would then be used to stabilize the newly formed CdTe/CdS particles.

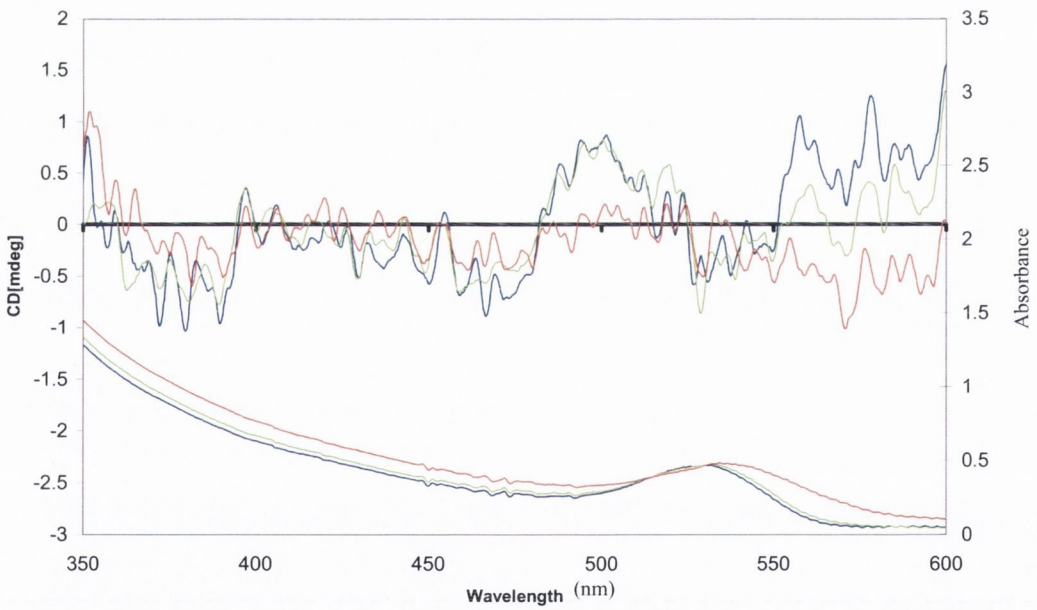

Figure 5.17 CD and Abs spectra of Cys-CdTe particles before, (blue), and after 10, (lime) and 20, (red) minutes exposed to the Hg lamp. The disappearance in what little CD structure is present indicates a removal of surface defects by the lamp.

However photoannealing also has the secondary effect of essentially burning off defects on nanoparticles surfaces, while it was hoped reducing the particles exposure to the lamp would minimise this effect it was not to be. In fact the weak chiral response of the initial Cys-stabilised CdTe particles was lost after only 20mins of

exposure to the lamp as can be seen from the CD spectra in **Figure 5.17**. Again the intense red shift in the emission spectra indicates particle size growth, (**Figure 5.18**).

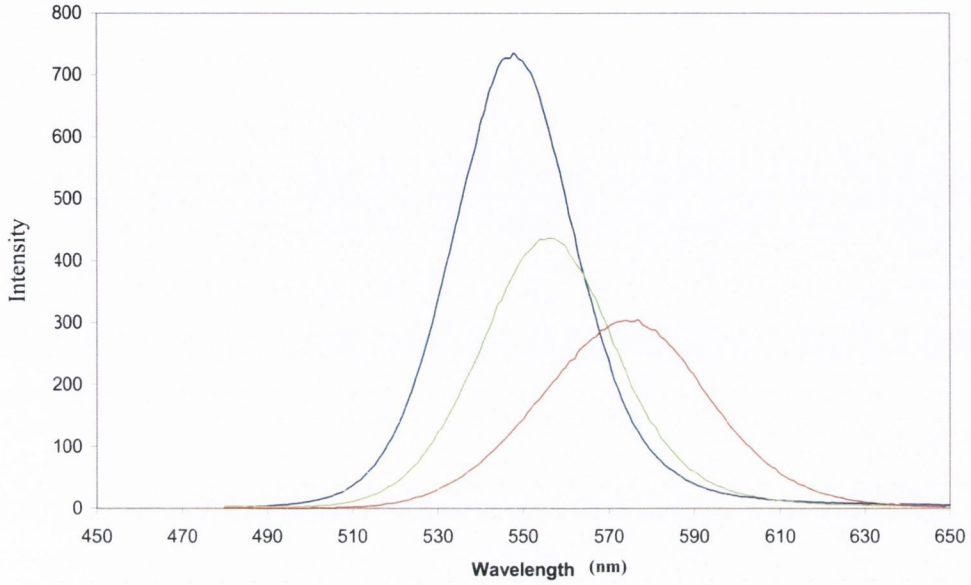

Figure 5.18 Emission spectra of Cys-CdTe particles before, (blue), and after 10, (lime) and 20, (red) minutes exposed to the Hg lamp. The red shift in the emission maxima indicates particle growth as CdS is deposited onto the CdTe core

Since no extra reactants have been introduced into the system we can only assume that this particle growth is due to the formation of a CdS shell on the CdTe core particles. However none of the above mentioned experiments seemed to work. While changes in the position and intensities of the various maxima did indicate shell deposition had occurred there was no notable increase in CD activity. This can be explained by the photoannealing of any chiral defects. Thus in all our experiments we did not observe the formation of any chiral QD species. Therefore because of the failure of these experiments another approach to fabricate chiral CdTe was taken.

As cystein produces highly luminescent dots, while penicillamine capping results in chiral ones it was decided to make mixed Cys-Pen stabilizer dots to try and get the best of both systems.

5.4.7 Cystein- Penicillamine co-stabilized CdTe nanoparticles.

In order to produce CdTe nanocrystals which were both chiral and luminescent mixtures of Cysteine and Penicillamine were used as the stabilizing molecules without changing the overall stabilizer concentration. As expected a large decrease in

the Q.Ys of the dots was observed as penicillamine was introduced into the system. However as expected this decrease in quantum yield was accompanied by an increase in the intensity of the CD response. To produce dots which possessed the best of both characteristics, that is a large optical response without too much loss of luminescence, a small study was carried out in which purely cystein coated dots are first prepared and then subsequent batches are made where a ever increasing amount (20%) of the overall molar concentration of cystein was replaced with penicillamine. Purely penicillamine stabilized dots were not prepared in these experiments so therefore the final particle batch was composed of 80% penicillamine and 20% Cystein. It is important to note that the overall concentration of stabilizer never increased but remained constant. All particles were examined using absorption, emission and CD spectroscopy.

Table 5.2: Spectroscopic, size and quantum yield data for D- Cys/Pen stabilized CdTe nanoparticles.

D-CdTe	Abs	CD	Ems	FWHM	Ext	Q.Y	Size(nm)
1	516nm; 0.47	535nm; 0.94 496nm; -0.42 460nm; 0.6	542nm	33nm	537nm	44.5%	4.6
2	554nm; 0.26	540nm; 0.15 474nm; -1.0	576nm	39nm	573nm	33.3%	4.8
3	567nm; 0.16 492nm; 0.34	587nm; -1.0 485nm;-5.0 416nm; -3.5	587nm	45nm	578nm	12.6%	5.6
4	506nm; 0.25	498nm; -5.0 431nm; -4.0	587nm	55nm	557nm	4.8%	5.5
5	475nm; 0.31	507nm; -4.3 496nm; -5.5 465nm; -5.8	579nm	52nm	546nm	2.0%	4.5

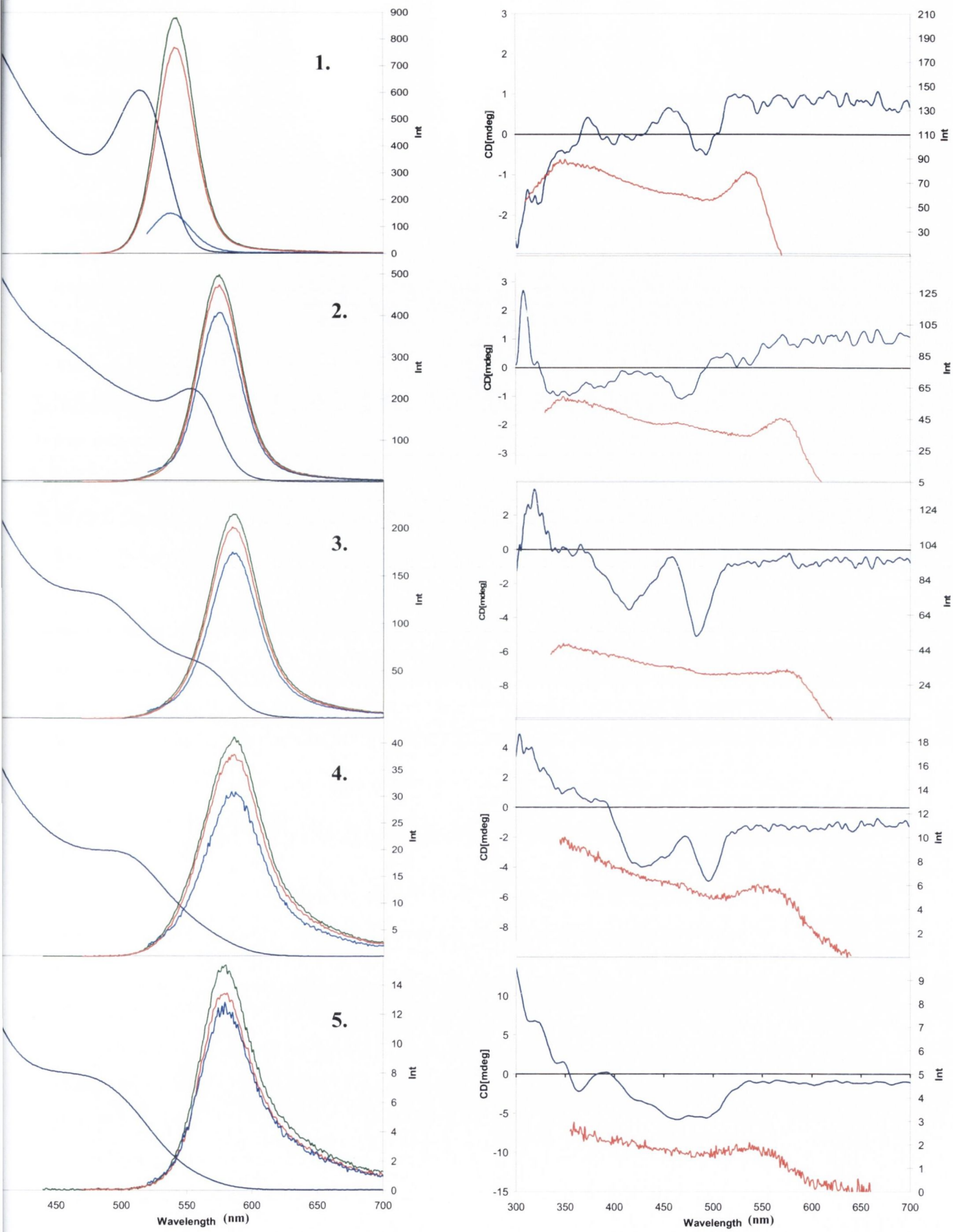

Figure 5.19 Left Absorption and emission spectra and **right** CD, (blue), and excitation, (red), spectra of D-Cys/Pen-CdTe. Cystein to penicillamine ratio is as follows **1.** 1:0. **2.** 0.8:0.2. **3.** 0.6:0.4. **4.** 0.4:0.6. **5.** 0.2:0.8. Particle size is at its largest when the ratio of Cys to Pen is at its lowest. Particles were excited at 420nm, 450nm and 500nm to ensure a high degree of monodispersity. Abs-Absorbance, Int-Intensity

Initially as the penicillamine to cystein ratio is increased we see not only an increase in CD activity, (with the subsequent decrease in quantum yield), but also an increase in the particle size which is accompanied by a red shift in both the absorbance and emission maxima's. However when we reach a level where the concentrations of Pen to Cys are almost equal we see a split in the band edge and the development of two distinct exciton peaks (**Figure 5.19-3**). Although these samples have been purified by size selective co-precipitation several times they do appear to contain two distinct particle shapes and or sizes. Also dots with an equal molar mixture of Cys to Pen, (not shown), were also synthesised and were found to have identical spectral characteristics. However sample 4 in which the Pen: Cys ratio is practically the same, (having just swung in the favour of pencillamine), does not contain these double peaks. This double peak also appears in the third L- batch. *This phenomenon will be dealt with more thoroughly at the end of this section.* As the penicillamine concentration is increased an exciton peak intermediate to the first and second peaks, (492nm), becomes dominant in the absorption spectra but as the excitation spectra clearly show the first exciton peak remains although it undergoes significant blue shifting as the penicillamine concentration is increased. This intermediate exciton peak begins then to blue shift as penicillamine becomes the dominant stabilizer with the final batch of dots possessing an absorption peak at 475nm, 41nm to the blue of the original cystein stabilized CdTe. This dramatic blue shift is attributed to the particles returning to an almost homogeneous stabilizer environment, coupled with the fact the penicillamine stabilized dots are normally smaller than their cystein coated counterparts, **Figure 5.2**.

Photoluminescent spectroscopy results were consistent with UV-Vis absorption spectra, although the spectra are not as complex as their corresponding absorption spectra. All batches were excited at multiple wavelengths to investigate the degree of homogeneity and monodispersity. As the penicillamine concentration is increased we see a constant red shift in the emission maxima up until batch four where it then remains stationary before beginning to blue shift in batch five. This initial red shift and eventual blue shift is again attributed to the inability of the mixed stabilizers to pack tightly around the quantum dot core with the eventual blue shift due to the formation of smaller dots caused by the almost complete penicillamine coverage in the final batch.

It is also in the emission spectra we can see an explanation for the increased optical activity in the dots as the pen concentration is increased. Although remaining intrinsic there is a continual increase in the FWHM of the emission peaks as we move down through the batches. The FWHM as explained earlier is a standard characterisation technique for determining the type of luminescence a dot exhibits. It is preformed by checking the number of nanometres between the emission lines at the half maximum and is usually ~30nm for intrinsically emitting dots and 120nm for defect emitting dots. Again we see an increase in this as the pen concentration increases and the dots become more optically active as a certain degree of defects are added to the dots surface. Excitation spectra follow the trend set by the emission spectra with a continued red and eventual blue shift.

As expected CD spectra show an increase in both the strength and structure of the CD signal as the Pen concentration is increased, however as the luminescent continues to falls to extremely low levels we begin to see a loss of structure in the CD signals and showing the link between luminescence and CD activity.

Although these experiments were initially only carried out using the D-enantiomers of each stabilizer due to their success they were repeated with the L- form of the amino acids. Similarly to the D-particles the L-CdTe particles display a noticeable red shift in their spectra, (**Figures 5.19 & 5.20**).

Table 5.3: Spectroscopic, size and quantum yield data for L- Cys/Pen stabilized CdTe nanoparticles. Note the increase in particle size as stabilizer ratio approaches 1 to 1. this is attributed to the inability of the stabilizers to pack effectively around the quantum dot core.

L-CdTe	Abs	CD	Ems	FWHM	Ext	Q.Y	Size(nm)
1	515nm; 0.47	529nm; -0.88 492nm; 0.42 454nm; -0.68	539nm	33nm	537nm	46.4%	4.2
2	524nm; 0.37	546nm; -0.9 466nm; -0.4	551nm	39nm	543nm	34.2%	4.5
3	566nm; 0.15 487nm; 0.34	487nm; 3.5 458nm; -0.2 411nmn; 2.3	585nm	43nm	640nm	13.3%	5.2
4	497nm; 0.27	532nm; 0.5 497nm; 4.4 453nm; 2.8	585nm	50nm	558nm	5.3%	4.9
5	501nm; 0.25	533nm; 0.5 500nm; 4.1 460nm; 3.8	590nm	55nm	551nm	2.3%	4.1

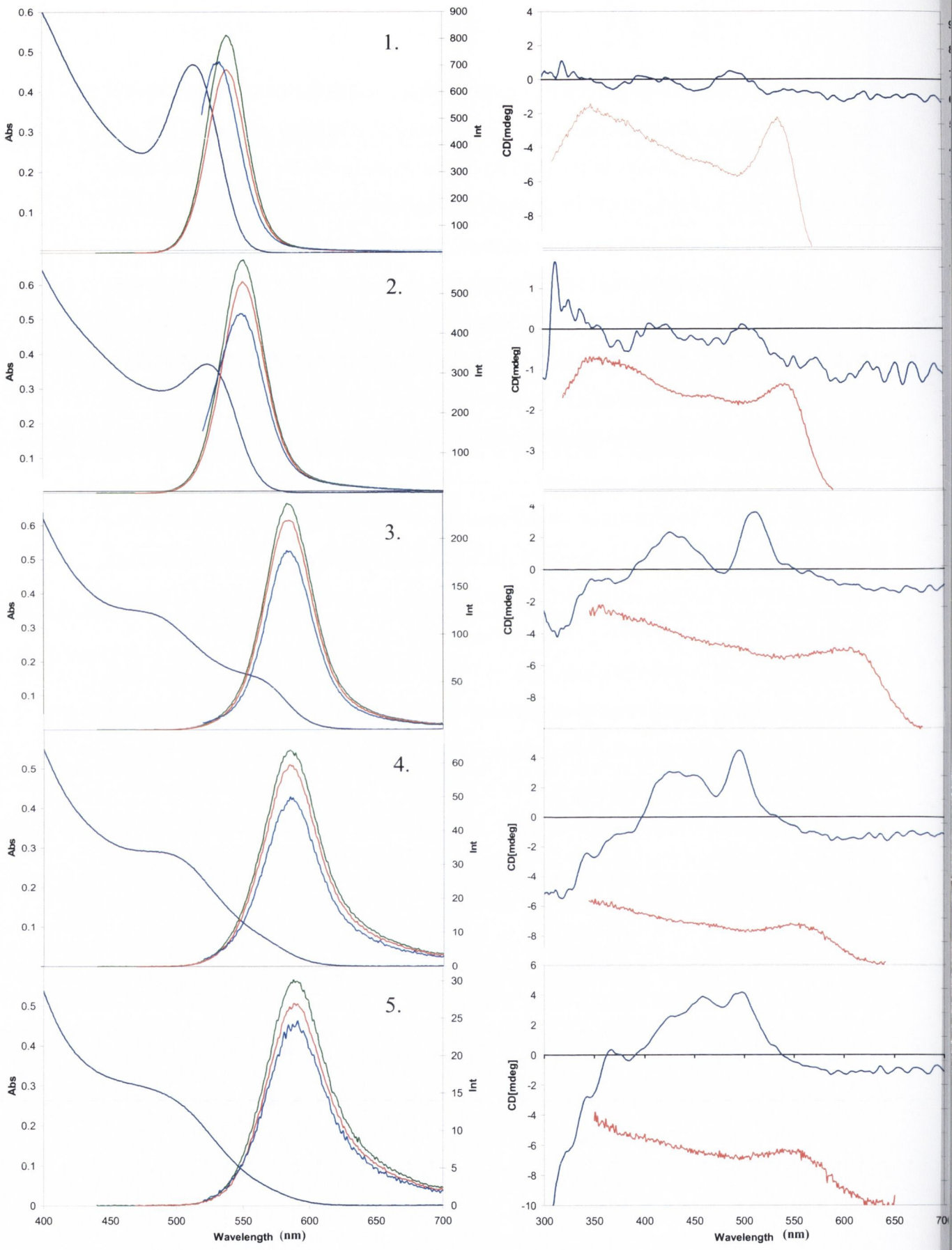

Figure 5.20 Left Absorption and emission spectra and **right** CD, (blue) and excitation, (red), spectra of L-Cys/Pen-CdTe. Cystein t penicillamine ratio is as follows **1.** 1:0. **2.** 0.8:0.2. **3.** 0.6:0.4. **4.** 0.4:0.6. **5.** 0.2:0.8. Particle size is at its largest when the ratio of Cy to Pen is at its lowest. Abs-absorbance, Int-intensity

Initially in D- stabilized particles we observe a 38nm red shift in the absorbance maxima accompanied by a 34nm red shift in the emission maxima, however the scale of these changes are not seen again with the second batch as the absorption and emission red shift by 13nm and 11nm respectively. In the case of the L- particles the red shift in the absorbance and emission spectra are only 9nm and 12nm respectively after the first addition of Pen. This however increases significantly after the second addition with red shifts of 34nm and 42nm for absorption and emission respectively. This reversal in behaviour is perhaps another example of the increased stability of L-stabilized particles in that it takes a much lower stabilizer ratio to destabilise the particles surfaces.

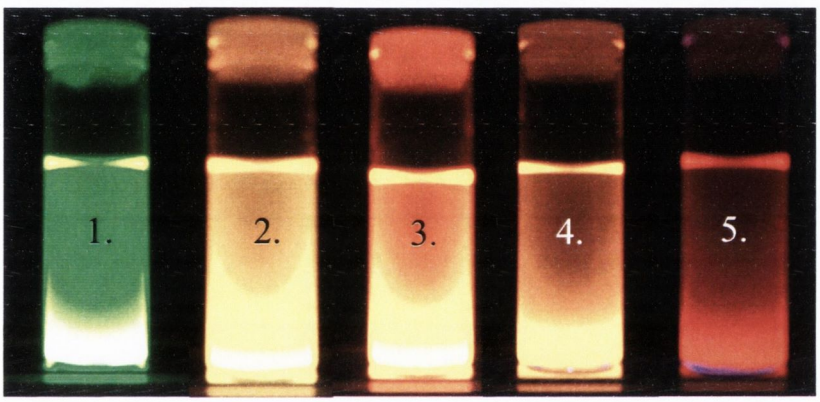

Figure 5.21: Photograph of batches 1-5 L-Cys/Pen stabilized CdTe nanoparticles. The dramatic change in colour is simply a result of varying the ratio of cystein to penicillamine, overall stabilizer; Cd and Te concentration do not change from batch to batch.

The spilt in the absorption spectra with two peaks at 487 and 566nm is observed for both D- and L-CdTe. D- and L- also appear show similar behaviour in batch four. However, while batch five shows a blue shift in D-, the particles continue to red shift for the L- enantiomer.

The FWHM also shows slight inconstancies between enantiomers especially in the latter batches. While both enantiomers display an increase in the FWHM, D-5 decreases by 3nm, as Pen concentration is increased indicating an increase in surface disorder this increase is slower with the L- particles again showing greater particle integrity.

Finally as was discussed in the previous chapters with the CdS and CdSe particles we believe that all particles which exhibit optical activity posses a third longer

"chiral" lifetime. With this in mind the emission lifetimes of all particles produced in this experiment were examined using a tri-exponential fit. A tri-exponential fit is used to highlight the presence of the lifetime contributing to chirality of the particles even though as seen in the previous section it is possible, due to their weak optical activity, to fit cystein coated CdTe particles with a bi-exponential component.

Again we see that the relative length of the lifetimes of the various particles does not agree with their respective quantum yields, **Tables 5.4 & 5.5.** Despite the fact that the quantum yields of both the D- and L- particles are decreasing as the penicillamine concentration is increased both the short, core and medium, shell, lifetimes do not follow any pattern. In fact it is only the longest lifetime which follows a pattern increasing, not decreasing as the QY goes down, except for batch 5 of the D-Cys/Pen particles where we see a dramatic decrease in all lifetimes including the longest one. Examination of the **B** factors is equally as puzzling, unlike the previously reported particles we do not see an increase in the contribution of the medium, shell, lifetime as the QY increases, or vice versa. This phenomenon can probably be explained by the presence of two stabilizers on the particle surface making it more difficult to fit these two dramatically different environments.

Table 5.4: Lifetime and QY data for mixed stabilizer CdTe dots. Note the increase in the contribution of the longest, (chiral lifetime) as the concentration of penicillamine is increased.

	Q.Y%	χ^2	A	τ_1(ns)	B_1	$B_{\%}$	τ_2 (ns)	B_2	$B_{\%}$	τ_3(ns)	B_3	$B_{\%}$
D1	44.5	1.2	10.6	**11.5**	15221	60.6	**29**	9469	37.7	**118**	392	2.7
D2	33.3	1.01	21.03	**13.3**	9503	55	**33**	7261	42	**115.7**	512	3
D3	12.6	1.11	22.13	**13.2**	10138	56	**34.3**	7391	40.8	**127**	571	3.2
D4	4.8	1.12	23.7	**12.4**	9392	57	**33.7**	6521	39	**127.8**	604	4
D5	2.0	1.0	45.1	**6.7**	3125	45	**24.4**	3328	48	**85.5**	494	7

Despite the complexity of the lifetime data acquired and the inconsistencies in the data collected for both the D- and L- stabilized particles, especially in the 5th batch, the presence of the longest lifetime is quite clear. As the penicillamine concentration is increased and the particles become more optically active there is an increase in not only the length of the longest lifetime but also its **B** factor, which is a measure of how much it contributes to the overall lifetime. Even in D5 where the longest lifetime

decreases its **B** factor continues to go up. This would suggest that it is indeed linked to the degree of optical activity which a particle possesses and as that particle has stronger CD response its longest lifetime becomes more dominant.

Table 5.5: Lifetime and QY data for mixed stabilizer CdTe dots. Note the increase in the contribution of the longest, (chiral lifetime) as the concentration of penicillamine is increased.

	Q.Y%	χ^2	A	τ_1(ns)	B_1	$B_{\%}$	τ_2 (ns)	B_2	$B_{\%}$	τ_3(ns)	B_3	$B_{\%}$
L1	46.4	1.05	15.4	**14.1**	10232	46	**31.3**	11621	52	**109**	389	2
L2	34.2	1.02	29.7	**16.3**	11597	58.5	**35.9**	7737	39	**124**	488	2.5
L3	13.3	1.05	19.9	**12.9**	11782	57	**32.9**	8222	40	**125**	579	3
L4	5.3	1.12	38.6	**12**	10759	54.2	**34.3**	8268	41.7	**126.8**	805	4.1
L5	2.3	1.08	30.1	**12.2**	9665	53.3	**38**	7601	41.9	**135.7**	874	4.8

Examination of batch 3 particles

As mentioned earlier the nanoparticles produced in batch number 3 for both the D- and L- particles posses two distinct absorption peaks, one at 487nm and one at 566nm. The simplest explanation for the presence of this second peak would be that this batch, (unlike any of the others), contains two distinctly different types of quantum dot. As TEM has ruled out the presence of nanorods, wires etc, it is assumed that batch number 3 contains isolated Pen-CdTe and Cys-CdTe, this seemed unlikely as the dots were co-precipitated in a mixture of Cys and Pen, however it must be considered. As pure cysteine particles absorb at 515nm we can therefore assign the peak at 566nm to them leaving the peak at 487nm to the penicillamine stabilized CdTe, (which normally absorbs at 510±20nm). These differences in the positions of the absorbance peaks, (when comparing the pure with the mixed dots), can be attributed to differences in the Cd to stabilizer ratios. However this explanation does not account for several spectroscopic features, i). the continued increase in the FWHM, which indicates the continued addition of defect creating Pen to intrinsic Cys emission, ii). the continued strengthening of the CD spectrum at 550nm, (the region assigned to the cystein shoulder), which is attributed to the inclusion of the defect creating Pen into the cystein stabilized dot, and finally iii). the lack of any Pen-CdTe emission peak despite the use of three different excitation wavelengths, (420, 450 and

500nm). This final feature is particularly interesting as due to L-Pen CdTe defect emission, (**Figure 5.4**), it should be easy to see despite the Cys-CdTe greater emission intensity. This also raises the question as to why extra fluorescent life times are not seen to account for the presence of two isolated dots, (**Tables 5.4 and 5.5**). However despite these inconsistencies, as the simplest explanation a mixture of dots must be considered.

Another possible explanation is that these bands are simply the first and second exciton peaks perhaps due to the presence of two distinct but equally concentrated surface stabilizers. However due to the lack of work on mixed ligand stabilization in the aqueous phase this is only speculation, although mixed ligand organic phase dots have been reported with multiple absorption peaks.[35, 36] Although it must also be noted that further functionalisation of cystein capped CdTe particles does sometimes lead to the appearance of a second exciton peak as observed by Mamedova et al.[8]

However despite this possible mixture this batch was chosen to produce CdTe nanowires. It was believed that as the best compromise between quantum yield and optical activity they represented the best batch for the experiment. Also as the wire growing method involved the lining up of individual dots and fusing them together it was believed that any wire produced would be a mixture of Cys and Pen stabilized dots.

5.4.8 Synthesis and studies of Chiral CdTe Nanowires

Semiconductor nanowires have many unique optical and chemical properties which allow them to be used as both light collectors and detectors as well as been potentially utilized in various opto-electronic devices[4, 37, 38] as well as temperature,[39] chemical[40] and p.H sensors.[41] In our work we attempted to produce chiral 1 D nanostructures which are expected to emit as well as absorb polarised light. Using a well known destabilization and growth technique,[16, 18, 42] we attempted to produce CdTe nanowires from the mixed ligand CdTe nanoparticles described above. Batch 3 was chosen for these experiments as it retained a high quantum yield while possessing a high degree of optical activity, (**Figure 5.22**).

Briefly, once the particles have been prepared they were reduced in volume to 1ml and 0.5ml aliquots of methanol and propan-2-ol are added until the colloid turns cloudy and turbid.[16] The particles are then centrifuged out and the supernatant is

decanted off. This process allows the removal of any remaining reactants, counter ions or excess stabilizer. However it must be noted that this technique was designed for mercapoethanoic acid stabilized CdTe in mind. Since the solubility of penicillamine and cystein in these solvents, (methanol and isopropanol), is quite low the stabilizers may simply precipitate along with the dots. Once the dots have been purified they were then placed under vacuum to remove any excess non-solvent. They were then redispersed in a mixture of 0.5ml of p.H 9 $NaOH_{(aq)}$ solution and 0.5ml of DMSO. The p.H 9 $NaOH_{(aq)}$ solution was prepared using Millipore water and NaOH. Once the particles were re-dispersed they were then placed in an oven at 80 ^{0}C and left for up to three hours. Samples were also taken and analysed at hour 2 for comparison. Once the colloids were removed from the oven they were made up to their original volumes using p.H 9 water. The colloids were examined using UV and PL, **Figure 5.22 &5.25**, TEM, **Figures 5.23, 5.24 & 5.26** and CD, (**Figure 5.27**). It is worth noting that while the L-stabilized particles were stable on addition of DMSO the D- stabilized dots began to crash out.

In both the D- and L- particle batches, "pearl-necklace" agglomerates such as the ones presented in **Figure 5.24** and **5.26** were observed. The actual recrystallisation itself probably occurs via Ostwald ripening with Cd^{2+} and Te^{2-} ions been transferred from smaller nanoparticle. The pearl-necklace aggregates are self-assembled from nanoparticles obtained after the precipitation of the original stable dispersion with organic solvent. These particles are considered to be "active" as the excess stabilizer whose electrostatic repulsion once compensated for the nanoparticle dipole-dipole interaction and kept the individual nanoparticles isolated is now gone. With the electrostatic repulsion now diminished the particles line up according to their dipoles. If the methanol/propan-2-ol precipitation and redispersion in water steps were excluded leaving the original excess thiol stabilizer in solution, nanowires would not form. Consequently, the chain aggregation step is initiated by the overall decrease in stabilizer concentration.

Also it must be noted that while Lilly et al. noted that excess DMSO prevents the above described pearl necklace step from taking place we stay below the >60% DMSO threshold needed for this to occur.[16] The DMSO is added to enhance the Oswalt ripening process.

Although both D- and L- particles were subjected to precisely the same treatment they both reacted quite differently to the DMSO treatment. After DMSO treatment all

CdTe samples have been characterised by UV-Vis and PL spectroscopy and TEM, (**Figure 5.23-5.28**).

Looking at D-Cys/Pen CdTe, (**Figure 5.23**), first we see a dramatic change in both the absorption and emission spectra of the dots after treatment with DMSO. In the UV-Vis spectrum we see the two exciton peaks at 567nm and 492nm have now been replaced with one at 559nm and a large degree of scattering is now present.

The scattering is expected due to the growth of the particles, however the loss of one of the exciton peaks suggests the individual particles are unstable and have been altered in some way by the heating process.

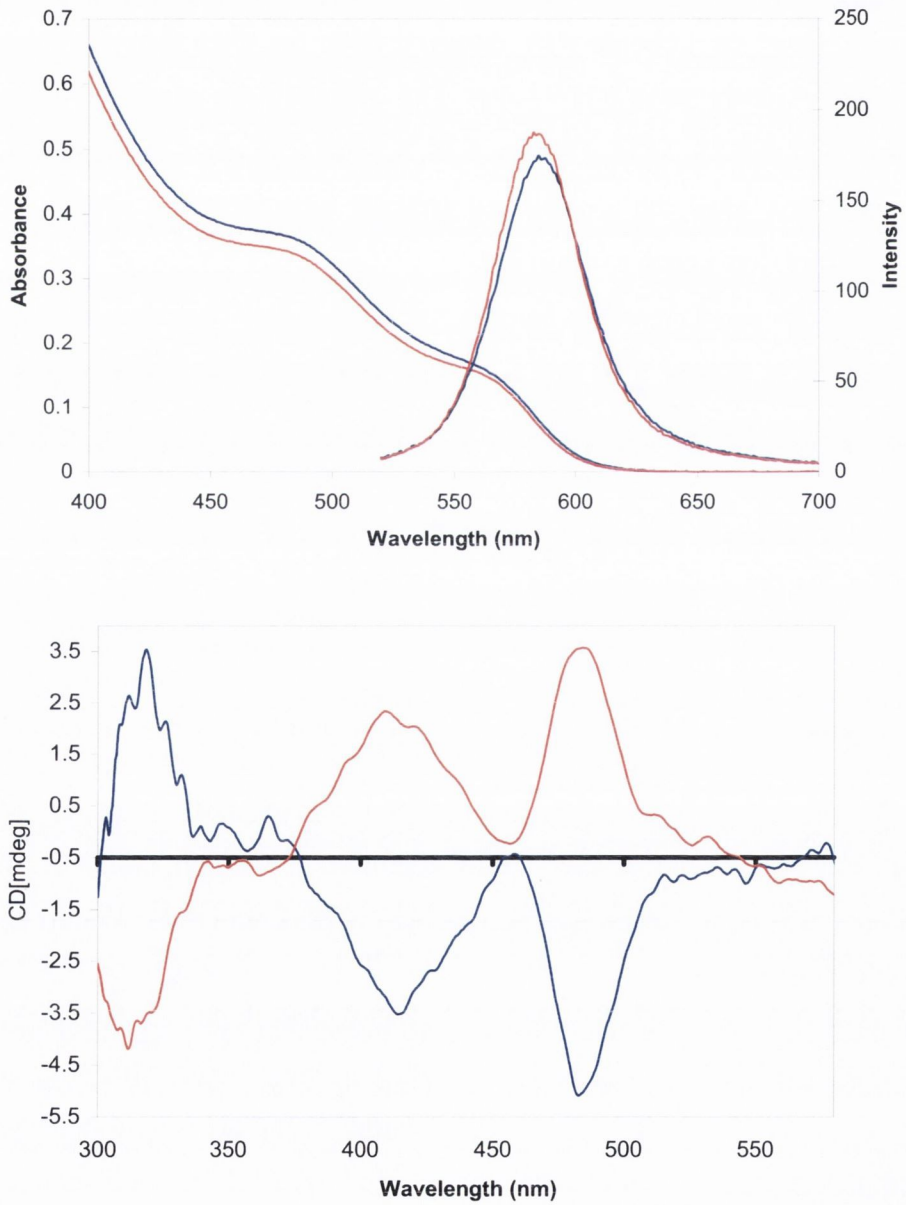

Figure 5.22: Top Absorption and emission spectra and bottom CD spectra of D- and L- Cys/Pen CdTe nanoparticles before treatment with DMSO.

Another explanation is that the two exciton peaks were indeed due to the presence of two different sized nanoparticles and that the smaller ones have been sacrificed as the larger ones begin to fuse end to end with the Cd and Te from the smaller particles been used to facilitate Oswalt ripening, as described above.

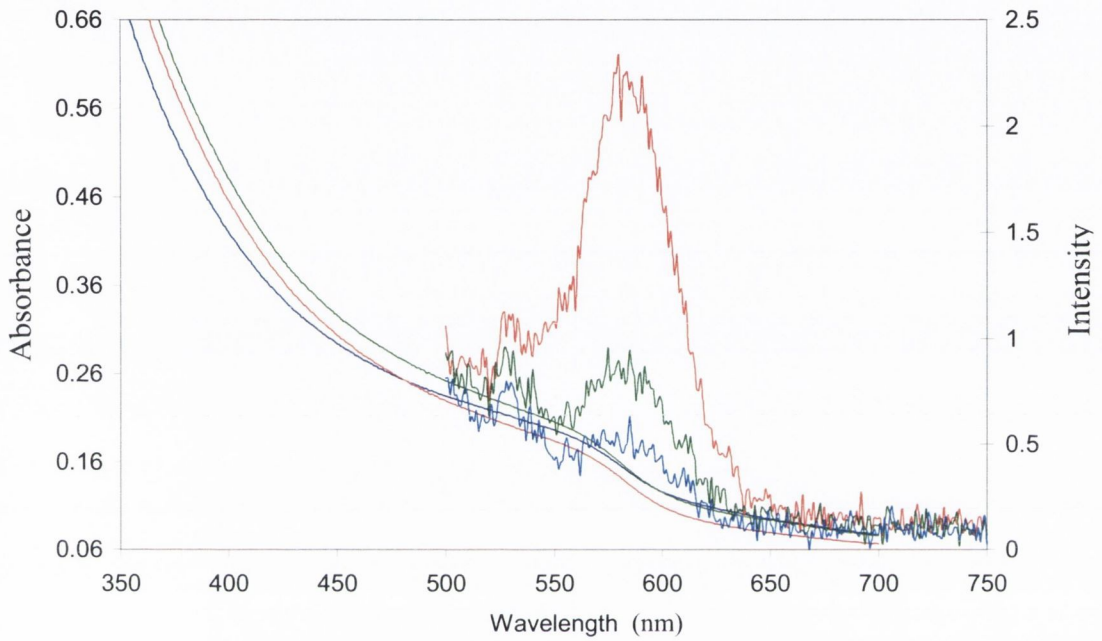

Figure 5.23: Absorption and emission spectra of D- Cys/Pen CdTe nanoparticles after treatment with DMSO, 1hr 2hrs and 3hrs. Note the increase in luminescence as the reaction proceeds.

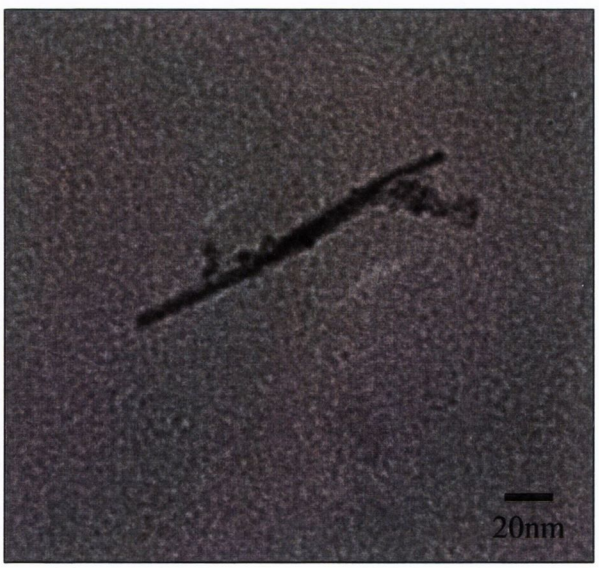

Figure 5.24: TEM image of D-Cys/Pen CdTe after 3hrs heating at 80^{O}C in DMSO and water. Note the 2.5nm particles on or as part of the 143nm long 7.5 nm wide nanowire.

Although, if this were the case the L-stabilized particles would also be expected to lose their second exciton peak and they do not, (**Figure 5.26**). The emission of the D-particles has decreased significantly but other than that has not changed, i.e. it has not red shifted, this is unusual where particle growth is expected, (**Figure 5.23**). A possible explanation for this is that the wires are either not luminescent or there emission has red shifted into the infra-red and can not be detected by this spectrometer. If this were so then the emission detected in figure 5.21 is that of the few remaining isolated quantum dots.

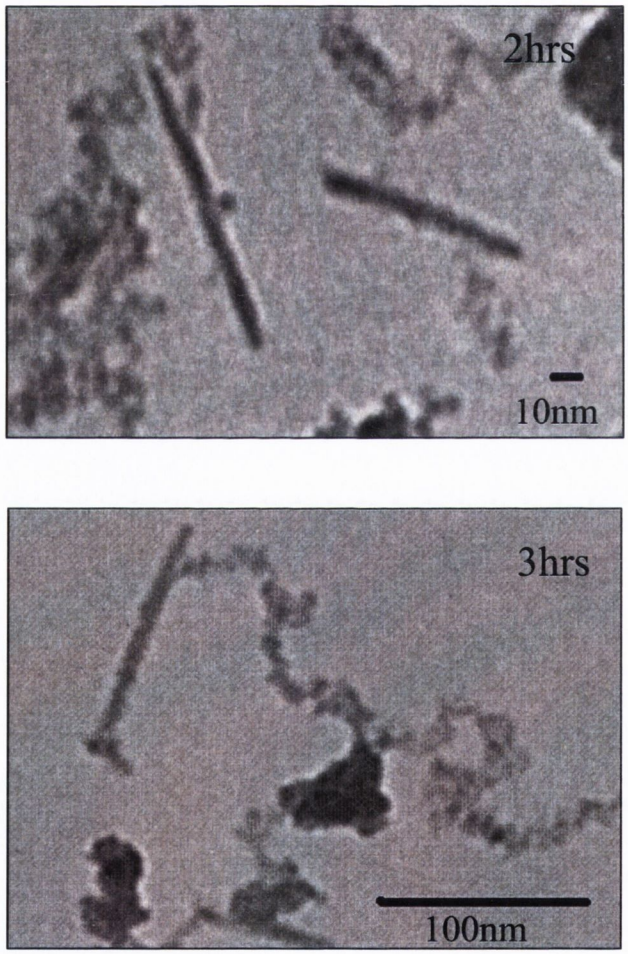

Figure 5.25: TEM images of D- Cys/Pen CdTe nanoparticles after treatment with DMSO, 2hrs, top, and 3hr bottom. While the width of the nanowires remains constant at 8.5±1.2nm the length increases from 99±9nm afte 2hrs of heating to 117nm ±5nm after 3hrs

Another possible explanation is that like the CdSe needles discussed in the previous chapter these nanowires are not solid objects but rather are composed of individual particles or bundles of much narrower nanowires held together by stabilizer. Although the diameter of dots before the growing process begins are ~3nm the resulting wires are ~8nm wide. As observed by Tang et al. the width of the wire produced usually corresponded to the diameter of the parent nanoparticles.[18] However as we are using the Lilly et al. modified method with DMSO we do expect an increase in wire diameter as individual wires may fuse along the long axis.[16] Lilly et al. saw red shifts in the emission maxima of the resulting wires while we do not. TEM imaging does seem to show 2.5nm particles "around" the nanowires which we have grown but whether they are part of a quantum dots stabilizer composite or simply sitting onto the surface of a solid CdTe nanowire is difficult to tell. One of the more noticeable occurrences during the wire growing step is that as the reaction is allowed to proceed while there is little change in the absorption spectra the emission intensity begins to recover. This increased luminescence may be due to the continued removal of surface defects formed during early nanowire formation. Another explanation is that it may possibly be a result of the increased length of the nanowires as they are left in the oven over a longer period of time. This would also explain the lack of movement in both the absorption and emission maxima's over the course of the experiment. As the position of the exciton is dependant on nanowire width and not length and although the wires increase in length between the second and third hour of heating there is very little difference on the width of the wires. Of course it may be simply due to the continued recrystallisation as the sample is heated.

The L-Cys CdTe particles have been treated using exactly the same procedure and conditions. However, the spectroscopic results as well as the resulting wires were quite different from those for D- Cys CdTe samples. While the affect of the DMSO treatment was to alter the photophysical characteristics of the D-capped dots, the L-dots remain virtually unchanged, (**Figure 5.26**). That is to say while the absorption spectra of the D-particles underwent significant changes, i.e. the loss of the second exciton peak, the L- particles retained both their exciton peaks.

Examination of the particles after one hour of heating in DMSO shows that while the first exciton peak has red shifted from 566nm to 569nm the secondary peak has done the opposite and blue shifted by 12nm from 487nm to 475nm. If these peaks truly represent the different chemical environments on the dots surface then perhaps

we are seeing preferential removal of one stabilizer over the other. However after three hours both exciton peaks are now red shifted, the primary peak to 573nm and the secondary to 487nm. This is due to the nanowires formation as opposed to simple pearl necklace nanostructures as confirmed by TEM (**Figures 5.27**-3hrs). At no time is either peak lost again indicating the greater stability of L- stabilized dots. The emission maxima red shifts from 585nm to 595 nm after one hour heating in DMSO however as the experiment continues and the luminescence increases it also blue shifts, an nm an hour. Thus that after 3hrs of heating the emission maxima now are shifted to 593nm. As TEM, **Figure 5.27**, shows very few nanowires were formed until the three hour mark, but the dots had none the less arranged into the distinctive pearl necklace structures which proceed nanowire formation. It is therefore quite probable that as the necklace structures begin to undergo Oswalt ripening and recrystallise occurs the stabilizer shell again packs tightly around the nanostructures causing these small blue shifts in their luminescence, (**Figure 5.26**).

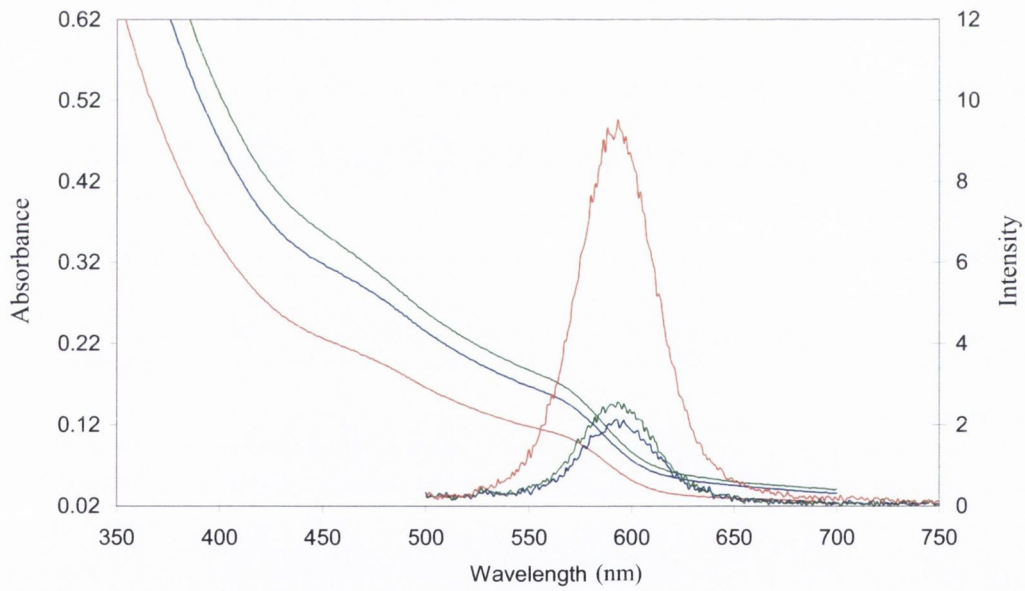

Figure 5.26: Absorption and emission spectra of L- Cys/Pen CdTe nanoparticles after treatment with DMSO, 1hr 2hrs and 3hrs. Note the increase in luminescence as the reaction proceeds.

Examination of the TEM and spectral data again allows us to suggest an increased stability of L- stabilized dots over their D- counterparts.

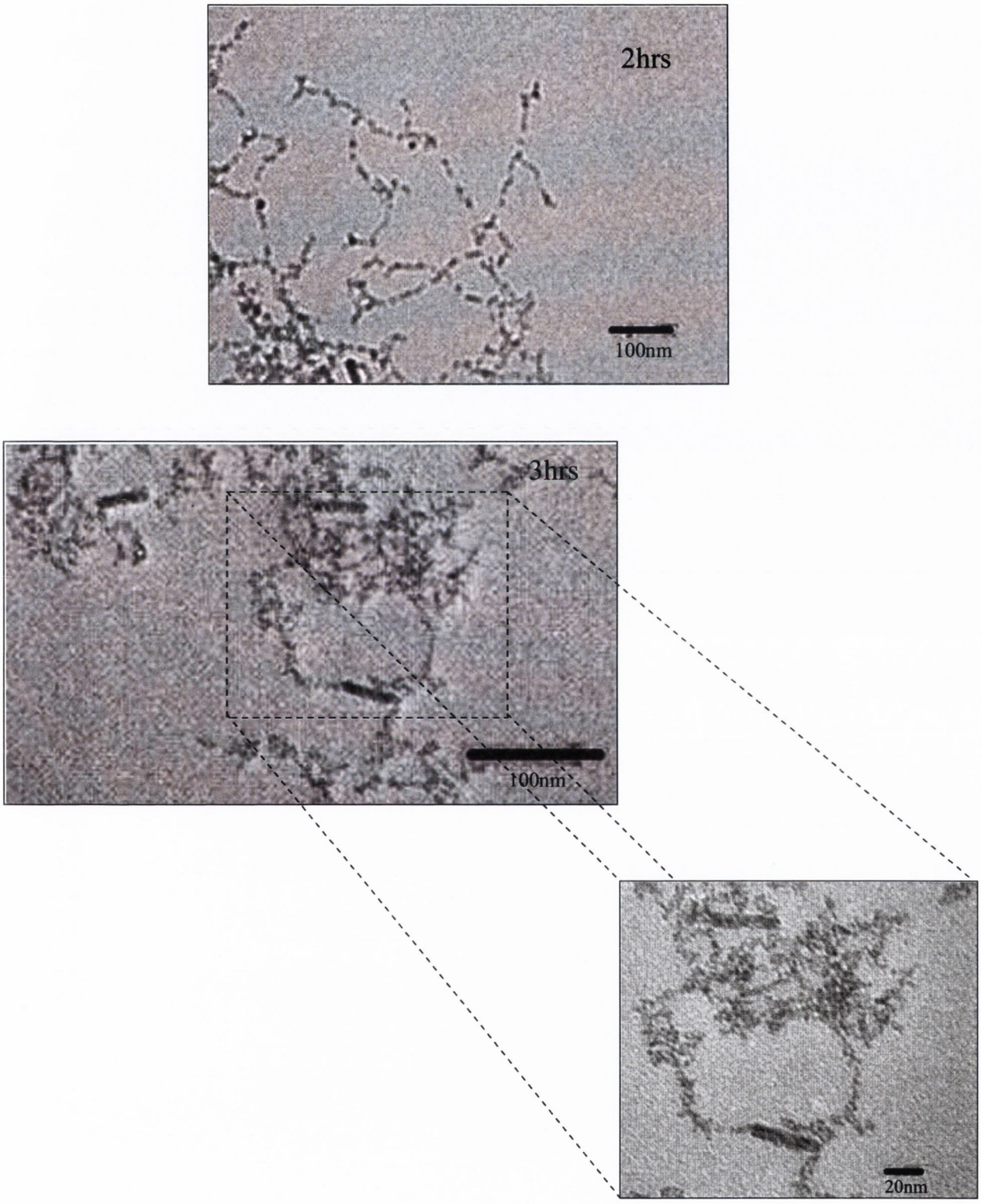

Figure 5.27: TEM images of L- Cys/Pen CdTe nanoparticles after treatment with DMSO, 2hrs, top, and 3hrs, bottom

While two hours of heating in DMSO was sufficient to produce nanowires in the D-sample the L-particles had only began to form pearl necklaces structures, with one or two nanowires visible within the entire grid. However after three hours the number of nanowires had increased dramatically, which may explain the sharpening of the UV-Vis exciton peaks, (**Figure 5.27**).

Finally, while both types of nanowires retained a certain degree of chirality most of the fine structure was lost. Appearing to be just scattering, both the D- and L-batches have CD profiles which appear to "scatter" with opposite chirality. That is, some fine structure is still visible at 540nm for D- and L-, (**Figure 5.28**). This wavelength is 40nm shifted to the red when compared to the maximum of the particles before treatment. Therefore, we can assume that this peak belongs to the wire themselves. Also, two peaks are clearly visible at 370nm and 340nm for D- and L- respectively which again suggests that the nanowires are chiral, as neither the stabilizers nor the metal stabilizer complexes absorb at this wavelength.

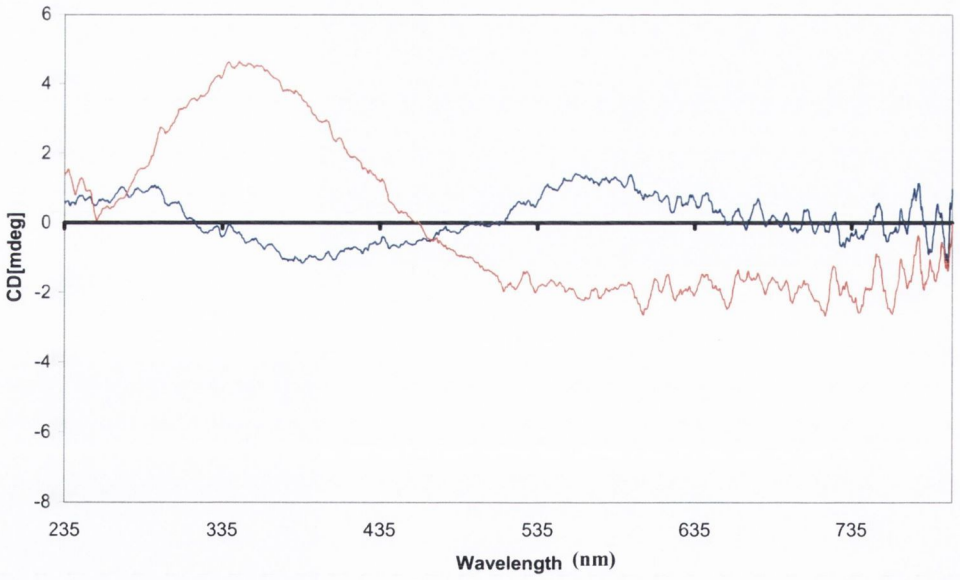

Figure 5.28: CD of D- and L- Cys/Pen CdTe nanoparticles after 3hr treatment with DMSO.

5.5 Conclusions

In summary, we have prepared strongly luminescent but weakly optically active cysteine stabilized CdTe quantum dots. The quantum efficiency of these dots is strongly dependant on the ratio of enantiomers used as stabilisers. It was found that the dots prepared using a racemic mixture of cysteine enantiomers results in QDs with higher quantum yields than those prepared with an enantio-pure stabilizer. We have demonstrated that the CD activity of CdTe QDs can be introduced by utilising a mixture of two different stabilisers (Pen and Cys) of the same chirality. This results in the enhanced CD activity, but causes a decrease in the quantum yield and a widening of the emission due to the presence of chiral defects on the nanoparticle surface. Further research will include detailed studies of the photophysical properties of CdTe QDs with different chiral stabilisers and the investigation of the electron transfer and energy transfer processes in these systems. We believe that our approach can be used for development of many other QDs with controlled chirality, quantum yield, photochemical and photophysical characteristics.

These CdTe QDs and nanowires could find important applications such as fluorescent chemical and biochemical chirality sensors and molecular recognition nanoprobes.

References

[1] H. Bao, Y. Gong, Z. Li, M. Gao, *Chem. Mater.* **2004**, *16*, 3853.

[2] Y. He, H. T. Lu, L. M. Sai, W. Y. Lai, Q. L. Fan, L. H. Wang, W. Huang, *J. Phys. Chem. B* **2006**, *110*, 13352.

[3] Y. He, L. M. Sai, H. T. Lu, M. Hu, W. Y. Lai, Q. L. Fan, L. H. Wang, W. Huang, *Chem. Mater.* **2007**, *19*, 359.

[4] Y. Wang, Z. Tang, S. Tan, N. A. Kotov, *Nano Lett.* **2005**, *5*, 243.

[5] P. Alivisatos, *Nat Biotech* **2004**, *22*, 47.

[6] M. Bruchez, Jr., M. Moronne, P. Gin, S. Weiss, A. P. Alivisatos, *Science* **1998**, *281*, 2013.

[7] W. C. Chan, nbsp, W, S. Nie, *Science* **1998**, *281*, 2016.

[8] N. N. Mamedova, N. A. Kotov, A. L. Rogach, J. Studer, *Nano Lett.* **2001**, *1*, 281.

[9] M. J. Meziani, H. W. Rollins, L. F. Allard, Y. P. Sun, *J. Phys. Chem. B* **2002**, *106*, 11178.

[10] S. Wang, N. Mamedova, N. A. Kotov, W. Chen, J. Studer, *Nano Lett.* **2002**, *2*, 817.

[11] D. L. Schulz, M. Pehnt, D. H. Rose, E. Urgiles, A. F. Cahill, D. W. Niles, K. M. Jones, R. J. Ellingson, C. J. Curtis, D. S. Ginley, *Chem. Mater.* **1997**, *9*, 889.

[12] J. A. Seabold, K. Shankar, R. H. T. Wilke, M. Paulose, O. K. Varghese, C. A. Grimes, K.-S. Choi, *Chem. Mater.* **2008**, *20*, 5266.

[13] K. C. Mandal, S. Basu, D. N. Bose, *J. Phys. Chem.* **1987**, *91*, 4011.

[14] S. Weng, M. Cocivera, *Chem. Mater.* **1993**, *5*, 1577.

[15] S. Coe, W.-K. Woo, M. Bawendi, V. Bulovic, *Nature* **2002**, *420*, 800.

[16] G. D. Lilly, J. Lee, K. Sun, Z. Tang, K. S. Kim, N. A. Kotov, *J. Phys. Chem. C* **2008**, *112*, 370.

[17] T. N. Sandeep Kumar, *Small* **2006**, *2*, 316.

[18] Z. Tang, N. A. Kotov, M. Giersig, *Science* **2002**, *297*, 237.

[19] J. Wang, M. S. Gudiksen, X. Duan, Y. Cui, C. M. Lieber, *Science* **2001**, *293*, 1455.

[20] M. W. Knight, N. K. Grady, R. Bardhan, F. Hao, P. Nordlander, N. J. Halas, *Nano Lett.* **2007**, *7*, 2346.

[21] S. Acharya, I. Patla, J. Kost, S. Efrima, Y. Golan, *J. Am. Chem. Soc.* **2006**, *128*, 9294.

[22] E. W. S. D. Haifeng Bao, *Small* **2006**, *2*, 476.

[23] E. Mullins, *Statistics for the quality control chemistry laboratory*, **2003**.

[24] Y. Chen, Z. Rosenzweig, *Anal. Chem.* **2002**, *74*, 5132.

[25] Y.-h. Zhang, H.-s. Zhang, X.-f. Guo, H. Wang, *Microchemical Journal, In Press, Corrected Proof.*

[26] Z. Tang, Y. Wang, S. Shanbhag, N. A. Kotov, *J. Am. Chem. Soc.* **2006**, *128*, 7036.

[27] S. D. Elliott, M. Moloney, x, chea, x, P. l, Gun, x, Y. K. ko, *Nano Lett.* **2008**.

[28] Y. He, H. T. Lu, L. M. Sai, W. Y. Lai, Q. L. Fan, L. H. Wang, W. Huang, *J. Phys. Chem. B* **2006**, *110*, 13370.

[29] S. J. Lee, K. N. Kim, P. K. Bae, H. J. Chang, Y.-R. Kim, J. K. Park, *Chemical Communications* **2008**.

[30] D. Wang, J. He, N. Rosenzweig, Z. Rosenzweig, *Nano Lett.* **2004**, *4*, 409.

[31] Q. Zeng, X. Kong, Y. Sun, Y. Zhang, L. Tu, J. Zhao, H. Zhang, *J. Phys. Chem. C* **2008**, *112*, 8587.
[32] C. L. Wang, H. Zhang, J. H. Zhang, M. J. Li, H. Z. Sun, B. Yang, *J. Phys. Chem. C* **2007**, *111*, 2465.
[33] S. K. Kulkarni, U. Winkler, N. Deshmukh, P. H. Borse, R. Fink, E. Umbach, *Applied Surface Science* **2001**, *169-170*, 438.
[34] S. J. Byrne, S. A. Corr, T. Y. Rakovich, Y. K. Gun'ko, Y. P. Rakovich, J. F. Donegan, S. Mitchell, Y. Volkov, *Journal of Materials Chemistry* **2006**, *16*, 2896.
[35] W. Liu, H. S. Choi, J. P. Zimmer, E. Tanaka, J. V. Frangioni, M. Bawendi, *J. Am. Chem. Soc.* **2007**, *129*, 14530.
[36] G. Shan, X. Kong, X. Wang, Y. Liu, *Surface Science* **2005**, *582*, 61.
[37] J. H. He, J. H. Hsu, C. W. Wang, H. N. Lin, L. J. Chen, Z. L. Wang, *J. Phys. Chem. B* **2006**, *110*, 50.
[38] J. Lee, A. O. Govorov, J. Dulka, N. A. Kotov, *Nano Lett.* **2004**, *4*, 2323.
[39] A. O. Govorov, G. W. Bryant, W. Zhang, T. Skeini, J. Lee, N. A. Kotov, J. M. Slocik, R. R. Naik, *Nano Lett.* **2006**, *6*, 984.
[40] C. S. Rout, S. Hari Krishna, S. R. C. Vivekchand, A. Govindaraj, C. N. R. Rao, *Chemical Physics Letters* **2006**, *418*, 586.
[41] S. J. N. Pearton, D. P.; Heo, Y. W.; Tien, L. C.; Ivill, M. P.;Li, Y.; Kang, B. S.;Ren, F.; Kelly, J.; Hebard, A. F., *J. Electron. Mater.* **2006**, *35*, 862.
[42] K. S. Cho, D. V. Talapin, W. Gaschler, C. B. Murray, *J. Am. Chem. Soc.* **2005**, *127*, 7140.

Chapter 6.

Penicillamine stabilized magnetic nanoparticles and their nanocomposites with CdS

Introduction 6.1

Magnetic Particles such as microspheres, nanospheres and ferrofluids have been widely studied over the past few decades with a number of real hi-tech applications in mind. These include their use in various emerging technological fields such as magneto-electronics or spintronics;[1-3] as well as the biological and medicinal applications such as enzyme and protein immobilization,[4-6] genetic studies,[7] as radio pharmaceuticals[8] and of course as next generation MRI (Magnetic Resonance Imaging) contrast agents.[9-13] However there are also applications for them in such fields as RNA and DNA purification, [14, 15] magnetic cell separation and purification,[7, 16-24] as well as magnetic controlled transport of various, (including anticancer), drugs.[22, 25-30] Another more radical use is the targeting and binding of functionalised magnetic nanoparticles to cancer and tumour cells allowing for the destruction of these cells by burning through a magneto-thermal effect.[31]

For many biological applications magnetic particles must meet a certain requirements including biocompatibility, low toxicity, water solubility and stability.
In addition magnetic iron oxide particle size must be below the 10nm size limit to express superparamagnetism. This is important especially in possible biological applications as a). small size makes cell entry more likely and b). by being superparamagneitc the particles will not retain any magnetism once the external field has being removed (i.e. MRI scanner) preventing their magnetic aggregation.

Unlike the previously discussed Cd based quantum dots -SH groups are not required for bonding to the magnetic iron oxide particles surface. The bio-molecules which are used to functionalise and stabilise iron oxide particles include nucleic acids, oligonucleotides, proteins and polymers (PEG, Dextran).[32] In addition when dealing with iron oxide particles various silanes such as 3-aminopropyl-triethoxysilane or 3-

mercaptopropyl-trimethoxysilane are commonly used to functionalise these types of particles. Once functionalised the exposed NH_2 or SH groups can then be further modified using basic peptide or sulphur chemistry respectively.

The main aim of this part of our work is to develop new water soluble chiral magnetic nanoparticles. We also plan to investigate interactions between chiral QDs and chiral magnetic nanoparticles and prepare corresponding core-shell structures and possibly "all in one" magnetic-fluorescent-chiral nanocomposites. We plan to synthesise chiral iron oxide based nanoparticles by introducing a chiral stabilizer (Penicillamine) into the reaction before particle formation by co-precipitation. By using penicillamine not only will the iron oxide particles be functionalised with either mercapto, amine or carboxyl groups, (depending on which group is pointing off the particles surface) but the Pen may also transfer its chirality onto the iron oxide particles as it has done in previous chapters with the Cd based quantum dots.

Synthesis 6.2

Synthesis of magnetic iron oxide nanoparticles was performed by well documented co-precipitation technique.[33-35] The co-precipitation method involves first the preparation of aqueous solutions of ferrous and ferric salts, in this case $FeCl_2.4H_2O$ and $FeCl_3.6H_2O$. These salts are then combined at a ratio 1:2 in a large volume of degassed Millipore water. The pH is then raised using strong base, in this case NH_4OH, causing the particles simultaneously to form and co-precipitate out of solution. They are then magnetically separated and washed several times using Millipore water. Magnetic separation of the particles from solution is quite easy due to their insolubility in water despite their functionalisation with –OH groups. Due to the lack of a stabilizer the particle sizes is controlled by the volume and type of base added, the ionic strength of the solution, (normally controlled by addition of NaCl), as well as the temperature of the iron salts solutions before co-precipitation.[35]

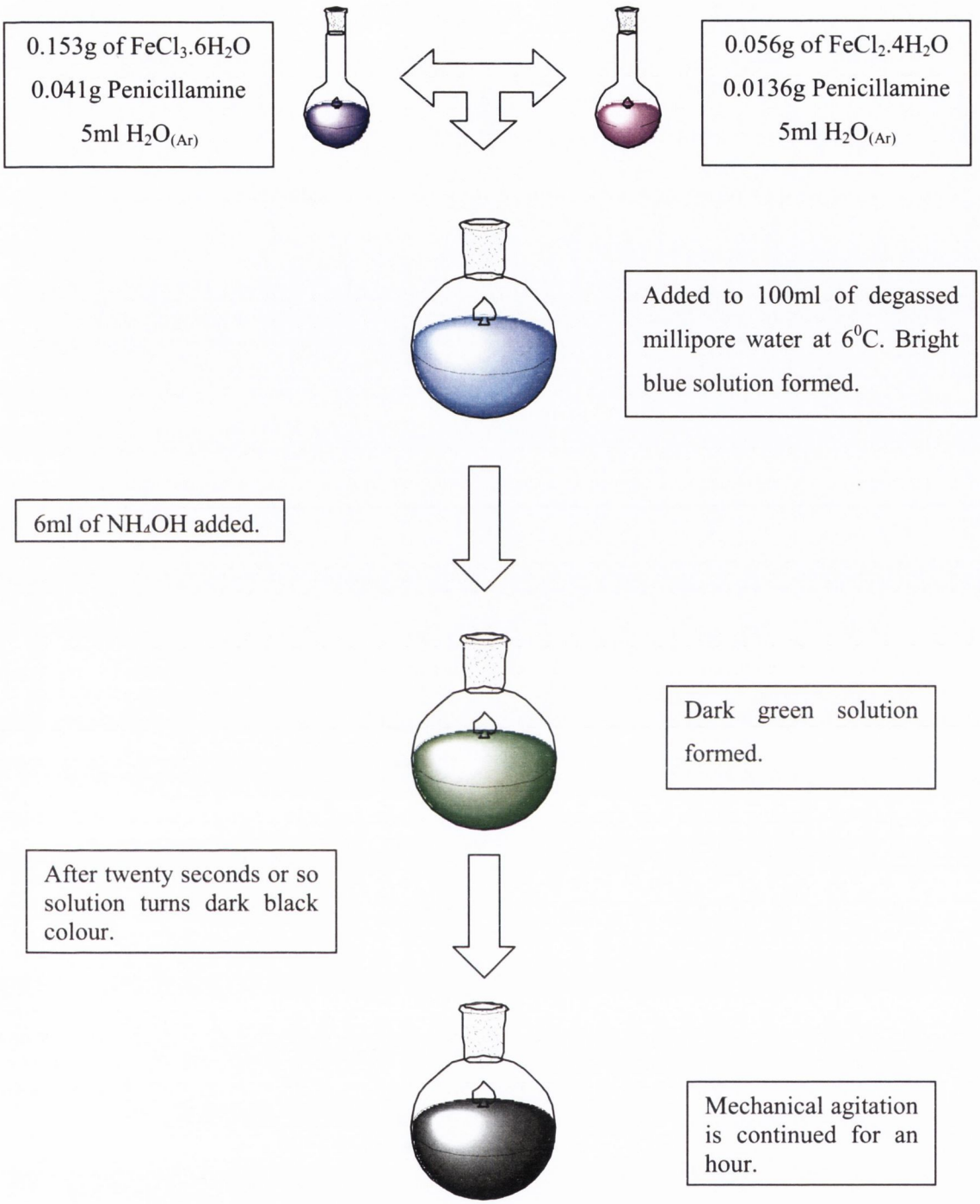

Figure 6.1: Scheme showing the preparation of Penicillamine stabilized Fe_xO_y. Fe(II)-Pen, 1:0.3, and Fe(III)-Pen, 1:0.5, were first prepared by the addition of pen to the respective iron salt in degassed Millipore water. Once the coloured complexes were formed they were then mixed in 100ml of degassed Millipore water, the final Fe ratio is 2:1 Fe^{3+}:Fe^{2+}. The p.H was then raised with the addition of 6ml of NH_4OH. Particles were mechanically shaken for at least an hour and then washed by magnetic separation.

In our work penicillamine coated iron oxide particles were prepared by the traditional co-precipitation route described above with a minor but important adjustment. Before

the iron solutions were combined an equimolar concentration of penicillamine was added to each iron salt. This generated the corresponding Fe(II)- and Fe(III)-Pen complexes. However, the addition of ammonia hydroxide to do this mixture resulted in the formation of a stable red solution without any precipitation of iron oxide. It was found that if high concentrations of Pen were used then the iron complexes formed were too stable and no particles are formed even after a large excess of ammonia added. Through a process of trial and error the correct ratio of iron to penicillamine was discovered to be 1:0.5 for Fe^{3+} and 1:0.3 for Fe^{2+} (**Figure 6.1**). We have also found that by using this route, instead of addition of penicillamine after particle formation we are able to better control the size of the particles and produce nanoparticles in the 3-6nm size range (depending on the enantiomer used) with excellent monodispersity. However, there is a drawback to this technique. Due to the small size of these particles, and the high solubility of penicillamine in water, magnetic retrieval of the particles for washing is quite difficult and time demanding. Therefore the process must be performed using small volumes and powerful magnets, this decreases the time spent on the purification of the iron oxide nanoparticles. Also it was noted that while the D- and L- coated particles gave a percentage yield of around 40%, the R- particles gave a much higher yield of around 60%. We believe that the higher yield for R-Pen stabilised nanoparticles is due to the hydrophobic nature of the racemate coating, which allows more effective precipitation of the particles out of the water.

6.3 Characterisation of magnetic nanoparticles

6.3.1 Raman spectroscopy studies

Although originally setting out to make magnetite, (Fe_3O_4), Raman spectroscopy confirmed that the particles produced were actually maghemite, (γ-Fe_2O_3), (**Figure 6.2**).[36] Maghemite has an inverse spinal structure and can be seen as an iron deficient form of magnetite. Its structural formula can be written as $Fe^{3+}_{21.33}\ _{2.67}\ O^{2-}_{32}$ where $_{2.67}$ signifies that there are 2.67 vacancies in the octahedral spinel sites.[37] Unlike magnetite, maghemite Raman bands are not well defined and the resolution of the bands is seemingly dependant on the method of sample preparation as it is directly

related to the degree of crystallinity of the material. It has been previously reported that in Raman measurements there is a possibility of thermal oxidation of magnetite under laser beam, that usually leads to the formation of hematite (α-Fe_2O_3) due to the high (>200°C) localised temperatures generated by the laser.[37, 38] This has been confirmed in the literature where the first recognisable signs of magnetite oxidation are the appearance of characteristic hematite bands at 300 and 410cm^{-1}.[38] In our Raman experiments to avoid the possible oxidation of iron oxide we have used reduced laser power (~3mW). Raman spectra of D-, L- and R- penicillamine stabilized maghemite are shown in Figure 6.2.

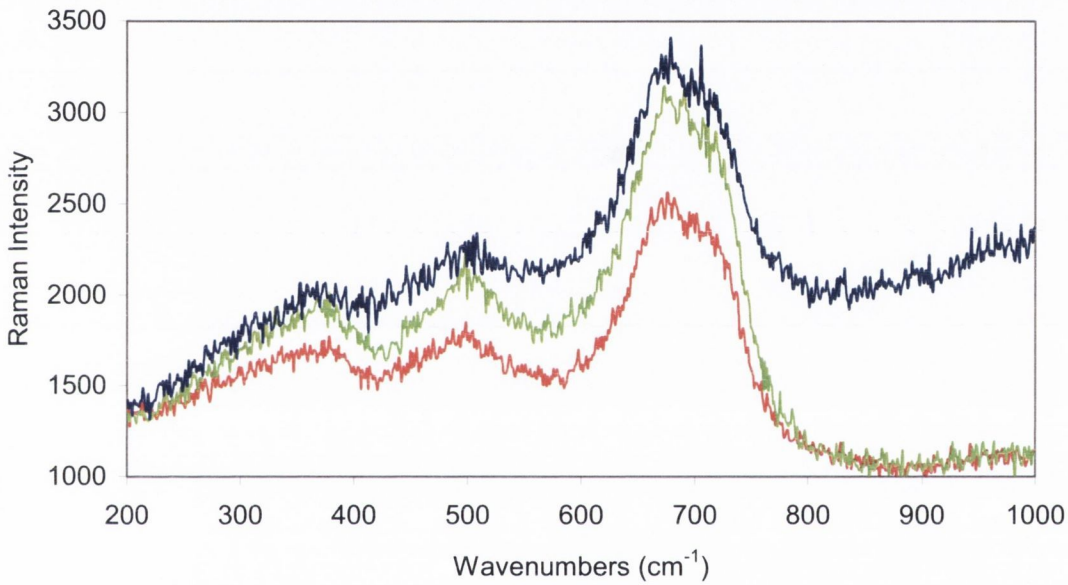

Figure 6.2: Raman spectra of D-, L- and R- Penicillamine stabilized Maghemite at 376, 506, 681 and 720cm^{-1}. The use of three different forms of penicillamine has had an effect on intensity and in the case of D- the degree of scattering exhibited by the particles. Although the most striking feature is the drop in intensity for all four peaks in the R- sample while the D- and L- samples have almost identical band intensities, despite the high level of noise in D-.

As stated above maghemite is characterised by its broad peaks, **Table 6.1** compares the peaks observed in the literature with those seen in **Figure 6.2.** The slight shifts in the wavenumbers are more than likely due to surface modification. Also there is a decrease in the relative intensity of the band at 720cm^{-1} when comparing functionalised with unfunctionalised maghemite. This phenomenon has also been reported in the literature where it was also the direct result of capping with a carboxy contain ligand.[36]

Table 6.1: Literature assigned wavenumbers, ($\acute{\upsilon}/cm^{-1}$), and modes for magnetite, maghemite and hematite, as well as the values for L-Pen Iron oxide presented in this chapter. The values for the L-Mag agree quite well with those of Maghemite although the Eg mode at $352cm^{-1}$ has red shifted to $376cm^{-1}$. This reduction in vibration energy may be due to covalent bonding to the stabilizer.

Hematite $\acute{\upsilon}/cm^{-1}$	Magnetite $\acute{\upsilon}/cm^{-1}$	Maghemite $\acute{\upsilon}/cm^{-1}$	L-Sample $\acute{\upsilon}/cm^{-1}$
$225(A_{1g})$		$193(T_{2g})$	
$247(E_g)$			
$293(E_g)$			
$299(E_g)$	$302(E_g)$		
$412(E_g)$		$352(E_g)$	**376**
$498(A_{1g})$	$513(T_{2g})$	$510(T_{2g})$	**506**
$613(E_g)$	$533(T_{2g})$	$678(E_g)$	**681**
	$663(A_{1g})$	$723(A_g)$	**720**
		1409	

6.3.2 FTIR spectroscopy studies

Infrared spectroscopy was particularly important in confirming the presence of penicillamine on the particles surface. Once prepared, the particles were magnetically separated and washed several times to remove any excessive penicillamine. CD and UV spectra were also carried out on the washings to confirm the absence of penicillamine from the final washing. After that the purified particles were examined using FTIR spectroscopy. FTIR spectra of all samples have shown characteristic bands of penicillamine (**Figure 6.3**.)

There were only some very minor differences noted between the FTIR spectra of the various enantiomer coated maghemite nanoparticles. The stretches of the Rac-penicillamine coated sample seemed to be more pronounced than either of the parent enantiomers. As these spectra are quite complex they will be broken up into different regions and the presence/or absence of the more important peaks, i.e. the mercapto, carboxyl and amine stretches, will be discussed. As the L-enantiomer gives the

sharpest peaks, no doubt due to it's greater purity, it will be used to highlight the various peaks.

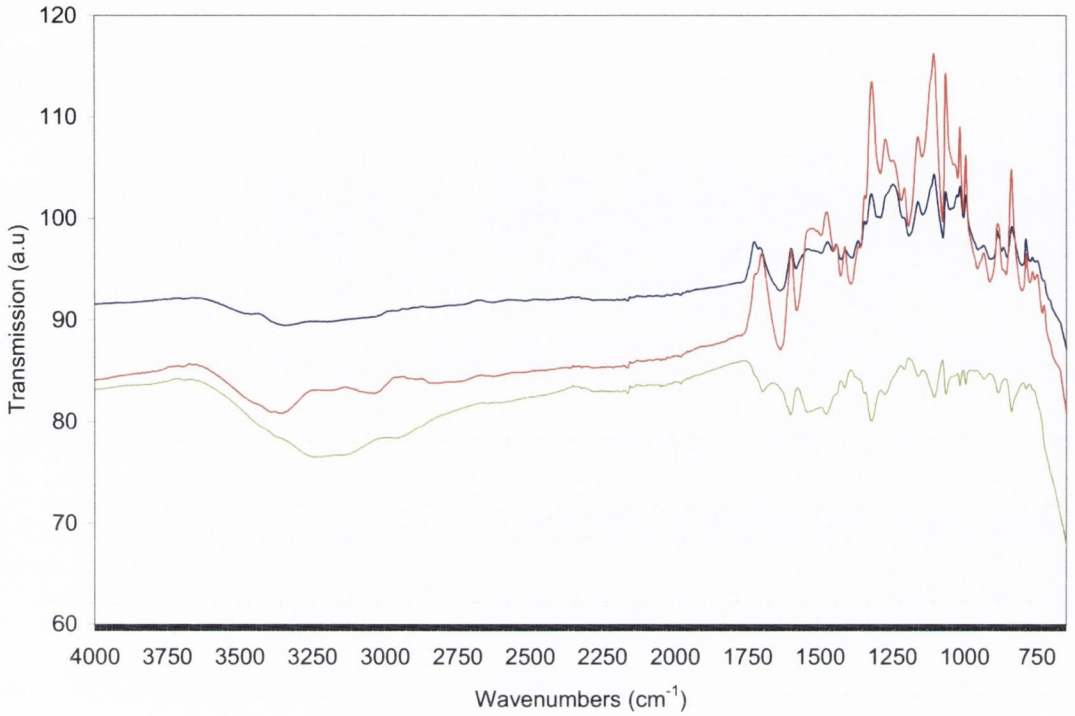

Figure 6.3: FTIR spectra of D- L- and R-Pen Maghemite. While the fingerprint region confirms the presence of penicillamine on the particles surface both the carboxyl and amino stretches are still visible while the mercapto stretch has completely vanished indicating it as the primary binding group. Also D- appears quite different from L- and R- , e.g. 1633 and 1578cm^{-1}.

To begin with the region containing the S-H stretch will be examined. Close examination of the L-stabilized particles at the region 2400-2700cm^{-1} showed that the S-H stretch as well as the –O-H stretching vibration, (which also occupies this region), were still present although greatly diminished and slightly red shifted. Due to the extraordinary decrease in the strength of these S-H bands, especially when compared with the amine and carboxyl peaks, it is possible that the mercapto and not the remaining functional groups is the primary point of attachment for penicillamine to the maghemites surface. Another possibility is that all three groups are involved in particle modification.

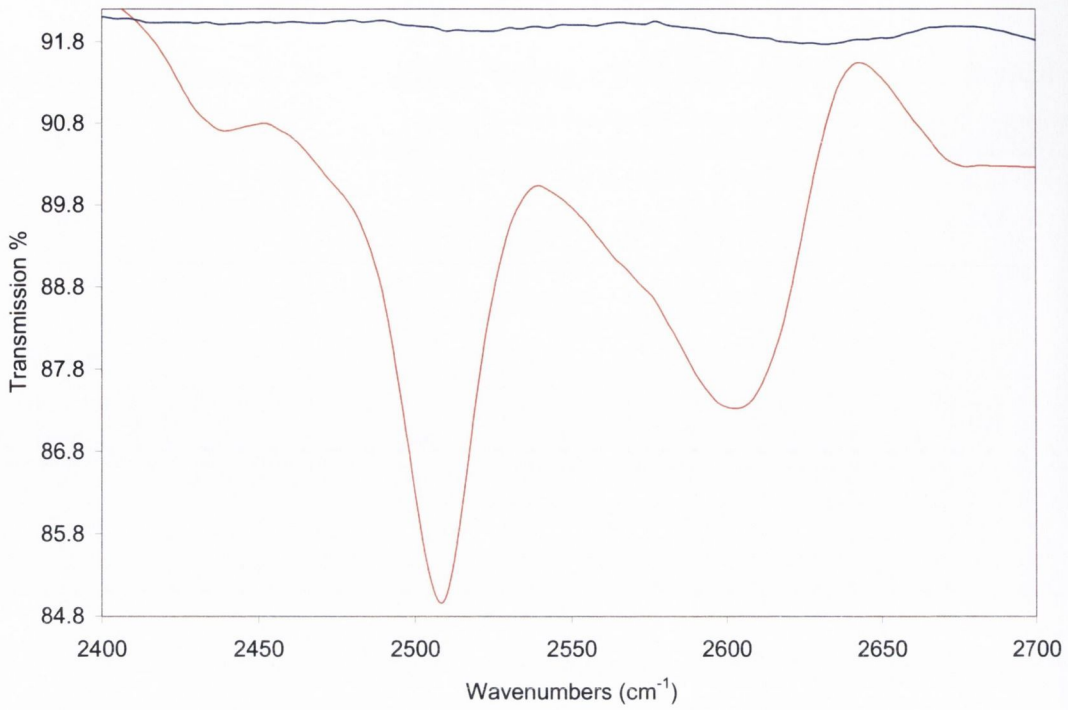

Figure 6.4: FTIR spectra of L-Pen and L-Maghemite. The strength of the peaks has been significantly reduced and both have red shifted from 2509 and 2604cm^{-1} to 2521 and 2630cm^{-1} respectively. As the frequency for a Pen S-H stretch is supposedly 2450cm^{-1} it could be either one.

Examination of the fingerprint region and beyond, (1000-1700cm^{-1}) shows that although the strength and position of the various amine and carboxyl stretches have been altered they have not been affected to the same extent as the mercapto groups. What is most noticeable though is that the penicillamine whether free or on the particles surface is present in both its anionic and zwitterionic forms as can be seen from figure 6.5. The most obvious difference between the free and attached Pen is the presence of broad hump at 1634cm^{-1} indicating the presence of N-H deformation and C-N stretching. This is probably due to bending of the molecule to allow direct attachment of the amine group to the maghemite surface. This would also partially explain the difference in the Raman spectra of the various enantiomers as chirality could only be introduced onto the particles if the amine, i.e. the chiral group, was involved in direct surface modification.

Therefore, though shifted from their original positions the various penicillamine peaks are clearly present indicating successful particle modification has taken place.

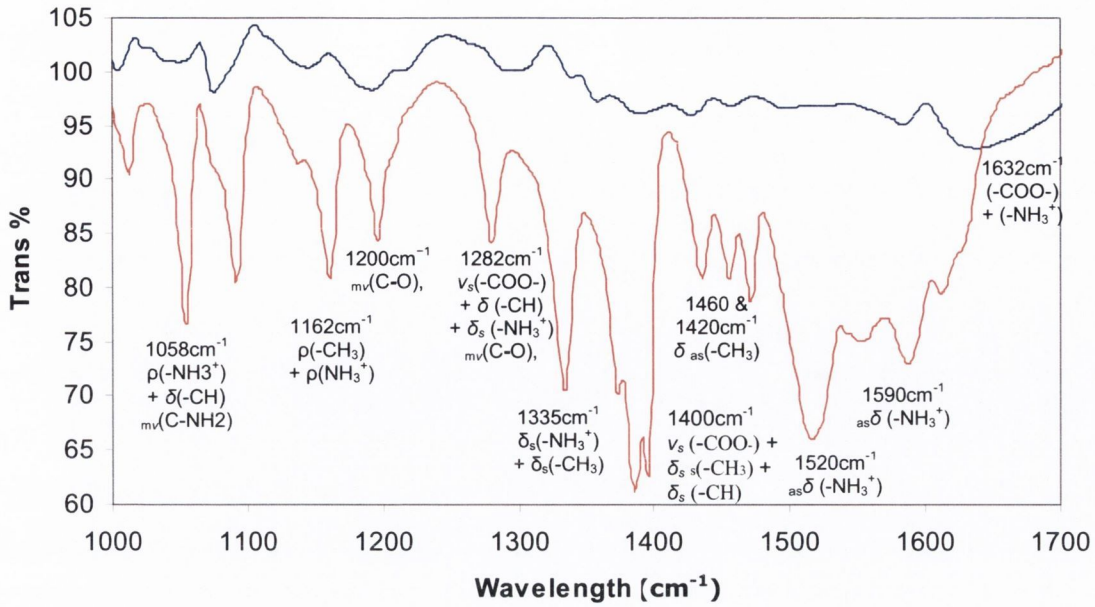

Figure 6.5: FTIR spectra of L-Pen and L-Pen stabilised-maghemite with the peak assignment.

6.3.3 TEM studies

TEM images of nanoparticles stabilised by both enantiomers as well as the R-modified particles confirm that all particles have sizes below 10nm and therefore should be paramagnetic (Figure 6.6).

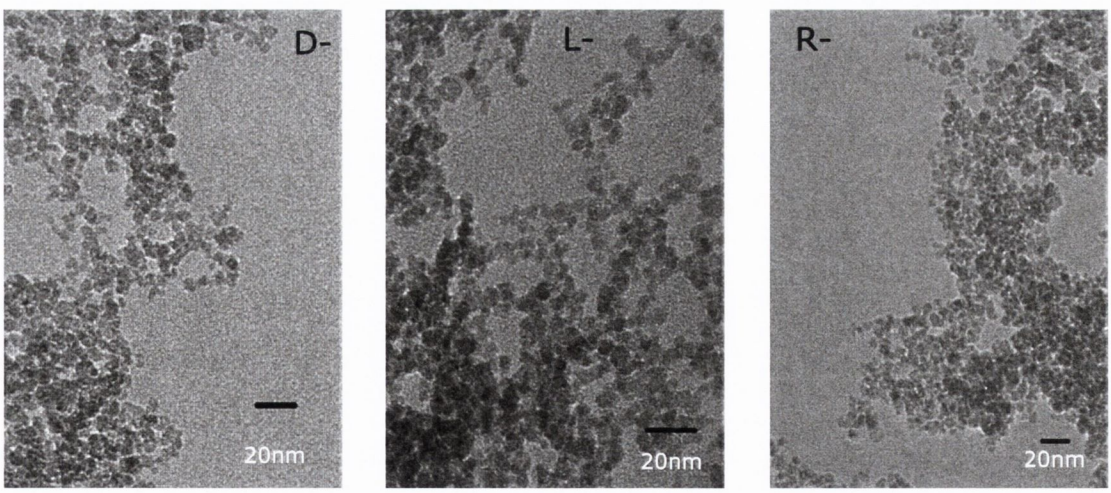

Figure 6.6: TEM images of penicillamine stabilized maghemite nanoparticles. All particle types, D-left, L-centre and R-right have diameters below 10nm. However due to the nature of the stabilizer used a good deal of aggregation is present.

All particle types are roughly spherical with D- and L- Pen stabilized particles being about the same size at 4.5±1nm while the R-Pen stabilized magnetic nanocrystals were almost one and half times as large with diameters of 6±1nm. Despite their larger size however R-Pen stabilized particles have a narrow distribution and they are well within the size range to be superparamagnetic.

6.3.4 Magnetisation measurements

The magnetic properties of all three types of particles were examined using a superconducting quantum interference device (SQUID)* magnometer, which shows magnetization as a function of magnetic field strength. Magnetisation curves for D- L- and R-Pen stabilized maghemite nanoparticles are shown in **Figure 6.7.**

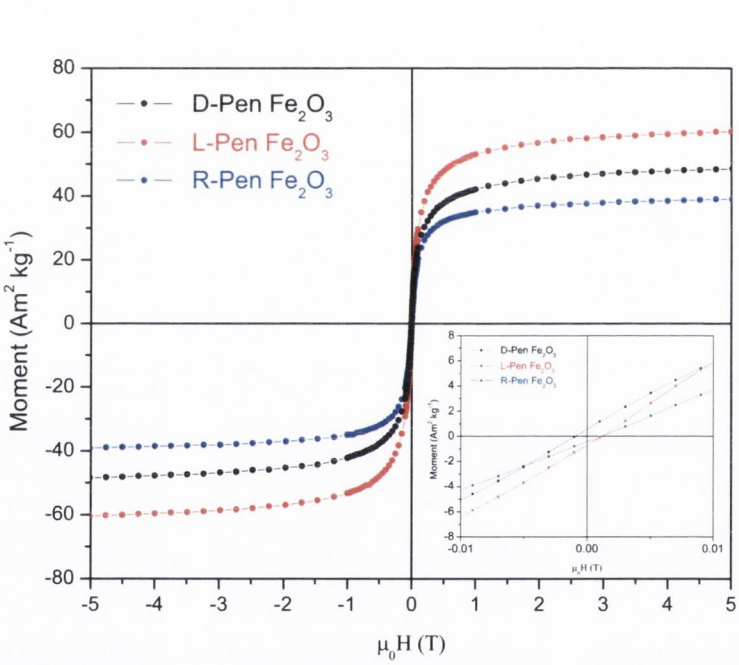

Figure 6.7: Hysteresis curves of penicillamine stabilized Maghemite nanoparticles. All particle types, D- L- and R- are superparamagnetic. However from the curves it is quite clear that the magnetic moment of the particles increases according to the chirality of stabilizer used.

The absence of the hysteresis loop and saturation in magnetization even at 5T field clearly indicate that all of these particles are superparamagnetic. For superparamagnetic material below Curie temperature, the thermal energy is sufficient to change the magnetisation of the whole particle. In this case, instead of each individual atom independently influenced by an external magnetic field, the magnetic

moment of the entire particle is aligned with the magnetic field. Even though the temperature is below the Curie temperature and the thermal energy is not sufficient to overcome the coupling forces between neighbouring atoms, the thermal energy is enough to change the direction of magnetisation of the entire crystallite. The resulting fluctuations in the direction of magnetisation cause the magnetic field to average to zero. The material behaves in a manner similar to paramagnetism, except that instead of each individual atom being independently influenced by an external magnetic field, the magnetic moment of the entire crystallite tends to align with the magnetic field. When the external field is shut off the particles do not retain any of their previous or "remnant" magnetism, this is an important feature of superparamagnetism.

While the coercivity and remanence values, i.e. where the loops insect the x and y axis's respectively, are miniscule for all three samples, {D (-0.001; 0.59), L (0.001;-0.67), and R (0.001;-0.43), inset **Figure 6.7**, the total magnetisation values for all three particles are radically different. Although still below the values for bulk γ-Fe_2O_3, 75Am^2kg^{-1} at μ_0H=2T, the moment for the L-Pen stabilized particles is much higher than the D- which is in turn higher than the R-functionalised particles. This would seem to suggest that depending on the chirality of stabilizer used maghemite nanoparticles with different magnetic moments have been produced. Also as the R-stabilized particles have the lowest over all magnetic moment it can be inferred that particles which are optically active have a higher overall magnetism than those which are not.

The decrease in the overall magnetisation of the R- particles when compared with the D- and L- particles is also possibly due to their larger size as seen in the TEM images, (**Figure 6.6**), although this does not account for the differences in the magnetism values between the D- and L- stabilized particles as they have practically the same diameter.

*A SQUID is a mechanism used to measure magnetic signals in the ~ *f*T range. SQUIDS work by employing a device known as a Josephson junction. (A Josephson junction is made up of two superconductors, separated by an insulating layer so thin that electrons can pass through.) A SQUID is made up of tiny loops of superconductive materials, for example gold or indium, employing Josephson junctions to achieve superposition. Superposition is when each electron moves

simultaneously in both directions. As the current is moving in two opposite directions, the electrons have the ability to perform as qubits. A qubit is the quantum computing analogue of the binary digit, or bit, in classic computing.

The data itself is displayed as the magnetic moment exhibited by the material being tested, y-axis, in the presence/or absence of an externally applied magnetic field, the x axis. Switching the applied field on and off, as well as reversing it, allows us to see whether the material retains away residual magnetism in the absence of an external field.

6.3.5 UV-Vis and CD measurements

Examination of the particles using UV-Vis spectroscopy showed that although the characteristic maghemite shoulder was present for all particles at 360 nm there was little evidence of the penicillamine at 234 nm although this could simply be due to its low concentration. This was also true of the CD spectra where little or no difference was seen between the D-, L- or R- Pen functionalised particles. While all three particle types did exhibit some optical activity at their UV-Vis active regions this was attributed to the defective spinel structure of the maghemite nanocrystals themselves and is not a result of their functionalisation.

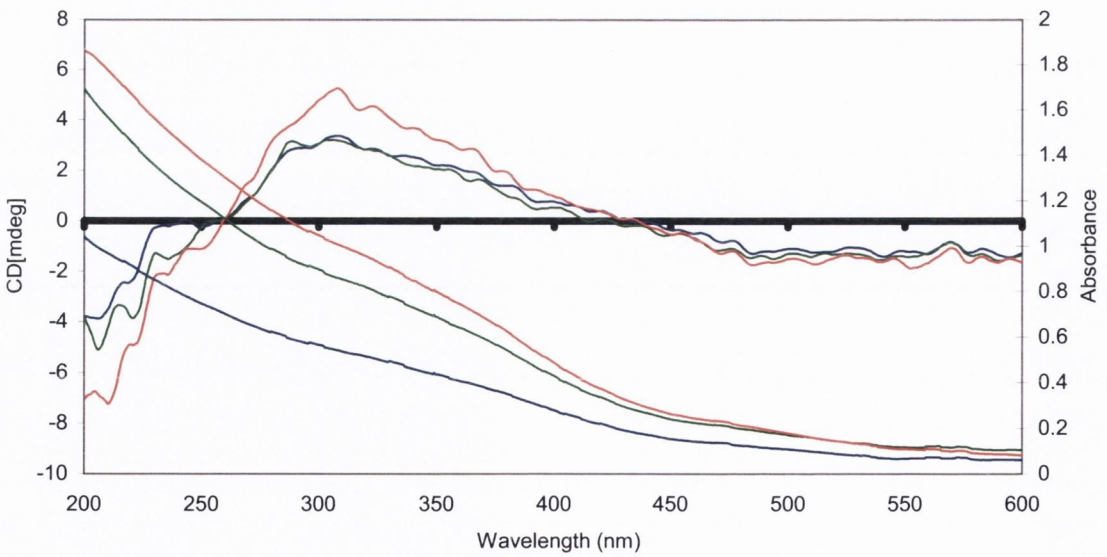

Figure 6.8: UV-Vis and CD spectra for D-, L- and R- Penicillamine Maghemite

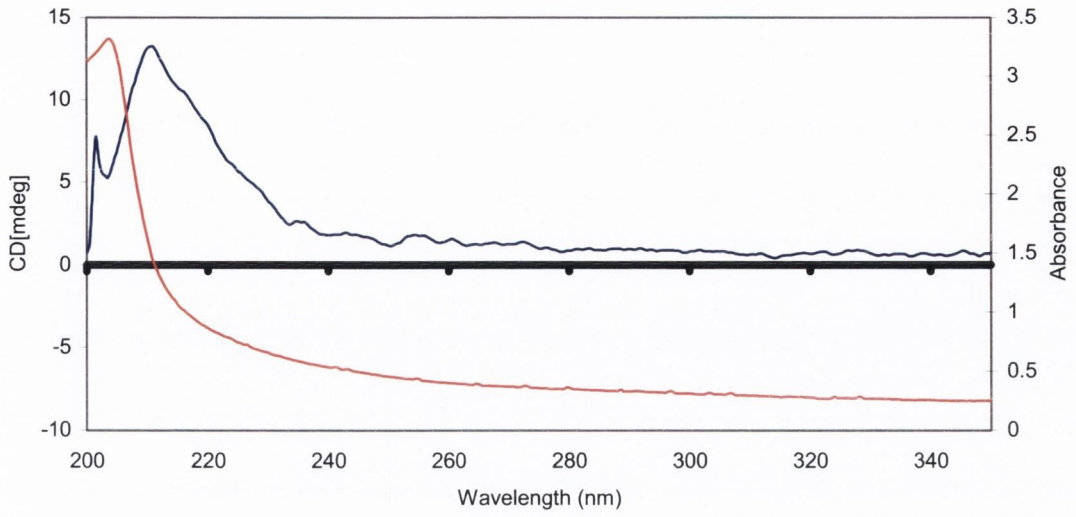

Figure 6.9: UV-Vis, (blue), and CD, (red) spectra of 1st washing taken after the preparation of L-Pen Maghemite. Note the lack of Pen or Fe-Pen complex signals indicating all Pen remains on the particles surface. The peak at 211nnm cannot be identified but it is present in the washing for both D- and L- and does not change chirality depending on the enantiomer used leading to the belief that its is some form of scattering.

Although not shown, unfunctionalised magnetic particles give similar CD responses, i.e. a strong hump like structure with a maxima at 320 nm. As mentioned earlier in the chapter, and shown above in **Figure 6.9**, the washings from the particles did not contain any free penicillamine or Fe-Pen complex. As there are no penicillamine molecules or Fe-Pen complexes in the washing, nor is it, (Pen), detectable by UV-Vis and CD on the particles surface despite FT-IR confirming its presence the only explanation is that the maghemite is somehow masking the Pen. In an effort to confirm this theory the entire reaction was monitored using UV-Vis and CD spectroscopy as was done in previous chapters. The lilac coloured Fe^{2+}-Pen while being weakly UV active appears to be the most optically active of the two precursor complexes with strong peaks at 273, 250 and 225 nm. The Fe^{3+} complex appears less chiral, despite it being more concentrated than the previous complex. It has weak CD bands at 237 and 220 nm, but is strongly UV active with a large hump like peak at 300 nm. Addition of the two complexes severely reduces their UV and increases the CD profiles; taking on appear of Fe^{2+}-Pen complex solution as opposed to a mixture of the both. Once ammonia has being added the particles are removed by magnetic separation and the supernatant is examined. The previous CD signals all but vanished while a strong signal appears at 205nm in both the UV and CD.

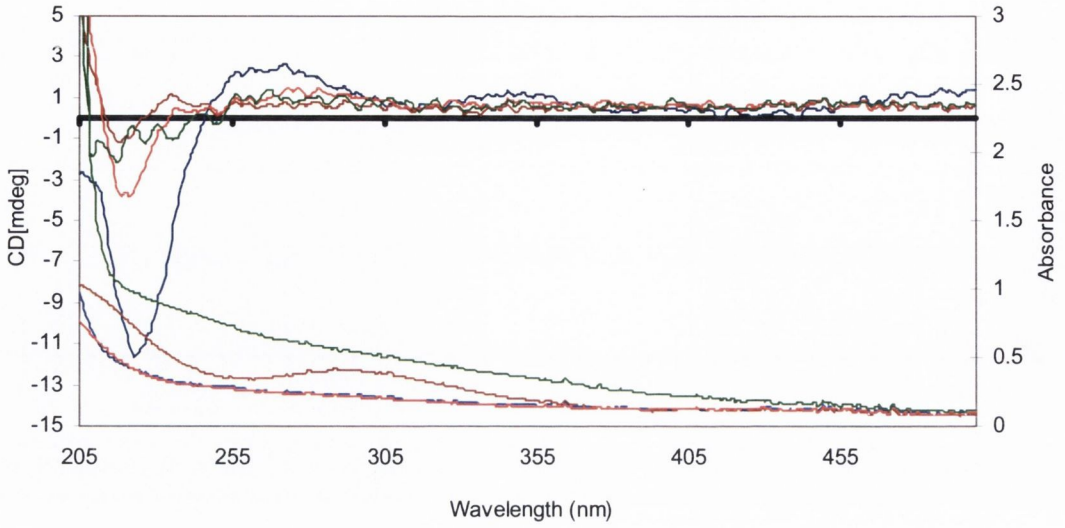

Figure 6.10: CD/Abs of D-Pen-Fe^{2+}, (blue), D-Pen-Fe^{3+}, (brown), the combined solutions, (red), and finally after the addition of ammonia hydroxide, (green).

While Fe^{2+}-Pen is a highly chiral supramolecular complex the Fe^{3+} equivalent is not. As the iron complexes are mixed together the loss in the CD signal may simply be attributed to dilution. However, it is clear from these experiments that Fe^{3+} complexes of penicillamine are not strongly chiral.

6.4 Magnetic-luminescencent nanocomposites

In this part of our project we have attempted to create "all in one" nanocomposites particles which are magnetic and luminescent.[39-42] This is an area which has been of large interest of late but we hope to bring something new to these composites in that they will be not only magnetic and luminescent but also chiral. Initially it was believed that the -SH groups of the penicillamine would be facing off the particles surface allowing for the deposition of Cd^{2+} ions onto the surface of the maghemite particles, with the eventual hope of growing a chiral luminescent CdS shell on the magnetic core. We also aimed to investigate interactions between magnetite nanoparticles and CdS QDs of different chirality. With this in mind D-Pen Maghemite was reacted with all three types of Pen-CdS, (D-, L-and R-), and both the resulting supernatant and the magnetically separated and washed particles were examined using UV-Vis, PL and CD spectroscopy.

Two different approaches were taken in the preparation of the "all in one "nanocomposites. The first method involved the mixing of the D-Pen maghemite with the CdS particles, (of any chirality), allowing them to stir overnight then magnetically separating them the following day, this approach is named as the addition route. The second approach was to *in situ* grow CdS shell on maghemite nanoparticles surface. This was achieved by adding Cd perchlorate salt to the maghemite particles under stirring , followed by addition of penicillamine, then by increasing the pH to 11 and then finally by the addition of thioactemide and microwave treatment of the sample for 70 seconds.

Examination of the magnetically separated maghemite particles using UV-Vis showed that while CdS QDs may be present on the magnetic cores surface, they are hidden by the presence of the characteristic maghemite peak, as can be seen in **Figure 6.11. Figure 6.11** shows UV-Vis spectra of unmodified Pen-maghemite, (red), alongside the UV-Vis spectra of Pen-maghemite after addition of CdS particles, (blue) and Pen-maghemite after in situ co-precipitation of CdS, (green). Although there does seem to be some difference between the modified and unmodified maghemite spectra the lack of any emission peak from these samples makes them of little use as

magnetic luminescent composites. Little difference was observed either between the added and co-precipitated samples or between the D-, L- or R- experiments.

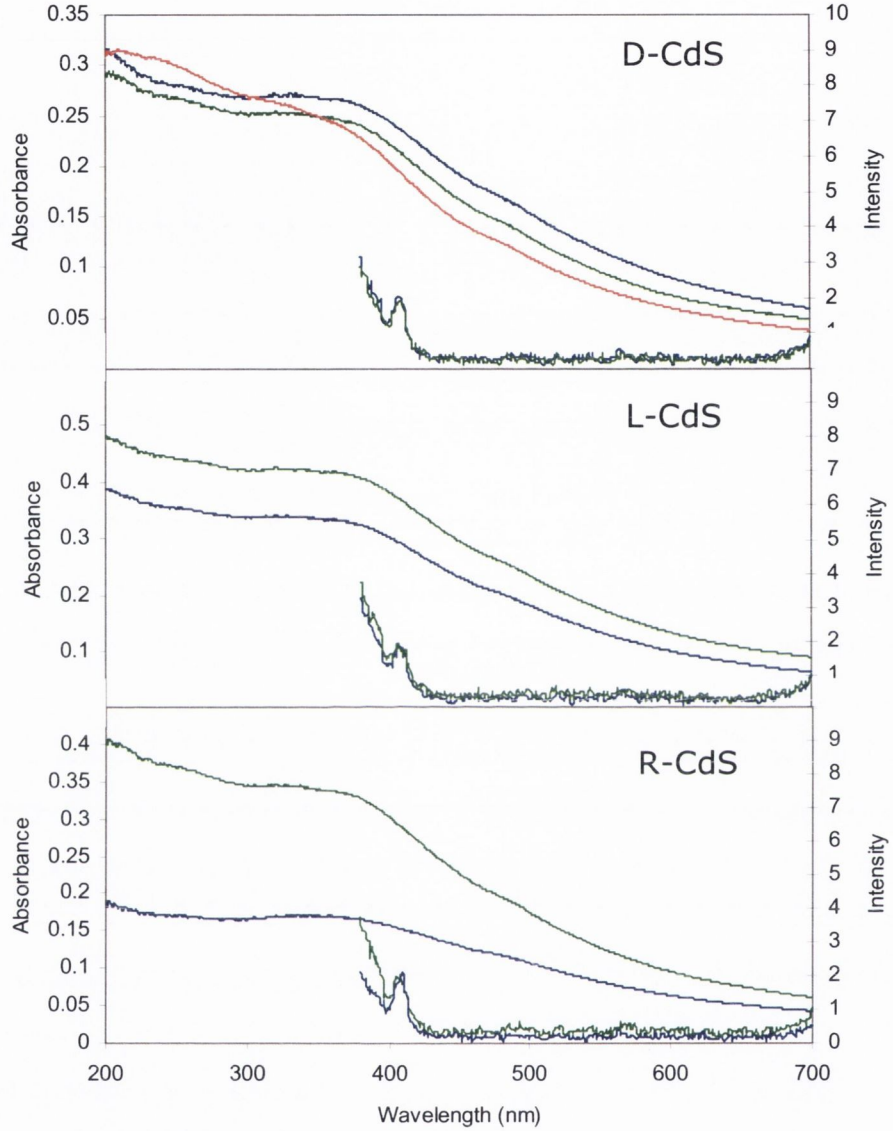

Figure 6.11: Absorption/Emission spectra of D-top, L-middle, and R-bottom CdS added to, (blue), or co-precipitated in the presence of, (green), D-Pen-maghemite. The top spectrum also contains unmodified D-Pen Maghemite for comparison, (red). Ems spectra were excited at 360nm.

6.4.1. Investigation of the interactions between chiral CdS and maghemite nanoparticles

Maghemite nanoparticle solution was added to freshly prepared Pen-CdS nanoparticles. The mixture was shaken overnight. The product was isolated by magnetic separation and washed several times with water. Examinations of the

washings lead to some interesting findings. Despite prolonged exposure to external magnetic fields it was impossible to remove all the maghemite from suspension; this could be seen by the very faint brown colour of the washings. Examination of the UV-Vis of these spectra showed that the CdS still absorbed deep in the UV region of the spectra and therefore could not be responsible for the colour.

Closer examination of the supernatant using UV-Vis, Pl, and CD spectroscopy showed that there were distinct differences between not only the co-precipitated and added reactions but more importantly between the D-, L- and R- particle conjugates.

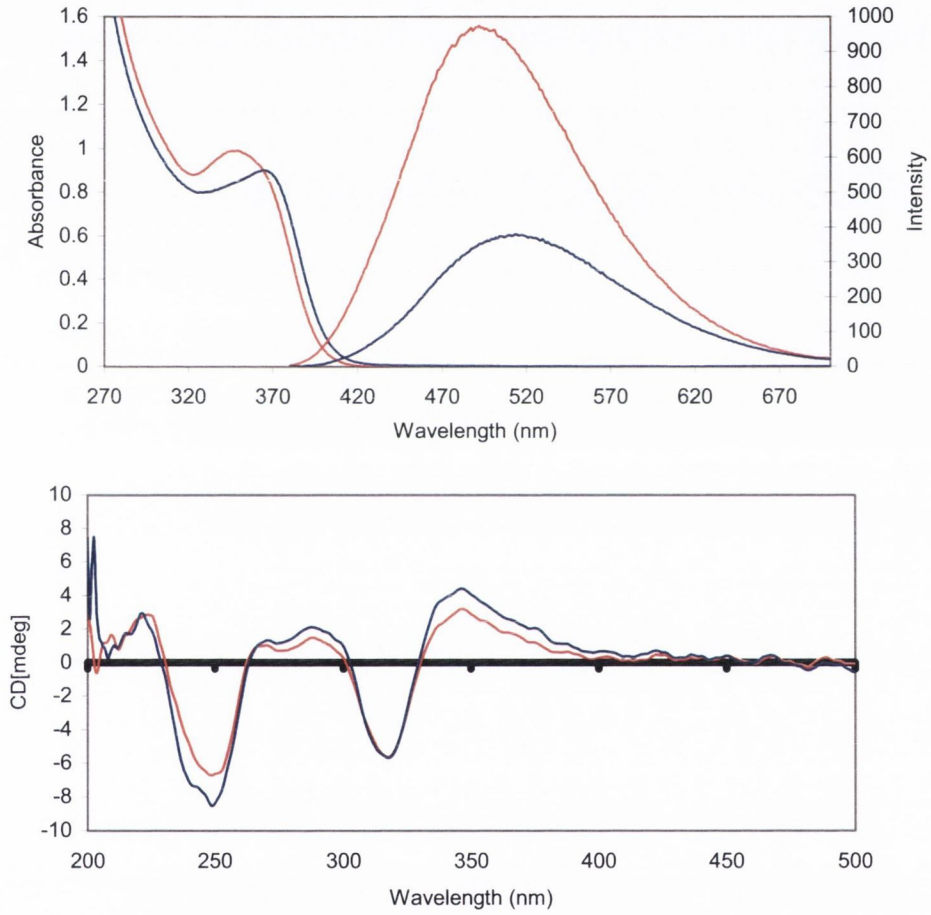

Figure 6.12: Absorption/Emission spectra, (top), and CD spectra, (bottom), of the first washing of D-CdS added to D-Maghemite, (blue). Red-Control, i.e. unmodified CdS. Pl spectra were excited at 360nm.

As expected we see a drop in emission intensity between the modified and unmodified CdS, (**Figure 6.12, 6.13 & 6.14**). This drop in the emission strength is clearly not just caused by the slight decrease in absorbance and is therefore an actual decrease in emission strength. By simply adding the as prepared D-CdS dots to D-Maghemite and leaving them to stir overnight we observe a red shift, i.e. increase in

QD size, in both the abs and ems of the D-CdS particles, (**Figure 6.12**). Also while the FWHM of the control is 124nm, the FWHM of the added particles has now increased to 135nm, indicating a higher degree of defectiveness on the particles surface. This red shift, in the luminescent suggests that larger particles are now present, while the increase in the strength of the CD spectrum, (despite the slightly lower abs), indicates a greater optically active character. This is perhaps due to the added presence of the D-Pen on the Maghemites surface.

In the case of the interactions between L-CdS and D-Maghemite a very different picture is observed (**Figure 6.13**).

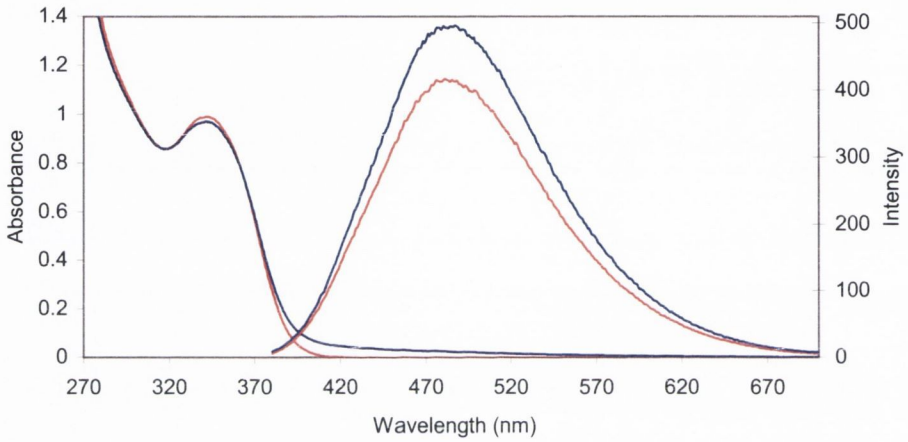

Figure 6.13a: Absorption/Emission spectra, (top) of the first washing of L-CdS added to D-Maghemite, (blue). Red-Control, i.e. unmodified CdS.

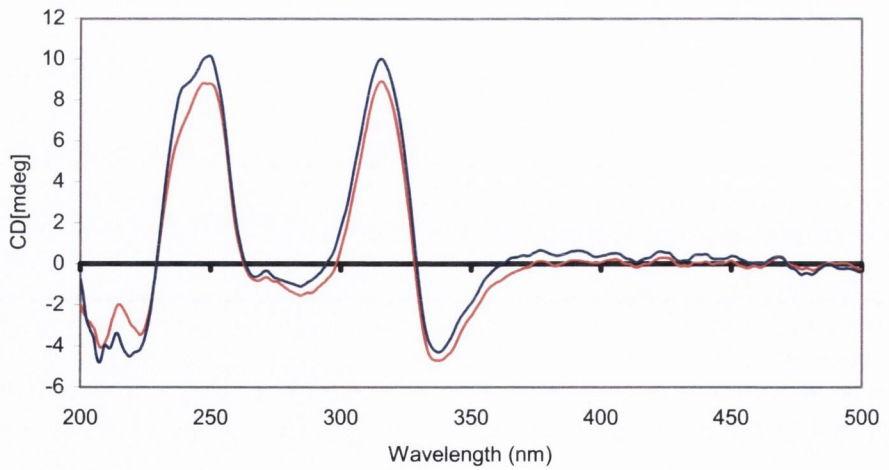

Figure 6.13b: CD spectra of the first washing of L-CdS added to D-Maghemite, (blue). Red-Control, i.e. unmodified CdS.

Firstly the added particles do not see a decrease but an increase in their luminescent intensity. As there is little change in the level of absorbance where both the added particles and control dots are excited, (360nm), this means the increase in intensity is not simply a result of changes in particle concentration but a real increase in luminescence. This increase in luminescent intensity combined with a 2nm red shift in the Pl maxima may be a result of increased QD proximity as they bind to the complimentary maghemite. Also although there is no change in the shape of the absorption shoulder, (**Figure 6.13**-red to blue), there is a good degree of scattering, unlike the D-CdS sample, indicating the presence of large sedimenting particles, again this is a sign of particle aggregation.

Lastly, the D-Maghemite and R-CdS were examined, (**Figure 6.14**). Although there are definite changes in the structure of the absorption spectra when comparing the added particles, (334nm), to the control there is little change in the peak position when compared with the control, (338nm).

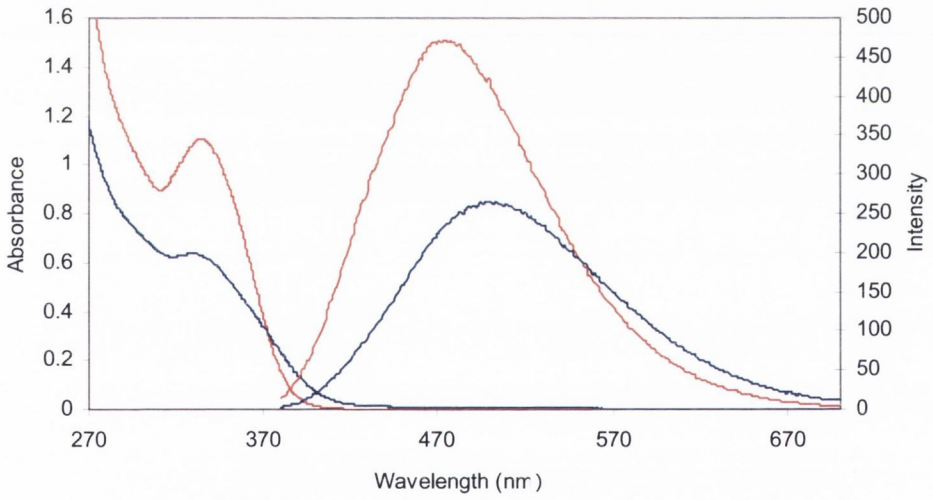

Figure 6.14a: Absorption/Emission spectra of the first washing of R-CdS added to D-Maghemite, (blue). Red-Control, i.e. unmodified CdS.

The drop in intensity of the emission spectra seems to be concurrent with the overall drop in absorbance so it can be disregarded as it is not a net change in luminescence. However there are distinctive red shift in the emission maximas of the added dots, (+26nm), when compared with the control dots. While the FWHM values for the control is 118nm the FWHM for the added dots has widened to 138nm. So while the changes to the R-CdS dots are not as distinctive as those for the D- and L- they are

present. This indicates that changes to the R-particles did occur as a direct result of exposure to the D-Maghemite.

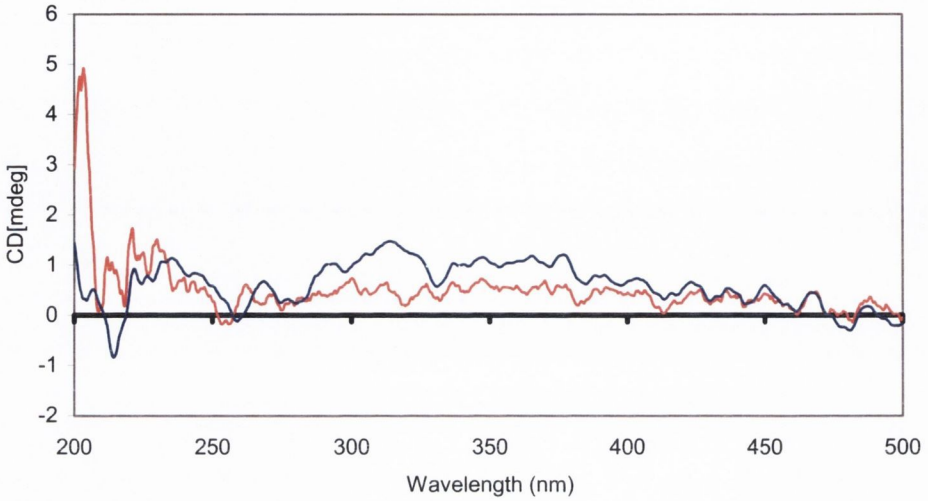

Figure 6.14b: CD spectra of the first washing of R-CdS added to D-Maghemite, (blue) and Red-Control. Pl spectra were excited at 360nm.

Examination of the CD spectrum of the control R-CdS particles shows as expected particles which are not optically active. However the added particles now show some degree of optical activity, (Figure 6.14b) While a possible explanation for this is that the D-Maghemite is preferably removing one enantiomer from the QDs making them chiral. This seems unlikely due to the strength of the Cd-S bond, although not impossible.[43].

6.4.2. In situ grow of CdS shell on maghemite nanoparticles

As expected there is also a drop in emission intensity, (**Figure 6.15**), for the in situ co-precipitated D-CdS. This drop could simply be a result of the smaller amount of particles formed, as can be seen from the absorption spectrum, in which case the quantum dots are actually brighter when formed with maghemite present. There seems to be very little difference between the control dots, (red), and the co-precipitated particles, (green), with respect to the emission maximas. The FWHM of both the control and co-precipitated particles were roughly the same 124 nm and 128

nm respectively, indicating little difference in the number of surface defects of each particle type.

While there are differences between the shape of the absorbance and CD spectra these could be simply put down to difference size particles. That is the co-precipitated particles appear to be smaller than the control dots. This could be due to the Cd^{2+} ions in solution being absorbed onto the surface of the penicillamine coated Maghemite before the QDs had a chance to form, this would explain the fact that not only are the dots smaller but there are also less of them.

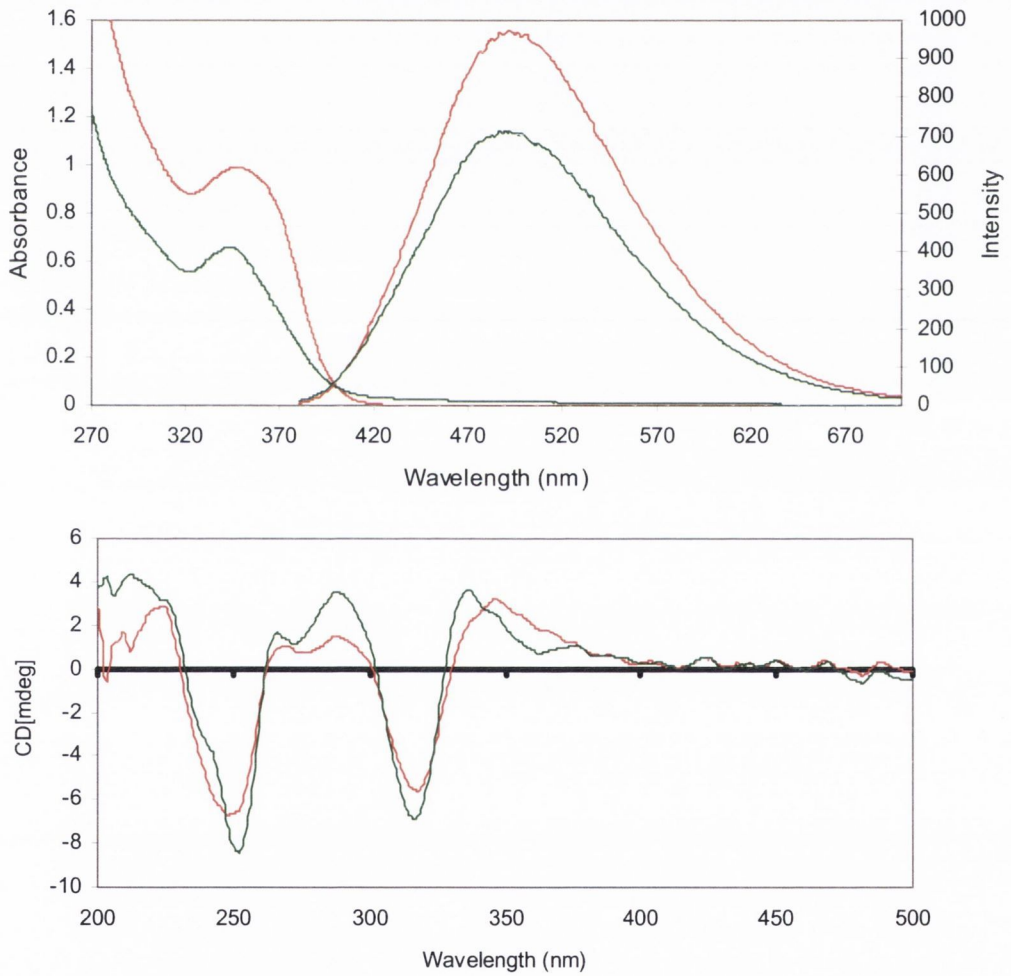

Figure 6.15: Absorption/Emission spectra, (top), and CD spectra, (bottom), of the first washing of D-CdS co-precipitated in the presence of D-Maghemite, (green). Red-Control. Pl spectra were excited at 360nm.

Interactions between L-CdS and D-Maghemite are shown in **Figure 6.16**. The co-precipitated particles are dramatically different from the control in both their

absorption and emission characteristics. Not only is the shape of the absorption shoulder different but the co-precipitated QDs have red shifted by 34nm indicating substantially larger particles. The luminescent intensity is considerably lower and has also red shifted, by 49nm. There is also a significant increase in the FWHM of the co-precipitated particles growing from 119nm, (control), to 168nm. The combination of the larger particle size, reduced luminescence and increased surface disorder, (as seen by the increased FWHM), suggests the present of Maghemite close to the CdS particles, this could be the result of the formation of core/shell or aggregated structures. What is for certain is that the results are in stark contrast to the co-precipitated reaction for the D-CdS particles indicating a chiral interaction has occurred.

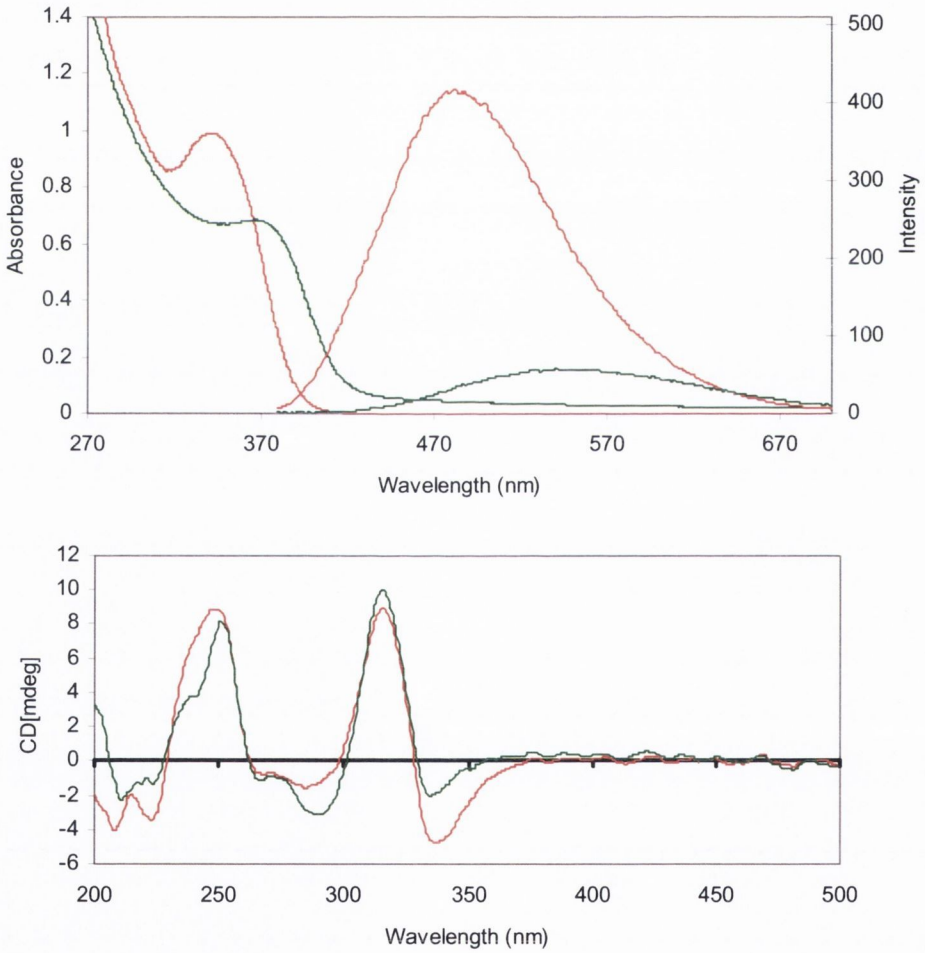

Figure 6.16: Absorption/Emission spectra, (top), and CD spectra, (bottom), of the first washing of L-CdS co-precipitated in the presence of D-Maghemite, (green). Red-Control. Pl spectra were excited at 360nm.

Finally D-Maghemite and R-CdS were combined and the results examined. Although there are definite changes in the structure of the absorption spectra for the co-precipitated, (334nm), there is little change in the position of the absorbance peak when compared with the control, (338nm). Also a slight degree of scattering is observed in the co-precipitated sample again indicating the presence of large sedimenting particles, (**Figure 6.17**).

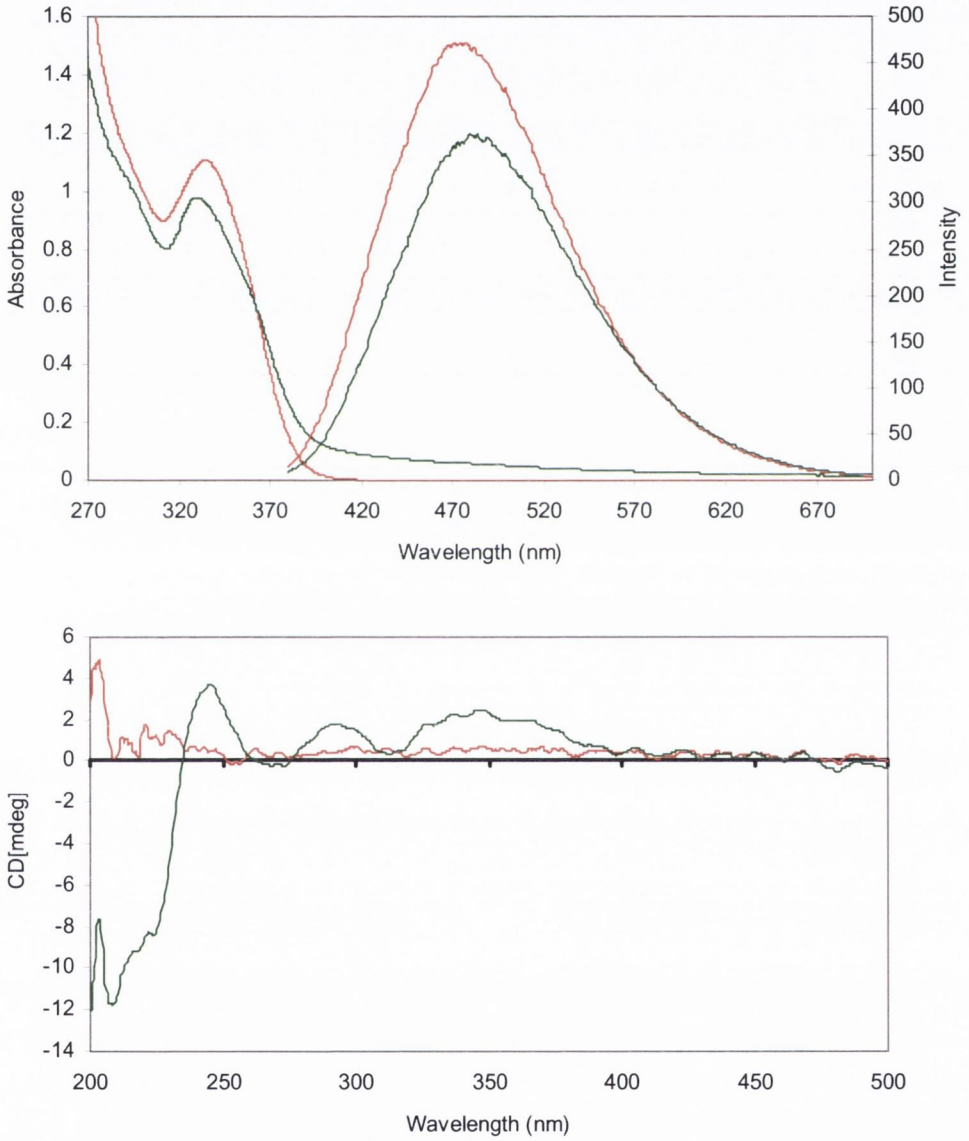

Figure 6.17: Absorption/Emission spectra, (top), and CD spectra, (bottom), of the first washing of R-CdS co-precipitated in the presence of D-Maghemite, (green). Red-Control. Pl spectra were excited at 360nm.

The drop in intensity of the emission spectra seems to be concurrent with the overall drop in absorbance so it can be disregarded as it is not a net change in luminescence. However there are distinctive red shift in the emission maximas of the co-precipitated

particles, (+6nm), when compared with the control dots. The FWHM values for the control and co-precipitated dots are also quite similar at 118nm and 121nm respectively. So again while the changes to the R-CdS dots are not as distinctive as the D- and L- they are present, again signifying that changes to the particles did occur as a direct result of exposure to the D-Maghemite. Examination of the CD spectrum of the control R-CdS particles shows as expected particles which are not optically active. However the co-precipitated particles now show a great degree of optical activity, (**Figure 6.17**). Close examination of the co-precipitated CD spectrum shows that the spectrum has elements of both the D- and L- particles. This suggests that both the D- and L-acids are being detected and are no longer cancelling each other out. This of course needs further examination.

6.4.3. TEM images of In situ grow of CdS shell on maghemite nanoparticles

In an attempt to show that the supernatant did indeed contain core/shell maghemite/CdS structures TEM imaging was preformed on D-, L- and R-CdS/ D-Maghemite co-precipitation reactions. Once magnetic separation had been preformed the supernatant was reduced in volume to around 2ml and isopropanol was added to precipitate out the particles. After centrifugation both maghemite and CdS could be seen in the pellets however these were probably a mechanical mixture of the two types of nanoparticles. However TEM confirmed that another type of particle, (core/shell), was also present, (**Figure 6.18**). While maghemite is clearly visible in all three samples it is L- and to a lesser extent the R-CdS samples that clear core/shell structures can be seen. Figure 6.18 shows D-Maghemite/L-CdS core shell particles. While plain maghemite is clearly present there are also particles with a 3.9nm maghemite core and 2nm CdS shell. The CdS modified maghemite is slightly smaller than the unmodified particles but this may simply be due to the compression brought on by the presence of the CdS on its surface. The large number of these structures may account for the red shifting and drop in strength of the L-CdS luminescence, (**Figure 6.16**). Less numerous core/shell particles were also found in the R-CdS samples. While the core sizes were on average 5.5nm with a high degree of monodispersity, the shell thickness ranged 2-3nm depending on the particle examined. Examination of the D-CdS particles at these magnification showed little evidence of

these core/shell structures there was evidence of them at much lower magnification with what appeared to be maghemite/CdS nanoparticles but now the size range of 460-590nm. These large aggregated structures are composed of 150±40nm maghemite cores with 140±24nm CdS shells. As there is in evidence for these large structures in the UV-Vis or Pl data we must assume that they are aggregates.

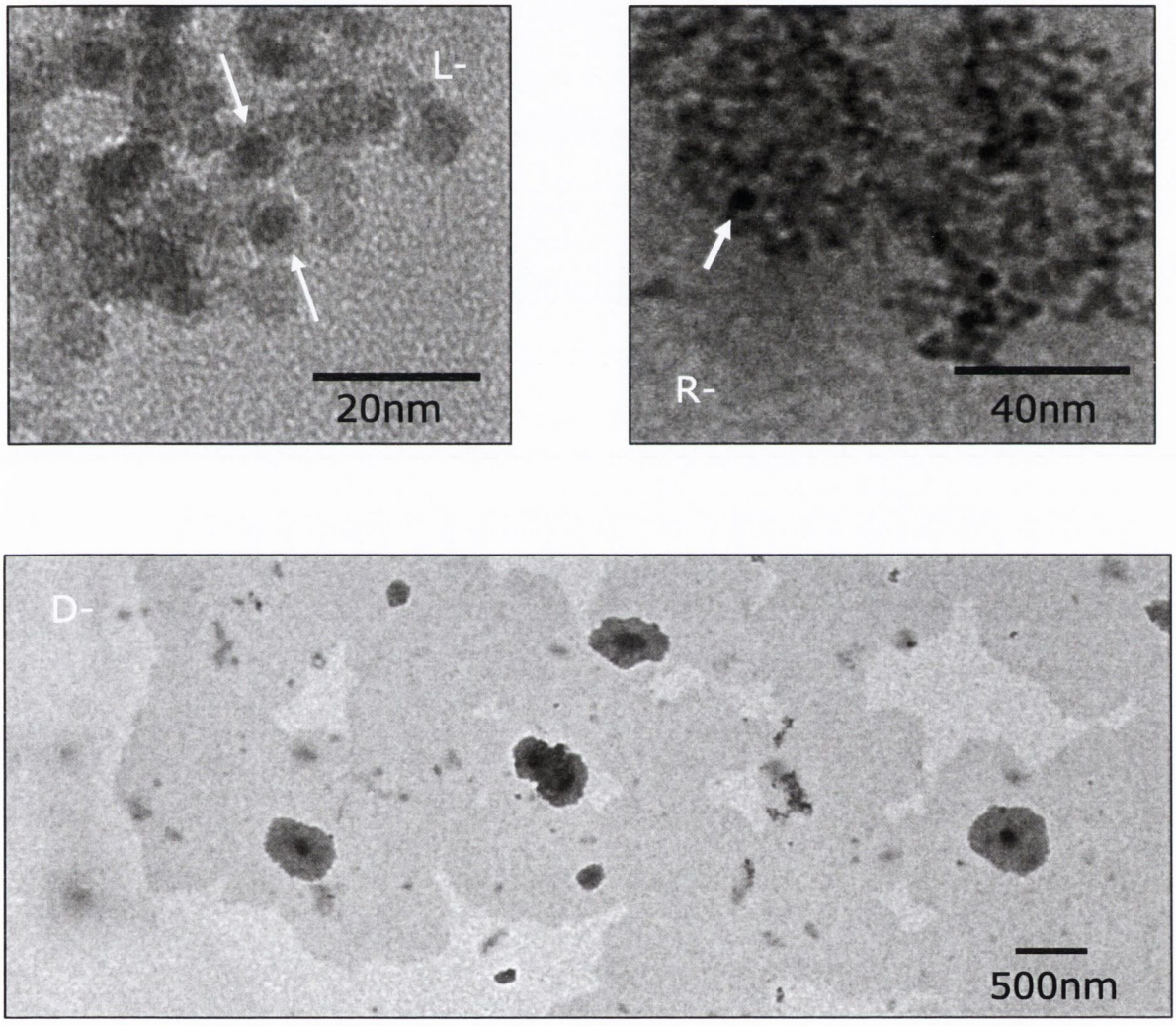

Figure 6.18: TEM images of D-Maghemite with in situ co-precipitated D-, L- and R- CdS shell.

6.5 Conclusions

Penicillamine coated maghemite nanocrystals have been successfully prepared. FTIR has confirmed the present of the ligand. TEM images demonstrated that the utilisation of Penicillamine stabilisers allowed us to control both the size and monodispersity of the magnetic particles. SQUID measurements have shown that the particles are indeed superparamagneitc. Also SQUID suggested a difference between the magnetism of the D-, L- and R- particles which can not be explained by simple nanoparticle size differences. CD measurements showed very little differences from the particles coated by non-chiral stabilisers. However, we believe that only VCD measurements could detect any effects of the chiral penicillamine stabilisers on maghemite particles.

Attempts to make "all in one" magnetic-luminescent-chiral composites resulted in some remarkable core-shell structures, which demonstrated interesting photophysical properties. However, there were some difficulties with the purification and clear identification of these nanocomposites. Obviously, significant efforts will be required to develop these nanosystems and investigate them in details. This will be a subject of our future work.

6.6 References

[1] S. A. Wolf, D. D. Awschalom, R. A. Buhrman, J. M. Daughton, S. von Molnar, M. L. Roukes, A. Y. Chtchelkanova, D. M. Treger, *Science* **2001**, *294*, 1488.

[2] P. P. C. Sartoratto, A. V. S. Neto, E. C. D. Lima, A. L. C. R. d. Sa, P. C. Morais, *Vol. 97*, AIP, **2005**, p. 10Q917.

[3] B. Gleich, J. Weizenecker, *Nature* **2005**, *435*, 1214.

[4] M. I. Shukoor, F. Natalio, M. N. Tahir, M. Divekar, N. Metz, H. A. Therese, P. Theato, V. Ksenofontov, H. C. Schröder, W. E. G. Müller, W. Tremel, *Journal of Magnetism and Magnetic Materials* **2008**, *320*, 2339.

[5] M. I. Shukoor, F. Natalio, H. A. Therese, M. N. Tahir, V. Ksenofontov, Pantho, x, M. fer, M. Eberhardt, P. Theato, Schro, x, H. C. der, Mu, x, W. E. G. ller, W. Tremel, *Chem. Mater.* **2008**, *20*, 3567.

[6] Y. Li, X. Xu, C. Deng, P. Yang, X. Zhang, *J. Proteome Res.* **2007**, *6*, 3849.

[7] A. F. Thunemann, D. Schutt, L. Kaufner, U. Pison, H. Mohwald, *Langmuir* **2006**, *22*, 2351.

[8] S. Liu, M. C. Ziegler, D. S. Edwards, *Bioconjugate Chem.* **2000**, *11*, 113.

[9] S.J. Saldanha, S.L. Piper, K.M. Ainslie, T.A. Desai, H.T. Kim, S. Majumdar, *European Cells and Materials Journal* **2008**, 17.

[10] M. Corti, A. Lascialfari, E. Micotti, A. Castellano, M. Donativi, A. Quarta, P. D. Cozzoli, L. Manna, T. Pellegrino, C. Sangregorio, *Journal of Magnetism and Magnetic Materials* **2008**, *320*, e320.

[11] S. Mornet, J. Portier, E. Duguet, *Journal of Magnetism and Magnetic Materials* **2005**, *293*, 127.

[12] H. Choi, S. R. Choi, R. Zhou, H. F. Kung, I. W. Chen, *Academic Radiology* **2004**, *11*, 996.

[13] C. W. Jung, P. Jacobs, *Magnetic Resonance Imaging* **1995**, *13*, 661.

[14] D. Shao, A. Xia, J. Hu, C. Wang, W. Yu, *Colloids and Surfaces A: Physicochemical and Engineering Aspects* **2008**, *322*, 61.

[15] C.-L. Chiang, C.-S. Sung, C.-Y. Chen, *Journal of Magnetism and Magnetic Materials* **2006**, *305*, 483.

[16] K.S. Wilson, L.A. Harris, J.D. Goff, J. S. Riffle, a. J. P. Dailey, *European Cells and Materials Journal* **2002**, *3*, 206.

[17] M. Ma, Y. Zhang, W. Yu, H.-y. Shen, H.-q. Zhang, N. Gu, *Colloids and Surfaces A: Physicochemical and Engineering Aspects* **2003**, *212*, 219.

[18] C. Bergemann, D. Müller-Schulte, J. Oster, L. à Brassard, A. S. Lübbe, *Journal of Magnetism and Magnetic Materials* **1999**, *194*, 45.

[19] D. K. Kim, M. Mikhaylova, Y. Zhang, M. Muhammed, *Chem. Mater.* **2003**, *15*, 1617.

[20] X.-C. Shen, X.-Z. Fang, Y.-H. Zhou, H. Liang, *Chemistry Letters* **2004**, *33*, 1468.

[21] D. Kenneth, S. Charles, L. Kevin, L. Guoda, G. Donald, J. Matthew, *Biomaterials* **2005**, *26*, 2061.

[22] T. Neuberger, B. Schöpf, H. Hofmann, M. Hofmann, B. von Rechenberg, *Journal of Magnetism and Magnetic Materials* **2005**, *293*, 483.

[23] D. M. Oliveira, Z. G. M. Lacava, E. Lima, C. D. lia, P. C. Morais, A. C. Tedesco, *Journal of Nanoscience and Nanotechnology* **2006**, *6*, 2432.

[24] A. L. Willis, N. J. Turro, S. O'Brien, *Chem. Mater.* **2005**, *17*, 5970.
[25] X. Yang, Y. Chen, R. Yuan, G. Chen, E. Blanco, J. Gao, X. Shuai, *Polymer* **2008**, *49*, 3477.
[26] G. A. Silva, *Surgical Neurology* **2007**, *67*, 113.
[27] R. Ganguly, A. P. Gaind, S. Sen, I. K. Puri, *Journal of Magnetism and Magnetic Materials* **2005**, *289*, 331.
[28] A. A. Kuznetsov, V. I. Filippov, R. N. Alyautdin, N. L. Torshina, O. A. Kuznetsov, *Journal of Magnetism and Magnetic Materials* **2001**, *225*, 95.
[29] M. I. Papisov, V. P. Torchilin, *International Journal of Pharmaceutics* **1987**, *40*, 207.
[30] F. L. Primo, P. P. Macaroff, Z. G. M. Lacava, R. B. Azevedo, P. C. Morais, A. C. Tedesco, *Journal of Magnetism and Magnetic Materials* **2007**, *310*, 2838.
[31] M. Krack, H. Hohenberg, A. Kornowski, P. Lindner, H. Weller, Fo, x, S. rster, *J. Am. Chem. Soc.* **2008**, *130*, 7315.
[32] S. Laurent, D. Forge, M. Port, A. Roch, C. Robic, L. Vander Elst, R. N. Muller, *Chem. Rev.* **2008**, *108*, 2064.
[33] A. P. Philipse, M. P. B. van Bruggen, C. Pathmamanoharan, *Langmuir* **1994**, *10*, 92.
[34] Y. S. Kang, S. Risbud, J. F. Rabolt, P. Stroeve, *Chem. Mater.* **1996**, *8*, 2209.
[35] X.-P. Qiu, *Chinese Journal of Chemistry* **2000**, *18*, 834.
[36] M. A. G. Soler, G. B. Alcantara, F. Q. Soares, W. R. Viali, P. P. C. Sartoratto, J. R. L. Fernandez, S. W. da Silva, V. K. Garg, A. C. Oliveira, P. C. Morais, *Surface Science* **2007**, *601*, 3921.
[37] D. L. A. de Faria, S. Venancio Silva, M.T. de Oliveira, Journal of Raman Spectroscopy 1997, 28, 873.
[38] O. N. Shebanova, P. Lazor, Journal of Raman Spectroscopy 2003, 34, 845.
[39] G. Beaune, C. Menager, V. Cabuil, J. Phys. Chem. B 2008, 112, 7424.
[40] N. Insin, J. B. Tracy, H. Lee, J. P. Zimmer, R. M. Westervelt, M. G. Bawendi, *ACS Nano* **2008**, *2*, 197.
[41] X. Liu, Q. Hu, X. Zhang, Z. Fang, Q. Wang, *J. Phys. Chem. C* **2008**, *112*, 12728.
[42] D. Wang, J. He, N. Rosenzweig, Z. Rosenzweig, *Nano Lett.* **2004**, *4*, 409.
[43] C. Gautier, T. Burgi, J. Am. Chem. Soc. 2008, 130, 7077

Chapter 7
Conclusion and Future Work

Over the course of the work we found that it was possible to induce the chirality into cadmium based II-VI quantum dots by using chiral stabilisers. This finding enabled us to prepare a series of chiral CdS, CdSe and CdTe based QDs. Initially we demonstrated that strongly emitting chiral *D*-Pen and *L*-Pen capped CdS QDs can be produced by synthesis of CdS particles in the presense of chiral penicillamine and cystein stabilizing molecules. These particles have shown both very strong and very broad luminescence spectra. CD spectroscopy studies have demonstrated that the CdS QDs are optically active and possess almost identical mirror images of one another in the range of 200-390 nm. Density functional theory calculations revealed that penicillamine strongly distorts surface of CdS transmitting an enantiomeric structure to the surface layers and associated electronic states. However, the quantum dot core is found to remain undistorted and achiral. Therefore the particles posses a chiral shell, but cores of the particles remain achiral. This chiral shell contains chiral defects induced by the chiral stabilizer, e.g. penicillamine, on the particle surface. Analysis of PL and CD spectra has shown that there is a clear relationship between defect emission and CD activity. Therefore we conclude that quantum dots must exhibit defect emission to posses CD activity. Although as the control experiment with non-chiral sodium citrate stabiliser showed, defect emitting dots not necessarily chiral. However, only chiral stabilisers can induce the light emitting chiral defect states. Circularly Polarised Luminescence spectroscopy (CPL) have shown no optical activity in the light emitted by the chiral QDs was observed. This indicates that the total emission from the defect trapped states on the surface of the particle does not result in circular polarised light. We have also found that while the penicillamine system did exhibit chiral shape determination, D- producing mainly spheres and L-producing mainly rods, this phenomenon was not fully understood. Future work will involve further investigation of these systems and targetted growth of chiral nanorod, e.g. by heating the QDs under reflux in pyrdine. We plan to explore the possibile formation of CdS based chiral nanorods and nanowires.

Penicillamine and cysteine stabilised chiral CdSe QDs have also been successfully synthesised and characterised. Again we have found that defect emission of these nanocrystals is strongly related to their CD properties. By comparing the CD and excitation spectra of individual particles it is possible to correlate the various CD peaks with those appearing on the excitation spectra. This apparently indicates a link between the various surface defects which contribute to the luminescence and those defects where allow the bandedge to be optically active. It was found that heating under reflux removes all surface defects creating a smoother trap free surface which allowed the particles to emit intrinsically, however by removing these surface defects we also removed the CD activity. This confirmed the strong link between emission type and particle chirality. Thus in our studies of chiral CdSe QDs, we have found that the defect luminescence again plays a vital role in the presence or absence of circular dichroism in nanoparticles.

We have also performed preliminary tests on sensing of selected chiral molecules using our new chiral CdSe QDs. While some sensing studies were carried out the results appear to be inconclusive and will need further study although it must be noted that the use of any material which can chelate Cd as an analyte, such as thiol-containing amino acids can partially destroy the particles. Interaction studies between chiral CdSe dots and DNA showed some interesting results. It was found that right handed DNA protects preferentially the L-Pen stabilised CdSe particles from the damaging affects of the EDTA buffer solution while both the D- and R- particles experienced a drop in luminescence. We believe this protection comes from the DNA's ability to selectively wrap more tightly around a complementary structure of L- stabilized particles. This demonstrates the potential of chiral CdSe based QDs as fluorescent chiral nano-sensors. This will compose the future work with these particles as we attempt to use them as fluorescent sensor with EDTA free DNA. Also lifetime experiments will be carried out on the Pen-CdSe to determine if these particles still exhibit the longest lifetimes after refluxing has removed the surface defects.

Also, we have successfully prepared strongly luminescent but weakly CD active cysteine stabilized CdTe quantum dots. The quantum efficiency of these dots was strongly dependant on the ratio of enantiomers used as stabilisers. It was found that the dots prepared using a racemic mixture of cysteine enantiomers results in QDs with higher quantum yields than those prepared with an enantio-pure stabilizer. We have

demonstrated that the CD activity of CdTe QDs can be introduced by utilising a mixture of two different stabilisers (Pen and Cys) of the same chirality. This results in the enhanced CD activity, but causes a decrease in the quantum yield and a widening of the emission due to the presence of chiral defects on the nanoparticle surface. Further research will include detailed studies of the photophysical properties of CdTe QDs with different chiral stabilisers and the investigation of the electron transfer and energy transfer processes in these systems. We believe that our approach can be used for development of many other QDs with controlled chirality, quantum yield, photochemical and photophysical characteristics.

We have also demonstrated that chiral luminescence nanowires can be produced from the mixture of chiral and non-chiral CdTe QDs. These CdTe QDs and nanowires could find important applications such as fluorescent chemical and biochemical chirality sensors and molecular recognition nanoprobes. However, detailed future investigations are required to investigate the formation of the chiral nanowires and origin of their circular dichroism. We also plan to perform Circularly Polarised Luminescence spectroscopy (CPL) studies of chiral CdTe nanowires, which could potentially serve as polarized light emitters.

We have also used our approach to induce chirality into metal oxide based nanoparticles. Penicillamine stabilised maghemite nanocrystals have been successfully prepared. TEM images demonstrated that the utilisation of Penicillamine stabilisers allowed us to control both the size and monodispersity of the magnetic particles. SQUID measurements have shown that the particles are indeed superparamagneitc. Also SQUID suggested a difference between the magnetism of the D-, L- and R- particles which can not be explained by simple nanoparticle size differences. CD measurements showed very little differences from the particles coated by non-chiral stabilisers. However, we believe that only VCD measurements could detect any effects of the chiral penicillamine stabilisers on maghemite particles. Therefore future studies involving VCD technique are required in order to investigate and fully explain the properties of penicillamine stabilised maghemite nanoparticles

Attempts to make "all in one" magnetic-luminescent-chiral composites resulted in some remarkable core-shell structures, which demonstrated interesting photophysical properties. However, there were some difficulties with the purification and clear identification of these nanocomposites. Obviously, significant efforts will be required

to develop these nanosystems and investigate them in details. This will be a subject of our future work.

Finally, although not included in this thesis we have recently produced chiral TiO_2 nanoparticles from titanium penicillamine-ethoxide precursors. The first of these precursors in the L- conformation was heated to reflux in propan-2-ol before EDA and $NaOH_{(aq)}$ were added to initiate a base hydrolysis reaction which co-precipitated chiral TiO_2 nanoparticles. The particles were isolated by centrifugation and redispersed in propan-2-ol and examined using UV-Vis and CD spectroscopy, (**Figure 7.1**). Future work will involve further synthesis and optimisation of TiO_2 nanoparticles using both enantiomers and racemic mixture of the precursors, as well as detailed studying chiral TiO_2 particles using TEM, spectroscopic and other techniques. Then we plan to investigate photocatalytic activity of new chiral TiO_2 nanoparticles in asymmetric photooxidation reactions.

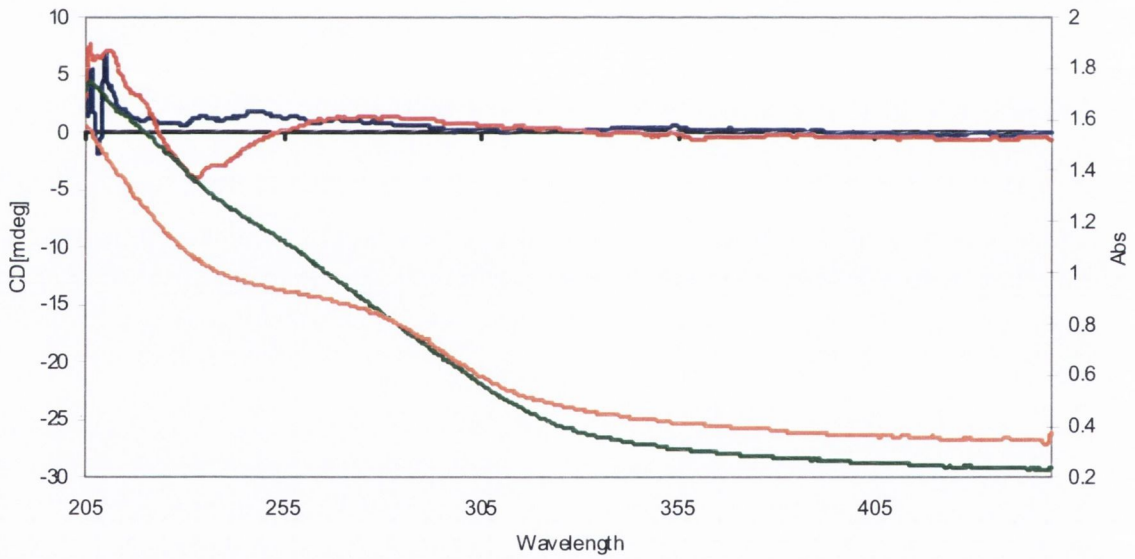

Figure 7.1: CD and UV-Vis scans of the Ti penicillamine-ethoxide precursor, (blue and green), as well as the co-precipitated TiO2 nanoparticles, (red and orange).

Some Personal Conclusions and Views

Initially we had anticipated that these quantum dots could be used as chiral fluorophores. However, the various chiral interactions studied returned results which are mixed at best. That is to say some of the results proved difficult to reproduce.

However, another possible application lies within there use in next generation opto-electronic devices. As we have shown it is possible to control not only the intensity of the emission but also the colour depending on the type and chirality of the stabilizer used. Also, by greater control of the nanoparticle shape we can move into the area of nanowires production. We hoped to be able to produce uniform, well defined nanostructures which not only absorb but also emit polarised light. This would allow us to start producing new pH or chemosensors. However, as was seen in chapter 5 the wire growing step had the effect of drastically reducing the strength of the emission. This is a problem that would have to be resolved if they are to be of use in this field.

Another aspect of this work which we would like to explore is that of reverse CPL. That is, instead of examining chiral quantum dots to see if they emit polarised light we would use polarised light of a specific handedness to excite either D- or L-stabilized particles. We hope that depending on the type of light used we would either do nothing or "switch on" the dot, i.e right handed light would excite D- but not L-dots and vice versa. This would allow us to begin constructing light gateways by simply adjusting the handedness of the light used.

With respect to the magnetic/luminescent work, the main problem is the complete separation of the nanocomposites from any remaining unmodified magnetic or luminescent particles. This is due to the fact that the magnetic washing of the nanocomposites also of course removes unmodified maghemite. Therefore this system will also require further study to improve washing step.

Lastly, as the field of nanoscience continues to grow the demand for higher quality TEM imaging also grows. However, by their very nature water based semiconductors which are coated with an insulating organic shell make poor candidates for imaging. While preparatory steps such as particle co-precipitation and overnight sample drying seem to help they are not the only answer. Perhaps it would be worth while to examine this further, i.e. finding the ideal particle concentration through combined UV and TEM, as well as investigating other cleaning techniques such as dialysis and gel chromatography separation.

Publications :

"Chiral shells and achiral cores in CdS quantum dots"; Simon P. Elliot, Mícheál P. Moloney, Yurii K. Gun'ko; Nanoletters 2008, (8) 2452-2457

"Chiral highly luminescent CdS quantum dots"; Mícheál P. Moloney, Yurii K. Gun'ko, John M. Kelly; *Chemical Communications*, 2007, (38), 3900

Oral communication:

Oral presentation at 3rd International Conference on Nanomaterials and Nanomanufacturing, 17-18 December 2007, Dublin, Ireland

Oral presentation at 20th International Symposium on Chirality, 6-9 July 2008, Geneva, Switzerland

Posters :

1. "Synthesis and modification of CdS and ZnS/CdS core/shell nanoparticles", Moloney, M., Kelly, J.M, PRTLI Winter Meeting December, 2002, Dublin, Ireland

2. "Preparation and characterisation of magnetic/luminescent composites", Moloney, M., Gun'ko Y.K, Annual Microspcopy meeting Dublin Institute of Technology 2004

3. "Luminescent Chiral Quantum Dots" Moloney, M., Gun'ko Y.K., Kelly J. M., Annual Irish Chemistry Colloquium, DCU 2006

4. "Chiral CdTe Nanoparticles »", Mary, C., Moloney, M., Gun'ko, Y., Sure Poster competition 2008